UNIVERSIDADE ESTADUAL DE CAMPINAS
Faculdade de Engenharia Mecânica

JAIR LEOPOLDO LOAIZA BERNAL

Study of the operation of an internal combustion engine, fueled by indirect injection of ethanol and direct injection of water into the combustion chamber.

Estudo do funcionamento de um motor de combustão interna, alimentado por injeção indireta de etanol e injeção direta de água na câmara de combustão.

CAMPINAS
2019

JAIR LEOPOLDO LOAIZA BERNAL

Study of the operation of an internal combustion engine, fueled by indirect injection of ethanol and direct injection of water into the combustion chamber.

Estudo do funcionamento de um motor de combustão interna, alimentado por injeção indireta de etanol e injeção direta de água na câmara de combustão.

Thesis presented to the School of Mechanical Engineering of the University of Campinas in partial fulfillment of the requirements for the degree of Doctor in Mechanical Engineering, in the area of Solid Mechanics and Mechanical Design.

Tese apresentada à Faculdade de Engenharia Mecânica da Universidade Estadual de Campinas como parte dos requisitos exigidos para a obtenção do título de Doutor em Engenharia Mecânica, na Área de Mecânica dos Sólidos e Projeto Mecânico.

Orientador: Prof. Dr. Janito Vaqueiro Ferreira

ESTE EXEMPLAR CORRESPONDE À VERSÃO FINAL DA DISSERTAÇÃO DEFENDIDA PELO ALUNO JAIR LEOPOLDO LOAIZA BERNAL, E ORIENTADA PELO PROF. DR. JANITO VAQUEIRO FERREIRA.

_____

ASSINATURA DO ORIENTADOR

CAMPINAS

2019

Ficha catalográfica
Universidade Estadual de Campinas
Biblioteca da Área de Engenharia e Arquitetura
Luciana Pietrosanto Milla - CRB 8/8129

L78s

Loaiza Bernal, Jair Leopoldo, 1973-
Study of the operation of an internal combustion engine, fueled by indirect injection of ethanol and direct injection of water into the combustion chamber / Jair Leopoldo Loaiza Bernal. – Campinas, SP : [s.n.], 2019.

Orientador: Janito Vaqueiro Ferreira.
Tese (doutorado) – Universidade Estadual de Campinas, Faculdade de Engenharia Mecânica.

1. Modelo estatístico-termodinâmico. 2. Modelagem termodinâmica. 3. Termodinâmica - Modelos matemáticos. 4. Evaporação. 5. Modelagem e simulação. I. Ferreira, Janito Vaqueiro, 1961-. II. Universidade Estadual de Campinas. Faculdade de Engenharia Mecânica. III. Título.

Informações para Biblioteca Digital

Título em outro idioma: Estudo do funcionamento de um motor de combustão interna, alimentado por injeção indireta de etanol e injeção direta de agua na camara de combustão
Palavras-chave em inglês:
Statistical-thermodynamic model
Thermodynamic modeling
Thermodynamics - Mathematical models
Evaporation
Modeling and simulation
Área de concentração: Mecânica dos Sólidos e Projeto Mecânico
Titulação: Doutor em Engenharia Mecânica
Banca examinadora:
Janito Vaqueiro Ferreira [Orientador]
Jose Eduardo Mautone Barros
Pedro Teixeira Lacava
Waldyr Luiz Ribeiro Gallo
Rogeiro Gonçalves dos Santos
Data de defesa: 16-04-2019
Programa de Pós-Graduação: Engenharia Mecânica

Identificação e informações acadêmicas do(a) aluno(a)
- ORCID do autor: https://orcid.org/0000-0002-5417-5637
- Currículo Lattes do autor: http://lattes.cnpq.br/1495692940617748

UNIVERSIDADE ESTADUAL DE CAMPINAS
FACULDADE DE ENGENHARIA MECÂNICA
COMISSÃO DE PÓS-GRADUAÇÃO EM ENGENHARIA MECÂNICA
DEPARTAMENTO DE MECÂNICA COMPUTACIONAL

TESE DE DOUTORADO ACADEMICO

Study of the operation of an internal combustion engine, fueled by indirect injection of ethanol and direct injection of water into the combustion chamber.

Estudo do funcionamento de um motor de combustão interna, alimentado por injeção indireta de etanol e injeção direta de água na câmara de combustão.

Autor: Jair Leopoldo Loaiza Bernal
Orientador: Prof. Dr. Janito Vaqueiro Ferreira

A Banca Examinadora composta pelos membros abaixo aprovou esta Dissertação/Tese:
Prof. Dr. Janito Vaqueiro Ferreira, Presidente
Instituição: Unicamp - FEM
Prof. Dr. Jose Eduardo Mautone Barros
Instituição: Universidade Federal de Minas Gerais
Prof. Dr. Pedro Teixeira Lacava
Instituição: Instituto Tecnológico de Aeronáutica - ITA
Prof. Dr. Waldyr Luiz Ribeiro Gallo
Instituição: Unicamp - FEM
Prof. Dr. Rogério Gonçalves dos Santos
Instituição: Unicamp - FEM
A Ata da defesa com as respectivas assinaturas dos membros encontra-se no processo de vida acadêmica do aluno.

Campinas, Abril 16 de 2019.

When one's expectations are reduced to zero, one really appreciates everything one does have. *(Stephen Hawking, 1942-2018)*

ACKNOWLEDGEMENTS

The author wishes to express his gratitude to the people and institutions that collaborated in different ways during the development of this research.

To the State University of Campinas (Unicamp) and its faculty of Mechanical Engineering (FEM) for giving me the opportunity to study in this institution. One of the best universities in the world.

To the professor Ph.D. Janito Vaqueiro Ferreira, for his guidance, support and collaboration in the development and advancement of this research.

To the professor Ph.D. Waldyr Luiz Ribeiro Gallo, for his guidance and timely collaboration for him to advance this investigation.

To the members of the research group, Laboratory of Biofuels Motors (LMB), the engineers Alessandro De Lima, Caio Rufino, Renato dos Santos and Ana Paula Mattos, for their friendship, patience, support, and guidance all the time.

To Mrs. Elizabeth de Oliveira Viana, secretary of the Department of Computational Mechanics, for her invaluable friendship and support.

To the engineer Rubén Darío Hernández, for his unconditional friendship.

To my friends and colleagues, Giovanna Zanoni, Carolina Corredor, Camilo Ariza, Maria Fernanda Rodriguez, German Castañeda, Diana Martinez, Oscar Rojas, Paola Gonzales, Jose Ilmar, in short, the list is endless.

Finally, I would like to thank FAPESP, for the opportunity to work on the granting of research grants and a scholarship, through project number 2015/20801-3.

"With a little help from my friends"

"An expert is a person who has found out by his own painful experience all the mistakes that one can make in a very narrow field".

(Niels Bohr 1885-1962)

RESUMO

Na busca contínua pelo aumento da eficiência e redução do impacto ambiental, devido ao uso de motores de combustão interna (ICE), a injeção de água tem sido uma das estratégias mais utilizadas para atingir esses objetivos. Várias foram e ainda são as metodologias que utilizam a água como método de controle de temperatura e redução de emissões. Antes do uso de turbinas de jato e durante o uso de motores de pistão na aviação militar e comercial, a injeção de água e soluções de água e álcool foi implementada como uma estratégia para controlar a temperatura interna do cilindro durante a combustão. Isso permitiu o aumento das taxas de compressão com o consequente aumento de potência, principalmente em operações críticas como decolagens e manobras evasivas durante o combate. As conseqüências da aplicação desta técnica têm sido extensivamente investigadas em motores que utilizam combustíveis derivados do petróleo (gasolina e diesel). No entanto, em dispositivos que utilizam combustíveis alternativos, como o etanol ou outros biocombustíveis, existem poucas referências à pesquisa que utiliza técnicas de injeção de água nesses motores. A pesquisa aqui apresentada mostra os resultados da implementação utilizando simulação computacional de um modelo termodinâmico de duas zonas que integra a injeção de água líquida diretamente na câmara de combustão, em um motor que utiliza etanol como combustível. O modelo proposto interpreta a partir da termodinâmica o comportamento da água no interior do cilindro quando é injetado na forma líquida durante qualquer momento do ciclo. Até agora, esse tipo de análise foi realizado por meio de testes experimentais. Aqui a influência da água do ponto de vista teórico é estudada usando simulação. O modelo é validado comparando seus resultados com os da pesquisa experimental que implementa a mesma técnica de injeção de água proposta. A pesquisa mencionada usa um protótipo de motor que usa gasolina como combustível. Ao comparar alguns dos parâmetros operacionais, como a pressão no interior do cilindro, o consumo específico de combustível efetivo ou a taxa de liberação de calor durante a combustão, verifica-se que o modelo se comporta muito próximo do que foi relatado nos dados experimentais. Outras variáveis, como as emissões de NOx, apresentam tendências semelhantes entre o comportamento experimental e o simulado, apesar da grande variabilidade dos dados experimentais. Por fim, o modelo apresenta grande flexibilidade, pois pode ser utilizado para simular diferentes geometrias de motores, regimes de rotação e uso de combustíveis como gasolina, etanol, etanol hidratado e misturas destes em diferentes proporções.

Palavras-chave: Modelo termodinâmico, duas zonas, evaporação de gotículas de água, modelo de simulação, injeção de água, pressão, fração de massa queimada.

ABSTRACT

In the continuous search for the increase in efficiency and the reduction of environmental impact, due to the use of internal combustion engines (ICE), water injection has been one of the strategies frequently used to achieve these objectives. Several have been and still are the methodologies that use water as a method of temperature control and emission reduction. Before the use of jet turbines and during the use of piston engines in military and commercial aviation, the injection of water and water and alcohol solutions was implemented as a strategy to control the internal temperature of the cylinder during combustion. This allowed the increase of compression ratios with the consequent increase in power, especially in critical operations such as takeoff and evasive maneuvers during the fighting. The consequences of the application of this technique have been extensively investigated in engines that use fuels derived from petroleum (Gasoline and Diesel). However, in devices that use alternative fuels such as ethanol or other bio-fuels, there are few references to research that uses water injection techniques in these engines. The research presented here shows the results of the implementation using computational simulation of a thermodynamic model of two zones that integrates the injection of liquid water directly into the combustion chamber, in an engine that uses ethanol as fuel. The proposed model interprets from thermodynamics the behavior of the water inside the cylinder when it is injected in liquid form during any moment of the cycle. So far, this type of analysis has been carried out through experimental tests. Here the influence of water from the theoretical point of view is studied using simulation. The model is validated by comparing its results with those of experimental research that implements the same water injection technique that is proposed. The research mentioned uses a prototype engine that uses gasoline as fuel. When comparing some of the operating parameters, such as the pressure inside the cylinder, the specific fuel consumption at brake or the rate of heat release during combustion, it is found that the model behaves very closely to what was reported in the experimental data. Other variables such as NOx emissions present similar trends between experimental and simulated behavior, despite the great variability of the experimental data. Finally, the model presents great flexibility because it can be used to simulate different engine geometries, rotation regimes and the use of fuels such as gasoline, ethanol, hydrated ethanol and mixtures of these in different proportions.

Keywords: Model thermodynamics, two zones, simulation model, water droplet evaporation, water injection, pressure, mass fraction burned.

LIST OF FIGURES

LIST OF TABLES

LIST OF ABBREVIATIONS AND ACRONYMS

C = Carbon.

H = Hydrogen.

O = Oxygen.

N = Nitrogen.

Ar = Argon.

P = Pressure.

V = Volume.

m = Molar mass.

R = Universal constant of ideal gases.

T = Temperature.

U = Internal energy.

Q = Heat.

W = Work.

t = Time.

h = Entalpy.

c_p = Specific heat at constant pressure.

s = Specific entropy.

K = Equilibrium constant.

W, X, Y and Z = Molar fraction of atmospheric air components.

v = Specific volume.

b = burned.

u = unburned.

IVC = Intake Valve Close.

EVO = Exhaust Valve Open.

l = length of the rod.

A = Area.

Nu = Nusselt number.

Re = Reynolds number.

D_{AB} = Binary diffusivity of the spices A in a medium composed by the species B.

Y_A = Mass fraction of the species A (or B).

m_A = Mass flow of the species A (or B).

k = Thermal conductivity.

B_y = Conduction potential.

D = Diameter.

P_r = Prandtl number.

w = Water.

MW = Molar Weight.

L = length of rupture of the Levich jet.

TDC = Top Dead Center.

$BTDC$ = Before Top Dead Center.

$ATDC$ = After Top Dead Center.

$ABDC$ = After Bottom Dead Center.

$BBDC$ = Before Bottom Dead Center.

LIST OF SYMBOLS

θ = Crank angle.

ω = Rate of rotation of he engine.

ξ = Property.

ϕ = Equivalence ratio.

ε = Balance for the stoichiometric condition.

$\alpha, \beta, \gamma, \delta$ = Numbers of the atoms of each elements

ΔG° = Ground state of the Gibbs free energy.

ρ = Density.

λ = Wavelength.

CONTENTS

1 INTRODUCTION

The concept of water injection has often been associated with the history of the development of energy conversion processes through combustion. It is possible to find initial references on this association, in the patents of the first gas turbines, around 1791, where the injection of water appears as an auxiliary technique to control the temperature of the combustion gases and prevent damage in the later section of the turbines (HOPKINSON, 1913),(RICARDO, 1953). Towards the second half of the 19th century, coal and other solid fuels were progressively replaced by liquids, hence steam was introduced as a way to improve the atomization of these liquid fuels. However, there are few references to the development of double atomizers, for the steam and fuels used. In the first decade of the 20th century, steam was frequently used for atomization processes, due to the problems generated by the mechanical atomization systems used in large oil boilers and natural gas shortage (DRYER, 1977).

As well as boilers and turbines, the addition of water by injection techniques are also associated with the evolution of internal combustion engines (ICE). Bertrand Hopkinson used this concept around 1913 in the development of power plants that used water as a cooling agent (HOPKINSON, 1914). Hopkinson's idea was not new; however, at that time , he was the only one who managed to implement it in a practical, successful way.

Towards the First World War (1914), the use of water and ethanol-methanol-watermixtures played a leading role in increasing the operating efficiency of Otto engines (KOENIG; HEISER, 1943), however; antiknock agents, soluble in fuels, were discovered and developed by 1922. These investigations, together with the high costs and complexity of storage systems for water and water/alcohol mixtures, discouraged the use of these substances in the engines of the automobiles of that time.

A few years before the start of the Second World War and during its development, the research on supercharged engines for airplanes returned the interest in the injection of water and alcohol. (KOENIG; HEISER, 1943). Aircraft engines presented a severe tendency to detonate and overheat, which limited the uses of overfeeding and also the increase in compression ratios used until then for a high load operation. With the aspiration of water/alcohol emulsions, it helped to avoid the formation of ice and allow aircraft to reach the maximum power widely, during takeoffs and combat maneuvers (BELL, 1944). After the end of the war, water injection was implemented in turboprop engines and the first reactors for commercial aircraft. The company Pratt and Whitney offered the injection of water/alcohol as an option within its line of JT9D engines, used in passenger aircraft (DRYER, 1977).

Simultaneously with these developments and, as a consequence of the cost increase of automotive-grade fuel compatible with existing engines; great efforts were made to increase the

compression ratio used. That research kept the interest in the addition of water/alcohol mixtures to prevent detonation. During the period between 1944 and 1956, several papers were published on internal refrigeration and control of detonation in spark ignition engines (SI) (PETERS; STEBAR, 1976). Additionally, in the auto parts market devices to dose water and alcohol appeared. The relative success of these mechanisms in the market , led to the Oldsmobile® division of General Motors to present a supercharged V-8 engine (compression ratio 10.25 to 1), which used small amounts of a mixture of water and methanol to limit detonation in high load (LASHERAS *et al.*, 1979).

In 1947, Zeldovich reported on the formation of Nitric Oxide from molecular Nitrogen (ZELDOVICH *et al.*, 1947). This paper together with the discovery of the relation between chemical pollution in the air and NOx (WEISS; RUDD, 1959),(PETERS; STEBAR, 1976), motivated the interest in the investigation of water injection of water as a method for the emission control of polluting agents (KOPA *et al.*, 1963), (KLAPATCH; KOBLISH, 1971b). Investigations related to the control of emissions through the addition of water and applied to compression ignition and spark ignition engines have been published in the last decades (URBACH *et al.*, 1997).

Other investigations that measure the effects on efficiency with various methods water addition have been made during recent years. Experimental works such as the published Lanzafame (LANZAFAME, 1999) and (BORETTI, 2013), about the consequences of the addition of water in the intake duct, just before the corresponding valve and between the turbocharger and the inlet port to the cylinder, show that the injected water has a noticeable effect in reducing the maximum pressure and the combustion temperature. The added water absorbs heat from the air/fuel mixture and evaporates. This effect has a positive influence on the performance of the engine, as these investigations show.

In technical literature are experimental studies, where it is reported how some of the performance parameters of ICE SI, which use gasoline as fuel, are affected by the addition of water by means of an injector located in the chamber combustion area (KIM *et al.*, 2016), (THEWES *et al.*, 2015). Also, it is possible to find simulations in Computational Fluid Dynamics (CFD) of the water injection process before the intake valve (BERNI *et al.*, 2015). However, theoretical studies that simulate the process of direct injection of water into the combustion chamber, using quasi-dimensional thermodynamic models of multiple zones and ethanol as fuel, have not been found.

In the work presented here, the injection of water in a liquid state is modeled in an ICE SI employing an injector located in the combustion chamber. The injection of water can be done during the closed phase (Compression, Combustion, and Expansion) of the work cycle of an internal combustion engine, ignited by a spark and that uses ethanol as fuel. The main objective is to theoretically analyze and validate, comparatively, through the computational simulation of the process, the influence of this water injection technique on the performance of this type of

engines.

In chapter two, a bibliographic review is presented. This review covers multizone thermodynamic modeling, a review of some of the applications of this type of thermodynamic models, the water evaporation model implemented and some of the modifications that have been proposed to improve its interpretation.

The quasi-dimensional thermodynamic model of two zones is extensively explained. This particular model was chosen because it is a multi-zone model, since the gases contained in the cylinder and the combustion chamber, during the combustion reaction process, are divided into two zones; a zone of burned gases and another of unburned gases, separated by a layer of infinitesimal thickness, called the flame front. This separation allows analyzing, with better accuracy, the temperature variations present in each zone during the reaction. The considerations and assumptions necessary for the configuration of the model are also enunciated and explained in this chapter. Likewise, the considerations and assumptions necessary for the deduction of the water evaporation model are enunciated and explained.

In chapter three, it is presented present the deduction of the equations for the quasi-dimensional model of two zones, which include the injection of water. It also presents the model of heat transfer implemented, the model of water injection and other models necessary for the interpretation of the phenomenology of the water injection process. All the modeling presented in this chapter is implemented in a Matlab® program to simulate the behavior of the water during the process, and the influence that the injection and subsequent evaporation of the water have on the work cycle of an internal combustion engine, spark-ignition, using ethanol as fuel. The mathematical model includes the possibility of injecting water in the open phase (Admission and Exhaust) or during the closed phase (Compression, Combustion, and Expansion).

Chapter four shows the results of the implementation of the mathematical model proposed in chapter three, in a program built on Matlab®. This simulation allows observing how the injection of water affects the variables of pressure, temperature, mass contained in the cylinder and NOx emissions. The injection of water is done in three instants of the closed phase of the cycle. Two of the water injection positions occur before the start of combustion and one after the start of combustion. The amount of water injected is determined using a ratio of water mass/mass of fuel in percentage. In addition to the variables mentioned, the program also delivers the values of power, torque, specific and instantaneous consumption, for a single-cylinder engine.

The geometrical characteristics, the valve command, the amount of fuel injected per cycle, the inlet pressure and the wall temperature are data taken from the engine supplied by the Peugeot® company and that is analyzed in the global project of which this work is part. For validating the result of the program, it is used the data reported by Kim (KIM *et al.*, 2016) which correspond to an experimental test of direct water injection in a gasoline engine. The

comparison with the results reported by this paper allows obtaining an assessment of the quality of the approach proposed.

Chapter five presents the conclusions and the proposal for future work by the author.

1.1 MOTIVATION AND JUSTIFICATION.

In the current technological moment that our civilization is going through, speaking of motors that use fossil fuels, seems to go against the environmentalist logic and the electric tendency prevailing in mobility. However, more than 80% of land transport vehicles, both public and cargo, use internal combustion engines, either diesel or spark ignition.

Additionally, the production of this type of electric vehicles is still far from reaching the levels needed to displace vehicles that use combustion engines in the market especially in developing countries, electric vehicles will take a few decades to reach the final consumer with prices that allow the consumption rates at levels presented by fossil fuel vehicles today.

Electric technology is expensive and it still needs to overcome the autonomy barrier to reach levels of combustion engines. Also, the development and evolution of ICE (Internal Combustion Engines) have been continuous and sustained for more than 100 years, and its technology has allowed progress in mobility.

The previous arguments together with the current environmental and energy problems justify the research and development of techniques that make ICE more efficient and less polluting, at least during the decades that will pass until the electric cars become massive. Among the techniques that have helped achieve the goals of improving efficiency and reducing ICE contamination, the use of bio-fuels such as ethanol and water injection appear. The two alternatives, both with independent and combined uses, have always been present in these developments.

1.2 OBJECTIVES.

The objective of this work is to contribute with the knowledge about the behavior of an internal combustion engine fueled by ethanol and to which water is subsequently added using the direct injection into the combustion chamber. The interest in this research is based on the growing need to design cleaner and more efficient engines that use alternative fuels (bio-fuels) to fossils (petroleum derivatives such as gasoline or diesel).

The secondary objectives are:

- To compare the behavior of a real engine (powered by ethanol or gasoline) with the results obtained through simulation, under the same conditions.. Additionally, to establish the convergence of both models.

- To study the possible effects of the combustion reaction, that can occur as a result of the addition of water directly to the combustion chamber.
- To compare the engine behavior (running on ethanol or gasoline) that incorporates the direct injection of water into the combustion chamber with the simulated results in the same conditions. Moreover, to establish the similarities and differences between the models.
- To verify the operating parameters and performance reported in the literature through simulated tests in the proposed model.
- To analyze the influence of direct water injection on the reduction of NOx emission.
- To compare the way direct water injection affects performance parameters such as thermal efficiency, instant fuel consumption and power generated.
- To verify if the technique of direct water injection effectively reduces the tendency to knock when the engine works at high load and low rotation.

2 LITERATURE REVIEW

The literature review developed for this dissertation includes topics related to thermodynamic models that describe the power cycle of a four (4) stroke spark ignition (SI) engine. Initially, a brief review is presented in which some of the most representative spark ignition engine simulation models are analyzed. Each shown model has a particular type of simulation approach within the so-called multi-zone thermodynamic models for engines. Afterward, it's reviewed an explicit mathematical model of two zones, in which the simplifications considered for the construction of the model are established. These simplifications are necessary due to the difficulty encountered in coupling the mathematical expressions involved in the descriptions of each stage of the model. The last part of the discussion concerns water injection systems in SI internal combustion engines. In addition, a description of a droplet evaporation model is included, together with the above description, serves as the basis for the deduction of the direct water injection model into the combustion chamber.

2.1 THERMODYNAMIC MODELS OF POWER CYCLE OF A 4-STROKE ENGINE.

In the 70's, mostly due to the oil crisis, designers began to think seriously about the design needs and to build more efficient and compact engines. These two important parameters are directly influenced by the way how the heat engine transforms the energy contained in a fuel into mechanical energy.

It can be stated that most of the engine models found in the literature are, in generic terms, similar. These models are called "Multi-zone thermodynamic models of engines" and include in their definition the so-called zero-dimensional, multidimensional and multi-zone thermodynamic models. The basic structure of the zero and multi-dimensional models is based on the conservation equations of mass and energy, therefore they only depend on time. These considerations result in a set of ordinary differential equations. Furthermore, multidimensional models incorporate, besides the set of equations mentioned in chapter one, the Navier-Stokes equations that govern the behavior of fluid also depend on spatial coordinates and take the form of partial differential equations. (VERHELST; SHEPPARD, 2009).

Due to the great difficulty in the approach and calculation, which is presented by the multidimensional models this document will only refer to the multi-zone thermodynamic models. Within these multi-zone models, some sub-models are used to explain the stages of the four-stroke engine operating cycle. Blumberg (BLUMBERG *et al.*, 1979) presented a review of the state of the art in this type of models, emphasizing that the detailed application of mathematical calculations can facilitate the development of phenomenological models that better explain engine behavior. From that period until now, a notable progress has been made to fully

understand the operation of thermal engines.

It is important to clarify it's difficult to establish a mathematical model that explains in a detailed and precise way the series of physical and chemical phenomena which occurs during the four stages of an engine is difficult. The appearance of turbulence and the speed of the chemical reactions during combustion make it almost impossible to describe the sequence of energetic events and processes by means of mathematical expressions. For this reason, researchers use a series of simplifications, which diminish the accuracy of the interpretation, but allow finding a remarkably close approximation of phenomenology.

Within the above simplifications it can be cited: (VERHELST; SHEPPARD, 2009)

- During the entire four-stroke cycle (intake, compression, power stroke and exhaust) the pressure is invariably assumed to be uniform throughout the cylinder.
- Burned and unburned gas regions are, each, in chemical equilibrium and they are assumed separated by a thin layer of infinitesimal thickness, called the flame front.
- No heat transfer between burned and unburned gas zones.
- All gases are considered ideal gases; possible invalidity of the ideal gas law at high pressures is counterbalanced by the associated high temperatures under engine combustion conditions.

Practically the total of the models here mentioned obey the previous considerations. A cylinder interior scheme is showed in (Fig.2.1), in which the two corresponding zones can be clearly appreciated; a zone of burnt gases and another zone of unburned gases.

In 1975, it was published by Benson (BENSON W. J. D. ANNAND, 1975) a comprehensive mathematical model for the simulation of a spark ignition engine, including the intake and exhaust processes. In this model, the authors applied an empirical correction factor for flame front turbulence and the calculation of NO (nitrogen oxide) emission. The authors also explain the dynamics of the gases in the exhaust pipe, including chemical reactions along path lines. In the document, it is a made a description of the mechanism of spread of flame, the ignition and the appearance of both zones (burned and unburned gases), and the thermodynamic equilibrium of the combustion reaction, considering 12 chemicals agents involved.

In 1985, Carpenter published a new mathematical model for a spark ignition engine (CARPENTER; RAMOS, 1985). This new model includes the study of delivered power, heat loss and emission of unburned hydrocarbons, using a system of two equations for turbulence, as opposed to Benson (BENSON W. J. D. ANNAND, 1975) where an empirical correction factor was used. The combustion is modeled by means of a single-stage irreversible chemical reaction whose speed is controlled by an expression of the Arrhenius type. The numerical results indicate that, during the intake stroke, two eddies are formed and persist in the compression stroke. It

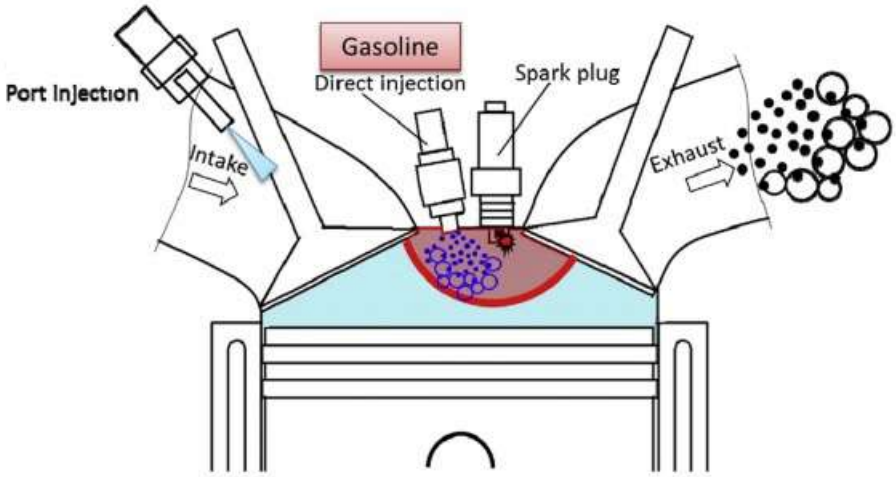

Fig. 2.1 – Scheme of the interior of a cylinder of an internal combustion engine and ignited by spark, during the cycle of power. The two zones (burned gases (Red) and unburned (Blue)) are clearly visible. Source:(LIU *et al.*, 2015)

is assumed that the flame kernel generated by the spark plug is spherical and the emission of unburned hydrocarbons amounts is 7.41 % of the admitted fuel into the cylinder.

The models mentioned previously use the method presented by Annand (ANNAND *et al.*, 1963) to calculate the heat loss by convection between gas and cylinder walls. The modifications of this model, that not only takes into account the convective effects but also the radiative, are presented in Woschni (WOSCHNI, 1967).

In 2001, a predictive model called quasi-two zones was published by Alla (ALLA *et al.*, 2001). The model was developed to predict the behavior of the combustion process in dual fuel engines. Methane is used as the main fuel and a small amount of liquid fuel was used as a pilot (Activator) injected through a similar system to that used in traditional diesel engines. This model presents a special emphasis on the activity of chemical kinetics of pre-mixed gaseous fuel. The complexity of the analysis is considerable if it is taken into account that 178 stages of elementary reactions and 41chemical species were considered to describe the oxidation of the gaseous fuel. The main goal was to estimate the concentrations of the exhaust gases. A more recent approach was made by Bozza (BOZZA *et al.*, 2005) using fractal mathematical techniques to perform a one-dimensional approach compared with experimental data.

Both, zero-dimensional and multi-zone models, are delimited by the simplifications mentioned previously which has allowed these models to evolve towards the analysis of the turbulent phenomena effects and how they affect combustion efficiency. Also, their the models' complexity has increased towards the understanding of the chemical kinetics of the reaction, where an increasing number of species involved gives rise to the increase in the number of reactions that must be analyzed. The fundamental objective is to study mechanisms that allow the

biggest reduction of greenhouse gas and pollutant emissions without affecting the mechanical performance of the engine.

2.2 COMPUTATIONAL MODELS OF THE POWER CYCLE OF A 4-STROKE ENGINE.

Some of the mathematical descriptions that are presented below on the working cycle of four-stroke engines and spark ignition, aim to be implemented in simulation models that allow predictions on the behavior of the variables that govern the cycle. These predictions support design decisions that include performance improvements, reductions in polluting gas emissions and, in general, in general, a better use of fuel energy to make the engine more efficient and less polluting.

In the literature, there are several computational models built in programming languages such as Fortran or C (FERGUSON; KIRKPATRICK, 2001). Different researchers have make modifications, in order to be closer to an accurate description of the phenomena involving the cycle. Some of these investigations are cited in this section.

2.2.1 SPARK IGNITION INTERNAL COMBUSTION ENGINE MODELING USING MATLAB®.

In the paper presented by Buttsworth, (BUTTSWORTH, 2002) several routines implemented in Matlab® are presented and described for calculations of combustion and thermodynamic simulation of the operation of the internal combustion engine and spark ignition. The functions are described to find the coefficients of the thermodynamic curve for a variety of fuels, air and combustion products.

Several routines included in this paper are essentially Matlab® versions of the programs implemented in FORTRAN and presented by Ferguson for spark ignition engine calculations (FERGUSON; KIRKPATRICK, 2001). A version in Matlab® of the Olikara and Borman method (OLIKARA; BORMAN, 1975) is also used by the author (BUTTSWORTH, 2002) to determine the state of equilibrium of the combustion products. Finally, additional routines specifically designed for spark ignition engine modeling are described.

For the calculation of the temperature of the adiabatic flame, a function presented in Turns is used (TURNS, 1996; JERZEMBECK *et al.*, 2009). By comparing the results delivered by the new routines built in Matlab® with the results previously obtained with the routines built in FORTRAN, it can be concluded that the new results are reliable. This assertion is based on the fact that the average standard deviation of the comparison between the results obtained in Matlab® and the old results, obtained with the routines programmed in FORTRAN, is close to 1%.

The most outstanding contribution presented in this article is related to the updating of

the programs presented by Ferguson in his book, since this programming was elaborated in 1986 and at that time FORTRAN was used as programming language, with the difficulties that the programming process presented.

The use of Matlab as a programming language proved to be adequately adapted to the objectives originally proposed by Ferguson (FERGUSON; KIRKPATRICK, 2001), in addition to allowing the use of more advanced computers that improved the execution times of the routines. Additionally, it was possible to improve some aspects of the programming that generated difficulties in the execution of the original programs.

2.2.2 NUMERICAL SIMULATION OF A SPARK IGNITION ENGINE OPERATING CYCLE.

The model presented for Morea-Roy (MOREA-ROY *et al.*, 1999) differs from the commonly used formulation, because the derivatives of the functions that describe the main variables (pressure, temperature, volume, mass flow) are concerning to the time and not to the crankshaft rotation angle. The researchers include, inside the model of the properties of transport, a model for the viscosity of the gas mixture, proposed by Pucher (PUCHER; SPERLING, 1986) beside resorting to some semi−empirical correlations observed in Reid (REID *et al.*, 1987) to calculate the coefficient of convective heat transfer h_c.

In reference to heat transfer by radiation, the model proposed by Morea (MOREA-ROY *et al.*, 1999) includes the formulation presented by Reyes (REYES, 1993) considered in the area of flared gases. In the same way, a version of the Wiebe function based on H.C. Yee's proposal is in use, for the solution by hyperbolic methods of some conservation equations (LEVEQUE; YEE, 1990).

The results provided by the model show that as the fraction of the recirculated exhaust gases increases, the start of combustion is delayed, the heat transfer of the gases to the cylinder walls increases and the emission of NOx pollutants decreases. In addition, the pressure calculation shows a variation of up to 6% between experimental and simulated data.

This model proved to be quite accurate in engines with low compression ratios (6.23 to 1); however, no experimental evidence is presented with compression ratios closer to those observed in commercial engines (10.5 to 1), and no data are presented for different engine rotation speeds, this fact limits the application of the model in studies of engines using high compression ratios.

2.2.3 QUASI-DIMENSIONAL MODELING OF A FAST-BURN COMBUSTION DUAL-PLUG SPARK-IGNITION ENGINE WITH COMPLEX COMBUSTION CHAMBER GEOMETRIES.

This article, presented by Altin (ALTIN; BILGIN, 2015) proposes a formulation to make a quasi-dimensional simulation (QD) of the thermodynamic cycle of a spark ignition and multiple injection internal combustion engine, based on previous research presented by Migita (MIGITA *et al.*, 2002), in which it is analized the effect of multiple fuel injection ports and how their location affects the performance parameters. The geometric shape of the combustion chamber is simplified by assuming it in the form of a simple cylinder.

In order to provide QD model adaptable to complex combustion chamber geometries, the authors consider a dual approach, which is used in the elaboration of the proposed code by them in Altin (ALTIN; BILGIN, 2015). A simulation of the advance of the flame front was carried out in Solid Works®, according to the models presented by Mattavi and Sezer (MATTAVI, 1980; SEZER; BILGIN, 2008) and the maps provided by the CAD, which include the possible radius for the section of the sphere that simulates the flame front according to the position of the spark plug, the time of ignition and the location of the piston with respect to the top dead center. These data are tabulated and stored in matrices that are then loaded into the MatLab® subroutines and that are configured under the same parameters that Ferguson (FERGUSON; KIRKPATRICK, 2001) proposes in his book. The simulation results are compared with the commercial production engine, belonging to a Honda Fit® vehicle, to validate the parametric study and thus establish the accuracy of the predictions made with the model that the authors propose.

The developed method allows allows to accurately obtain the geometrical characteristics of the flame front for a combustion chamber of the SI engine that has an actual complex geometry. This method allows to eliminate the restrictions of applicability of previous thermodynamic models quasi-dimensional with respect to the simplified and idealized geometries of the combustion chamber which greatly improves the predictions about the behavior of the flame front. The main limitation of this development is referred to the computational cost, since it implies the use of two computer programs (Solid Works® and Matlab®), together with the large size of the matrices resulting from the initial parametrization, consuming a large amount of calculation resources and simulation time. Despite the aforementioned estimation, the method application results prove to be a step forward in terms of the combustion simulation process.

2.2.4 STUDY OF A MODEL OF ENGINE COMBUSTION AND SPARK IGNITION FOR THE ANALYSIS OF CYCLICAL VARIATION AND STABILITY OF COMBUSTION, UNDER LEAN OPERATION.

A basic and fundamental model of an internal combustion and spark ignition engine is simulated and studied in Wu (WU, 2013). The model is built using Simulink tool of Matlab®

to simulate the work cycle. The results of the program are shown in terms of the mass fraction burned during combustion and the pressure changes inside the cylinder for various operatin The combustion model uses Wiebeg conditions. function (HEYWOOD *et al.*, 1988) and it includes a formulation of turbulent eddies in the propagation-based flame front enunciated by Ayala (AYALA; HEYWOOD, 2007). However the turbulence propagation and eddy burning processes are simulated by zero-dimensional method and the flame front is assumed as sphere.

The equations defining pressure and temperature variations apply to the particular case in which the engine uses lean air-fuel mixture, as indicated in (Sec.2.2) in the two-zone thermodynamic model presented by Ramachandran (RAMACHANDRAN, 2009). The results predicted by the model proposed by Wu (WU, 2013) are consistent with experimental data taken during the different operating conditions of a Ford Ecoboost 3.5L V6 petrol engine configured to operate at low load and lean mix. The comparison between the experimental data and the data provided by the simulation show a variation of less than 10% in all the cases studied.

The combustion process is described by means of the Wiebe function (HEYWOOD *et al.*, 1988) and incorporates turbulent flame propagation and large eddy burning with laminar flame speed. With the assumption of the spherical geometry of the flame and the use of a two-zone thermodynamic model, the combustion model presented is able to predict the temperature and pressure variables inside the cylinder. The results of the pressure simulation in the cylinder and MFB (mass fraction burned) roughly coincide with the experimental data of the engine under various operating conditions. The functionality of the model and its flexibility show the great capacity provided by Matlab® for this type of simulations, taking into consideration that the model is not built by means of programming but using the Simulink tool of Matlab®.

2.2.5 A USER-FRIENDLY, TWO-ZONE HEAT RELEASE MODEL FOR PREDICTING SPARK-IGNITION ENGINE PERFORMANCE AND EMISSIONS.

In this thesis, developed by Cuddihy (CUDDIHY, 2014) in order to predict the performance and efficiency of an engine Yamaha YZ250F, the author uses the heat release model proposed by Klein and Stone (KLEIN, 2004; STONE, 1999) within a general model of a zone which also includes a model that predicts friction losses depending on engine speed, proposed by Blair (BLAIR, 1999), the calculation of combustion efficiency for different engine operating points, the thermodynamic properties depending on temperature and residual gas fractions, the latter two based on the models proposed by Ferguson (FERGUSON; KIRKPATRICK, 2001).

The initial single-zone model is divided in order to construct a two-zone model using fractions of volume of burned and unburned gases (BLAIR, 1999; GUEZENNEC; HAMAMA, 1999). The high burned area temperature provided by the two-zone model was used by the author Cuddihy (CUDDIHY, 2014) to predict NOx and UHC (unburned hydrocarbons) emissions according to arguments presented by Hamrin (HAMRIN; HEYWOOD, 1995) and Rakopoulos (RAKOPOULOS *et al.*, 2003). This model was tested comparing its results with data obtained

from a Yamaha YZ250F engine mounted on a parasitic current dynamo-meter. The points chosen among the information are several positions of the accelerator, between operating speeds of 4,500 to 9,000 RPM. In comparing model predictions with the actual data, it was found that all predictions had an accuracy of about 3% with respect to power, while all predictions on BSFC (Brake Specific Fuel Consumption) showed an accuracy of 10%. Finally, when comparing the emission predictions with the experimental data, it was found that all the predictions made by the program had an accuracy of 15%.

Unlike the previous model Wu (WU, 2013), which is implemented using Matlab's Simulink tool ®, the one presented here, Cuddihy (CUDDIHY, 2014), is developed entirely by programming using Matlab ®, in which several fundamental sub-models for the simulation of the combustion process are integrated, such as the Wiebe function (HEYWOOD *et al.*, 1988) for the simulation of burned and unburned gas zones, as well as the heat transfer model proposed by Hohenberg (HOHENBERG, 1979). The predictions of the model fit remarkably well with experimental data, reiterating the flexibility of Matlab ® as a platform for the development of such models.

2.2.6 COMPUTATIONAL MODELING OF INTERNAL COMBUSTION ENGINES

In this paper, Cro (CRÓ *et al.*, 2013), the authors propose a computer simulation model for internal combustion and spark ignition engines, which uses ethanol as fuel. The model incorporates the finite duration condition of combustion as well as a model of instant heat transfer and mass flow processes during the intake and exhaust stages. The solution proposed by the authors, Cro (CRÓ *et al.*, 2013), calculates the thermodynamic properties (pressure, temperature and mass flow) at each instant, discretizing the engine cycle and using the engine geometry, fuel properties, air and valve command as input data. Is uses the formulation proposed by Zacharias (ZACHARIAS, 1967) for the treatment of ideal gases of the mixture fuel-air during the combustion. In the same direction (CRÓ *et al.*, 2013), adopts the methodology presented by Gallo (GALLO, 1990) for the analysis of the phenomena of heat transfer with the walls of the cylinder and the processes of intake and leak.

The phenomenon of combustion is modeled using the Wiebe function (HEYWOOD *et al.*, 1988), besides, it is adopted in the treatment of the combustion process, a coefficient called combustion efficiency, proposed by Alla (ALLA *et al.*, 2001). To validate the results predicted by the simulation model developed, the conditions used by Gallo (GALLO, 1990) are reproduced by Cro (CRÓ *et al.*, 2013) and the results are compared. The configuration data used for validation are shown in (Table 2.1).

The main contribution of the approach shown in the paper is that the thermodynamic and computational model is, according to the authors, less complex and their configuration is simpler, greatly reducing simulation times (CRÓ *et al.*, 2013). (Fig.2.2) and (Fig.2.3) illustrate the results of simulations of the instantaneous pressure and the instantaneous temperature versus

Table 2.1 – Configuration data for validation of the program. (CRÓ *et al.*, 2013)

Ambient Pressure (P_0)	101325	N/m^2
Ambient Temperature (T_0)	298.15	K
Displaced Volume (V_c)	1598	cc^3
Number of Cylinders	4	
Stroke (L)	79.5	mm
Bore (d)	80	mm
Connecting Rod (l)	128	mm
Compression Ratio (l)	12:01	
Number of valves	8	
Intake valve size $(diameter(d_{va})/lift(e_{va}))$	30.93/9.28	mm
Exhaust valve size $(diameter(d_{ve})/lift(e_{ve}))$	28.27/8.48	mm
Angle duration of intake valve lift (α_a)	230	◦
Angle duration of exhaust valve lift (α_e)	245	◦
Crankshaft angle to the intake valve starts to open	700	◦
Crankshaft angle to the exhaust valve starts to open	490	◦
Engine speed (N)	5200	RPM
Intake manifold pressure (P_{adm})	86000	N/m^2
Exhaust manifold pressure (P_{exh})	115000	N/m^2
Cylinder wall temperature (T_p)	520	K
Ignition angle (θ)	340	◦
Low heat value anhydrous ethanol (PCH)	27.72	MJ/kg

the crank angle, respectively, for the chosen compression ratios.

As in previous cases ((CUDDIHY, 2014), Wu (WU, 2013)), this model was programmed in MatLab ® and integrates some of the submodels mentioned earlier in other investigations (Zacharias (ZACHARIAS, 1967), the Wiebe function (HEYWOOD *et al.*, 1988)), for the treatment of ideal gases from the mixture of air and fuel during combustion. However, it is worth noting that the model was entirely developed by Brazilian researchers at UNICAMP, demonstrating the potential of higher education institutions when this type of projects are developed.

The model is constructed from the consideration of a zone, which limits predictive capacity by not taking into account the multi-zone model, in particular the temperature behavior in the areas of burned and unburned gases during combustion, which prevents, for example, establishing the time of the start of the combustion reaction and how it is affected by modifying the values of variables such as the advance of the spark and the delay in the start of combustion.

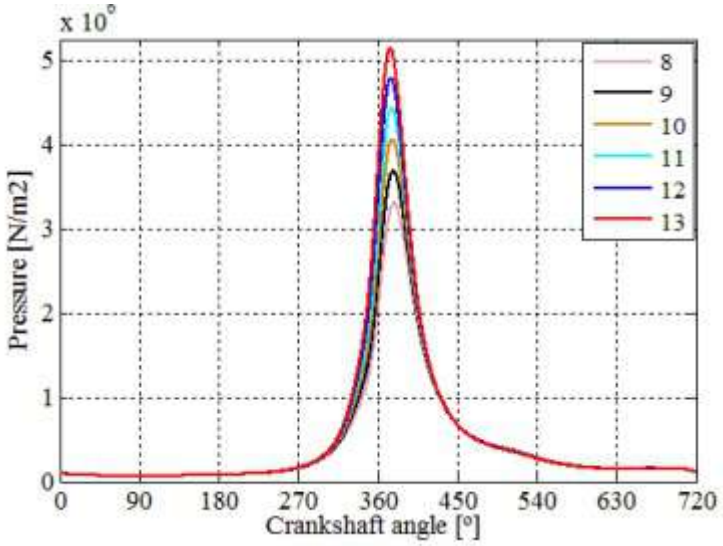

Fig. 2.2 – Pressure versus crank angle for different compression ratios. Source:(CRÓ *et al.*, 2013)

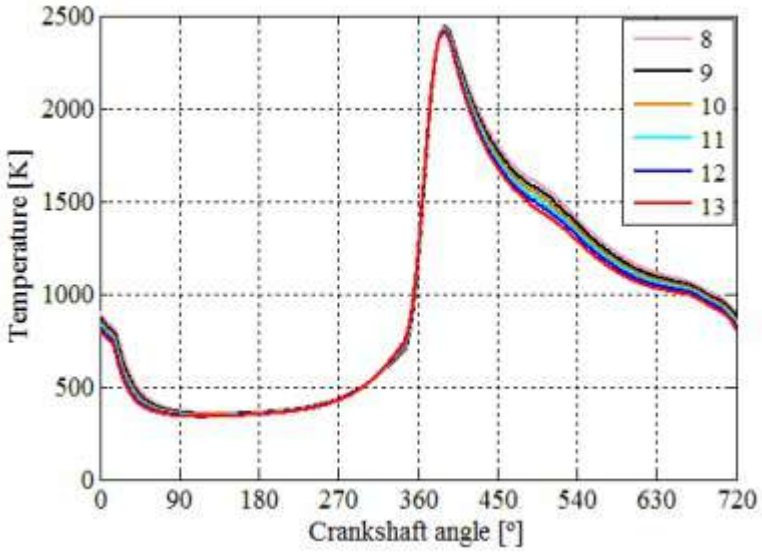

Fig. 2.3 – Temperature versus crank angle for different compression ratios. Source:(CRÓ *et al.*, 2013)

Tables 2.2 and 2.3 contain a comparison between the previously referenced computational models whose emphasis is placed on their main contributions proposed by each one and the most relevant weaknesses found in them.

The model proposed in this article integrates some of the most important features mentioned in the models previously described (Cuddihy (CUDDIHY, 2014), Wu (WU, 2013), Altin (ALTIN; BILGIN, 2015) and Buttsworth (BUTTSWORTH, 2002)) (table 2.2 and table 2.3), among which are found:

- The use of the two zone model (burned and unburned gases) during combustion.
- The use of the heat transfer model proposed by Hohenberg (HOHENBERG, 1979), be-

Table 2.2 – Comparison between the different computational models for spark ignition engines, referenced.

Type and Title of Document	Authors	Publication Year	Main Contributions	Disadvantages
(Scientific Article) Numerical simulation of the operating cycle of a provoked ignition engine	**Morea-Roy J., Muñoz M., Moreno F.**	**1999**	**The model presented differs from the commonly used formulation because the derivatives of the functions that describe the main variables (pressure, temperature, volume, mass flow) refer to the time and not to the rotation angle of the crankshaft specifically. Heat transfer by radiation is modeled by means of the formula presented by Reyes (REYES, 1993) considered in the area of gases burned. The version of the Wiebe function used is based on H.C.Yee's proposal for the solution by hyperbolic methods of some conservation equations (LEVEQUE; YEE, 1990).**	**This model proved to be quite accurate in engines with low compression ratios (6.23 to 1). However, no experimental evidence is presented with compression ratios closer to those observed in commercial engines (10.5 to 1), and no data are presented for various engine rotational speeds, which limits the application of the model in engine design studies.**
(Report) Spark Ignition Internal Combustion Engine modelling Using MatLab®	**Buttsworth David R.**	**2002**	**The update of the program presented by Ferguson (FERGUSON; KIRKPATRICK, 2001) in his book, which was originally developed in FORTRAN as a programming language, and dates back to 1986. The conversion to Matlab® was well adapted to the original objectives, also allowed the use of more advanced computers that improved the execution times and the correction of some of the inaccuracies presented by the original programs.**	**In addition to the update and transcription of the programs presented by Ferguson from Fortran to MatLab®, no significant input is shown on issues related to the modeling of internal combustion and spark ignition engines.**
(Scientific Article) Computational Modeling of Internal Combustion Engines: Influence of Compression Ratio in the Indicated Performance Curves	**Rodrigues Cró N., Ferreira J., Gallo W. and Tanikawa M.**	**2013**	**The approach used for the construction of the thermodynamic and computational models are less complex and their configuration is simpler, which reduces considerably the simulation times. The phenomenology of the 4-stroke spark ignition engine cycle using ethanol as fuel is studied. It is adopted in the treatment of the combustion process, a coefficient called combustion efficiency, proposed by Alla (ALLA *et al.*, 2001). The model is fully programmed in MatLab®.**	**The model is approached from the consideration of a zone, which limits its predictive capacity by not taking into account the multi-zone model, in particular the behavior of temperature in the areas of gases burned and not burned during combustion, which prevents, for example, establishing the time of the start of the combustion reaction and how it is affected by modifying the values of variables such as the advance of the spark and the delay in the start of combustion.**

Table 2.3 – Comparison between the different computational models for spark ignition engines, referenced. (Continued)

Type and Title of Document	Authors	Publication Year	Main Contributions	Disadvantages
(Dissertations, Master's Theses). Study of spark ignition engine combustion model for the analysis of cyclic variation and combustion stability at lean operating conditions	**Wu Hao**	**2013**	**The combustion process is described by means of the Wiebe function (HEYWOOD *et al.*, 1988) and incorporates the propagation of turbulent flames and the burning of eddies with laminar flame velocity.The functionality of the model shows the great capacity and flexibility provided by Matlab® for this type of simulations, bearing in mind that the model is not built by programming, but uses Matlab's Simulink® tool.**	**The model is only validated with a particular type of engine and at low load. Only two rotation regimes (1500 and 2000 RPM) are used. No full load results for the same rotations.**
(Dissertations, Master's Theses). A User-Friendly, Two-Zone Heat Release Model for Predicting Spark-Ignition Engine Performance and Emissions	**Cuddihy J.**	**2014**	**The model combines programming in MatLab® with the use of the Simulink® tool. The Blair model (BLAIR, 1999) is included to calculate the friction losses depending on the speed of rotation of the engine. A prediction is made about NOx and UHC (Unburned Hydrocarbons) emissions. For the transfer of heat between the cylinder walls and the gas mixture, the model proposed by Hohenberg (HOHENBERG, 1979) is implemented.**	**Model validation is performed with a single engine type, which limits the ability to explore the proposed simulation model to interpret geometries of different engines and the use of other fuels. The rotation regimes chosen for the calculation of emissions are between 4500 and 9000 RPM (high rotation). No low rotation data are presented.**
(Scientific Article) Quasi-dimensional modeling of a fast-burn combustion dual-plug spark-ignition engine with complex combustion chamber geometries	**Altın I. and Atilla B.**	**2015**	**Quasi-dimensional simulation and use of two fuel injectors in the combustion chamber. A 3D CAD model is implemented to describe the advance of the flame front. The data supplied by the CAD model of the flame front are then loaded into MatLab® to simulate the advance of the front during combustion. The method developed allows the geometric characteristics of the flame front to be obtained with great precision for an SI engine combustion chamber that has a real complex geometry.**	**The main limitation of this development refers to the computational cost, since it implies the use of two computer programs (Solid Works® and Matlab®), along with the large size of the matrices resulting from the initial parametrization of the CAD model, consuming a large amount of calculation resources and simulation time.**

tween the cylinder walls and the gases contained in the cylinder.

- The use of the Wiebe function (HEYWOOD *et al.*, 1988).
- The model can be used for gasoline engines, ethanol engines or mixtures of these two fuels.
- The use of MatLab® as a programing language.

In addition to the foregoing, the proposal presented in Chapter three of this document makes it possible to evaluate the performance of engines of different construction geometries working in a wide range of rotational speed regimes. The programming style used, by means of functions, increases the flexibility of the final simulation program as it allows the insertion of applications such as water injection, a water evaporation model, the combustion model under the treatment of chemical kinetics and a function that allows the analysis of the tendency to detonation during the operation of the engine under analysis.

2.3 DESCRIPTIVE MATHEMATICAL MODEL OF TWO ZONES OF THE WORKING CYCLE OF A SPARK-IGNITED ENGINE.

A thermodynamic model of two zones is presented here. As already mentioned, all models of this type are based on the same criteria and simplifications. The one that is described here corresponds to a version of the proposed one by Ramachandran, (RAMACHANDRAN, 2009), which is, in general terms, similar to that used by most researchers referenced. The model considers 14 resulting species after the combustion process:

$$O_2, N_2, CO_2, H_2O, H_2, OH, NO, CO, O, H, N, Ar, NO_2, HO_2$$

The fuel input is limited to form C-H-O-N. (Carbon, Hydrogen, Oxygen, Nitrogen).

The Wiebe function is used to determine the ratio of burned fuel mixture and control the rate at which the fuel mixture, air and residual gases are transformed into burning gases (HEYWOOD *et al.*, 1988). In addition to the above, the conservation equations of mass and energy together with the state equations make up the set of model governing equations.

2.3.1 MASS AND ENERGY BALANCE EQUATIONS.

The equation of state for ideal gases is:

$$PV = mRT. \tag{2.1}$$

With:

- P = Pressure.

- V = Volume.
- m = Molar mass.
- R = Universal constant of ideal gases.
- T = Temperature.

The reason of change of the mass into any open system is the net flow of mass through the system boundaries. Therefore, for the volume of control that contains the air-fuel mixture, we have:

$$\frac{dm}{dt} = \sum_k \dot{m}_k. \tag{2.2}$$

Where: (dm/dt) is the reason of change of mass with respect to time and k represents all the mass flows that cross the boundary of the control volume.

The first law of thermodynamics applied to the performance of an open system results in the energy equation can be expressed as:

$$\dot{U} = \dot{Q} - \dot{W} + \sum_k \dot{m}_k h_k. \tag{2.3}$$

With:

- U = Internal energy.
- Q = Heat.
- W = Work.
- h = Enthalpy.

(Eq.2.2) and (Eq.2.3) can be described as a function of the crankshaft speed that is assumed constant during the time interval of analysis, it is established that:

$$dt\omega = d\theta. \tag{2.4}$$

$$\frac{dm}{d\theta} = \sum_k \frac{dm_k}{d\theta} \tag{2.5}$$

$$\frac{dmu}{d\theta} = \frac{dQ}{d\theta} - p\frac{dV}{d\theta} + \sum_k h_k \frac{d\dot{m}_k}{d\theta} \tag{2.6}$$

where ω in (Eq.2.4) is the rate of rotation of the engine. (Eq.2.5) corresponds to the total mass inside the cylinder. (Eq.2.6) it does not take into account the changes in the kinetic and potential energy in the control volume.

2.3.2 AIR AND PRODUCTS OF COMBUSTION DATA.

In Gordon and McBride (GORDON; MCBRIDE, 1976), they propose the following expressions, which correspond to the curves tabulated by JANAF's tables (STULL D R ; PROPHET, 1971).

$$\frac{c_p}{R} = a_1 + a_2T + a_3T^2 + a_4T^3 + a_5T^4 \tag{2.7}$$

$$\frac{h}{RT} = a_1 + \frac{a_2}{2}T + \frac{a_3}{3}T^2 + \frac{a_4}{4}T^3 + \frac{a_5}{5}T^4 + \frac{a_6}{T} \tag{2.8}$$

$$\frac{s}{R} = a_1 lnT + a_2T + \frac{a_3}{2}T^2 + \frac{a_4}{3}T^3 + \frac{a_5}{4}T^4 + a_7 \tag{2.9}$$

where c_p is the specific heat at constant pressure, h is the specific enthalpy and s is the specific entropy.
Coefficients a_1 to a_7 are calculated for two different temperature ranges: **1)** 300<T<1000 K and **2)** 1000<T<5000 K and they can be taken from (GORDON; MCBRIDE, 1976).
The following are the species of interest during combustion; CO_2, H_2O, N_2, O_2, CO, H_2, H, O, OH, and NO (FERGUSON; KIRKPATRICK, 2001).

2.3.3 FUEL DATA.

To represent the thermodynamic properties of the fuel, Heywood (HEYWOOD *et al.*, 1988), uses similar expressions to those shown in (Eq.2.7), (Eq.2.8) and (Eq.2.9).

$$\frac{c_p}{R} = a_1 + a_2T + a_3T^2 + a_4T^3 + a_5\frac{1}{T^2} \tag{2.10}$$

$$\frac{h}{RT} = a_1 + \frac{a_2}{2}T + \frac{a_3}{3}T^2 + \frac{a_4}{4}T^3 - a_5\frac{1}{T^2} + \frac{a_6}{T} \tag{2.11}$$

$$\frac{s}{R} = a_1 lnT + a_2T + \frac{a_3}{2}T^2 + \frac{a_4}{3}T^3 - \frac{a_5}{2}\frac{1}{T^2} + a_7 \tag{2.12}$$

The data for calculating the coefficients can be obtained from Gordon (GORDON; MCBRIDE, 1976; CHASE *et al.*, 1975; KEE *et al.*, 1990)
To differentiate properties such as specific heat or the entropy of each of the species, it is propose the model expressed in (Ec.2.13). With ξ representing the property and x being the fraction

of mass burned. (RAMACHANDRAN, 2009).

$$\xi_{mixture} = \sum_{k=1}^{N} x_k \xi_k \tag{2.13}$$

with ξ referring to the property and x is the burnt mass fraction.

2.3.4 EQUIVALENCE RATIO.

The equivalence ratio ϕ for a single fuel model is given by Ferguson, (FERGUSON; KIRKPATRICK, 2001):

$$\phi = \left(\frac{\left(\frac{F}{Air}\right)_{Act}}{\left(\frac{F}{Air}\right)_{St}} \right) \tag{2.14}$$

where F is fuel, Act means current and St refers to stoichiometric.

For mixtures of hydrocarbons and alcohols with hydrogenated fuel (H), the equivalence ratio becomes (AL-BAGHDADI, 2007):

$$\phi = \frac{\left(\frac{F}{Air - \left(\frac{H}{(H/Air)_{St}}\right)} \right)}{\left(\frac{F}{Air}\right)_{St}} \tag{2.15}$$

As in equation 2.14, the terms correspond to:

- ϕ: The equivalence ratio
- F: Fuel
- H: Hydrogenated fuel
- Act: Means current
- St: Stoichiometric

2.3.5 COMBUSTION PROCESS AND FORMATION OF POLLUTING GASES.

The process of the combustion reaction and the formation of pollutants (NO_x and CO) in spark ignition engines presented in this section, corresponds to the work developed by Lima (LIMA *et al.*, 2017).

Two mathematical models are developed in order to predict the formation of regulated pollutant gases in spark ignition engines that use ethanol as fuel. The initial model uses the

information obtained from the study of a thermodynamic model of combustion of two zones with chemical equilibrium and chemical kinetics. The second model uses the same two-zone thermodynamic model, shown in the first model, to calculate unburned hydrocarbon emissions by applying the crevice and flame quenching HC-mechanisms (LIMA *et al.*, 2017).

The first model of chemical kinetics was developed for air under the thermodynamic conditions of a spark ignition engine. The main objective was to analyse the behaviour of reactions related to the formation of NO_x at high temperatures, such as those obtained during combustion and power stroke. Within the development, a constant temperature and volume model is considered and the results obtained from parameters such as reaction ratios and NO_x formation ratios are subsequently interpreted. In this model three reactions and five chemical species were considered.

Subsequently, a second model is developed for a mixture of gases at the operating conditions of an internal combustion engine and spark ignition (*SI*). The variation profiles for pressure, volume and temperature (P,V,T) are considered for a typical engine, instead of the constant conditions used in the first model. This analysis involved 12 chemical species, and, as in the previous model, we sought to study the formation of NO_x influenced by more chemical reactions, in addition to evaluating the formation of CO.

This second model of chemical kinetics is used as the basis to be implemented within a simulation model of the operation of a spark ignition (*SI*) engine that uses ethanol as fuel. The latter is a zero-dimensional model of two zones: one for unburned gases and one for burned gases. The Wiebe function (HEYWOOD *et al.*, 1988) is used for the development of the burned gas zone during the advance of combustion, and; at the same time, the unburned gas zone provides the air-waste gas-fuel mixture to the burned mixture.

2.3.6 **FROZEN COMPOSITION.**

The model shown in Depcik (DEPCIK, 2000) can only be applied between 600 and 4000 K. Ferguson (FERGUSON; KIRKPATRICK, 2001) uses a model to calculate combustion species in the range of 300 to 600 K, which assumes that species prevailing in the exhaust gases are CO_2, H_2O, N_2, Ar, CO, O_2 and H_2. The general reaction is taken of:

$$\begin{gathered}\frac{\varepsilon}{\phi}C_\alpha H_\beta O_\gamma N_\delta + (WO_2 + XN_2 + YAr + ZCO_2) \rightarrow \\ x_1CO_2 + x_2H_2O + x_3N_2 + x_4O_2 + x_5CO + x_6H_2 + x_7Ar\end{gathered} \tag{2.16}$$

where W,X,Y and Z are the molar fractions of atmospheric air components.

(Eq.2.16), is the formulation for the stoichiometric case $(\phi = 1)$ wherein $x_4 = x_5 = x_6 = 0$. In the case of the poor mixture $(\phi \leq 1)$, $x_5 = x_6 = 0$ and for rich mixture $(\phi > 1)$, $x_4 = 0$. Developed the atomic equilibrium for the stoichiometric case and solving the coefficients, it is

obtained:

$$C : \phi\varepsilon\alpha + Z = x_1 \Rightarrow \qquad x_1 = \phi\varepsilon\alpha + Z \tag{2.17}$$

$$H : \phi\varepsilon\beta = 2x_2 \Rightarrow \qquad x_2 = \frac{\phi\varepsilon\beta}{2} \tag{2.18}$$

$$O : \phi\varepsilon\gamma + 2W + 2Z = 2x_1 + x_2 \tag{2.19}$$

$$N : \phi\varepsilon\delta + 2X = 2x_3 \Rightarrow \qquad x_3 = \frac{\phi\varepsilon\delta + 2X}{2} \tag{2.20}$$

$$Ar : Y = x_7 \Rightarrow \qquad x_7 = Y \tag{2.21}$$

$$\varepsilon = \frac{W}{\alpha + \frac{\beta}{4} - \frac{\gamma}{2}} \tag{2.22}$$

From the above, the ratio fuel/air stoichiometric is (RAMACHANDRAN, 2009):

$$\left(\frac{[F]}{Air}\right)_{St} = \frac{\varepsilon\,(12.011\alpha + 1.008\beta + 16.0\gamma + 14.01\delta)}{31.998W + 28.012X + 38.948Y + 44.009Z} \tag{2.23}$$

This last expression (Eq.2.23), is used in (Eq.2.14) and (Eq.2.15) to calculate the ratio of equivalence. This formulation is given by the simplified combustion.

2.3.7 THERMAL PROPERTIES.

The present model considers two zones, one of unburned gases and one of burned gases, as separate open systems. Therefore, the specific energy **u** and the specific volume **v** are expressed as:

$$\mathbf{u} = \frac{U}{m} = x u_b + (1 - x)\, u_u \tag{2.24}$$

$$\mathbf{v} = \frac{V}{m} = x v_b + (1 - x)\, v_u \tag{2.25}$$

where subscripts b and u refers to burning zone and unburned respectively. Assuming that the pressures of the burned and unburned areas are equal, v_b and v_u are functions of T_b, T_u and p. Thus:

$$\frac{dv_b}{d\theta} = \frac{\partial v_b}{\partial T_b}\frac{dT_b}{d\theta} + \frac{\partial v_b}{\partial p}\frac{dp}{d\theta} \tag{2.26}$$

$$\frac{dv_u}{d\theta} = \frac{\partial v_u}{\partial T_u}\frac{dT_u}{d\theta} + \frac{\partial v_u}{\partial p}\frac{dp}{d\theta} \tag{2.27}$$

Substituting the logarithmic derivatives from (DEPCIK, 2000) in equations (Eq.2.26) and (Eq.2.27), it is obtained:

$$\frac{dv_b}{d\theta} = \frac{v_b}{T_b}\frac{\partial \ln v_b}{\partial \ln T_b}\frac{dT_b}{d\theta} + \frac{v_b}{p}\frac{\partial \ln v_b}{\partial \ln p}\frac{dp}{d\theta} \tag{2.28}$$

$$\frac{dv_u}{d\theta} = \frac{v_u}{T_u}\frac{\partial \ln v_u}{\partial \ln T_u}\frac{dT_u}{d\theta} + \frac{v_u}{p}\frac{\partial \ln v_u}{\partial \ln p}\frac{dp}{d\theta} \tag{2.29}$$

Similarly, the same treatment is applied to the internal energy of areas of burned and unburned gases under the same condition of equal pressure. Including the logarithmic derivatives, it is obtained:

$$\frac{du_b}{d\theta} = \left(c_{p_b} - \frac{pv_b}{T_b}\frac{\partial \ln v_b}{\partial \ln T_b}\right)\frac{dT_b}{d\theta} - v_b\left(\frac{\partial \ln v_b}{\partial \ln T_b} + \frac{\partial \ln v_b}{\partial \ln p}\right)\frac{dp}{d\theta} \tag{2.30}$$

$$\frac{du_u}{d\theta} = \left(c_{p_u} - \frac{pv_u}{T_u}\frac{\partial \ln v_u}{\partial \ln T_u}\right)\frac{dT_u}{d\theta} - v_u\left(\frac{\partial \ln v_u}{\partial \ln T_u} + \frac{\partial \ln v_u}{\partial \ln p}\right)\frac{dp}{d\theta} \tag{2.31}$$

2.3.8 MASS CAUGHT IN VOLUME CONTROL.

The trapped mass in the engine cylinder at various periods is given by Chan (CHAN; ZHU, 2001):

- For the intake $\theta_{IVC} \geq \theta \geq -360^{\circ}CA$ where CA is the crank angle (a revolution before the intake valve closes), the trapped mass is:

$$m = \frac{V(\theta)}{v_u} \tag{2.32}$$

where V(θ): Volume as a function of the angle of rotation of the crankshaft (θ).

- For $\theta_{EVO} \geq \theta \geq \theta_{IVC}(\text{Valve} - \text{Closed})$

$$m = m_{IVC}e^{-C_b(\theta-\theta_{IVC})/\omega} \tag{2.33}$$

where C_b is the coefficient of blowby, ω is angular speed and IVC it refers to Intake Valve Close

- For $360^{\circ}CA \geq \theta \geq \theta_{EVO}$(blowdown and exhaust.) (A revolution after the exhaust valve opens)

$$m = \frac{V(\theta)}{v_b} \tag{2.34}$$

EVO refers to Exhaust Valve Open.

The equation relating the volume of the cylinder with respect to the crank angle at any instant is:

$$V(\theta) = V_c \left\{ 1 + \frac{r-1}{2} \left\{ 1 - \cos\theta + \frac{1}{\varepsilon} \left[1 - \left(1 - \varepsilon^2 \sin^2\theta \right)^{0.5} \right] \right\} \right\} \tag{2.35}$$

where V_c is the volume between the combustion chamber and the piston top when the latter is in the top dead center and:

$$\varepsilon = \frac{stroke}{2 \times l} \tag{2.36}$$

where *stroke* refers to the travel of the piston within the cylinder l the length of the rod.

2.3.9 RATIO OF BURNT MIXTURE MODEL.

Some models show that the ratio of fuel/air mixture burnt depends mainly on the shape of the combustion chamber and the position of the plug. Function *Wiebe* represents the fraction of burnt mass, x_b, in relation to the crankshaft angle.

$$x_b(\theta) = 1 - \exp\left\{ -a \left[\frac{(\theta - \theta_0)}{\Delta\theta} \right]^{m+1} \right\} \tag{2.37}$$

The vast majority of the models use values a=5 and m=2 (HEYWOOD *et al.*, 1988). So models are able to represent different types of combustion chambers with different positions of the spark plug, only adjusting the values of a and m (KODAH *et al.*, 2000)

2.3.10 HEAT TRANSFER MODEL.

The heat transfer to the interior of a thermodynamic system, expressed in terms of the heat losses.

$$\frac{dQ}{d\theta} = \frac{-Q_l}{\omega} = \frac{-\dot{Q}_b - \dot{Q}_u}{\omega} \tag{2.38}$$

where:

$$\dot{Q}_b = h \sum_{i=h,p,l} A_{bi}(T_b - T_{wi}) \tag{2.39}$$

$$\dot{Q}_u = h \sum_{i=h,p,l} A_{ui}(T_u - T_{wi}) \tag{2.40}$$

Here A_{bi} and A_{ui} are the areas of the burned and unburned zones in contact with combustion chamber components; temperature T_{wi} and subscripts h, p, l refers to the cylinder head (head), piston crown (crown) surface and the cylinder wall (linear). The equations describing the geometry of these terms are defined in Ferguson (FERGUSON; KIRKPATRICK, 2001) and shown below:

$$A_{bi} = A_i x^{0.5} \tag{2.41}$$

$$A_{ui} = A_i \left(1 - x^{0.5}\right) \tag{2.42}$$

$$A_h = \frac{\pi b^2}{2} \tag{2.43}$$

$$A_p = \frac{\pi b^2}{4} \tag{2.44}$$

$$A_l = \frac{4V(\theta)}{b} \tag{2.45}$$

- A_{bi} : Area corresponding to the gases burned.
- A_{ui} : Area corresponding to unburned gases.
- A_h : Area corresponding to cylinder head.
- A_p : Area corresponding to piston crown.
- A_l : Surface and the cylinder wall (linear).
- T_{wi} : Cylinder wall temperature.

In (Eq.2.41) and (Eq.2.42) the subscript i, on the right side of the equations, refers to the admission phase and in (Eq.2.43) to (Eq.2.45) b, on the right side of the equations, represents the cylinder's diameter.

2.3.11 HEAT TRANSFER CORRELATIONS.

In (Eq.2.39) and (Eq.2.40), h is the instantaneous coefficient of heat transfer. Woschni proposes in (WOSCHNI, 1967) a correlation of the form:

$$Nu = 0.035 Re^{0.8} \tag{2.46}$$

where Nu is the Nusselt number and Re is the Reynolds number. Now, assuming an average speed for the gas in the cylinder, h is transformed in:

$$h = 0.83 b^{-0.2} (p \cdot 10^{-3} \cdot c)^{0.8} T^{-0.53} \tag{2.47}$$

with h is the coefficient of heat transfer, p is the pressure and c=6.18 cm. (For the gas exchange process (RAMACHANDRAN, 2009)).

$$T = xT_b + (1-x)T_u \tag{2.48}$$

(Eq.2.48) defines the temperature T for equation (Eq.2.47).

2.3.12 ENERGY LOSSES BY BLOWBY MODEL.

Enthalpy loss due to blowby is expressed as Ferguson (FERGUSON; KIRKPATRICK, 2001):

$$h_l = (1-x^2)h_u + x^2 h_b \tag{2.49}$$

That indicates that there is a major proportion of the leakage of the unburned gas in comparison with the leakage of the burned gas in the beginning of the combustion.

2.3.13 MAIN GOVERNMENT EQUATIONS OF THE MODEL.

Differentiating the (Eq.2.25) with respect to the crank angle and taking into account the (Eq.2.26) and (Eq.2.27) gives (FERGUSON; KIRKPATRICK, 2001):

$$\begin{aligned}\frac{1}{m}\frac{dV}{d\theta} + \frac{VC_b}{m\omega} = x\frac{v_b}{T_b}\frac{\partial \ln v_b}{\partial \ln T_b}\frac{dT_b}{d\theta} + (1-x)\frac{v_u}{T_u}\frac{\partial \ln v_u}{\partial \ln T_u}\frac{dT_u}{d\theta} + \\ \left[x\frac{v_b}{p}\frac{\partial \ln v_b}{\partial \ln p}(1-x)\frac{v_u}{p}\frac{\partial \ln v_u}{\partial \ln p}\right]\frac{dp}{d\theta} + (v_b - v_u)\frac{dx}{d\theta}\end{aligned} \tag{2.50}$$

Here C_b is the coefficient of blowby and is given by:

$$C_b = \frac{\dot{m}_l}{m} \tag{2.51}$$

and $\dot{m}_l$ corresponds to the leakage due to blowby.

Expressing the heat loss of burnt and unburned gases as a function of the ratio of change of specific entropy (s) is obtained:

$$-\dot{Q}_b = m\omega x T_b \frac{ds_b}{d\theta} \tag{2.52}$$

$$-\dot{Q}_u = m\omega(1-x)T_u\frac{ds_u}{d\theta} \tag{2.53}$$

where:

$$\frac{ds_b}{d\theta} = \left(\frac{c_{pb}}{T_b}\right)\frac{dT_b}{d\theta} - \frac{v_b}{T_b}\frac{\partial \ln v_b}{\partial \ln T_b}\frac{dp}{d\theta} \tag{2.54}$$

$$\frac{ds_u}{d\theta} = \left(\frac{c_{pu}}{T_u}\right)\frac{dT_u}{d\theta} - \frac{v_u}{T_u}\frac{\partial \ln v_u}{\partial \ln T_u}\frac{dp}{d\theta} \tag{2.55}$$

Expressing heat loss from the flue gases and unburned as a function of the rate of change of specific entropy by combining (Eq.2.39) to (Eq.2.40) and (Eq.2.47) to (Eq.2.50)

$$c_{pb}\frac{dT_b}{d\theta} - v_b\frac{\partial \ln v_b}{\partial \ln T_b}\frac{dp}{d\theta} = \frac{-h\sum_{i=h,p,l}A_{bi}(T_b - T_{wi})}{m\omega x} \tag{2.56}$$

$$c_{pu}\frac{dT_u}{d\theta} - v_u\frac{\partial \ln v_u}{\partial \ln T_u}\frac{dp}{d\theta} = \frac{-h\sum_{i=h,p,l}A_{ui}(T_u - T_{wi})}{m\omega(1-x)} \tag{2.57}$$

Differentiating the (Eq.2.35) and (Eq.2.37) and incorporating the (Eq.2.4), (Eq.2.24), (Eq.2.25) to (Eq.2.31) and (Eq.2.38) to (Eq.2.49) into the (Eq.2.5), is possible to establish the following relations (RAMACHANDRAN, 2009):

$$\frac{dp}{d\theta} = \frac{f_1 + f_2 + f_3}{f_4 + f_5} \tag{2.58}$$

$$\frac{dT_b}{d\theta} = \frac{-h\sum_{i=h,p,l} A_{bi}\left(T_b - T_{wi}\right)}{m\omega c_{pb} x} + \frac{v_b}{c_{pb}}\frac{\partial \ln v_b}{\partial \ln T_b}\frac{dp}{d\theta} + \frac{h_u - h_b}{x c_{pb}}\left[\frac{dx}{d\theta} - \left(x - x^2\right)\frac{C_b}{\omega}\right] \tag{2.59}$$

$$\frac{dT_u}{d\theta} = \frac{-h\sum_{i=h,p,l} A_{ui}\left(T_u - T_{wi}\right)}{m\omega c_{pb}\left(1-x\right)} + \frac{v_u}{c_{pu}}\frac{\partial \ln v_u}{\partial \ln T_u}\frac{dp}{d\theta} \tag{2.60}$$

where:

$$f_1 = \frac{1}{m}\left(\frac{dV}{d\theta} + \frac{VC_b}{\omega}\right) \tag{2.61}$$

$$f_2 = \frac{h}{m\omega}\left[\frac{v_b}{c_{pb}}\frac{\partial \ln v_b}{\partial \ln T_b}\frac{\sum_{i=h,p,l} A_{bi}\left(T_b - T_{wi}\right)}{T_b} + \frac{v_b}{c_{pu}}\frac{\partial \ln v_u}{\partial \ln T_u}\frac{\sum_{i=h,p,l} A_{ui}\left(T_u - T_{wi}\right)}{T_u}\right] \tag{2.62}$$

$$f_3 = -\left(v_b - v_u\right)\frac{dx}{d\theta} - v_b\frac{\partial \ln v_b}{\partial \ln T_b}\frac{h_u - h_b}{c_{pb}T_b}\left[\frac{dx}{d\theta} - \left(x - x^2\right)\frac{C_b}{\omega}\right] \tag{2.63}$$

$$f_4 = x\left[\frac{v_b}{c_{pb}T_b}\left(\frac{\partial \ln v_b}{\partial \ln T_b}\right)^2 + \frac{v_b}{p}\frac{\partial \ln v_b}{\partial \ln p}\right] \tag{2.64}$$

$$f_5 = (1-x)\left[\frac{v_u}{c_{pu}T_u}\left(\frac{\partial \ln v_u}{\partial \ln T_u}\right)^2 + \frac{v_u}{p}\frac{\partial \ln v_u}{\partial \ln p}\right] \tag{2.65}$$

(Eq.2.61) to (Eq.2.65) are the functions of p, T_u and T_b in terms of θ.

2.4 WATER INJECTION SYSTEMS IN INTERNAL COMBUSTION ENGINES AND SPARK IGNITION.

In 1913, Bertram Hopkinson indicated that "the idea of introducing water in the internal combustion engines is not new". The use of water to eliminate detonation and internally cool the gas engines was very successful and Hopkinson decided to design power plants that only used water as a cooling system (HOPKINSON, 1913; DRYER, 1977). Nevertheless, the discovery of anti-explosive agents soluble in fuel in 1922, and the complexity and cost of control systems and water storage required for use, discourages the use of the addition of water and alcohol for automobile engines (MIDGLEY; BOYD, 1922). The supercharged engine development aircraft, both before and during the Second World War, rejuvenated interest in water and alcohol aspirated internal combustion engines (KUHRING, 1938). Adding water was also instituted early in turboprop engines and jet engine, to extend the limit of performance and to increase the power and, in fact, technical survived as an optional feature in the commercial aircraft engine such as Pratt & Whitney *JT9D* (WEISS; RUDD, 1959).

Numerous articles were published between 1944 and 1959 for example, those elaborated by Weiss (WEISS; RUDD, 1959) and VanHartesveldt (HARTESVELDT, 1959), where it refers to systems of internal refrigeration and relief in Otto cycle engines with characteristics that promoted the appearance of the detonation and, at the same time, diverse devices to measure the water and the alcohol that were injected in the engines, appeared in the commercial market.

Zeldovich work (ZELDOVICH *et al.*, 1947) on the nitric oxide formation from molecular nitrogen and the discovery of the relationship NO_x in the chemical formation of the residual toxic gas engines formulated in Kopa (KOPA *et al.*, 1963), suggested a new motivation for adding water: reduction of emissions NO_x generated by combustion engines. Extensive research on this concept has been applied to compression ignition engines (GREEVES *et al.*, 1977), spark ignition engines (NICHOLLS *et al.*, 1969), (BARTON *et al.*, 1971) gas turbines (NELSON, 1972), (KLAPATCH; KOBLISH, 1971a) and external combustion systems (boilers, etc.) (TURNER *et al.*, 1972).

Lanzafeme (LANZAFAME, 1999) performs a validation on the advantages of water injection as a NOx emission control technique. In spite of the multiple analysis carried out by several investigations, the technique of water injection in spark ignition engines (SI-ICE) does not produce consistent results, due to the different types of engines used for the experiments. In Lanzafame's work, (LANZAFAME, 1999), the effects of water injection into the intake pipe were investigated, both theoretically and experimentally. Pressure diagrams as a function of time were recorded in a motor CFR Single cylinder in AGIP PETROLI in Priolo Catania. The tests were performed according to the method Motor Research (ASTM).

The water is supplied by a continuous injection system, including a high pressure pump, while the engine is supplied with low quality petrol (cheap products, intermediate refining pro-

cesses). Water is added as a proportion of the fuel mass flow, which ranges from 0 to 1.5 times. *NOx* emission measurements confirm the effectiveness of water injection in reducing engine emissions and impacting the environment. Test data were used to implement a detonation model that predicts the effects of water injection. The results showed that the injection of water actually represents a new way to avoid detonation, reduces the work during the compression and allows controlling the formation of *NOx* in the engines *SI* (LANZAFAME, 1999).

In later work Brusca (BRUSCA; LANZAFAME, 2003) took the same configuration of Lanzafame's work, but varied flow ratio in the addition of water in the inlet, between 0 to 2 fold relative to the amount of fuel. The author states that for low-octane gasolines, the observed behavior resembles high-octane gasolines, proving once again the benefits of water use as antiknock.

In 2006, Subramanian, study the impact of water injection on emissions of nitrogen oxides in an internal combustion engine with spark ignition and hydrogen-powered (SUBRAMANIAN *et al.*, 2007). One of the main problems with hydrogen, when it is used to feed internal combustion engines, is the high level of *NOx* issued, due to rapid combustion. The use of diluents loading the mixture into the cylinder and the delay in the ignition time of the spark can reduce the levels of *NOx* in the engines fed on hydrogen. In his work, a single cylinder engine was fueled with hydrogen and operated with different ratios of fuel equivalent maximum demand. *NOx* levels were found after an increasing equivalence ratio of 0.55 and the maximum value was approximately 7500 ppm. High reductions in the emission of *NOx* were not possible without a significant fall in the thermal efficiency, with delay ignition times of the spark. The most drastic drops in levels of *NOx*, even below 2490 ppm, were observed with water injection. Despite the reduction in the rate of heat release (HRR), no significant loss was observed in brake thermal efficiency (BTE). It was not observed a significant influence on the stability of combustion or emission levels UHC.

In 2013, Boretti (BORETTI, 2013) conducted an exploratory work, comparing the performance of an engine two liters and four cylinders, powered by ethanol and water injection, with the results achieved by a commercial program for engine design. The document describes the use of water injection in the turbo of a spark ignition engine. A water injection port is located in the conduit that joins the turbo with the intake ports and its efficiency is numerically demonstrated in the reduction of the detonation tendency and the control of the temperature of the gases in the turbine. With the injection of water in selected operating conditions, the engine may operate at higher compression ratios, and more near the maximum value of the torque to the brake, to improve the power of exit and the peak of efficiency besides the capacity in partial load. The document suggests the introduction of this ancient technique that is now used in parts, assemblies to improve performance and possibly evolve to direct water injection in the design stage of new turbo engines.

Recently, Mingrui (MINGRUI *et al.*, 2016) reported the results of their study on the

influence of water injection with variable mass in the performance characteristics and emissions of a direct injection engine (GDI) under light load conditions. The study involves injecting water into the cylinder when the crank angle (CA) was worth 640° a duration of 10° CA. Gasoline is injected directly into the cylinder with a fixed duration from 660° to 680° CA. The results indicated that a water injection 15% in mass (in comparison with the load of fuel/ air), when used together with fuel, gave the best engine performance due to the increase in the average effective pressure and indicated efficiency resulting from the cooling some parts of the engine. The water injection also showed decreased NOx emissions (ppm), and pollutant emissions.

2.4.1 EVAPORATION MODEL FOR ONE DROP.

Here it is presented a simple model of droplet evaporation of a single-component liquid substance within a hot gaseous environment, implementing a simulation program that was developed for engines.

2.4.1.1 *Introduction to mass transfer.*

Because during the evaporation process of substance A in a medium composed of substance B, a mass transfer from A to B occurs, the mass change ratio of the mass drop of substance A is equivalent to the mass evaporation ratio, which can be obtained from Fick's diffusion law (TURNS, 1996):

$$\dot{m}_A'' = Y_A \left(\dot{m}_A'' + \dot{m}_B'' \right) - \rho_A \mathbf{D}_{AB} \frac{dY_A}{dx} \tag{2.66}$$

with:

- $\dot{m}_A$= Mass flow of the species A (or B).
- Y_A= Mass fraction of the species A (or B).
- ρ_A= Density of species A (or B).
- $\mathbf{D}_{AB}$=Binary diffusivity of the species A in a medium composed by the species B. The Binary Diffusivity $\mathbf{D}_{AB}$ is a property of the mixture and is given in $\frac{m^2}{s}$.
- $\frac{dY_A}{dx}$= Ratio of change of the mass fraction of the species A respect to the distance x.

The mass flow is then defined as the mass flow ratio of species A per unit area, perpendicular to the direction of flow (TURNS, 1996):

$$\dot{m}_A'' = \frac{\dot{m}}{A} \tag{2.67}$$

(Eq.2.67) is also valid for medium B, but because area B is substantially larger than area A, and medium B is considered static (no motion), (Eq.2.67) is zero for the latter case (TURNS, 1996). Organizing and replacing in (Eq.2.66) yields:

- Mass flow of the species *A* (TURNS, 1996).

$$\dot{m}_A'' = Y_A \left(\dot{m}_A'' + \dot{m}_B'' \right) = Y_A \dot{m}_A \tag{2.68}$$

- Diffusional flow of the species *A* (TURNS, 1996).

$$-\rho_A \mathbf{D}_{AB} \frac{dY_A}{dx} = \dot{m}_{A,diff}'' \tag{2.69}$$

Thus (TURNS, 1996):

$$\dot{m}_A'' = Y_A \dot{m}_A + \dot{m}_{A,diff}'' \tag{2.70}$$

in which $\dot{m}_{A,diff}''$ is proportional to the mass fraction gradient. Similarly, conduction heat diffusion can be written in a similar way to Fourier heat conduction law (TURNS, 1996):

$$\dot{Q}_x'' = k \frac{dT}{dx} \tag{2.71}$$

(Eq.2.70) and (Eq.2.71) provide the basis for the analysis of droplet evaporation in hot and inactive environments, i.e. where no chemical reactions occur.

2.4.1.2 *Evaporation of drops.*

The evaporation of a drop of liquid in an inactive and hot gaseous environment is a version of Stefan's problem (STEFAN, 1891), where a spherical coordinate system is used (TURNS, 1996). The problem illustrates one of the ways to apply the basic concepts of mass transfer presented above (Sec 2.4.1.1). (Fig. 2.4) describes a system of spherical coordinates. The radius r is the variable and is located on the horizontal axis. The center of the drop determines the origin of the coordinate system and the distance from the center of the drop to the liquid vapor interface is called r_s. Moving away from the surface of the drop ($r \to \infty$), the mass fraction of the steam drop is $Y_{F,\infty}$ (TURNS, 1996) . Physically, the heat emitted by the gaseous medium provides the energy needed for the evaporation of the liquid droplet, and the resulting vapor is then diffused from the surface of the droplet (liquid-steam interface) into the gaseous medium. The loss of mass causes the radius of the drop to be reduced until the drop disappears when it evaporates completely. The complete mathematical description of this process requires the following conservation laws (TURNS, 1996):

- Drop: Conservation of mass and energy.
- On the surface of the drop, steam is mixed with the surrounding gaseous medium ($r_s < r < \infty$): In this zone the laws of conservation of mass, species and energy apply.

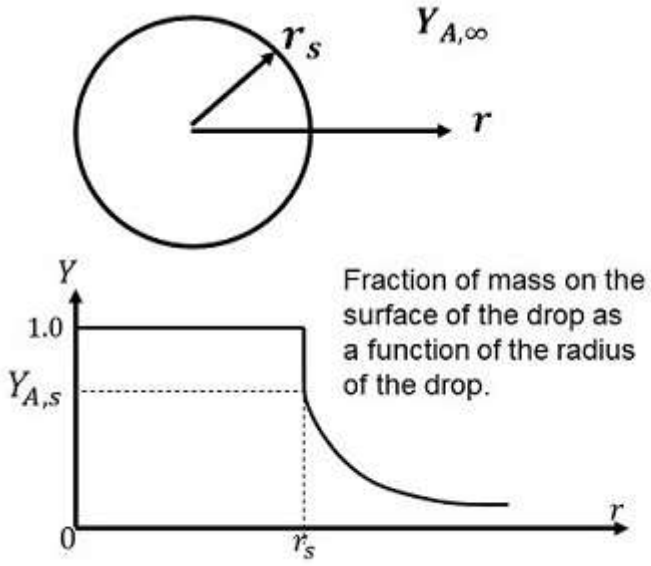

Fig. 2.4 – Spherical coordinate system for the analysis of drop evaporation. Source:(TURNS, 1996).

The following assumptions are also necessary for the model description (TURNS, 1996):

- The evaporation process is quasi-stable. This means that for any instant of time the process can be described as being in steady state. This assumption eliminates the need to deal with partial differential equations.
- The temperature of the drop is uniform and therefore the temperature is assumed to be below the boiling point of the liquid for a given pressure. Some problems of transient heating of the liquid does not significantly affect the lifetime of the drop (TURNS, 1996). The determination of the temperature at the surface of the drop depends on the ratio of heat transfer to the drop. Thus, the assumption of a specific temperature eliminates the need to apply conservation of energy to the gases around the drop and towards the drop itself.
- The vapor mass fraction at the drop surface is determined by the liquid-vapor balance at the drop temperature.
- It is also assumed that thermophysical properties, especially the product $\rho \mathbf{D}_{AB}$, are constant. Although the properties may vary strongly as the gas phase advanced from the surface of the drop to the surroundings, the constant properties allow a solution of closed form.

2.4.1.3 *Ratio for evaporation.*

Taking the description presented in section 2.4.1.2, it is possible to find an evaporation ratio according to the reason of the change of mass in relation to time, $\dot{m}$, and a function for the

droplet radius, also in terms of time $r_s(t)$, writing species conservation equation for the vapor of the drop and mass conservation equation for the liquid part of the drop. With the conservation of the species, it can be determined the ratio of evaporation $\dot{m}$ and thus, obtaining $\dot{m}(t)$, easily find the size of the drop as a function of time. Bearing in mind that it is assumed that there is no movement of the droplet with respect to the gaseous medium in which it is found and that, in addition, it is assumed that the gaseous medium has no movement either, it is necessary to modify the approach of Stefan's problem considering the change of coordinates. The deduction of the equation relating the ratio for change of mass as a function of time, $\dot{m}$, with the variation of the fraction of mass on the surface of the droplet, $Y_{A,s}$ can be found in (TURNS, 1996). The final result establishes the droplet evaporation ratio as the variation of the droplet mass in terms of the fraction of mass on the droplet surface (TURNS, 1996).

$$\dot{m} = 4\pi r_s \rho \mathbf{D}_{AB} \ln\left(\frac{(1-Y_{A,\infty})}{(1-Y_{A,s})}\right) \tag{2.72}$$

Defining the dimensionless number By as the "driving potential" for mass transfer or the Spalding mass transfer number (NI, 2010) and taking the logarithm argument, it is obtained that (TURNS, 1996):

$$1 + B_y = \frac{1-Y_{A,\infty}}{1-Y_{A,s}} \tag{2.73}$$

or

$$B_y = \frac{Y_{A,s}-Y_{A,\infty}}{1-Y_{A,s}} \tag{2.74}$$

Applying (Eq.2.73) in (Eq.2.72) it is found (TURNS, 1996):

$$\dot{m} = 4\pi r_s \rho \mathbf{D}_{AB} \ln(1+B_y) \tag{2.75}$$

2.4.1.4 *Conservation of the mass in the drop.*

The ratio in which the radius of the droplet (or diameter) decreases is proportional to the ratio in which the liquid that makes up the droplet evaporates.(TURNS, 1996):

$$\frac{dm_d}{dt} = -\dot{m}, \tag{2.76}$$

in which the mass of the drop can be taken as (TURNS, 1996):

$$m_d = \rho_l V = \rho_l \pi \frac{D^3}{6} \tag{2.77}$$

in which ρ_l, is the density of the liquid of the drop, V is the volume and $D = 2r$ is the diameter of the drop respectively. Substituting (Eq.2.75) and (Eq.2.77) into (Eq.2.76), rearranging and differentiating, gives (TURNS, 1996):

$$\frac{dD}{dt} = -\frac{4\rho \mathbf{D}_{AB}}{\rho_l D} \ln(1+B_y) \tag{2.78}$$

In the literature of combustion, it is more common to find this expression in terms of D^2, so (TURNS, 1996):

$$\frac{dD^2}{dt} = -\frac{8\rho \mathbf{D}_{AB}}{\rho_l}\ln(1+B_y) \tag{2.79}$$

This last equation shows that the derivative with respect to the time of the square of the diameter of the drop is constant, so that D^2 varies linearly over time t and its slope is (TURNS, 1996):

$$-\frac{8\rho \mathbf{D}_{AB}}{\rho_l}\ln(1+B_y) \tag{2.80}$$

The slope is defined as the evaporation constant K (TURNS, 1996):

$$-K = -\frac{8\rho \mathbf{D}_{AB}}{\rho_l}\ln(1+B_y) \tag{2.81}$$

(Fig.2.5) shows the relationship between time (t) and the diameter variation of the droplet squared, where K is the slope of the line.

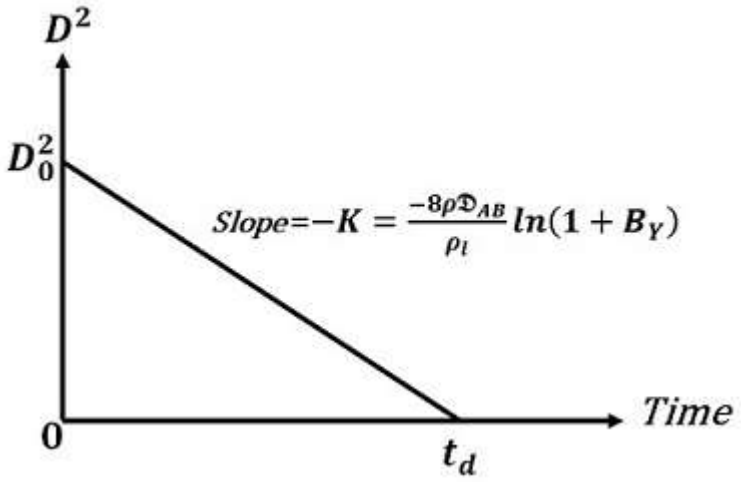

Fig. 2.5 – Relationship between the time and the diameter of the drop squared during the evaporation process. The slope of the line is –K. Source: (TURNS, 1996).

It is possible to find the time a given size drop takes to evaporate completely. Being t_d the life time of the drop (TURNS, 1996):

$$\int_{D_0^2}^{0} dD^2 = -\int_0^{t_d} K dt \tag{2.82}$$

As a result:

$$t_d = \frac{D_0^2}{K}. \tag{2.83}$$

By changing the limits of (Eq.2.82), it is possible to establish a general relation to express the variation of the diameter D with respect to time t (TURNS, 1996):

$$D^2(t) = D_0^2 - Kt_d \tag{2.84}$$

(Eq.2.84) is known as the law of D^2 for the evaporation of drop.

2.4.2 EMPIRICAL CORRELATIONS:

It begins with a summary of the empirical correlations used to find the Nusselt number (Nu) (RENKSIZBULUT; YUEN, 1983). The first is given by the expression:

$$N_{uf} = \left(\frac{2 + 0.57 R_{e_f}^{\frac{1}{2}} P_{r_f}^{\frac{1}{3}}}{(1 + b_f)^{0.7}} \right) \tag{2.85}$$

in which (CHIANG *et al.*, 1992):

$$B_f = \frac{c_{pv}(T_g - T_s)}{L} \left(1 - \frac{|\dot{q}_d|}{|\dot{q}_c|} + \frac{|\dot{q}_R|}{|\dot{q}_c|} \right) \tag{2.86}$$

- $|\dot{q}_d|$: Reason why the heat is spent in raising to liquid drop temperature.
- $|\dot{q}_c|$ and $|\dot{q}_R|$: Heat ratios supplied to the drop by convection and radiation, respectively.
- L: Latent heat of evaporation.
- $R_{e_f} = \frac{2R_d \rho_{g\infty} |v_g - v_d|}{\mu_{gf}}$, where f indicates the value of the film parameters surrounding the drop.
- R_d: Drop Radius.
- T: Temperature and subscripts g and s indicate gas phase and drop surface respectively.
- $\frac{T_g + T_s}{2}$: Film temperature.
- R_e: Reynolds number.
- P_r: Prandtl number.
- The vapour mass fraction is given by $\frac{Y_{v\infty} + Y_{vs}}{2}$, where $Y_{v\infty}$ and Y_{vs} are the vapor mass fractions away from the drop and in the vicinity of the droplet, respectively.

It is assumed that the droplets can be treated as black bodies with emissivity of 0.95 this model is acceptable when the droplet radio range from 0.5 to 3 mm. With smaller radii the predictions are not acceptable (SAZHIN, 2014). In cases where $|\dot{q}_d| = |\dot{q}_R| = 0$, B_f is taken as the Spalding number of heat transfer. When there is no evaporation, $B_f = 0$. Now, h_m is defined as the mass coefficient used to describe the evaporation of the drop. This coefficient can be expressed as follows:

$$m_d^{''} = h_m(\rho_{vs} - \rho_{v\infty}) \tag{2.87}$$

with: $m_d^{''} = \frac{\dot{m}_d}{4\pi R_d^2}$ and $\rho_{vs}, \rho_{v\infty}$ are the densities of vapor on the droplet surface, and away from it $|\dot{m}_d|$: is the absolute value of the evaporation ratio of the droplet (RENKSIZBULUT; YUEN,

1983). For steady evaporation of the droplet, regardless of the gas movement speed in the drop vicinity in the vicinity of the drop (Stefan flow), the expression for h_m becomes in:

$$h_m = \frac{\mathbf{D}_g}{R_d} \tag{2.88}$$

with: $\mathbf{D}_g$: Binary diffusion coefficient of the vapour in the gas (described as $\mathbf{D}_{AB}$). For general cases the mass transfer coefficient is dimensionless and is introduced by means of the Sherman number(Sh), which is defined as (BERGMAN; INCROPERA, 2011).

$$Sh = \frac{2R_d h_m}{\mathbf{D}_g} \tag{2.89}$$

For cases of steady evaporation of the drop in the void or when Stefan's flow is not important $(Sh = 2)$. Similarly, the correlation of the Sherman number for drops evaporating in motion can be obtained from:

$$Sh_f = \frac{\left(2 + 0.87 Re_f^{\frac{1}{2}} Sc_f^{\frac{1}{3}}\right)}{(1 + B_m)^{0.7}} \tag{2.90}$$

in which:

$$B_m = \frac{\rho_{vs} - \rho_{v\infty}}{\rho_{gs}} = \frac{Y_{vs} - Y_{v\infty}}{1 - Y_{vs}}. \tag{2.91}$$

This is defined as the Spalding number of mass transfer (SAZHIN, 2014).

Sc_f is defined as the Schmidt number and is established by the ratio between the specific volume of the fuel (v_f) and its diffusivity in the corresponding medium $(\mathbf{D}_f)$,

$$Sc_f = \frac{\nu_f}{\mathbf{D}_f} \tag{2.92}$$

(Eq.2.90) is applicable for values of Re_f in the range of 20 to 2000. The term $(1 + B_m)^{0.7}$ implies that the velocity of the gas around the drop must be taken into account (Stefan flow). The value of ρ_{vs} is connected to the vapour saturation pressure p_{vs} and at the surface temperature by means of the ideal gas law and the Clausius-Clapeyron equation (SAZHIN, 2014). For example, for the case of the saturated surface of a drop of n-dodecane, we have:

$$p_{vs} = p_{ref} \exp\left(\frac{T_s - T_{ref}}{a_{pres}}\right) \tag{2.93}$$

in which:

- p_{ref} = 70.44 Pa; T_{ref} = 300.18 K; a_{pres} = 22.37 K when $T_s \leq$ 440.00 K.
- p_{ref} = 46204.48 Pa; T_{ref} = 449.87 K; a_{pres} = 56.97 K when $T_s >$ 440.00 K.

An alternative correlation for *Sh* is (KULMALA *et al.*, 1995),

$$Sh = \left(2.009 + 0.514 Re^{\frac{1}{2}} Sc^{\frac{1}{3}}\right) \tag{2.94}$$

The following correlation was obtained for the reference temperature T_{ref}, using the rule of $\frac{1}{3}$:

$$T_{ref} = T_s + \frac{1}{3}(T_g + T_s) \tag{2.95}$$

- T_g: Gas temperature in the surroundings.
- T_s: Temperature on the surface of the drop.

The correlation of (Eq.2.94) is valid when the contribution of Stefan's flow is small.

The correlation of (Eq.2.95) is widely used in the combustion literature for calculations of numbers *Nu* and *Sh* (SAZHIN, 2014).

3 METHODOLOGY

In this section, it is presented a detailed explanation of the working cycle model of a spark ignition engine with direct water injection in the combustion chamber. This section has been divided into two main parts. First, the mathematical treatment of the thermodynamic equations corresponding to the two-zone model during the combustion phase is shown; the combustion chamber is divided into two zones corresponding to the regions of burned and unburned gases, separated by a thin layer called the flame front. This model was previously developed within the research group of the Bio-Fuels Engine Laboratory (LMB), and was the model taken as the basis For the development of its modifications, which includes the effects of injection and evaporation of a specific amount of water within the combustion chamber. This modifications include variations in the behavior of the main parameters to be observed, more specifically the pressure, temperature and mass inside the cylinder, once a defined volume of water is injected in a pulverized form and liquid state. The equations are presented in such a way that the injection of water is not limited exclusively to the cycle closed phase, but can also be done in the open phase. The second part of the chapter describes the water evaporation model used and implemented within the simulation program developed in MatLab® to model the phase change of the water inside the combustion chamber in the different instants in which it is possible to perform the water injection. The spray model is also included.

Finally, it is made a physical description of the engine used for the corresponding simulations. For the validation and verification of the proposed model, the geometrical and kinematic configuration of the engine performed by Kim (KIM *et al.*, 2016) is used. This paper presents the results of a series of experimental tests for a spark ignition engine that uses gasoline as fuel. The engine was adapted as a water injection system directly in the combustion chamber. The other parameters corresponding to the operating conditions for each RPM (revolutions per minute) are presented tabulated in the results section.

3.1 MODEL OF TWO-ZONES FOR THE WORKING CYCLE OF AN INTERNAL COMBUSTION AND SPARK IGNITION ENGINE, WITH WATER INJECTION.

The mathematical development of a two-zone thermodynamic model for the duty cycle of an internal combustion engine and spark ignition is shown below. The initial model is based on what is shown by Verhelst (VERHELST; SHEPPARD, 2009), Cruz (CRUZ *et al.*, 2016), Cuddihy (CUDDIHY, 2014) together with the considerations made by Rufino (RUFINO, 2017). In this two-zone model there are three unknowns: T_u, T_b and P (Temperature of unburned gases (u), Temperature of burned gases (b) and Pressure, respectively). The volumes are calculated

using the law of ideal gases, once the temperature of each zone are established (RUFINO, 2017).

$$V_u = \frac{m_u R_{mix} T_u}{P}, \tag{3.1}$$

$$V_b = \frac{m_b R_{prod} T_b}{P}. \tag{3.2}$$

For the ideal gas constants in the mixture R_{mix} and in products R_{prod} are calculated as a function of molecular weight M of the mixture and the respective product and the Universal Constant of the Ideal Gases R, so:

$$R_{mix,prod} = \frac{R}{M_{mix,prod}} \tag{3.3}$$

The masses are calculated using the Wiebe function:

$$m_b = m_{adm} X_b \tag{3.4}$$

$$m_u = m_{adm}(1 - X_b) \tag{3.5}$$

Where each variable means:

- m_b : Mass of burned gas.
- m_u : Mass of unburned gas.
- m_{adm}: Admission Mass.
- X_b : Fraction of burned substance.
- T_b : Temperature of burned gases.

The equations used throughout this description are:

1. Energy balance for the burned gas region: T_b.
2. Energy balance for the region of unburned gases: T_u.
3. Pressure balance: P.

3.1.1 ENERGY BALANCE IN THE BURNED GASES REGION.

Using the first law of thermodynamics for a control volume during the combustion process, we have:

$$\frac{dU_b}{d\theta} = \delta Q_b - \delta W_b + h\frac{dm_b}{d\theta} \tag{3.6}$$

The terms contained in (Eq.3.6) are described below (RUFINO, 2017):

1. Internal energy differential:

$$\frac{dU_b}{d\theta} = \frac{d}{d\theta}(m_b Cv_p T_b). \tag{3.7}$$

So:

- m_b : Mass of burned gas.
- Cv_p : Specific heat at constant volume of combustion products.
- T_b : Temperature of burned gases.

2. Heat transfer:

$$\delta Q_b = \delta Q_{comb} + \delta Q_{conv,b}. \tag{3.8}$$

Where:

- δQ_b : Differential of heat released.
- δQ_{comb} : Combustion heat differential.
- $\delta Q_{conv,b}$: Convection heat differential of the combustion gases.

3. Differential of Work (δW_b):

$$\delta W_b = P\frac{dV_b}{d\theta}. \tag{3.9}$$

where:

- P : Pressure.
- $\frac{dV_b}{d\theta}$: Volume variation as a function of crankshaft angle of rotation.

4. Enthalpy of mass transfer between areas of burned and unburned gases:

$$h = Cp_{mix} T_u. \tag{3.10}$$

Where:

- h : Enthalpy.
- Cp_{mix} : Specific heat at constant pressure of the gas mixture.
- T_u : Temperature of unburned gases

The terms of the heat transfer by convection (Eq.3.8) and the energy released by combustion (Eq.3.9) are obtained as follows: $(\delta Q_{comb} = \delta Q_c)$ and $(\delta Q_{conv,b} = \delta Q_{c,b})$.

$$\delta Q_{c,b} = -\frac{hA_b(T_b - Tw)}{\omega}. \tag{3.11}$$

Where:

- $\delta Q_{c,b}$: Convection heat transfer by the mass of burned gas.
- h : Enthalpy.
- A_b : Burnt gas area in contact with cylinder wall.
- T_b : Burned gas temperature.
- T_w : Cylinder wall temperature.
- ω : Crankshaft rotation speed.

$$\delta Q_c = n_f m_f LHV_f dX_b. \tag{3.12}$$

Whit:

- δQ_c : Combustion heat transfer.
- LHV : Lower Heating Value of the fuel.
- m_f : Molecular mass of fuel.
- X_b : Fraction of burned substance.
- n_f : Number of moles of fuel.

Considering that within the energy balance for the region of burned gases all forms of energy exchange should be included, in (Eq.3.6) the term corresponding to the entry of the water fraction in a liquid state must be added. With the equation mentioned above it can be stated as follows: $(\delta Q_{comb+covn} = \delta Q_{c+c})$

$$\frac{dU_b}{d\theta} = \delta Q_{c+c} + \delta Q_w - P\frac{dV_b}{d\theta} + \sum h_i \frac{dm_i}{d\theta} \tag{3.13}$$

in which the last term, $(\sum h_i \frac{dm_i}{d\theta})$, corresponds to the sum of all the mass exchange processes that can happen to the interior of the combustion chamber.

(Fig.3.1) illustrates a diagram of the evaporation process of a water droplet in a hot gaseous environment.

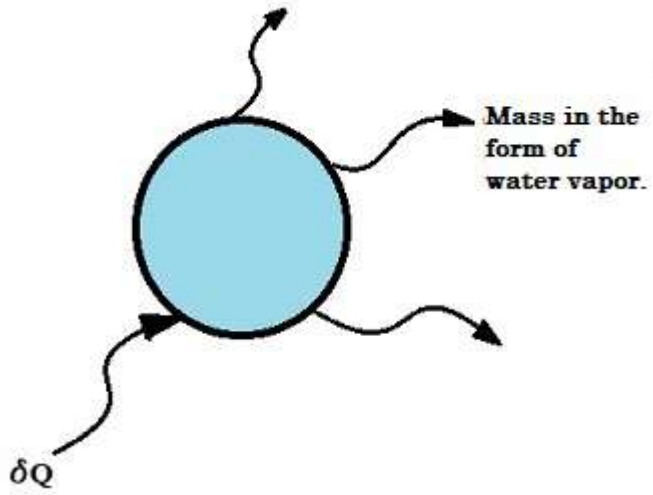

Fig. 3.1 – Simplified model of the phenomenology of the evaporation of a drop of water

.

A fraction of heat (δQ_w) is absorbed by the liquid by raising the temperature of the latter, if the amount of heat available is sufficient so that the temperature of the drop is raised until reaching the value corresponding to the saturation of the liquid for the pressure of the hot gaseous medium, the liquid will start a phase change process until the drop disappears and becomes thoroughly steam. The above description can be written as follows:

$$\frac{dU_l}{d\theta} = \delta Q_w - h_v \frac{dm_w}{d\theta} \tag{3.14}$$

in where $(\frac{dU_l}{d\theta})$ corresponds to the energy used by the drop during the phase change.

The first term to the right of the (Eq.3.14), δQ_w, can be approximated as the difference between the enthalpies of vapor and liquid (h_v, h_l) for the fraction of water mass $(\frac{dm_w}{d\theta})$ which enters the control volume:

$$\delta Q_w \approx (h_v - h_l) \frac{dm_w}{d\theta} \tag{3.15}$$

Replacing in (Eq.3.13) and simplifying, it is got:

$$\frac{dU_b}{d\theta} = \delta Q_{c+c} + h_l \frac{dm_w}{d\theta} - P\frac{dV_b}{d\theta} + h_u \frac{dm_c}{d\theta} \tag{3.16}$$

The ideal gas law allows the third term of (Eq.3.16), corresponding to the work $(P\frac{dV_b}{d\theta})$, to become:

$$P\frac{dV_b}{d\theta} = PV_b \left(\frac{dm_b}{d\theta}\frac{1}{m_b} + \frac{dT_b}{d\theta}\frac{1}{T_b} - \frac{dP}{d\theta}\frac{1}{P} \right) \tag{3.17}$$

Simplifying and reordering:

$$P\frac{dV_b}{d\theta} = \left(R_b T_b \frac{dm_b}{d\theta} + m_b R_b \frac{dT_b}{d\theta} - V_b \frac{dP}{d\theta}\right) \tag{3.18}$$

Replacing (Eq.3.18) in (Eq.3.16) yields:

$$\frac{dU_b}{d\theta} = \delta Q_{c+c} + h_l \frac{dm_w}{d\theta} - \left(R_b T_b \frac{dm_b}{d\theta} + m_b R_b \frac{dT_b}{d\theta} - V_b \frac{dP}{d\theta}\right) + h_u \frac{dm_c}{d\theta} \tag{3.19}$$

Taking the mass of burnt gases (m_b) in the combustion chamber during the combustion process as the sum of the gases produced by the reaction(m_{bnt}) plus the fraction of water that has already been transformed into steam (m_w^v), likewise: $m_b = m_{bnt} + m_w^v$. Replacing in (Eq.3.19) and rearranging:

$$\frac{dU_b}{d\theta} = \delta Q_{c+c} + h_l \frac{dm_w}{d\theta} - R_b T_b \frac{dm_b}{d\theta} - m_b R_b \frac{dT_b}{d\theta} + V_b \frac{dP}{d\theta} + h_u \frac{dm_c}{d\theta} \tag{3.20}$$

Now, from the application of the first law of thermodynamics regarding the specific heat at constant volume, it is know that:

$$\frac{dU_b}{d\theta} = \frac{d}{d\theta}(m_b C_{vb} T_b) = C_{vb} T_b \frac{dm_b}{d\theta} + m_b C_{vb} \frac{dT_b}{d\theta} + m_b T_b \frac{dC_{vb}}{d\theta} \tag{3.21}$$

Replacing the previous expression (Eq.3.21) in (Eq.3.20)

$$C_{vb} T_b \frac{dm_b}{d\theta} + m_b C_{vb} \frac{dT_b}{d\theta} + m_b T_b \frac{dC_{vb}}{d\theta} = \delta Q_{c+c} + h_l \frac{dm_w}{d\theta} - R_b T_b \frac{dm_b}{d\theta} - m_b R_b \frac{dT_b}{d\theta} + V_b \frac{dP}{d\theta} + h_u \frac{dm_c}{d\theta} \tag{3.22}$$

Starting from equation (Eq.3.22), simplifying and clearing $(\frac{dT_b}{d\theta})$, an expression is obtained for the variation of the temperature inside the combustion chamber which takes into account the injection of water, which is performed moments after the combustion reaction has started in the burned gas zone. Taking into account that$\left(\frac{dC_{vb}}{d\theta} = \frac{\partial C_{vb}}{\partial T_b}\frac{dT_b}{d\theta}\right)$ and substituting in (Eq.3.22), it is got:

$$\frac{dT_b}{d\theta} = \frac{\delta Q_{c+c} + h_{unt}\frac{dm_c}{d\theta} + h_l \frac{dm_w}{d\theta} - C_{pb} T_b \frac{dm_b}{d\theta} + V_b \frac{dP}{d\theta}}{m_b \left(C_{pb} + T_b \frac{\partial C_{vb}}{\partial T_b}\right)} \tag{3.23}$$

3.1.2 ENERGY BALANCE IN THE UNBURNED GAS REGION.

Within the initial considerations, it was stated that the injection of water would take place instants after the ignition to ensure that the most significant amount of liquid water enters the burned gas area directly (LOAIZA, 2016). However, is possible that the model allows making the injection of water at any time of the cycle, would imply that it is possible to inject the water

fraction not only in the region of burnt gases, after ignition, but also in the part of unburned gases before the spark. For this reason, the energy balance for the area of unburned gases is presented, equally based on the considerations that can be observed in Rufino (RUFINO, 2017). Again starting from the first law of thermodynamics and taking into account the description shown in (Fig.3.1), (Eq.3.14) and (Eq.3.15), the energy for the region of unburned gases can be described as follows:

$$\frac{dU_u}{d\theta} = \delta Q_{u+c} - P\frac{dV_u}{d\theta} + h\frac{dm_u}{d\theta} - \delta Q_w + h_v\frac{dm_w}{d\theta} \tag{3.24}$$

in which the subscript u refers to the zone of unburned gases. The term δQ_w is the same as described in (Eq.3.15). The last term $\left(h_v\frac{dm_w}{d\theta}\right)$ corresponds to the fraction of water that is evaporating. In the same way as in (Eq.3.21), $\frac{dU_u}{d\theta}$ can be written as:

$$\frac{dU_u}{d\theta} = C_{vu}T_u\frac{dm_u}{d\theta} + m_uC_{vu}\frac{dT_u}{d\theta} + m_uT_u\frac{dC_{vu}}{d\theta} \tag{3.25}$$

It's known that $\frac{dC_{vu}}{d\theta} = \frac{\partial C_{vu}}{\partial T_u}\frac{dT_u}{d\theta}$. Substituting (Eq.3.16) and (Eq.3.25) in (Eq.3.24) and applying the law of ideal gases gives:

$$m_u\frac{dT_u}{d\theta}\left(C_{vu} + T_u\frac{\partial C_{vu}}{\partial T_u}\right) = \delta Q_{uc} - R_uT_u\frac{dm_u}{d\theta} - R_um_u\frac{dT_u}{d\theta} - C_{vu}T_u\frac{dm_u}{d\theta} + V_u\frac{dP}{d\theta} + h\frac{dm_u}{d\theta} + h_l\frac{dm_w}{d\theta} \tag{3.26}$$

As $C_{pu} - C_{vu} - R_u = 0$ and $h\frac{dm_u}{d\theta} = C_{pu}T_u\frac{dm_u}{d\theta}$ so:

$$m_u\frac{dT_u}{d\theta}\left(C_{vu} + T_u\frac{\partial C_{vu}}{\partial T_u}\right) = \delta Q_{uc} - R_um_u\frac{dT_u}{d\theta} + V_u\frac{dP}{d\theta} + h_l\frac{dm_w}{d\theta} \tag{3.27}$$

Separating $\frac{dT_u}{d\theta}$, an expression for the temperature of the zone of unburned gases with addition of water is reached, as follows:

$$\frac{dT_u}{d\theta} = \frac{\delta Q_{uc} + V_u\frac{dP}{d\theta} + h_l\frac{dm_w}{d\theta}}{m_u\left(C_{pu} + T_u\frac{\partial Cvu}{\partial T_u}\right)} \tag{3.28}$$

3.1.3 VOLUME BALANCE FOR THE COMBUSTION CHAMBER.

Obtained the corresponding expressions for the variation of the temperature in the burned and unburned gas zones, it is necessary to find another one for the variation of the pressure. Starting from the balance of volume and the ideal gases law, it has:

$$\frac{dV}{d\theta} = \frac{dV_b}{d\theta} + \frac{dV_u}{d\theta} + \frac{dV_w^l}{d\theta} \tag{3.29}$$

in which $V_b = V_{bnt} + V_w^v$ with V_{bnt} is the volume of flue gases generated during the combustion reaction and V_w^v corresponding to the volume of water steam. From the ideal gases law, it is known that:

$$\frac{dV}{d\theta} = V_b\left(\frac{dm_b}{d\theta}\frac{1}{m_b} + \frac{dT_b}{d\theta}\frac{1}{T_b} - \frac{dP}{d\theta}\frac{1}{P}\right) + V_u\left(\frac{dm_u}{d\theta}\frac{1}{m_u} + \frac{dT_u}{d\theta}\frac{1}{T_u} - \frac{dP}{d\theta}\frac{1}{P}\right) + \frac{dV_w{}^l}{d\theta} \tag{3.30}$$

in which subindices b and u refer to burned and unburned respectively, indicating each of the zones of the gases during the combustion reaction in the combustion chamber. In the same manner, $m_b = m_{bnt} + m_w^v$ with m_{bnt} corresponding to the mass of the flue gases resulting from the reaction and m_w^v being the mass of water steam. V_w^l indicates the volume of water remaining liquid. Taking the well-known expression:

$$PV = mRT \Rightarrow \frac{PV}{m} = RT \tag{3.31}$$

and taking into account that $V_G = V_b + V_u$ is the volume of total gases at the time of analysis, (Eq.3.29) can be simplified and rewritten as follows:

$$\frac{dP}{d\theta}(V_G) = R_b T_b \frac{dm_b}{d\theta} + R_b m_b \frac{dT_b}{d\theta} + R_u T_u \frac{dm_u}{d\theta} + R_u m_u \frac{dT_u}{d\theta} + P\frac{dV_w^l}{d\theta} - P\frac{dV}{d\theta} \tag{3.32}$$

Separating $\frac{dP}{d\theta}$ and replacing the expressions for the region of burned gases (Eq.3.23) and unburned gases temperature (Eq.3.28) (RUFINO, 2017), and in (Eq.3.32) and after applying some algebra equation (Eq.3.33) it is obtained (For simplicity and space $\delta Q_{comb+conv} = \delta Q_{cc}$ corresponds to the heat transfer model and $dm_{comb} = dm_c$ mass of combustion gas):

$$\begin{aligned}\frac{dP}{d\theta}(V_G) = R_b T_b \frac{dm_b}{d\theta} + R_b m_b \left(\frac{\delta Q_{cc} + h_{unt}\frac{dm_c}{d\theta} + h_l \frac{dm_w}{d\theta} - C_{pb} T_b \frac{dm_b}{d\theta} + V_b \frac{dP}{d\theta}}{m_b \left(C_{pb} + T_b \frac{\partial C_{vb}}{\partial T_b} \right)} \right) + \\ R_u T_u \frac{dm_u}{d\theta} + R_u m_u \left(\frac{\delta Q_{uc} + V_u \frac{dP}{d\theta} + h_l \frac{dm_w}{d\theta}}{m_u \left(C_{pu} + T_u \frac{\partial C_{vu}}{\partial T_u} \right)} \right) + P\frac{dV_w^l}{d\theta} - P\frac{dV}{d\theta}\end{aligned} \tag{3.33}$$

Once more, by taking (Eq.3.33), simplifying and organizing gives the expression for the pressure variation:

$$\frac{dP}{d\theta} = \left(\frac{P\frac{dV}{d\theta} - P\frac{dV_w^l}{d\theta} - R_b T_b \frac{dm_b}{d\theta} - R_u T_u \frac{dm_u}{d\theta} - \frac{R_u}{C_{pu} + T_u \frac{\partial C_{vu}}{\partial T_u}}(A) - \frac{R_b}{C_{pb} + T_b \frac{\partial C_{vb}}{\partial T_b}}(B)}{\frac{R_u V_u}{C_{pu} + T_u \frac{\partial C_{vu}}{\partial T_u}} + \frac{R_b V_b}{C_{pb} + T_b \frac{\partial C_{vb}}{\partial T_b}} - V_G} \right) \tag{3.34}$$

in which:

$$(A) = \left(\delta Q_{uc} - h_l \frac{dm_w}{d\theta} \right) \tag{3.35}$$

and:

$$(B) = \left(\delta Q_{cc} - h_u \frac{dm_c}{d\theta} - h_l \frac{dm_w}{d\theta} + T_p C_{pb} \frac{dm_b}{d\theta} \right) \tag{3.36}$$

(Eq.3.34) represents the pressure variation within the combustion chamber. The set of equations (Eq.3.23), (Eq.3.28) and (Eq.3.34) describe the pressure and temperature conditions within the combustion chamber during the combustion reaction and with the addition of a fraction of liquid water is injected at any time during the closed phase and is transformed into steam by absorbing part of the heat available in the gaseous medium, due to the increase in temperature during compression and/or due to the combustion reaction. The system is solved through

the implementation of a program in Matlab®, using the numerical method Runge-Kutta of fifth order.

The model shown so far corresponds to the closed phase of the engine cycle (compression, combustion, and expansion). These three stages have in common that the amount of mass inside the cylinder and the combustion chamber remains constant, but the temperature, volume and pressure vary. The equations described so far for pressure and temperature variations were deduced as volume functions, but during the open phase (intake and exhaust) the amount of mass inside the cylinder varies. It is assumed that these two processes occur at constant pressure and this corresponds to the pressure in the intake manifold. So it is only necessary to deduce an expression for the temperature variation.

(Fig.3.2) illustrates an outline of the open phase of the engine work cycle including water injection.

Fig. 3.2 – Diagram of the open phase

.

As already mentioned, this phase is assumed to occur under constant pressure and this pressure is very close to the atmospheric pressure of the geographical place where the engine works. The mass inside the cylinder constantly changes throughout the phase. The latter is the main difference for the closed phase, since it is assumed that during the closed phase the mass is the variable whose value always remains constant. For the analysis, a change in the nomenclature is made, there will be no more arguments about burned and unburned gases (*b* and *u*), now the letters are used for the subscripts *e* for the escape and *a* for admission.

The energy balance for the open phase can be written as follows:

$$\frac{dU}{d\theta} = \delta Q - P\frac{dV}{d\theta} - P\frac{dV_w}{d\theta} + h_a\frac{dm_a}{d\theta} - h_e\frac{dm_e}{d\theta} + h_w\frac{dm_w}{d\theta} \tag{3.37}$$

in which the terms third and last correspond to the injection of water. Applying the same equivalence seen in (Eq.3.25) and substituting in (Eq.3.36), it can be written:

$$C_vT\frac{dm}{d\theta} + C_vm\frac{dT}{d\theta} + mT\frac{dC_v}{d\theta} = \delta Q - P\frac{dV}{d\theta} - P\frac{dV_w}{d\theta} + h_a\frac{dm_a}{d\theta} - h_e\frac{dm_e}{d\theta} + h_w\frac{dm_w}{d\theta} \tag{3.38}$$

where:

$$\frac{dC_v}{d\theta} = \frac{\partial C_v}{\partial T}\frac{dT}{d\theta} \tag{3.39}$$

and

$$h_e dm_e = C_{pe}T_e dm_e \tag{3.40}$$

$$h_a dm_a = C_{pa}T_a dm_a \tag{3.41}$$

Once more substituting and simplifying in (Eq.3.38), it is obtained:

$$\frac{dT}{d\theta}\left(C_vm + mT\frac{\partial C_v}{\partial T}\right) = \delta Q - P\left(\frac{dV}{d\theta} + \frac{dV_w}{d\theta}\right) + \left(C_{pa}T_a\frac{dm_a}{d\theta}\right) - \left(C_{pe}T_e\frac{dm_e}{d\theta}\right) + h_w\frac{dm_w}{d\theta} - \left(C_vT\frac{dm_a}{d\theta}\right) - \left(C_vT\frac{dm_e}{d\theta}\right) \tag{3.42}$$

Separating $\frac{dT}{d\theta}$, the equation for the temperature variation in the open phase is:

$$\frac{dT}{d\theta} = \frac{\delta Q - P\left(\frac{dV}{d\theta} + \frac{dV_w}{d\theta}\right) + \frac{dm_a}{d\theta}\left(C_{pa}T_a - C_vT\right) - \frac{dm_e}{d\theta}\left(C_{pe}T_e - C_vT\right) + h_w\frac{dm_w}{d\theta}}{m\left(C_v + T\frac{\partial C_v}{\partial T}\right)} \tag{3.43}$$

(Eq.3.43) describes the temperature variation in both the intake and the exhaust. When analyzing the admission terms with the subscript e, corresponding to the escape, are made 0, and during the escape, the same thing happens with the terms with subscript a.

As for the closed phase, the equation can be solved by implementing a program in Matlab®, using the numerical method Runge-Kutta of fifth order.

3.1.4 MODEL OF THE COMBUSTION PROCESS AND FORMATION OF POLLUTING GASES.

The chemical kinetics model is one of the algorithms of the simulation model and provides the reaction ratios and composition of burned and unburned gases. Additionally, these compositions allow the main simulation model to calculate the thermodynamic properties (P, V, T) (LIMA *et al.*, 2017). The kinetic model starts at the beginning of the compression stroke.

The air-residual gas-fuel mixture is assumed inside the cylinder. An assumption is also made of the residual gases in the mixture which is refined during later iterations of the main simulation model. The universal gas constant, R, is calculated from this mixture (LIMA *et al.*, 2017). In the initial iteration, the residual gas is calculated by means of the complete combustion model described in (FERGUSON; KIRKPATRICK, 2001). Once in combustion, the amount of burned gas increases with the advance of the crankshaft angle. The mixed reactant gases are taken as the input for the adiabatic flame temperature, which is assumed to be the initial temperature in the combustion zone of gases obtained by chemical equilibrium (LIMA *et al.*, 2017).

It is assumed that the initial composition of the gases in the burned zone is the same as the chemical equilibrium composition, except for nitric oxide NO_x; the latter is assumed to be the same as its molar fraction in the residual gases in the immediately preceding cycle (ANNAND *et al.*, 1963). The Wiebe function continuously adds mass in the burned gas zone and this mass is considered in the chemical kinetics model as an input. The system of differential equations obtained is solved by means of the procedure proposed by Lima (LIMA *et al.*, 2017) resulting in the new composition of the burned gas zone. The next iteration of the crankshaft angle provides new mass from the area of unburned gases to the area of burned gases by means of the procedure described above and this additional mass is mixed with the mass of burned gases already present in the corresponding area. The process happens until the Wiebe function indicated that no longer exists mass of unburned gases for the reaction, them where the mass inside the cylinder is considered a product of combustion.

The process of chemical kinetics continues to calculate the thermodynamic compositions in each iteration until the combustion temperature reaches $1500K$ (T_{frezze}). This limit is considered the freezing temperature where the indices of chemical kinetics are devalued and can be ignored. This frozen composition becomes the composition of the residual gases for the following cycle. In this way it is possible to predict the formation of NO_x and CO for each position of the crankshaft angle and therefore of the exhaust gases.

The chemical kinetic model works for each step of a two-zone combustion model for an SI engine. In this way it is possible that the chemical kinetic model performs the calculations under constant volume and temperature conditions for each step. The above assumption allows the thermodynamic conditions (P, V, T, dV, dT, dP) of the two-zone model of a normal spark ignition engine not to vary considerably. This is the most important assumption of the model, because the derivatives of molar concentration $\frac{dC_i}{dt}$ will not depend on the volume derivative of the piston-cylinder assembly $\frac{dV}{dt} = \omega\frac{dV}{d\theta}$, which simplifies the model without diminishing the precision of its results. Other additional assumptions considered in model construction are (LIMA *et al.*, 2017):

- During each iteration, the thermodynamic conditions of the burned gas zone are applied to the chemical kinetics model (V_b, T_b, P_b).

- The model considers the following 12 chemical species (Ar, CO, CO_2, H, H_2O, OH, O, O_2, N, N_2, NO).
- The index i represents each of the chemical species considered (i=1 to 12). The order of the indices is equal to the sequence of chemical species mentioned in the previous numeral (Ar=1, CO=2, CO_2=3).
- With respect to the consideration related to the freezing of compositions, this occur when the temperature is low, which does not allow the chemical kinetics to be activated. Chemical reactions are considered to occur more slowly, i.e. the ratio of reactions is low enough to ignore the influence of chemical kinetics on the system.

3.1.5 DETONATION MODEL.

The model for the prediction of detonation, implemented within the two-zone main model for the work cycle of an internal combustion engine that includes the direct injection of water into the combustion chamber, corresponds to the work developed by (JÚNIOR, 2017).

The model is based on the development presented by (DOUAUD; EYZAT, 1978) and is called KIM (Knock Integral Method). The method calculates the value of a variable called τ, which represents the autoignition delay time of the air-fuel mixture at constant pressure and temperature conditions. The equation for the calculation of τ, (Eq.3.44) proposed by (JÚNIOR, 2017), includes the values for temperature (T) and pressure (P) and determined by means of equations (Eq.3.28) and (Eq.3.34), respectively. The values of the proposed constants are the result of the calibration of the model, applied by the researchers (JÚNIOR, 2017).

$$\tau = 17.13 \left(\frac{ON}{100}\right)^{3.402} P^{-1.7} e^{\frac{3400}{T}} \frac{\left(N^{0.1}\right)}{2.15} \tag{3.44}$$

Where:

- P: Pressure (Eq.3.34)
- T: Temperature (Eq.3.28)
- ON: Is the RON octane rating of the fuel
- N: Engine rotation speed in RPM

3.1.6 HEAT TRANSFER MODEL.

The modeling of heat transfer can be carried out from two main approaches: global or zonal. The zonal approach establishes the transfer of heat in specific places. Therefore, it is possible to implement turbulence models because the effect of the phenomenon is restricted.

One way to develop this approach is to consider that heat transfer occurs by conduction in a boundary layer. Other approaches work with the kinetic theory of gases (MOREL; KERIBAR, 1985).

In the global approach, empirical or semi-empirical models are implemented, which provide an average film coefficient for the entire boundary of the system. The definition of the system establishes the corresponding analysis region. The heat transfer is determined by Newton's law of cooling.

In 1963, Annand proposed a model (ANNAND *et al.*, 1963), based on dimensionless groups. In addition to convection, the film coefficient takes into account the heat transfer by radiation. Another widely used model is the one proposed by Woschni in 1967 (WOSCHNI, 1967). Another outstanding model is the one developed by Hohenberg in 1979 (HOHENBERG, 1979).

In 1988, Gallo (GALLO, 1990) showed that the results provided by the named models are quite close. Based on Gallo's conclusions, the model implemented in this document corresponds to the one proposed by Hohenberg, in addition to Newton's law of cooling.

3.1.6.1 *Newton's Law of Cooling.*

To calculate the temperature difference between a body and the environment that surrounds it, when this difference is not large, the heat transferred per unit time from the body or towards the body, by convection, conduction and radiation, is approximately equal to the difference of temperatures between the body and its surroundings. It is possible to raise the following energy balance:

$$\frac{dQ}{dt} = \alpha S(T - T_a) \tag{3.45}$$

where:

- Heat flow Q, as a function of time t $\frac{dQ}{dt}$
- Heat transfer coefficient α.
- Body area S.
- Body temperature T.
- Temperature of the medium surrounding the body T_a.

(Eq.3.45) can be transformed, to express the flow of heat in terms of the angle of rotation of the crankshaft. Defining $\alpha = h_c$ and establishing the heat flow for each zone, burned gases (b) and unburned (u), it is got:

$$\frac{dQ}{d\theta} = \frac{-Q_b - Q_u}{\omega} \tag{3.46}$$

where:

- ω, is the speed of the crankshaft.
- Q_b, Heat transferred through the area of burned gases.
- Q_u, Heat transferred through the area of unburned gases.

The heat transferred by the gas zones, burned and unburned, is defined by the following expressions:

$$Q_b = h_c A_b \left(T_b - T_w\right) \tag{3.47}$$

$$Q_u = h_c A_u \left(T_u - T_w\right) \tag{3.48}$$

where T_w corresponds to the wall temperature.

3.1.6.2 *The Hohenberg model.*

The Hohenberg model (HOHENBERG, 1979) establishes the following correlation for the calculation of h_c:

$$h_c = C_1 V^{-0,06} P^{0,8} T^{-0,4} \left(C_2 - v_{mp}\right)^{0,8} \tag{3.49}$$

where:

- C_1 and C_2, are the constants of Woschni and Hohenberg.
  - C_1 = 130
  - C_2 = v_p+1.4, where v_p = (2*L*N/60) whit L = Connecting rod length and N = Engine revolutions
- V, Internal volume of the cylinder.
- P, Pressure inside the cylinder.
- T, Temperature inside the cylinder
- v_{mp}, Average piston speed

3.2 EVAPORATION MODEL OF DROP.

Droplet evaporation is a phenomenon that can be experienced in daily life. When it is raining, some of the raindrops evaporate during the fall to the ground. That is, the liquid on the surface of the drop evaporates and mixes with the air around it, and as a result of this condition, it is possible to easily measure the resulting increase in moisture in the air after the rain. The evaporation of the drops is also a phenomenon of great interest in some industrial applications. It is the case of what happens in some restaurants in Sweden, where the air around these is

heated due to the emission of steam from the heaters of their kitchens, or in warm countries, external zones are cooled using the evaporation of drops emitted by evaporative coolers (Fig.3.3) (HOLDER, 2012).

Fig. 3.3 – Evaporative coolers. Source:(HOLDER, 2012)

.

The spray of fine drops is injected into the surrounding air. When these droplets evaporate in hot air, the energy required to break the molecular structure of the liquid state is called Latent Heat of Vaporization. This energy is taken by the drop from the air that surrounds it. Therefore, the latter lowers its temperature.

However, the main application of this droplet evaporation process is in the engines and the liquid fuel turbines. The fuel is injected into the combustion chamber. Due to the aerodynamic interaction with the surrounding fluid, instabilities are developed on the surface of the liquid jet, which leads to the disintegration of the liquid jet core and the creation of extended irregular liquid structures. The sequence of ruptures continues until a liquid spray is formed. At this point, the mass of liquid that is still connected is relatively small, and the forces of surface tension tend to give the liquid a spherical shape, dominating the inertial forces that tend to form structures. When the liquid structures are small and spherical, they are called drops.

When the first jet of liquid disintegrates into fine droplets, the surface/volume ratio increases significantly. As evaporation occurs at the liquid interface−gas, reduction in droplet size accelerates the evaporation process. The designer of a combustion chamber usually wants the drops to evaporate quickly and mix with the surrounding air, which improves the quality of the subsequent combustion, regarding efficiency and the level of exhaust gas. It is therefore of great interest to predict the evaporation of the drops analytically or numerically.

Based on the deduction shown in section 2.4.1, a simple drop model is defined, taking into account the assumptions that are listed in the same section.

3.2.1 SIMPLE MODEL OF DROP EVAPORATION.

In this section, a simple model of drop evaporation, applied to water, is implemented. The development shown here is based on the description presented in section 2.4.1 of this document, which is, in turn, based on the description found in (TURNS, 1996). It is required to determine the evaporation constant K, which relates the time of life of the drop, t_d, and the diameter of the same, D (Fig.2.5).

The initial data that are required for the calculation of the constant K are:

- The initial diameter of the droplet, D_0.
- The pressure of the gas where the droplet evaporates, P_r.
- The density of the liquid of the droplet, ρ_l.
- The temperature of the liquid, T_l, at the moment it enters the gaseous medium.
- The temperature of the gaseous medium,$\overline{T}_r$, which is taken as a reference to perform the correction of the density of the medium at that temperature, $\overline{\rho}$.

The required properties are:

- The temperature of saturation of the liquid for the pressure of the gaseous medium where it evaporates, T_{sat}.
- The enthalpy liquid-vapor of the evaporating liquid, h_{fg}.
- The molar weight of the evaporating liquid, MW_A.
- The diffusivity of the liquid that evaporates in the medium where it evaporates, D_{AB}. This is a property that is found in the combustion bibliography.

Once these properties are determined, using the data reported in the literature, the Spalding number for mass transfer is calculated B_Y, (Eq.2.93). This requires the fraction of mass of the substance that evaporates, A, on the surface of the drop. The Clausius-Clapeyron equation is integrated to find the saturation pressure at the temperature of the surface of the given drop (TURNS, 1996) .

$$\frac{dP}{P} = \frac{h_{fg}}{R_u/MW_A}\frac{dT}{T^2} \tag{3.50}$$

where R_u is the universal constant of ideal gases. For the reference state (P=P_r and T=T_{sat}) to the state at T_r.

$$\frac{P_{sat}}{P} = \exp\left[-\frac{h_{fg}}{(R_u/MW_A)}\left(\frac{1}{T_r}-\frac{1}{T}\right)\right] \tag{3.51}$$

The mole fraction of a component in a gas mixture is proportional to the partial pressure of the component within the mixture. Therefore, knowing P_{sat} from (Eq.3.51), it is possible to set X_A, which is the mole fraction of the component A in the liquid-vapor interface, on the surface of the drop

$$X_A = \frac{P_{sat}(T_l)}{P_r}. \tag{3.52}$$

Known X_A, the mass fraction of the $Y_{A,s}$ of component A can be established on the surface of the drop

$$Y_{A,s} = X_A \frac{MW_A}{X_A MW_A + (1-X_A)MW_B} \tag{3.53}$$

where MW_B is the molar weight of the gas where the drop evaporates.

Determined $Y_{A,s}$, it is possible to apply (Eq.2.73) to find B_Y, supposing that the mass fraction of component A, away from the drop, $Y_{A,\infty}$, is equal to 0.

The (Eq.2.80) shows that it is required to establish the ρD_{AB} product. From the literature, the diffusivity of substance A in medium B (D_{AB}) is known for a reference condition (Generally at P_{ref} = 1 Atm and T_{ref} = 298 K). Therefore, to find the value (D_{AB}) for the given conditions, the expression shown in (TURNS, 1996) is used, which relates the D_{AB} diffusivity with the temperature and pressure, to the given conditions.

$$D_{AB}(\overline{T}_r) = (D_{AB})_{ref}\left(\frac{\overline{T}_r}{T_{ref}}\right)^{(3/2)} \tag{3.54}$$

Once the value of the diffusivity of substance A in medium B has been established as a function of temperature, it is possible to calculate the product ρD_{AB}, where ρ corresponds to the density of the gaseous medium, to the given conditions, therefore it is also necessary to correct this value, for which the law of ideal gases is applied.

Known the product ρD_{AB} and B_Y, it is possible to apply (Eq.2.80) and determine the evaporation constant K. Once the value of K is established and with the initial diameter of the known drop, D_0, the (Eq.2.82) is applied to determine the drop's time of life, t_d.

The method described so far, allows to find the drop's time of life, t_d, when it evaporates in a gaseous medium constant pressure and temperature.

Because the conditions of pressure and temperature inside the cylinder change constantly, the method is implemented in a Matlab®function, to determine the fraction of mass droplet (or droplets) that evaporate during each step of the solution process.

3.2.2 MEAN DIAMETER MODEL FOR THE CALCULATION OF THE INITIAL SIZE OF THE DROP.

To estimate the average diameter of a drop formed by the breaking of a cylindrical jet of liquid, it is assumed that the drop is proportional to λ_{mu}^{n}, where $0 < n \leq 1$ is a coefficient determined by the breaking regime considered (For example $n = 1$ for the case of Rayleight break) (BALABEL; WILSON, 2013).

This implies that:

$$d_m = \beta \lambda_{mu}^{n} \tag{3.55}$$

in which β is a coefficient determined by the volume balance of the liquid jet in the nozzle and which depends mainly on the diameter of the emission nozzle d_0.

For the analysis shown here, N is the number of spherical drops, with an average diameter d_m and which are produced over a period of time Δt. It is considered that the total volume of the jet emitted by the nozzle during time interval, with an average speed u_{av} is equal to the total volume of the droplets formed during the break (BALABEL; WILSON, 2013), so:

$$\frac{\pi d_m^3}{6} N = \frac{\pi d_0^2}{4} u_{av} \Delta t \tag{3.56}$$

The rupture of the liquid jet in droplets is controlled almost exclusively by a very unstable wave disturbance in the early and subsequent stages of jet instability. Assuming that there is a direct relationship between the diameter of the droplets formed and the unstable wave disturbance at the surface of the jet (REITZ; BRACCO, 1982), this perturbation can be taken as a continuous phase and dispersed phase function depending on the dimensional characteristics of the nozzle.

From the above, it is possible to assume that:

$$u_{av} \Delta t = \sum_{i}^{N} \lambda_i = N \lambda_{mu} \tag{3.57}$$

Using (Eq.3.57) in (Eq.3.56), gives an expression for the mean diameter of the drop, (BALABEL; WILSON, 2013), so:

$$d_m = (1.5 d_0^2 \lambda_{mu})^{\frac{1}{3}} \tag{3.58}$$

Otherwise:

$$d_m = d_0 \left(\frac{1.5\pi}{\xi_{mu}} \right)^{\frac{1}{3}} \tag{3.59}$$

in which $\xi_{mu} = \frac{2\pi r_0}{\lambda_{mu}}$ is the dimensionless wave number.

The results of this model are compared with those of a series of experimental tests carried out for different types of nozzles (BALABEL; WILSON, 2013). From the results obtained, the

researchers established the following empirical relationship that follows the form proposed in (Eq.3.59) (BALABEL; WILSON, 2013).

$$d_m = \frac{a d_0^{\frac{3}{2}}}{p^{\frac{1}{3}}} \tag{3.60}$$

in which p is the pressure of the jet at the outlet of the nozzle, a=8.7066932 (BALABEL; WILSON, 2013) if p is in bar and if d_0 is in meters.

The results between the two models (theoretical (Eq.3.59) and empirical (Eq.3.60)) show error percentages between -3.4% and 1.9%. In the experiments, water was used as liquid in the nozzle and air as medium where the liquid is dispersed (BALABEL; WILSON, 2013).

This model was implemented within the program of simulation of drop evaporation since the substances used correspond to those assumed for the same.

3.2.2.1 **Jet breaking model.**

The primary rupture of the highly unstable initial drops is artificially modeled increasing its useful life in such a way that they coincide with the experimentally observed rupture lengths (ASHGRIZ, 2011). With greater accuracy, the value for the time of rupture, t_{bu}, is obtained from the experimental correlation of the length of rupture of the Levich jet (LEVICH, 1962).

$$L = u_0 t_{bu} = C_\lambda \sqrt{\frac{\rho_d}{\rho_g} d_0} \tag{3.61}$$

When the value of d_0 corresponds to the diameter of the nozzle, in the present case it is replaced by the value of the diameter of the injector hole, and u_0 corresponds to the exit velocity of the liquid through the hole. The constant C_λ depends on the nozzle, and the value of C_λ = 0.7 is the one that best corresponds to the observed experimental results. (ASHGRIZ, 2011). ρ_d corresponds to the density of the discharge liquid (water) and ρ_g corresponds to the density of the medium where the discharge is made (air).

The velocity, u_0, is estimated using the method found in (SAZHIN, 2014), where again the constant C_λ, also called the discharge coefficient, the pressure in the injector, Δp, and the density of the liquid, $\rho_d = \rho_l$, are related. This relation is deduced from the application of the classic wave model to experimental observations.

$$u_0 = C_\lambda \sqrt{\frac{2\Delta p}{\rho_l}} \tag{3.62}$$

3.2.2.2 **Drop size distribution model.**

Measuring the size of the drops and determining the distribution of their diameters, have been for years, the subject of research that, in the vast majority, are experimental. The

researchers develop methodologies to determine the size of the drops and, later, they propose statistical models that adjust with the relatively low percentages of error, to the observed data. However, the vast majority of these models is empirical and requires values that must be adjusted conveniently, for the data set of the sample, corresponding adequately with the proposed model.

Once the value of the average diameter is established, it is possible to choose the probability distribution function of the drop diameters. The chosen model corresponds to the one proposed by Rosin-Rammler (BABINSKY; SOJKA, 2002). This model was chosen because only two parameters are required to establish the distribution function. One of these parameters is the mean diameter which is known from equation (Eq.3.60), the other is an empirical factor q, which depends on the width of the spraying area of the spray. Small q values correspond to broad sprinkler areas while large q values correspond to narrow sprinkler areas. In the bibliography consulted the values of q are taken between 3 and 5, and for the case presented here it is assumed that q = 3 (LEFEBVRE; MCDONELL, 2017). (Eq.3.63) describes the probability distribution function used:

$$f_0(D) = q\overline{D}^{-q} D^{q-1} \exp\left[-\left(\frac{D}{\overline{D}}\right)^q\right] \tag{3.63}$$

where $\overline{D}$ corresponds to the mean diameter ($\overline{D} = dm\ in$ (Eq.3.60)), D the value of the diameter whose probability is to be established.

3.3 GEOMETRICAL AND KINEMATIC CHARACTERISTICS OF THE DEVICE (ENGINE) USED FOR THE IMPLEMENTATION OF THE DESCRIBED MODEL.

For the verification of the model described here, the geometric and kinematic description of an ICE SI type device is required. Parameters such as cylinder diameter, piston stroke, compression ratio, number of cylinders, type of fuel injection system and water and total volumetric displacement, among others, are necessary for the implementation of the simulation model.

Table 3.1 shows the values of these parameters that are considered in the different cases proposed for the implementation and validation of the simulation model described in this chapter, with an engine that uses gasoline as fuel. Since these values are constant and do not depend on atmospheric conditions or operating regime, it is only necessary to establish them once.

Table 3.2 shows the values of the parameters mentioned above, which are considered in the different cases proposed for the implementation and validation of the simulation model, with an engine that uses ethanol as fuel.

The geometrical description in table 3.2 corresponds to an ethanol engine located at the MAUA Institute of Technology and whose performance and performance data are used in this research to validate the performance of the proposed simulation program.

Table 3.1 – Engine Specifications for simulation (Gasoline) (KIM *et al.*, 2016)

Engine Specifications for simulation (Gasoline).	
Bore (*mm*)	77
Stroke (*mm*)	85.4
Compression ratio	13.5
Number of cylinders	1
Displacement of cylinder (mm^3)	398.8
Fuel injection system	Fuel injection port
Water injection system	Direct injection

Table 3.2 – Engine Specifications for Simulation (Ethanol).

Engine Specifications for Simulation (Ethanol).	
Compression Ratio	12.25
Connecting rod length (*mm*)	145.6
Eccentricity Piston-Crankshaft	0.0069
Bore (*mm*)	75
Ratio Stroke-Diameter	90.473/75
Cylinder volume (mm^3)	400
Number of cylinders	1
Fuel injection system	Fuel injection port

The operating parameters that are not constant and depend on the rotation regime and the atmospheric conditions are listed in the results section together with the data delivered by the simulation model for each case studied.

4 RESULTS AND ANALYSIS

This chapter presents the results of the computational implementation of the mathematical models enunciated in chapter three. It begins with the functional verification of the droplet evaporation model together with the droplet size probability distribution function, the latter is determined once the average droplet diameter is known, which is calculated from the diameter of the water injector orifice. The evaporation model shows how the diameter of the droplet varies as a function of time when the droplet is evaporating in a hot gaseous medium. This model is incorporated in the thermodynamic model of an ICE SI cycle with direct water injection in the combustion chamber. The validation of the model is carried out by comparing the results of the simulations with two experimental data sources.

Initially the comparison is presented with the results of an investigation where a system of direct injection of water into the combustion chamber was implemented in one of the cylinders belonging to an ICE SI atmosphere engine that uses gasoline as fuel (KIM *et al.*, 2016). All known parameters of engine geometry and performance are entered as input data into the simulation program built from the proposed set of models (droplet evaporation, droplet size distribution and two-zone thermodynamic model) of the cycle operation of an ICE SI engine with direct water injection into the combustion chamber. The results of this validation are evaluated and analyzed to determine the level of similarity between the data obtained through simulation under the operating conditions presented in (KIM *et al.*, 2016) and the experimental data consulted in (KIM *et al.*, 2016). The step used is 0.05° of the angle of the crankshaft, with θ as the independent variable. The water is injected in liquid form at a temperature of 373.15 K and a pressure of 50 bar, using an injector located in the area of the combustion chamber. The spray pattern and droplet formation correspond to those shown in (LEVICH, 1962), (BALABEL; WILSON, 2013) and (LEFEBVRE; MCDONELL, 2017) where the distribution of the droplet diameter, calculated from the diameter of the water injector orifice is included.

The results of a second comparison with experimental data are presented later. This data was provided by the MAUA Institute of Technology and is the result of a series of tests carried out there on an ICE SI atmospheric engine that uses ethanol as fuel but does not have a water injection system. In the same way as in the previous case, all the parameters of the geometry and the functioning of the engine necessary to execute the simulation, are entered into the program as input data. Although this engine does not have water injection, the results of the comparison have special relevance since they allow to establish the level of flexibility of the program and its capacity to interpret the phenomenology of the operation and performance of engines of different geometries and the once use different fuels. As in the case of gasoline or ethanol.

The final part of the chapter corresponds to the results of the simulation of the process of direct injection and evaporation of water, in an atmospheric engine that uses ethanol as fuel.

Using the geometrical and operating parameters of the engine studied by the MAUA Institute of Technology, the simulation is performed to determine the possible advantages and disadvantages of the direct injection of water techinique water into the combustion chamber in this type of engines widely used in Brazil.

4.1 RESULTS OF THE EVAPORATION MODEL OF WATER DROPLET

The droplet evaporation model described in the section 2.4.1, establishes a linear relationship between the lifetime of the drop (t_d), and the initial diameter of the droplet (D_0) using the evaporation constant K (Eq.2.83). This relationship is valid for constant pressure and temperature conditions of the gaseous medium where the water drop evaporates. It is known that inside the cylinder the conditions of pressure and temperature are not constant and vary according to the movement of the piston. However, it is mentioned at the beginning of chapter 3, that for the numerical solution of the equations deduced in sections 3.1 and 3.2, the Runge-Kutta method of 5th order was implemented, which uses a discretization step of 0.05° of the angle of the crankshaft. It is during this step of discretization that the conditions are assumed to be constant, and therefore it is possible to apply the droplet evaporation model.

The mean diameter (d_m) is calculated from (Eq.3.59) which is a function for the calculation of the mean diameter of the drop, depending on the diameter of the orifice of the injector. Once the mean diameter is known, the droplet size distribution function described in section 3.2.2.2 can be applied. The distribution function used establishes the probability of occurrence for each of the droplet diameter length ranges, within the total group of drops released by the injector. For the particular case discussed here, an injector diameter of 0.6 mm was chosen, and the droplet size ranges were restricted to 0.005 mm, for a total of 120 possible droplet size ranges. The mean diameter (d_m) calculated by applying the (Eq.3.59) is 34,73 microns. (d_m in (Eq.3.59) is $\overline{D}$ in (Eq.3.62)).

(Fig.4.1) presents the probability distribution function for the previous parameters supplied to the (Eq.3.62). (Fig.4.2) illustrates the evolution in time for 10 different initial droplet diameters, within the ranges established for the probability distribution function.

4.2 VALIDATION OF SIMULATION RESULTS COMPARED TO EXPERIMENTAL DATA.

4.2.1 VALIDATION OF THE SIMULATION PROGRAM TO THE OPERATING CONDITIONS OF THE GASOLINE ENGINE AND WATER INJECTION SYSTEM.

The validation of the model is carried out using the geometric configuration presented in Table 3.1 (KIM *et al.*, 2016). (Fig.4.3) illustrates a schematic diagram of the combustion chamber and cylinder assembly with the arrangement of the water and fuel injectors. In addition

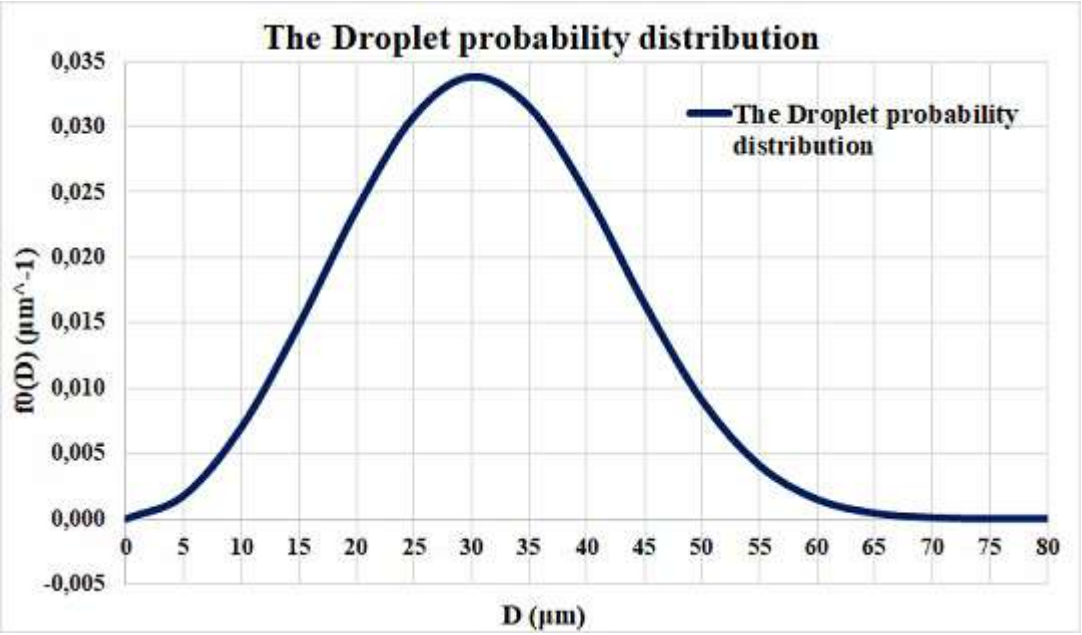

Fig. 4.1 – Droplet size probability distribution function.

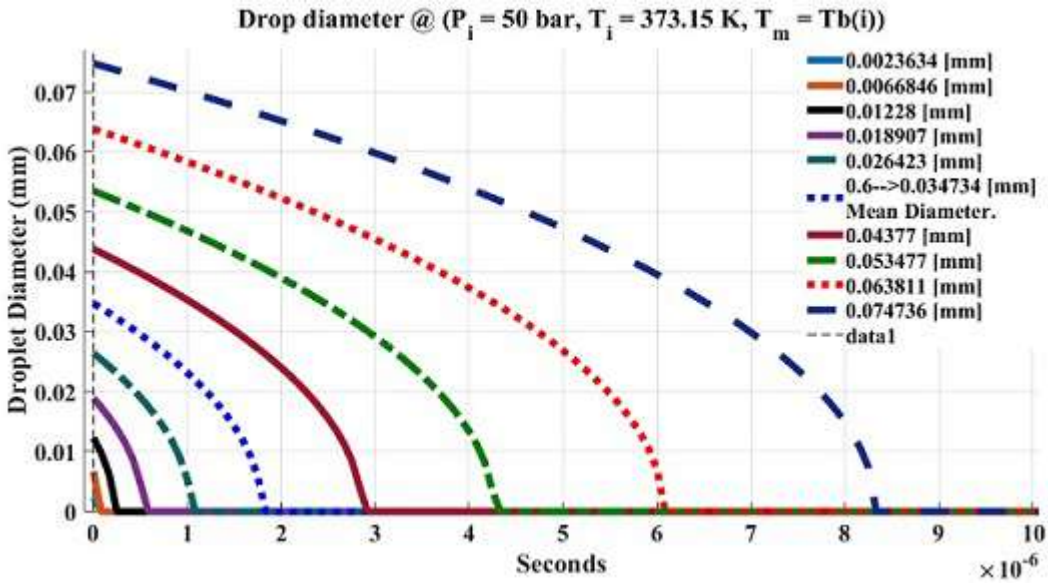

Fig. 4.2 – Evaporation time vs. Droplet diameter. (P_i = Injection pressure, T_i = Injection temperature, T_m = T_b = Temperature of the burned gases)

to the information on the geometrical configuration, the valve command used in the tests is provided and reproduced in the simulations (Table 4.1). The fuel used in the experiments is gasoline, and the operating regime is 2000 RPM, with 90 Nm of breaking load.

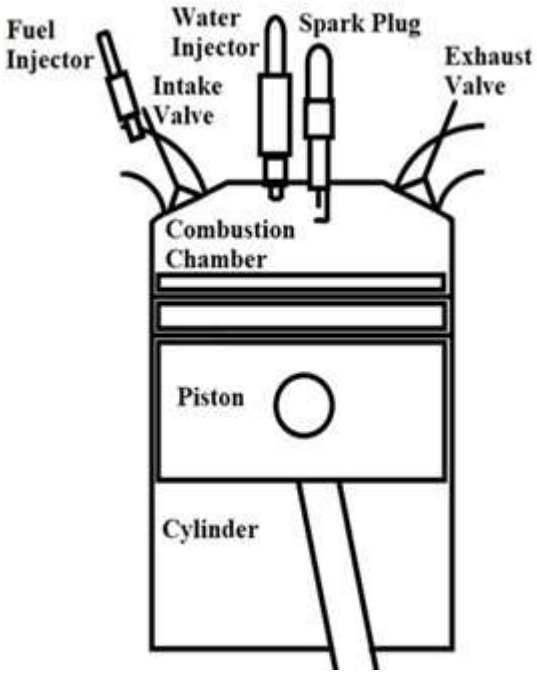

Fig. 4.3 – Schematic diagram of the water and fuel injection systems used in the simulations.

Table 4.1 – Valve timing condition. BTDC (Before Top Dead Center), ATDC (After Top Dead Center), ABDC (After Bottom Dead Center). BBDC (Before Bottom Dead Center)(KIM *et al.*, 2016)

Valve Timings	
Parameters	
Intake valve opening	43° **BTDC**
Intake valve closing	28° **ABDC**
Exhaust valve opening	17° **BBDC**
Exhaust valve closing	26° **ATDC**
Valve Overlap	69°

Table 4.2 illustrates the relationship established to determine the amount of water injected in the experiment. The experiment reports that two spark advance values were used in relation with the compression top dead center, the experiment reports that two spark advance values were used were $-8.3°$ and $-14.2°$. The water is injected 240° after the TDC, at the end of the exhaust and the beginning of the intake. The degrees are measured according the rotation of the crankshaft.

Table 4.2 – Water/Fuel Ratio used to determine the amount of water injected. 2000 RPM. (KIM *et al.*, 2016)

Fuel Mass (kg)	Water Mass (kg)	Ratio Water/Fuel
$1.98E-05$	$0.00E+00$	0%
$1.98E-05$	$5.46E-06$	28%
$1.98E-05$	$9.92E-06$	50%
$1.98E-05$	$1.98E-05$	100%

To compare the simulated data with the experimental data, the results of pressure and fraction of mass burned presented in (KIM *et al.*, 2016) were digitized using the free distribution Engauge Digitizer®software.

The case initially analyzed corresponds to the test without water injection. For this case, the average relative error for the pressure, when comparing the results of the simulation model with the experimental data provided by (KIM *et al.*, 2016) is 2.12% (Fig.4.4).

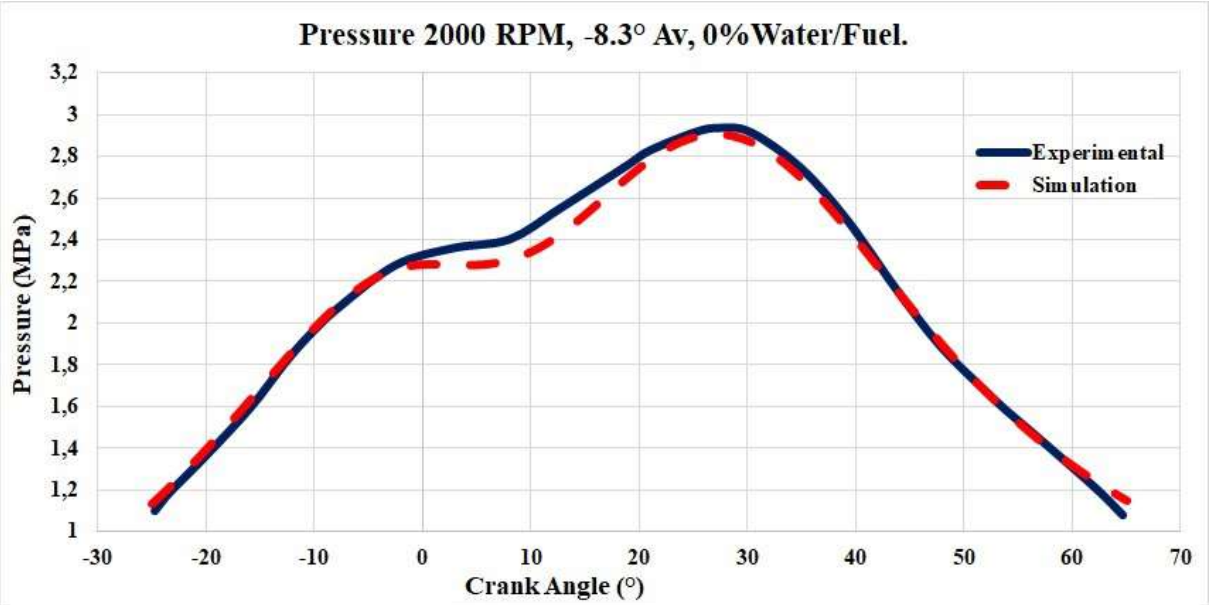

Fig. 4.4 – Comparison of pressure curve for $-8.3°$ of advance, without water.

However, for the fraction of mass burned (Fig.4.5), the relative error has a behavior that is strongly influenced by the large difference presented by the comparison between the data at the beginning of the curve. By carefully observing the behavior of the fraction of mass burned at the beginning of the curve of the experimental data (KIM *et al.*, 2016), it is possible to observe that there are negative values of up to -2.07%.

On the other hand, in the simulated data, the lowest value calculated for that same part of the curve of the mass fraction burned is -0.75%. These negative values indicate that heat transfer

at the beginning of combustion occurs from the walls of the cylinder to the contained gases, heating the mixture as the mass of burned gas increases, this tendency reverses. In consequence of not being able to establish with more precision the model of heat transfer between the walls of the cylinder and the gases contained in it, at the beginning of the combustion, a notable difference between the two data sets is observed. Therefore, in the case of the fraction of mass burned, a particular point was taken to make the comparison between the experimental data and those provided by the simulation. The experimental point used to compare, in which the percentage of burning reaches 50% of the mass contained in the cylinder, is (27.35° Crank Angle). For this condition, the relative error between the experimental data and that obtained by the simulation is 9% (Fig.4.5).

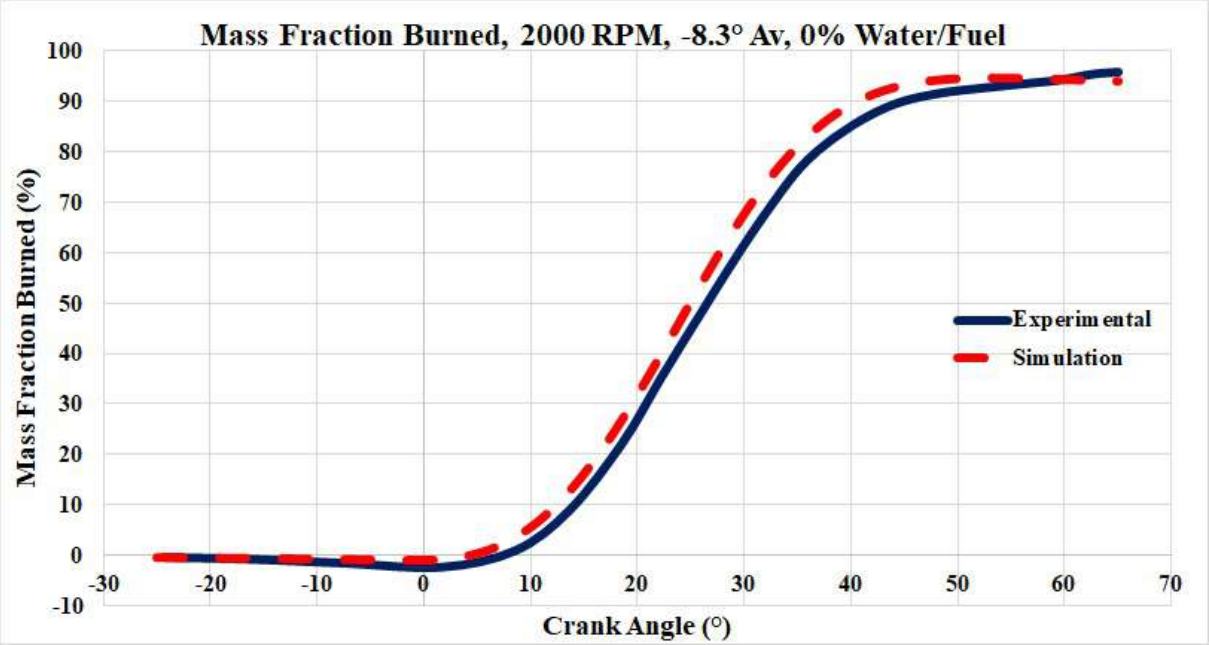

Fig. 4.5 – Comparison of the mass fraction burned to $-8.3°$ of advance, without water.

Afterward, the first case is analyzed with water injection (Fig.4.6). The average relative error found when comparing experimental and simulated data is 2.37%. The trend observed above (Fig. fig4.4) is maintained for this case.

On the other hand, the behavior of the burned mass fraction (Fig.4.7), for the point where 50% of the mass contained in the cylinder is reached, presents a relative error between the experimental data and the simulation data of 13% ($-8.3°$ spark advance and 28% water/fuel).

(Fig.4.8) and (Fig.4.9) again illustrate the experimental and simulated behavior of the pressure and mass fraction burned, respectively with 5.4 mg of injected water (28% water/fuel, Table 4.2) but with an advance of $-14.2°$. For this condition, the average relative error found for the pressure is 2.15%. In the three conditions compared, it is observed that the error between the simulation and the experimental data is less than 2.5% in the case of pressure.

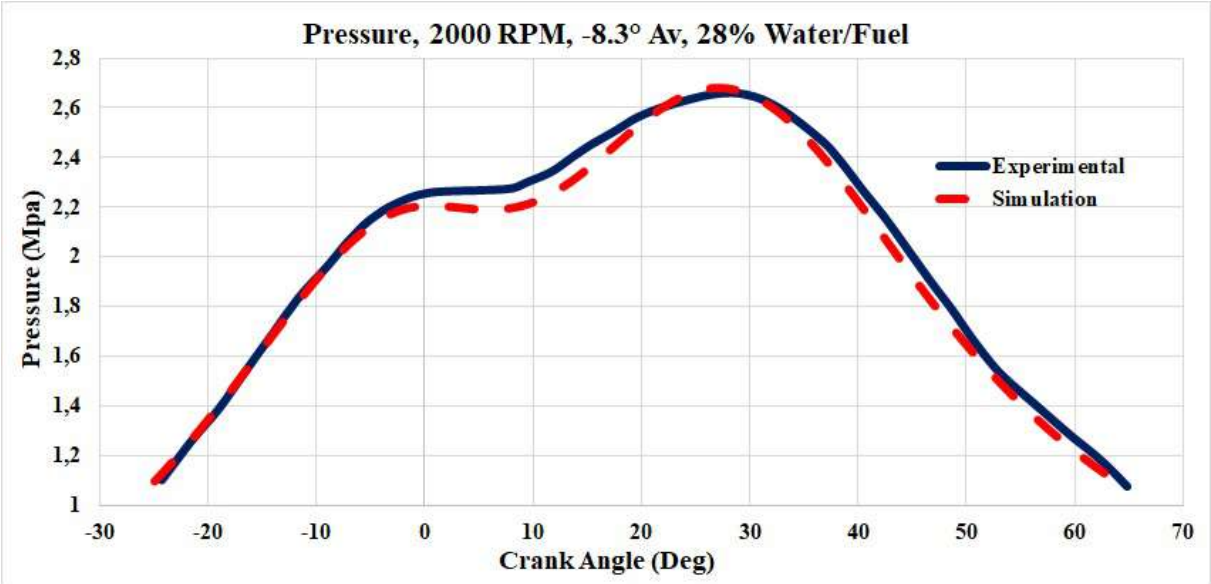

Fig. 4.6 – Comparison of pressure curve for $-8.3°$ of advance, 28% Water/Fuel.

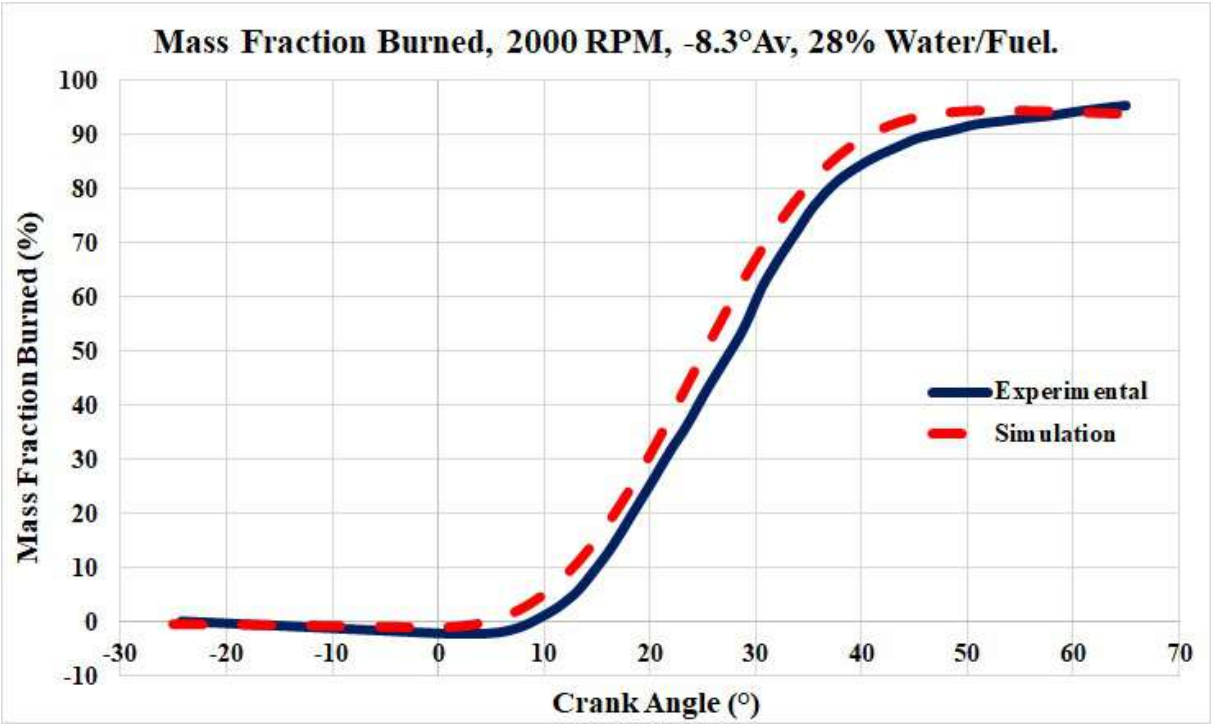

Fig. 4.7 – Comparison of the mass fraction burned to $-8.3°$ of advance, 28% Water/Fuel.

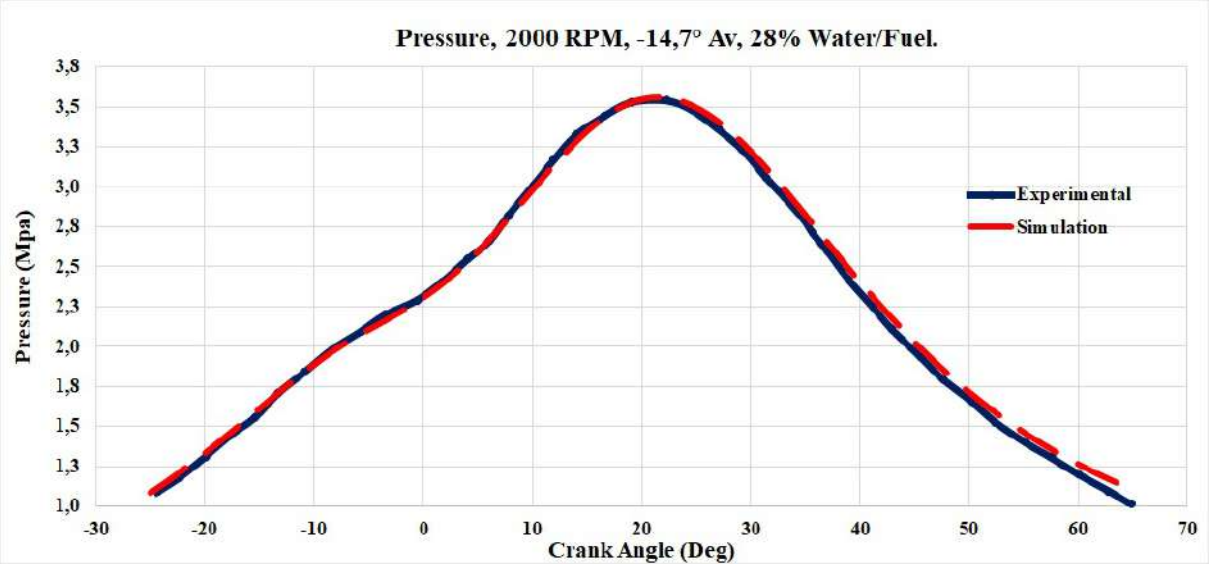

Fig. 4.8 – Comparison of pressure curve for $-14.2°$ of advance, 28% Water/Fuel.

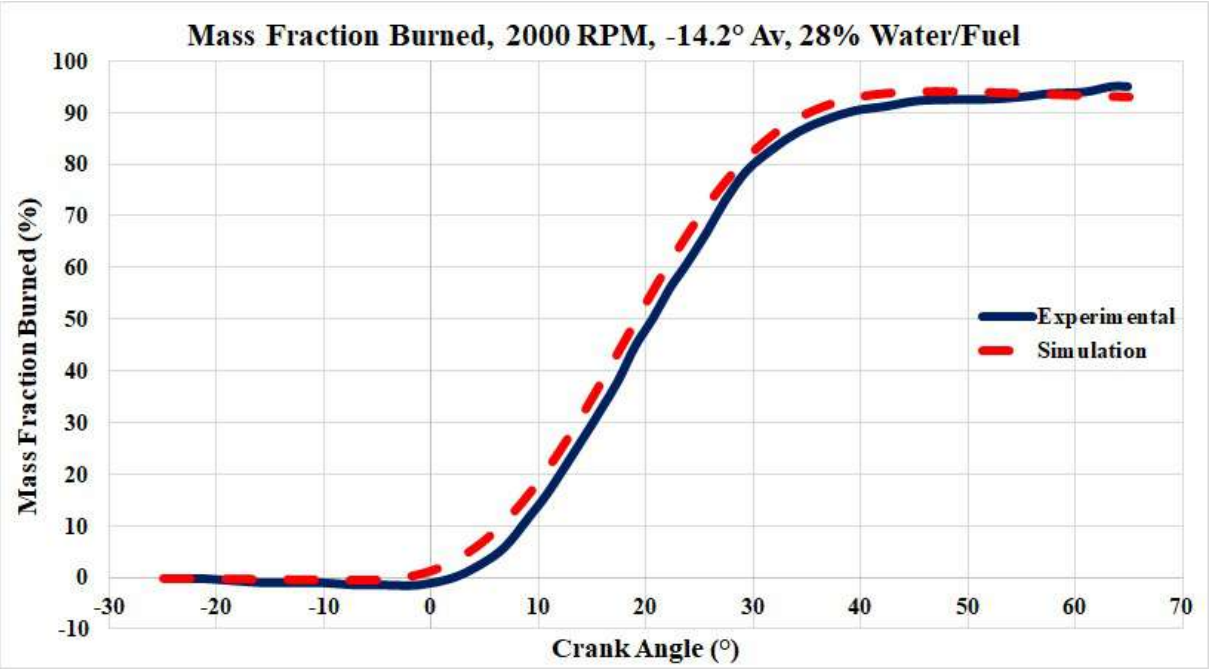

Fig. 4.9 – Comparison of the mass fraction burned to $-14.2°$ of advance, 28% Water/Fuel.

It is important to confirm that, in none of the cases compared so far in this validation, the trend of the simulation model has presented differences in its behavior. This is demonstrated by observing that the values of the relative error calculated for the pressure are very close in the three cases (2.12% first case without water, 2.36% second case, with 5.4 mg water and -8.3° advance and 2.15% third case, with 5.4 mg of water and -14.2° of advance). These actions are repeated with the fraction of burnt mass. For the third comparison condition, the relative error calculated between the point where the experimental data reported 50% of the burned mass (20.58°) and the percentage of mass burned for the same point reported by the simulation is 10.42%.

Although the values of the relative error calculated for the percentage of mass burned are markedly greater than for the case of pressure (9% for the first case without water, 16.36% second case with 28% water/fuel and $-8.2^{\circ}$of advance and 10.42% of the third case with 28% water/fuel and -14.2° of progress) showing coherence, since the trend of the approach does not change.

Another variable that can be compared corresponds to the specific fuel consumption at brake (BSFC) (Table 4.3). The results provided by (KIM *et al.*, 2016) are in the first column, for the three cases analyzed thus far. The second column contains the results delivered by the simulation model. Columns three and four identify each of the cases, specifying the advance of the spark and the water/fuel ratio used for water injection. Finally, column five calculates the value of the relative error between the data. As it can be seen, this is less than 2% in all three cases.

Table 4.3 – Comparison of BSFC. 2000 RPM.

BSFC g/kWh				
Experimental	**Simulate**	**Advance (°)**	**Water/Fuel**	**% Error**
275.6	273.62	-8.3	0	0.72
283.3	279.48	-8.3	28	1.35
265.5	268.41	-14.2	28	1.09

In addition, the maximum pressure in the different conditions was analyzed. When comparing the values of the maximum pressure for the same advance condition (-8.3°) without water (Fig.4.4) and with water (Fig.4.6), it can be seen that in the case where the water injection was used, the value of the maximum pressure is lower than for the waterless condition, both in the experimental and simulated data (Fig.4.10).

This decrease in pressure is a consequence of the heat demand of the liquid water that enters during the injection. The water absorbs part of the available energy of the hot gases contained in the cylinder and changes phase. Consequently, internal temperatures decrease ((Fig.4.11) and (Fig.4.12)) due to the relationship between pressure and temperature given

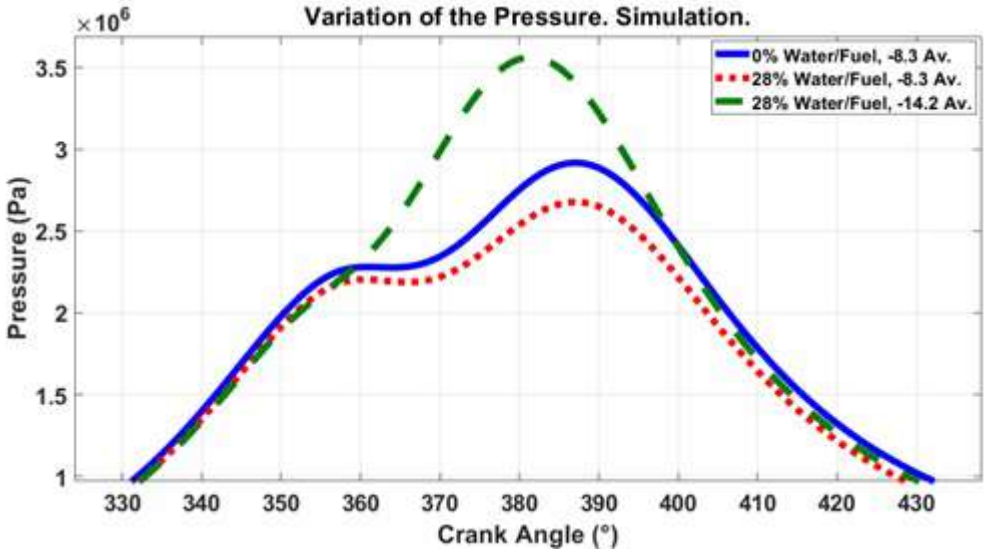

Fig. 4.10 – Comparison of the behavior of the pressure, for the three cases subject to analysis. Simulation.

by the ideal gas law, which states that when the temperature decreases, so does the pressure (Fig.4.10), while the volume remains constant. The assumption of constant volume is related to the step taken for the resolution of the model in Matlab. At the beginning of this chapter, it was established that the step used corresponds to 0.05° of the angle of the crankshaft. It is during this time (the length it takes the crankshaft to rotate 0.05°) that the volume is assumed to be constant. Therefore the statement made above regarding the relationship between pressure and temperature for a constant volume is valid.

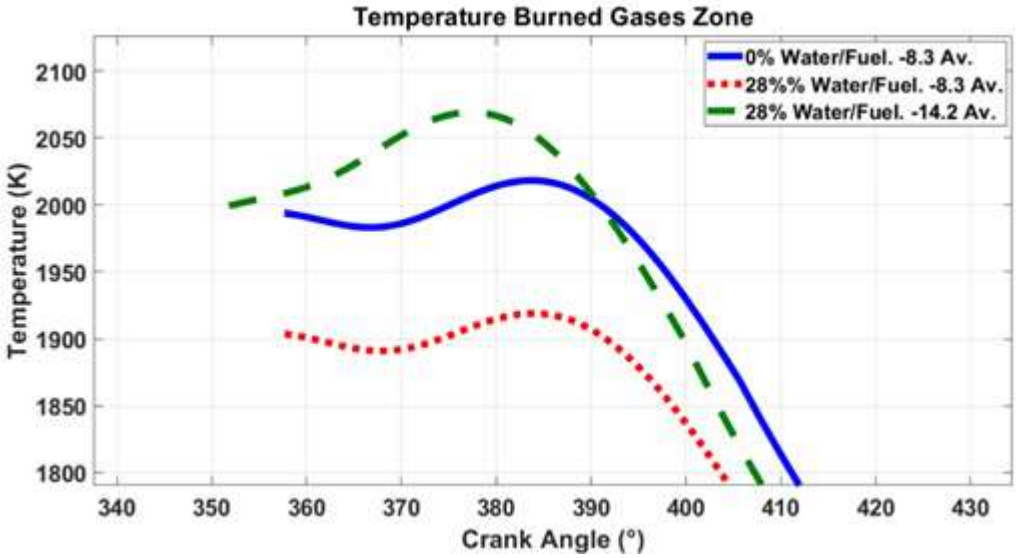

Fig. 4.11 – Comparison of the behavior of the temperature in the burned gases zone, for the three cases subject to analysis. Simulation.

The maximum pressure decreases with water injection (Fig.4.10), for the same spark advance condition, ($-8.3°$, blue line without water and red line with 28% water/fuel). This

effect is more noticeable in the temperature of the area of burned gases (Fig.4.11), where the injection of water used (28% water/fuel) decreases close to 100 K of the temperatures reached inside the cylinder from the start of combustion. On the other hand, this effect on the temperature observed in (Fig.4.11) is less noticeable for the temperature of the area of unburnt gases (Fig.4.12), although a slight decrease in the maximum temperature is still observed.

The behavior of the pressure and temperature curves, for an advance of $-14.2°$ and 28% water/fuel of the injection water, are the result of the advance value. This is due to the time it takes for combustion to reach the maximum temperature value in relation to the time when the piston reaches the TDC.

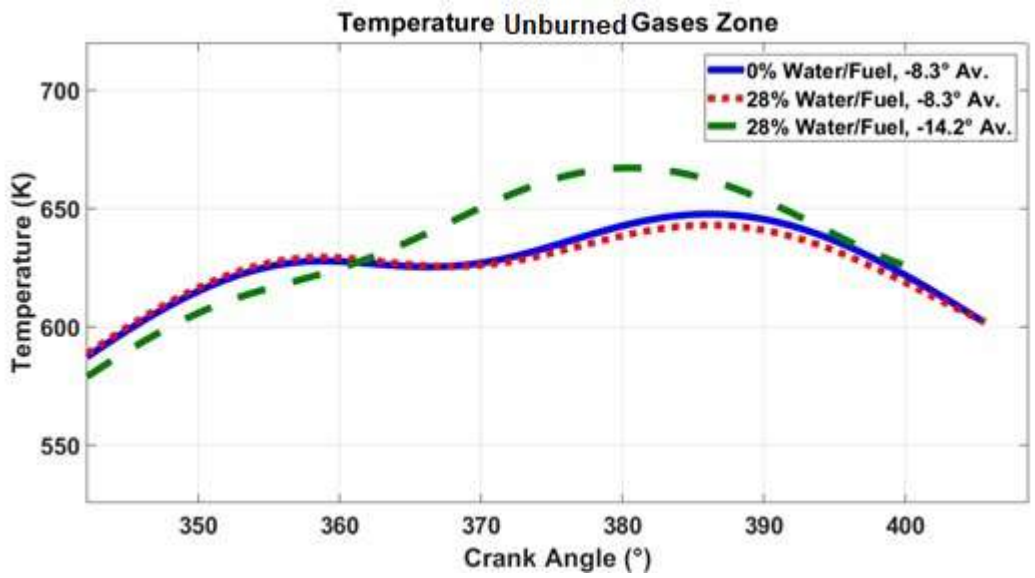

Fig. 4.12 – Comparison of the behavior of the temperature in the unburned gases zone, for the three cases subject to analysis. Simulation.

The last comparison presents a spark advance of $-29.3°$ and a water/fuel ratio of 100%, for the same conditions of rotation and load (2000 RPM and 90 Nm of load at brake).

For the latter case, the relative error obtained when comparing the experimental data and those delivered by the 0.92% simulations (Fig.4.13).

Based on the comparisons it is possible to concluded that the engine model implemented in the simulation demonstrates a great consistency and precision in the prediction of the behavior of the pressure inside the cylinder during the closed phase, both without injection of water and for the different spark advance conditions and quantities of added water.

Moreover, when comparing the behavior of the data for the fraction of burned mass (Fig.4.14), it is appreciated that in the first part of the curves, between 0 and 60% of burned mass, the trend that was observed in previous analysis is maintained (Fig.4.5), (Fig.4.7) and (Fig.4.9). Even when calculating the relative error between the simulation model and the experimental data, for the point where 50% of burned mass was reached, this error is 9%. The error

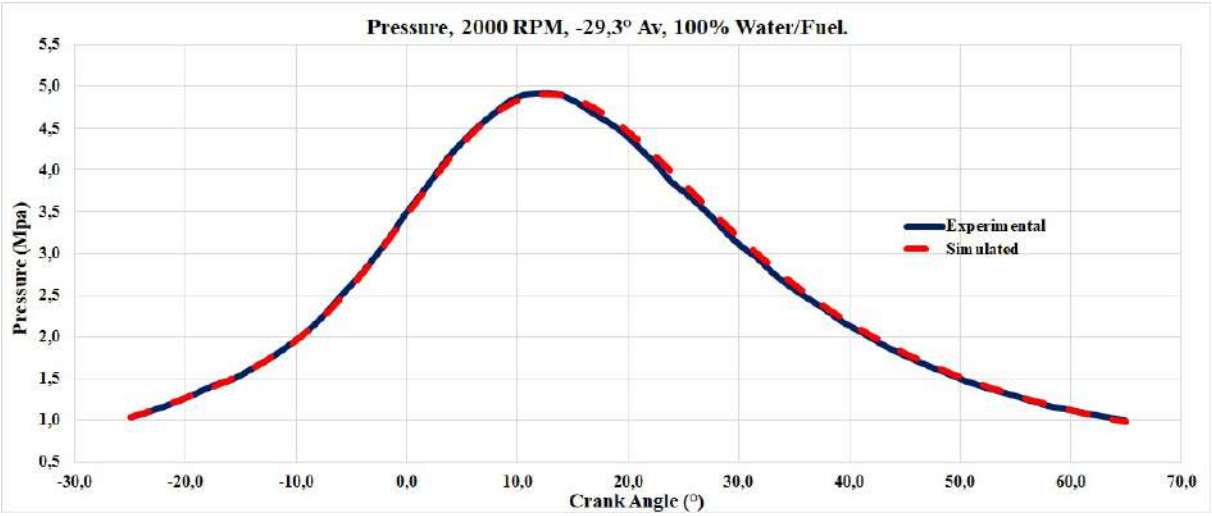

Fig. 4.13 – Comparison of pressure curve for −29.3° of advance, 100% Water/Fuel.

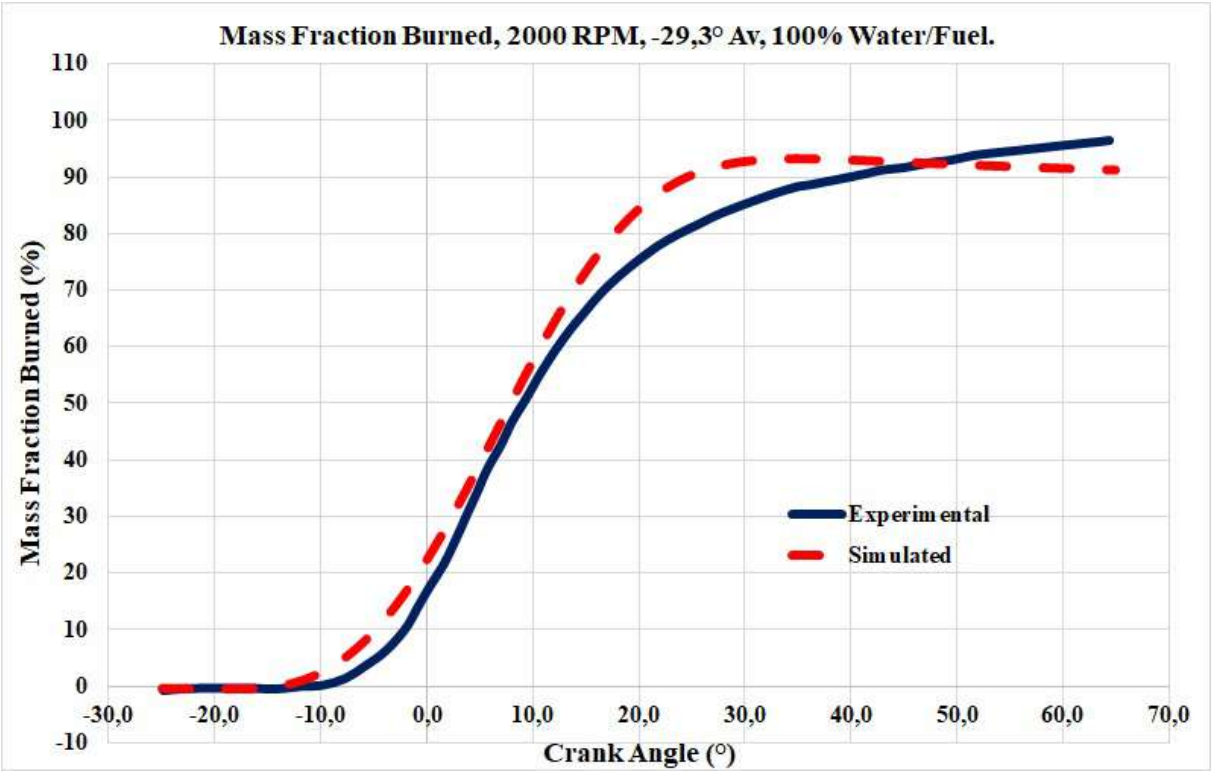

Fig. 4.14 – Comparison of the mass fraction burned to −29.3° of advance, 100% Water/Fuel.

value is in agreement with those calculated previously for the cases already analyzed.

However, from the point of 60% of the burned mass and until the end of the curves (Fig.4.14), a very clear divergence between the experimental data and the simulation model is observed. This divergence can be explained by the lack of knowledge of the model used by researchers to interpret heat transfer. In the simulation, it was established that the Hohenberg proposal is used (HOHENBERG, 1979), but due to the limited information available about the experiment reported in (KIM *et al.*, 2016), it is not possible to determine to what it extends the heat transfer model, implemented in the simulation corresponding to the experimental data. This consideration is also relevant to understand the oscillation values of the relative error between 9 and 13% for the three previous cases already discussed.

Table 4.4 – Comparison of BSFC. 2000 RPM. Full load condition.

2000 RPM			
Water/Fuel	**Experimental (KIM *et al.*, 2016)**	**Simulated**	**% Error**
	BSFC (g/kWh)	**BSFC (g/kWh)**	
0%	**301.14**	**290.9**	**3.4**
20%	**288.9**	**290.63**	**0.6**
40%	**281.14**	**291.19**	**3.57**
60%	**278.68**	**291.09**	**4.45**
80%	**273.77**	**291.18**	**6.36**
100%	**261.53**	**291.77**	**11.56**

Yet again, the specific fuel consumption to the brake (BSFC) is compared. Similar to what was previously used (Table 4.3), the rotation regime is the same (2000 RPM) but this time at full load. Besides, the data reported shows variation in the amounts of water injected and in the values for the advance of the spark (KIM *et al.*, 2016). Comparing the results provided by the simulation model with the experimental data (Table 4.4), it is observed that the relative error value varies from 0.60%, for the case without water injection, to 11,56% for the case with water injection, 100% water/fuel ratio. However, between 0% and 80% water/fuel ratio, the relative error does not exceed 7%, demonstrating once again that the simulation model is successful since it interprets the operation of the test engine.

Finally, the NOx emission index is compared to a regime of 1500 RPM and full load. It is observed that the differences between the experimental data (KIM *et al.*, 2016) and those provided by the simulation model are quite evident (Table 4.5), especially for the case without water injection, where the relative error is 29.09%.

On the other hand, for cases with water injection, the relative error is significantly lower and it shows a progressive decrease, showing that the trend in the values reported by the simu-

Table 4.5 – Comparison of NOx Emissions. 1500 RPM, Full load condition.

1500 RPM			
Water/Fuel	**Experimental (KIM *et al.*, 2016)**	**Simulated**	**% Error**
	NOx (PPM)	**NOx (PPM)**	
0%	**1836.1**	**1302**	**29.09**
20%	**1455.77**	**1253**	**13.93**
40%	**1289.33**	**1199**	**7.01**
60%	**1225.23**	**1142**	**6.79**
80%	**1112.78**	**1081**	**2.86**
100%	**1175.27**	**1016**	**13.55**

lation is the same as in the case of the experimental data. The simulation presents a very stable behavior and the reported values decrease as the amount of water injected increases (Fig.4.15).

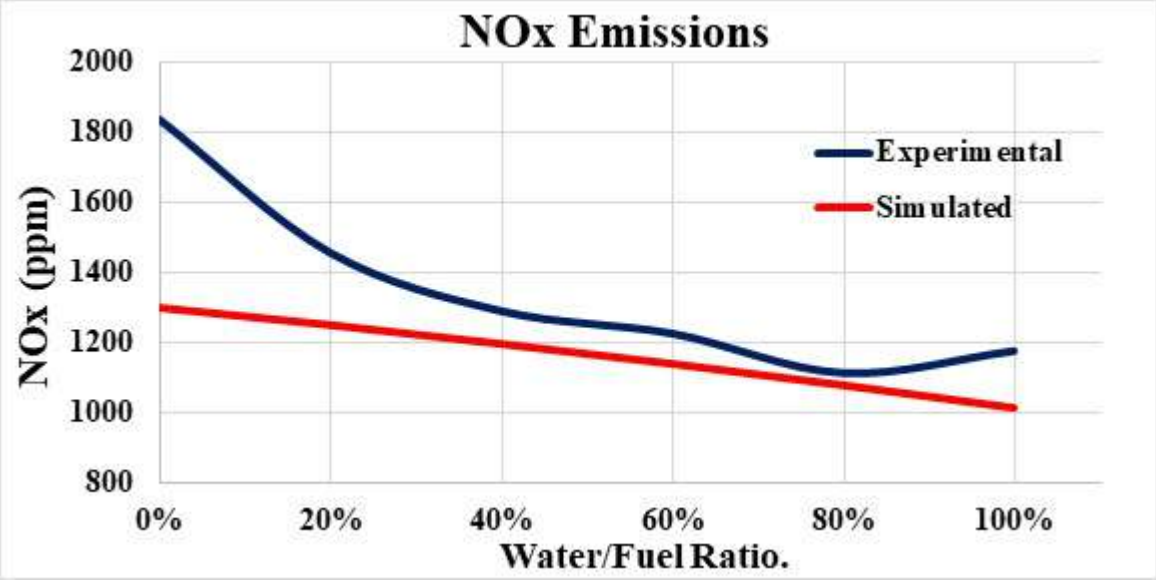

Fig. 4.15 – Comparison of NOx Emissions. 1500 RPM.

Although the experimental data shows a more random behavior, where the tendency to decrease emissions is evident between a 20% water/fuel ratio and 80% water/fuel, it tends to increase slightly when the water/fuel ratio is of 100% (Fig.4.15). The simulation again demonstrates a consistent behavior with that reported by (KIM *et al.*, 2016) and with the same tendency for most of the experimental results.

4.2.2 VALIDATION OF THE SIMULATION PROGRAM TO THE OPERATING CONDITIONS OF THE ETHANOL ENGINE WITHOUT WATER INJECTION. (MAUA).

The second validation of the performance and reliability of the proposed simulation program is performed by comparing the data from some of the experimental tests carried out at the MAUA Institute of Technology on an atmospheric engine, that uses ethanol as fuel and has no water injection system, with the results delivered by the simulation program, for the same conditions of geometry and operation.

Table 3.2, presented in chapter three, shows the geometric parameters of the test engine used in the MAUA Institute of Technology experiments. Table 4.6, presented below, contains the other operating parameters necessary for running the simulations under the same operating conditions of the engine used in the tests. Five engine rotation regimes were chosen to perform the simulations and compare the results with the experimental tests. These are: 1000, 2000, 3000, 4000, and 5000 RPM. Several rotation speeds were chosen to perform the comparison in order to verify the reliability of the simulation program under different operating conditions, all in full load.

Tables 4.7 to 4.11 present a comparison between the results of the simulation and the experimental data, for the performance parameters mentioned below: Power, Torque, Instantaneous Fuel Consumption, Specific Fuel Consumption, Mean Indicated Pressure, Maximum Value of the Pressure reached during compression, expansion and at the point, measured in degrees of crankshaft rotation, where its maximum pressure is reached.

Next to each table, the corresponding graph is presented, which compares the behavior of the pressure inside the cylinder during the cycle, both experimental and simulated. (Fig.4.16 to 4.20)

The first case of comparison corresponds to 1000 RPM at full load. It is observed that the values of the compared parameters do not exceed 3.5% error between the simulation data and the experimental data in most cases. Only for Instantaneous Consumption there is a relative error of 12.99% (Table 4.7). However, it is worth noting that the instantaneous consumption values are very close, even though the relative error seems to indicate a great difference between them. This discrepancy is due to the magnitude of these values (Instantaneous Consumption) which are less than 1.5 kg/h, besides it must be considered that the simulation program, despite it interpretes correctly the phenomenology of the processes inside the cylinder, as evidenced by the values of the other parameters and the proximity of the pressure curves (Fig.4.17), it does not take into account the variability present in the real test process and all the environmental alterations that may affect it directly, such as air quality and the fuel used on the day of the test.

The second case of comparison corresponds to the regime of 2000 RPM, again in full load. The trend observed in the previous case is maintained in this sample. The absolute value of the relative error between most of the simulation data and the experimental tests does not

Table 4.6 – Data Simulations for the ethanol engine without water injection. (MAUA).

Data Simulations for the ethanol engine without water injection					
	1000 RPM	**2000 RPM**	**3000 RPM**	**4000 RPM**	**5000 RPM**
Form factor	2.0	2.04	2.0	2.1	1.8
Duration of combustion (°)	34.5	38.7	43.4	46.1	49.2
Delayed start of combustion with respect to ignition (°)	5.0	6.1	5.0	4.0	7.0
Spark Advance (°)	-10.5	-16.3	-17.5	-18.3	-20.8
Combustion efficiency (%)	79.364	78.585	87	92	90.236
Lambda	0.90136	0.87087	0.89297	0.878904	0.850958
Inlet pressure (Pa)	91605.4	91275.79	90082.09	89750.36	89585.64
Cylinder wall temperature (K)	520	520	520	520	520
Load	1.0	1.0	1.0	1.0	1.0
Valve opening time (°)	245	245	245	245	245
Inlet valve opening (°)	-20	-20	-20	-20	-20
Close exhaust valve (°)	15	15	15	15	15
Over position of the valves (°)	35	35	35	35	35
Relative humidity (%)	50	80.3	50.77	78.78	62

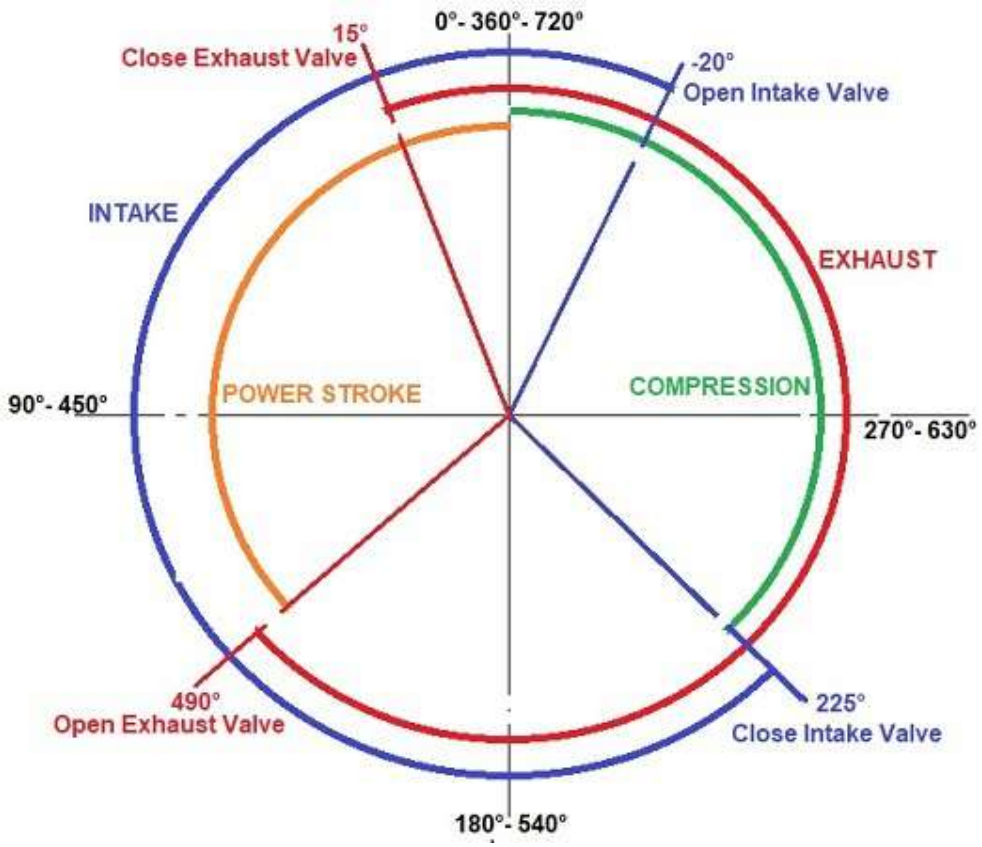

Fig. 4.16 – Duty Cycle.

Table 4.7 – 1000 RPM

1000 RPM			
Performance Parameters	**Simulation**	**Experimental**	**Error (%)**
Power (Kw)	***2.75***	***2.68***	***2.61***
Torque (Nm)	***26.26***	***25.70***	***2.19***
Instant consumption (kg/h)	***1.26***	***1.11***	***12.99***
Specific consumption (g/kWh)	***457.67***	***442.79***	***3.36***
Indicated average pressure (Bar)	***8.24***	***8.34***	***-1.22***
Mass of Injected Water (kg)	***0.0***	***0.0***	
Maximum Pressure Reached (Pa)	***5137223.75***	***5183502.04***	***-0.89***
Angle of the cycle corresponding to the maximum pressure reached (°)	***376.35***	***374.60***	***0.47***

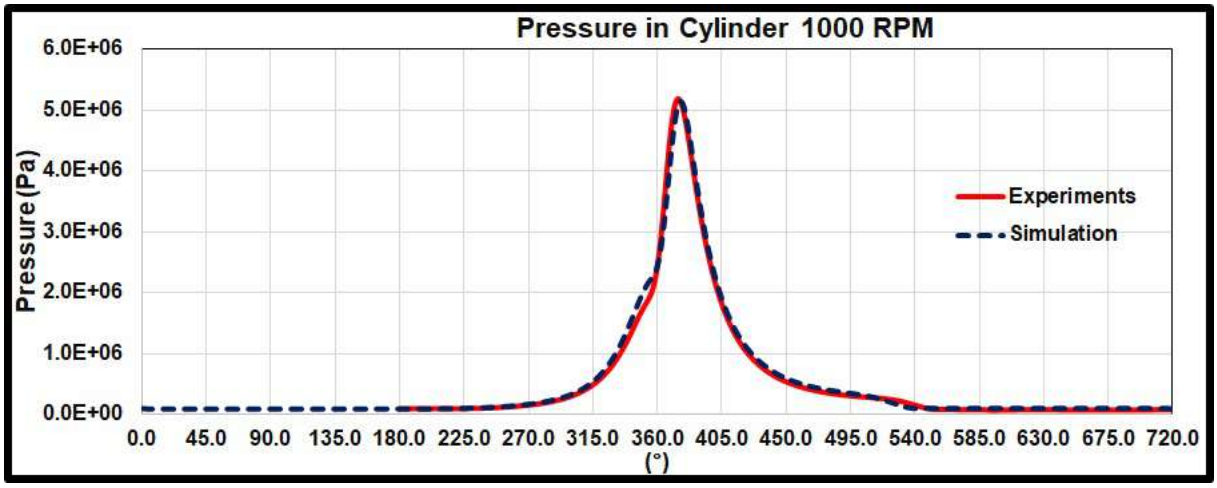

Fig. 4.17 – Comparison of Pressure in Cylinder 1000 RPM.

Table 4.8 – 2000 RPM

2000 RPM			
Performance Parameters	**Simulation**	**Experimental**	**Error (%)**
Power (Kw)	***6.88***	***7.05***	***-2.42***
Torque (Nm)	***32.87***	***33.69***	***-2.44***
Instant consumption (kg/h)	***3.04***	***2.85***	***6.44***
Specific consumption (g/kWh)	***441.31***	***430.82***	***2.44***
Indicated average pressure (Bar)	***10.31***	***10.70***	***-3.63***
Mass of Injected Water (kg)	***0.0***	***0.0***	
Maximum Pressure Reached (Pa)	***6446353.39***	***6507189.37***	***-0.93***
Angle of the cycle corresponding to the maximum pressure reached (°)	***374.30***	***374.40***	***-0.03***

exceed 3.63% as in the same way observed in the case of 1000 RPM, it is in the instantaneous consumption where the greater value of the error is appreciated; 6.44% (Table 4.8). However, this value is less than the 12.99% perceived in table 4.7 (1000 RPM).

(Fig.4.18) shows the comparison between the experimental and simulated pressures for 2000 RPM. It can be seen how the simulation program interprets satisfactorily the operating conditions of the test engine. This statement is supported by analyzing the absolute value of the relative error for the maximum pressure reached inside the cylinder and the point where it occurs. These percentages are 0.93% and 0.03% respectively.

In the case of 3000 RPM there is a notable change in the trend observed in the two previous cases. The absolute values of the relative errors calculated for the parameters of comparing

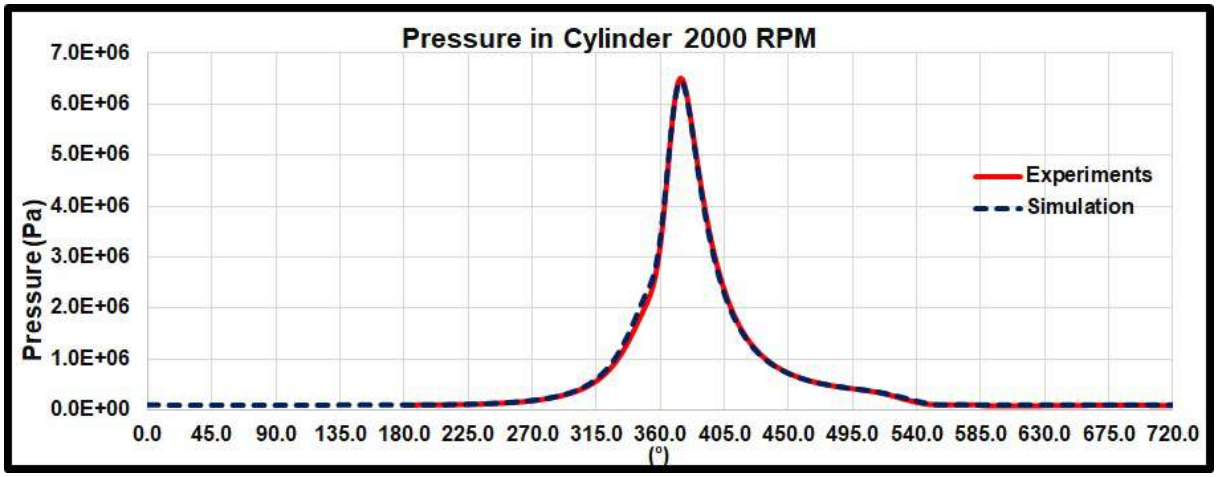

Fig. 4.18 – Comparison of Pressure in Cylinder 2000 RPM.

Table 4.9 – 3000 RPM

3000 RPM			
Performance Parameters	**Simulation**	**Experimental**	**Error (%)**
Power (Kw)	***12.00***	***12.99***	***-7.68***
Torque (Nm)	***38.18***	***40.64***	***-6.04***
Instant consumption (kg/h)	***4.74***	***4.98***	***-4.81***
Specific consumption (g/kWh)	***395.48***	***415.52***	***-4.82***
Indicated average pressure (Bar)	***11.98***	***13.13***	***-8.74***
Mass of Injected Water (kg)	***0.0***	***0.0***	
Maximum Pressure Reached (Pa)	***7090148.67***	***7143906.48***	***-0.75***
Angle of the cycle corresponding to the maximum pressure reached (°)	***374.30***	***375.40***	***-0.29***

power, torque, specific consumption and indicated mean pressure, increased markedly between the simulated and experimental data.

Table 4.9 shows that in the only parameters where the trend seen in tables 4.7 and 4.8 is kept, are the maximum pressure reached inside the cylinder during the cycle and the point where this maximum value is located (Fig.4.19). For these two parameters the absolute values of the calculated relative errors correspond to 0.75% and 0.29% respectively.

In the other parameters compared, the absolute values of the calculated relative errors range from 4.81%, as in the case of specific consumption, to 8.74% for the indicated mean pressure. On the other hand, it is important to point out that in the case of instantaneous consumption the tendency to decrease the absolute value of the calculated relative error is maintained. For

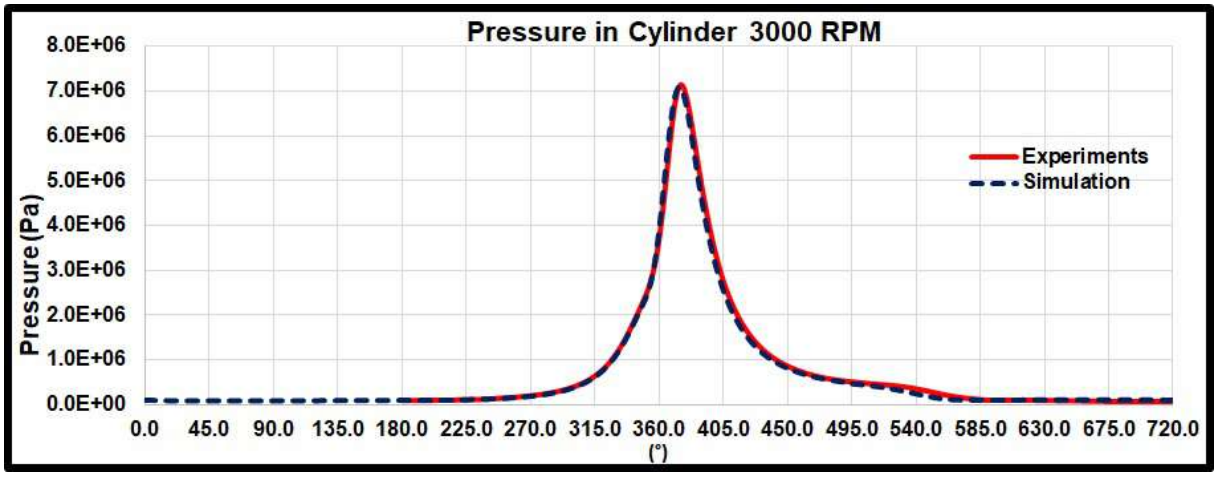

Fig. 4.19 – Comparison of Pressure in Cylinder 3000 RPM.

3000 RPM the corresponding figure is 4.81% (Table 4.9).

Table 4.10 – 4000 RPM

4000 RPM			
Performance Parameters	**Simulation**	**Experimental**	**Error (%)**
Power (Kw)	***16.13***	***16.45***	***-1.96***
Torque (Nm)	***38.50***	***39.29***	***-1.99***
Instant consumption (kg/h)	***6.08***	***6.27***	***-3.01***
Specific consumption (g/kWh)	***377.24***	***406.60***	***-7.22***
Indicated average pressure (Bar)	***12.08***	***13.23***	***-8.68***
Mass of Injected Water (kg)	***0.0***	***0.0***	
Maximum Pressure Reached (Pa)	***7253192.94***	***7250493.77***	***0.04***
Angle of the cycle corresponding to the maximum pressure reached (°)	***374.30***	***375.80***	***-0.40***

For 4000 RPM it is observed that the trend of the absolute values of the relative errors calculated for the comparison between the simulation data and the experimental tests, recovers the proclivity observed in the first cases (table 4.7 for 1000 RPM and table 4.8 for 2000 RPM) where these values do not exceed 3.5% (Table 4.10). However, it is observed that in the case of the specific consumption and the indicated mean pressure, the absolute values of the relative errors are at 7.22% and 8.68%, respectively.

The trend in the decrease of the relative error calculated for instantaneous consumption is maintained; at 4000 RPM the absolute value of the relative error calculated for this performance parameter is 3.1%. Also comparing the values of the maximum pressure reached inside the

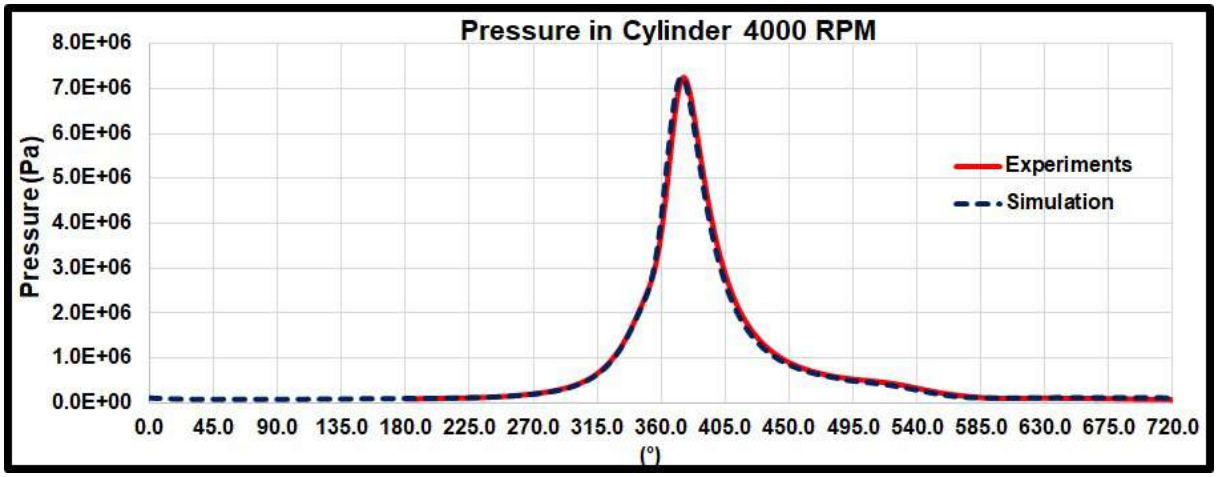

Fig. 4.20 – Comparison of Pressure in Cylinder 4000 RPM.

cylinder and its location within the cycle, between the results shown by the simulation program and the experimental data, the absolute value of the calculated relative error is still less than 1% as it has been observed in all cases.

(Fig.4.20) provides a better illustration of the behavior of the pressure inside the cylinder throughout the cycle. As in all previous cases the proximity of the experimental and simulated curves is remarkable confirming the correct interpretation of the phenomenology of the process by the simulation program.

Table 4.11 – 5000 RPM

5000 RPM			
Performance Parameters	**Simulation**	**Experimental**	**Error (%)**
Power (Kw)	***19.43***	***18.99***	***2.24***
Torque (Nm)	***37.10***	***36.26***	***2.28***
Instant consumption (kg/h)	***7.56***	***7.31***	***3.29***
Specific consumption (g/kWh)	***389.14***	***410.84***	***-5.58***
Indicated average pressure (Bar)	***11.64***	***12.78***	***-9.76***
Mass of Injected Water (kg)	***0.0***	***0.0***	
Maximum Pressure Reached (Pa)	***6800420.82***	***6800286.39***	***0.002***
Angle of the cycle corresponding to the maximum pressure reached (°)	***374.25***	***375.60***	***-0.36***

The last case presented corresponds to 5000 RPM. Table 4.11 contains the data regarding to the comparison between the variables in the simulation and experimental tests. According to the above, the trend is maintained in the absolute values of the relative error calculated for

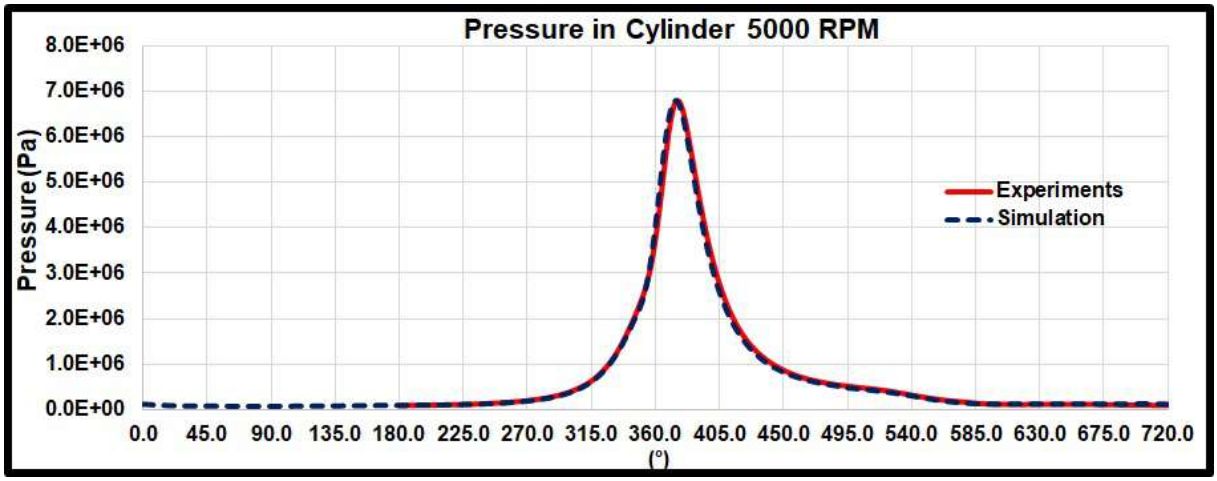

Fig. 4.21 – Comparison of Pressure in Cylinder 5000 RPM.

the performance parameters such as power, torque, instantaneous consumption, the maximum pressure reached inside the cylinder during the cycle and the position of this value with respect to the angle of rotation of the crankshaft. In the case of specific consumption, there is a decrease in the absolute value of the calculated relative error, altering the trend observed in relation with other comparisons where this particular value was gradually increasing from 3.36% for 1000 RPM (Table 4.7) to 7.22% in 4000 RPM (Table 4.10).

In the case of the Indicated average pressure, it is observed that the tendency to increase in the absolute value of calculated relative error is maintained and for 5000 RPM reaches its maximum value of 9.76% (Table 4.11). (Fig.4.21) presents the curves of the pressure behavior within the simulated and experimental cylinder and again it is observed that the simulation program reproduces in a remarkable way the variation of the pressure in the cylinder in the different stages of the cycle.

The validations have shown the qualities of the proposed simulation program, referring to its capacity to interpret and reproduce the phenomenology of the processes inside the cylinder in the cycle of an internal combustion engine and spark ignition.

It is observed that the data provided by the simulation was adequately adjusted to what was observed in the experiments carried out on this engine, that works with gasoline as fuel and in which a system of direct injection of water in the combustion chamber was adapted, with an absolute value of relative error calculated between 0.92%(Fig.4.13) and 2.37% (Fig.4.6) in the calculation of the maximum pressure inside the cylinder, taking into account that the first case (Fig.4.4) corresponds to the operation of the engine without water injection and the three subsequent cases (Fig.4.6), (Fig.4.8) and (Fig.4.13) correspond to conditions where a process of direct injection of water was applied to the combustion chamber in variable amounts of water related as a percentage by mass in relation with the amount of fuel injected (Table 4.2).

It was also observed how the simulation program reproduces the fraction of burned mass curve during the cycle (Fig.4.5), (Fig.4.7), (Fig.4.9) and (Fig.4.14) showing again the great consistency achieved in the program when interpreting the combustion process.

The satisfactory performance of the simulation program proposed in this particular first validation also demonstrates that the water droplet injection and evaporation model implemented (Fig.4.1) and (Fig.4.2) is adequate and accurate to predict the duty cycle influence of this technique in the engine studied.

The second validation of the proposed simulation program consisted in comparing the information provided by the program with the data supplied by the MAUA Institute of Technology on the tests carried out there on an atmospheric spark ignition engine that uses ethanol as fuel. This engine does not have a direct or indirect water injection system, for this reason, the simulations were carried out for cases without water injection. Five rotation speed regimes were chosen; 1000, 2000, 3000, 4000 and 5000 RPM, since the validation was carried out by the MAUA speeds operations references.

Table 4.6 shows the data of the engine operating conditions, reported by MAUA and this is the same data supplied in the simulation program, , together with the geometric characteristics of the engine shown in table 3.2, to perform the corresponding simulations.

Tables 4.7 to 4.11 present the results of the comparison between the values of some of the performance variables delivered by the simulation program and the values of the same variables supplied by MAUA from the experimental tests. Additionally, (Fig.4.17) to (Fig.4.21) present a comparison between the pressure curves throughout the duty cycle. For performance parameter cases such as power, torque, maximum pressure reached inside the cylinder and the location of this maximum value, the absolute value of the calculated relative error percentage does not exceed 3.5% in any of the 5 cases analyzed. This is easily verifiable by looking at the graphs of the pressure curves. Yet again it is confirmed that the simulation program correctly interprets the phenomenology of the process.

As for the other parameters compared: Instantaneous consumption, specific consumption and the indicated mean pressure, the calculated relative errors do not exceed 10%. Bearing in mind that these parameters are highly influenced by the specific conditions in which the experimental tests are carried out, it can be considered that the relative error is in reasonable ranges, although it is desirable that these error percentage values are lower.

The analysis described above consistently supports the predictive simulations with direct water injection into the combustion chamber presented below. Taking the geometric and functional characteristics of the last engine on which the validations were carried out, that is to say the engine that is in the Institute of Technology of MAUA (Table 3.2 and Table 4.6), (Fig.4.16). These simulations provide a clearer idea of the influence of this technique on the performance variables of the engine, such as power, torque and specific consumption, as well

as the ability of the same technique of water injection to control the temperature and pressure inside the cylinder, the prevention of the phenomenon of detonation and emission control.

4.3 PREDICTIVE SIMULATION RESULTS FOR AN INTERNAL COMBUSTION AND SPARK IGNITION ENGINE THAT USES ETHANOL AS FUEL WITH DIRECT WATER INJECTION INTO THE COMBUSTION CHAMBER.

As mentioned above, this section presents the analysis of the results obtained when simulating the process of injection and evaporation of water in the combustion chamber, using the simulation program built from the thermodynamic model proposed and described in Chapter 3.In addition to the data provided by tables 3.2 and 4.6, (Fig.4.16), referring to the geometry of the engine to the operating variables, respectively, it is required to establish the amount of water to be injected, the instants within the operating cycle of the engine where the injection of water is carried out and the time that the injection takes. The evaporation process is calculated by means of the model described in section 3.2.1 and the time it takes to evaporate depends on the conditions inside the cylinder and how these vary during injection and evaporation of water.

(Fig.4.1) shows a probability distribution of drop size based on the considerations mentioned in (BALABEL; WILSON, 2013) and (LEVICH, 1962). (Fig.4.2) presents a relationship between the drop diameter and the time in which this diameter decreases to be equal to 0 (TURNS, 1996).

To establish the quantity of water to be injected, we take as an example the relationship mentioned in (KIM *et al.*, 2016), where the quantity of water is established as a mass proportion of the quantity of fuel injected in each cycle (Table 4.2). Table 4.12 presents the equivalence between the degrees that the water injection takes, measured in relation to the angle of rotation of the crankshaft and the time that the crankshaft takes to travel through the angle of injection of water, for 5 different speeds of rotation of the crankshaft (1000, 2000, 3000, 4000 and 5000 RPM).

Table 4.12 – Ratio (Water Injection Time)/(Width of Injection Angle)

Ratio (Water Injection Time)/(Width of Injection Angle)						
Seconds	**1000 RPM**	**2000 RPM**	**3000 RPM**	**4000 RPM**	**5000 RPM**	**Ratio Water/Fuel**
3.33E-04	**2°**	**4°**	**6°**	**8°**	**10°**	**50% W/F**
6.67E-04	**4°**	**8°**	**12°**	**16°**	**20°**	**100% W/F**
1.00E-03	**6°**	**12°**	**18°**	**24°**	**30°**	**150% W/F**
1.33E-04	**8°**					**200% W/F**
1.67E-04	**10°**					**250% W/F**

In the last column of table 4.12, the relations in percentage of mass between the quantity of water injected and the quantity of fuel injected are presented (W/F). In this way, both the

duration of the injection and the amount of water injected during the injection time are defined for the 5 rotation speeds chosen for the predictive simulations.

Once the amounts of water injection and the times when it is carried out (Table 4.12) have been established, it is also necessary to establish the instants in which each injection is applied with respect to the engine's operating cycle. Four instants were chosen to perform the water injection, measured in relation to the rotation angle of the crankshaft. These injection moments are chosen to observe how the process of water injection and evaporation affects the cycle performance variables (power, thermal efficiency, specific fuel consumption), as well as their influence on the control of knock and NOx emissions.

The water injection moments chosen are: 180°, 240°, 330° and 370°, i.e. the first corresponds to the phase opened during admission (180°). The second corresponds to the closed phase at the beginning of compression (240°) and the third corresponds to the closed phase at the end of compression (330°). The fourth and last corresponds to the closed phase, shortly after ignition and during the beginning of the power stroke (370°).

The following graphs (Fig.4.22), (Fig.4.23) and (Fig.4.24) show in a characteristic way the behavior of the three parameters that are affected by the addition of a specific volume of water inside the combustion chamber, during the working cycle of an internal combustion engine that uses ethanol as fuel. These three parameters are : The pressure throughout the cycle (Fig.4.22), the variation of the temperature in the zones of burned and unburned gases during the cycle (Fig.4.23) and the variation of the mass contained in the cylinder during the cycle (Fig.4.24).

In each of the graphs mentioned above, a detail (box) of the graph interval is shown where the maximum pressure and temperature values are reached in the burned and unburned gas zones (Fig.4.22) and (Fig.4.23 Details 1 and 2) respectively, the variations of the total masses and gases inside the cylinder during the water injection and evaporation processes (Fig.4.24).

Initially it is analysed how the injection of water affects the behavior of the pressure inside the cylinder during an engine cycle. (Fig.4.25) presents the detail of the maximum pressure reached when the engine has a rotational speed of 1000 RPM and the water injection is done 180° ATDC Exhaust-Intake (Fig.4.16) in the four cases proposed in table 4.12 for the amounts of water injection.

As it can be seen, the pressure increases by about 274 KPa when the water/fuel ratio is 150%, i.e. the amount of water injected is 1.5 times the mass of fuel (ethanol) injected. It can also be seen that as the amount of water injected increases, the maximum pressure inside the cylinder also increases (53 KPa between 0% water/fuel and 50% water/fuel, 85 KPa between 50% water/fuel and 100% water/fuel and 136 KPa between 100% water/fuel and 150% water/fuel). In this case, the injection process is carried out in the open phase towards the end

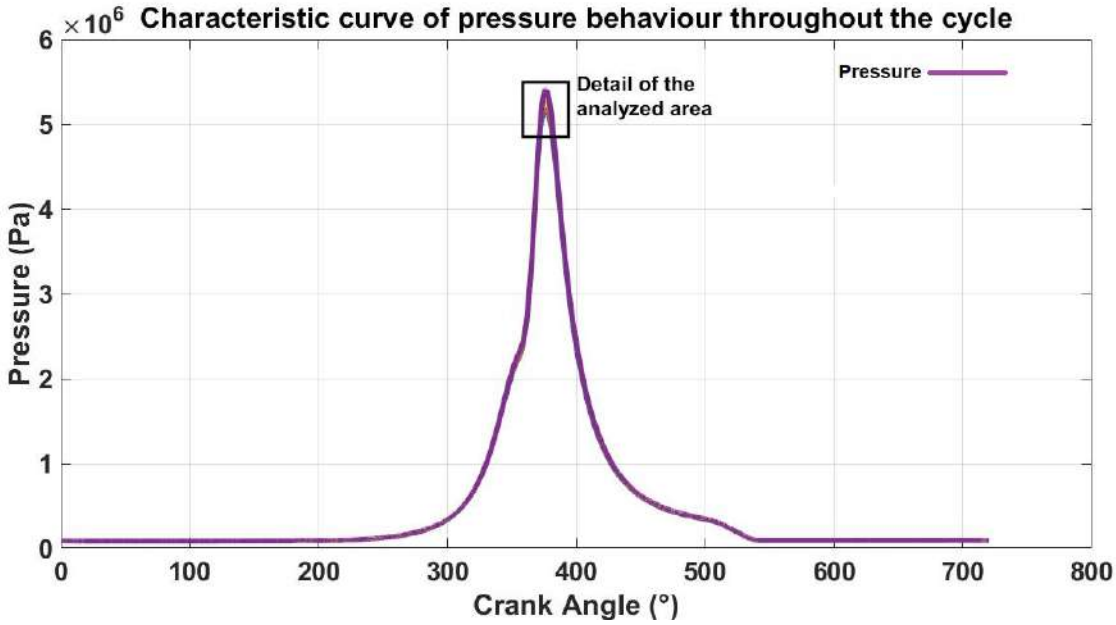

Fig. 4.22 – Characteristic curve of Pressure.

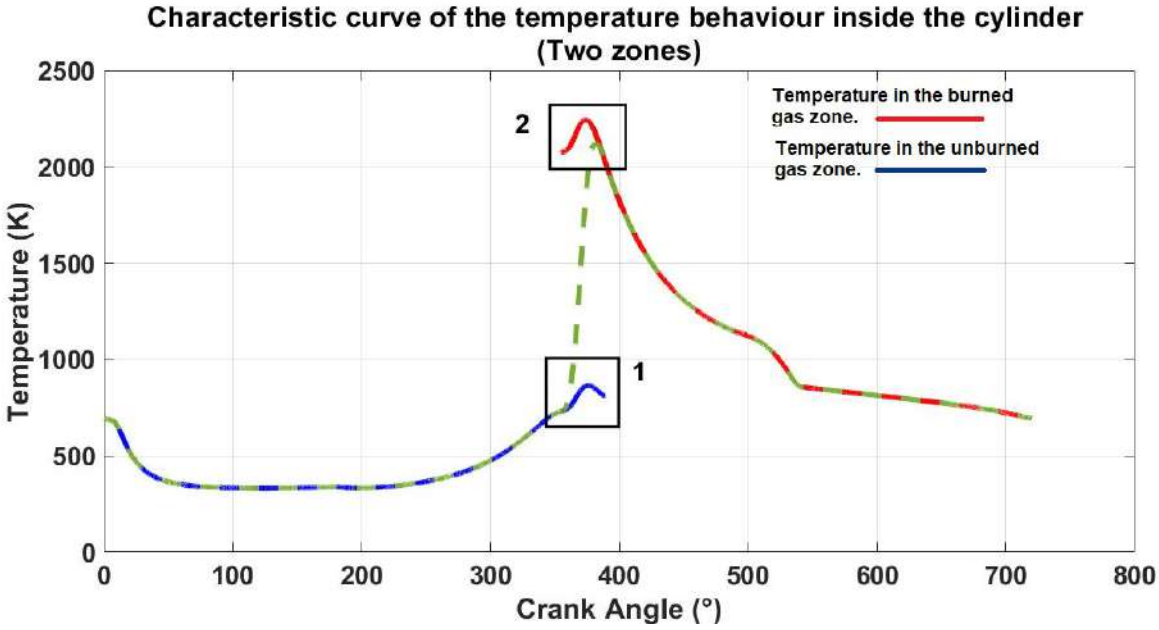

Fig. 4.23 – Temperature-Two Zones.

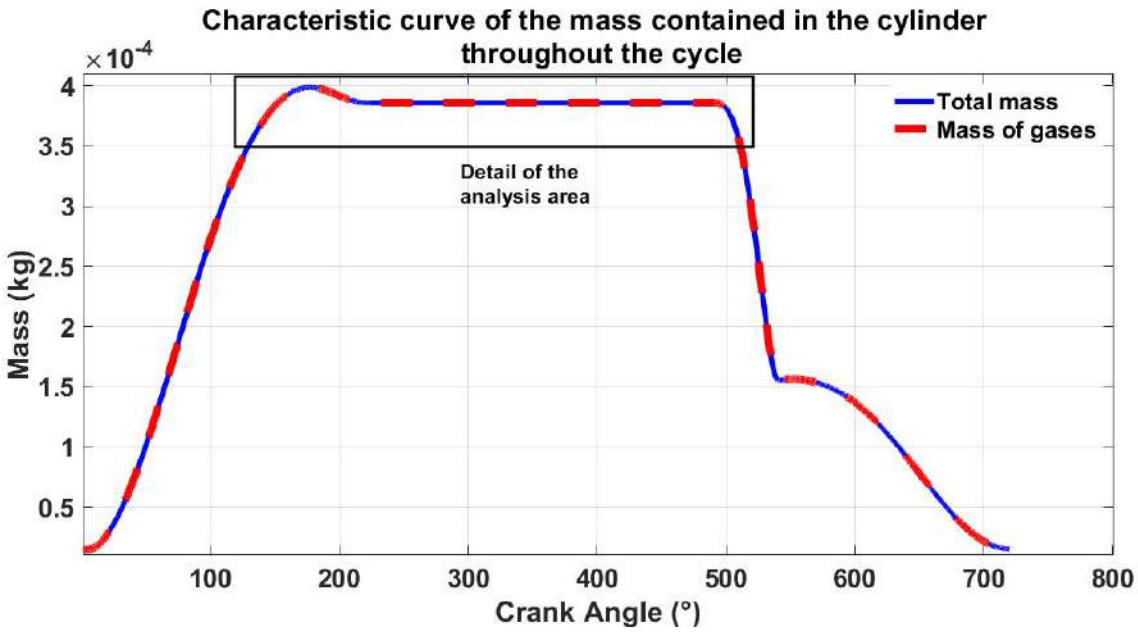

Fig. 4.24 – Mass-In Cylinder Normal.

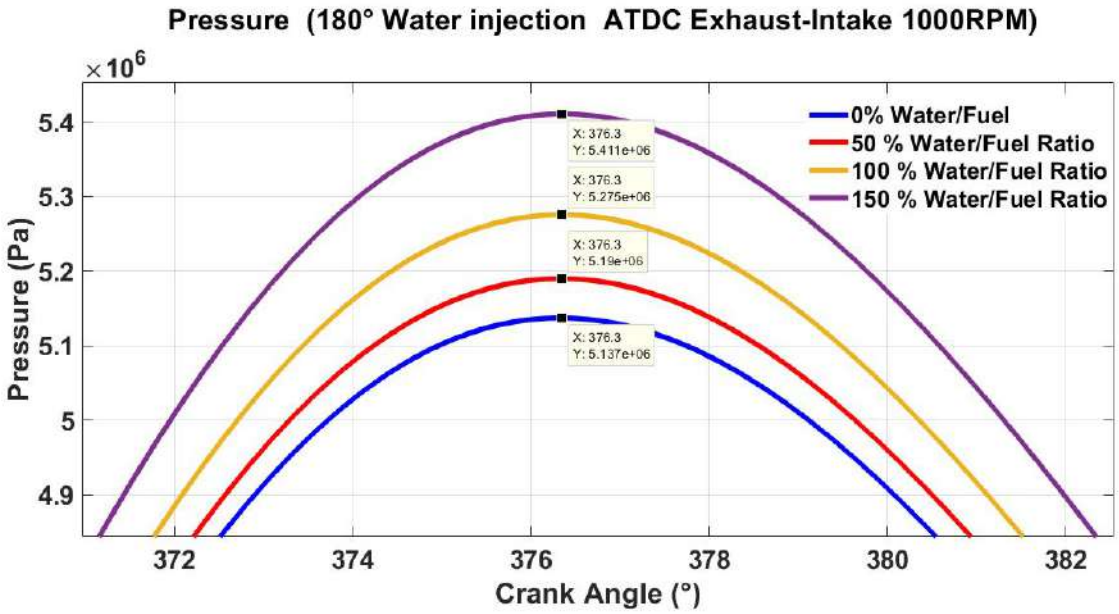

Fig. 4.25 – Comparison of Pressure in Cylinder 1000 RPM.

of the admission. Observing (Fig.4.26) it can be appreciated how the amount of mass inside the cylinder increases during the closed phase for each of the proposed cases of water injection. This increment in the internal mass explains the corresponding growth in the maximum pressure reached.

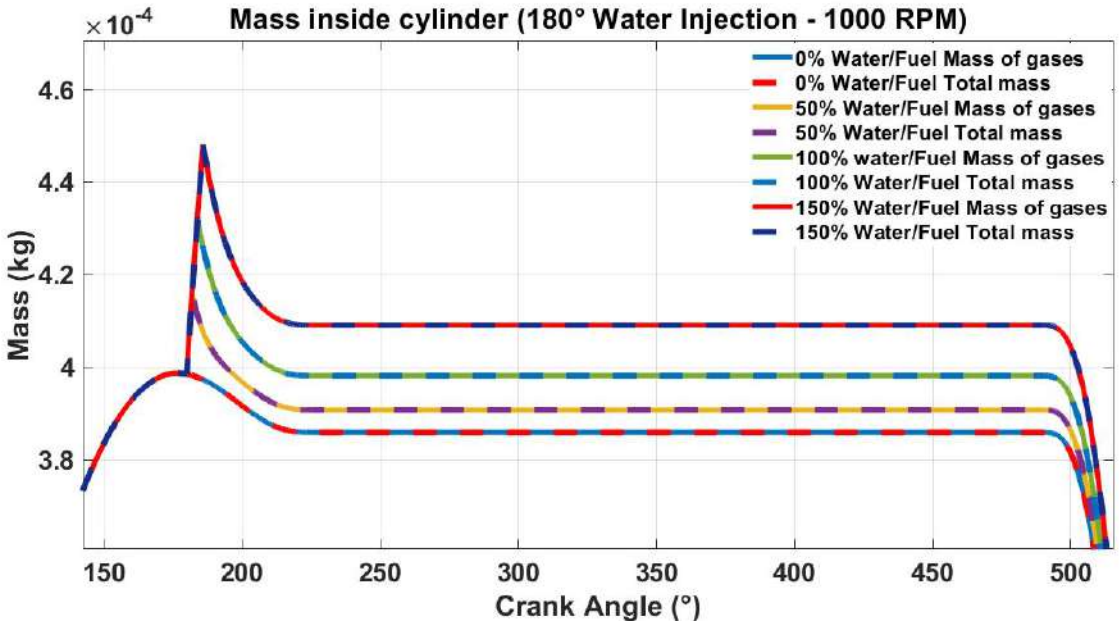

Fig. 4.26 – Mass-In Cylinder 180° water injection 1000 RPM.

The maximum temperatures reached in the burned and unburned gas zones are also affected by water injection. Although the effect is not as marked as it does occur in the pressure or mass inside the cylinder, there is a slight drop in the maximum temperature in the burned gas zone in direct proportion to the amount of water added in. (Fig.4.27) and (Fig.4.28). Likewise, the steam generated and the air/fuel mixture have a longer time to homogenize due to the fact that the water injection is carried out in the lower dead point of the admission, for this reason the effect on the maximum temperatures reached by each of the gas zones at the end of the compression is low when compared with the cases that will be shown later.

As the entire process occurs while the intake valve is closing and the initial part of the compression, the heat absorption for the change phase does not directly affect the maximum pressure reached inside the cylinder, as this pressure is achieved at the end of the compression and for that instant the water vapor and air/fuel mixture behave as a single gas.

This same condition is present in the maximum values of the temperature in the zone of unburned gases (Fig.4.29) and (Fig.4.30).

Both in the burned gas zone and in the unburned gas zone, the values of the temperature reduction intervals are quite close. 12 K for the burned gas zone and 12.6 K for the unburned gas zone.

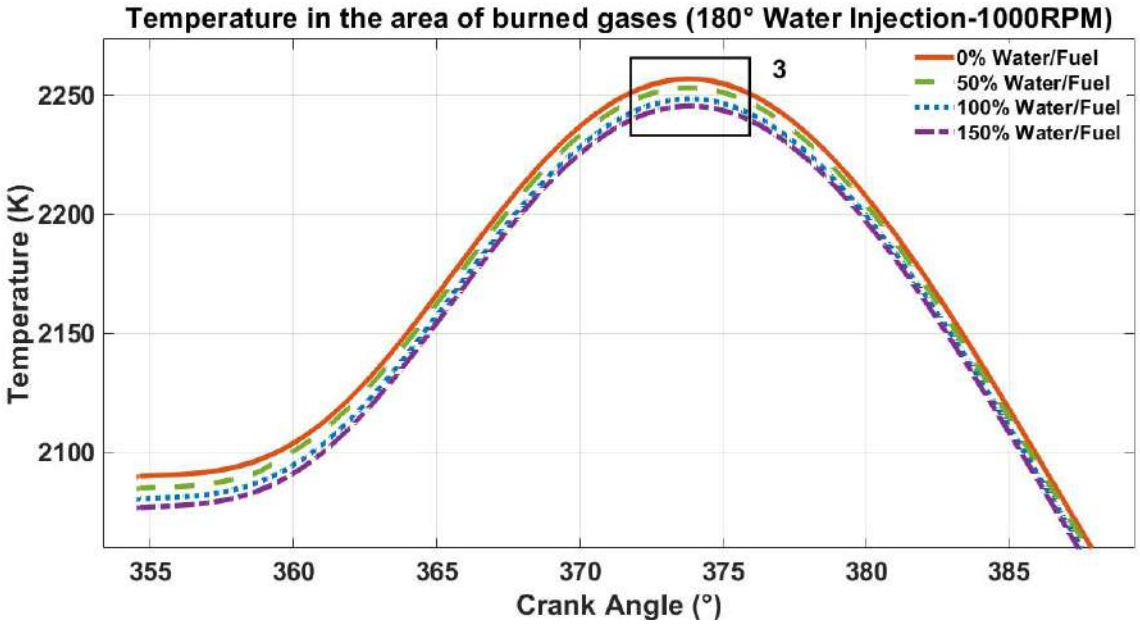

Fig. 4.27 – Temperature 180° water injection Burned zone 1000 RPM. Detail (2).

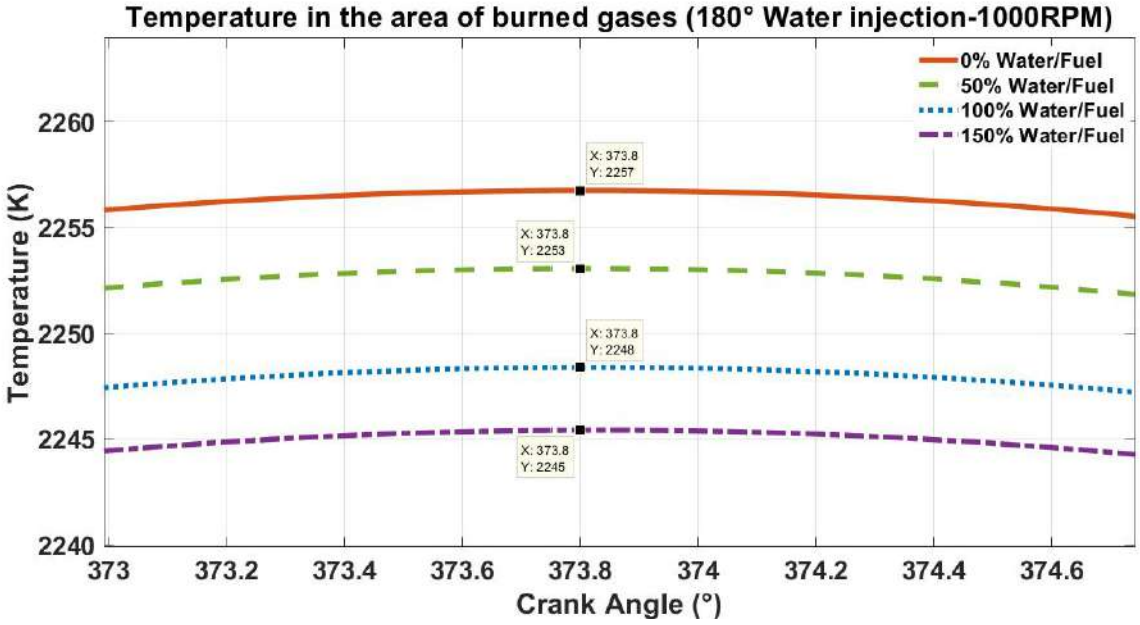

Fig. 4.28 – Temperature 180° water injection Burned zone 1000 RPM. Detail (3).

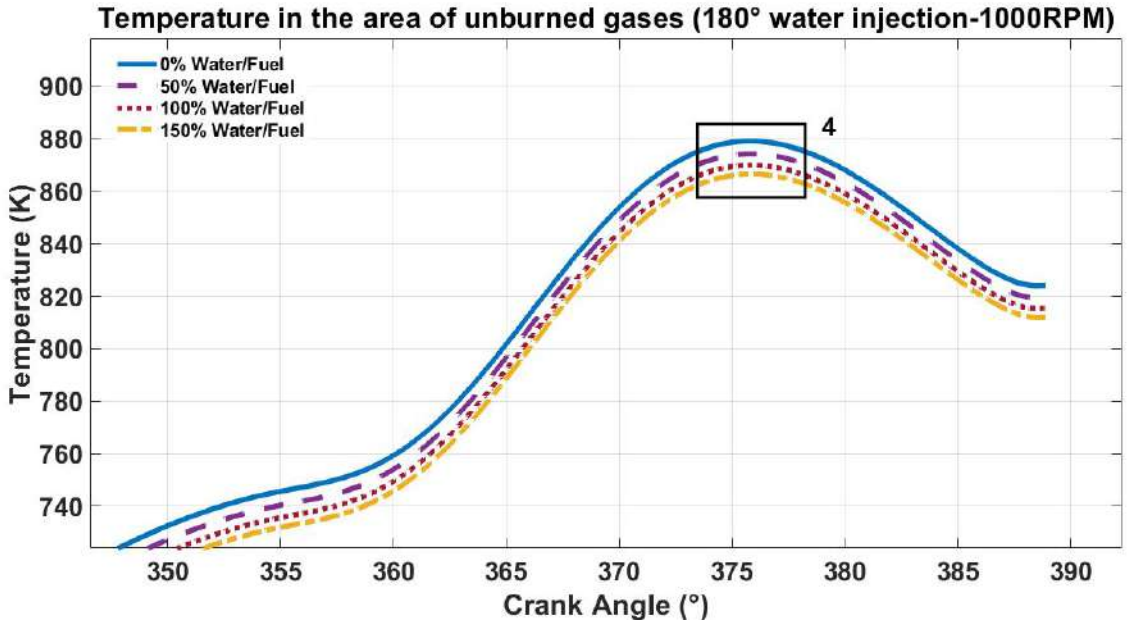

Fig. 4.29 – Temperature 180° water injection Unburned zone 1000 RPM. Detail (1).

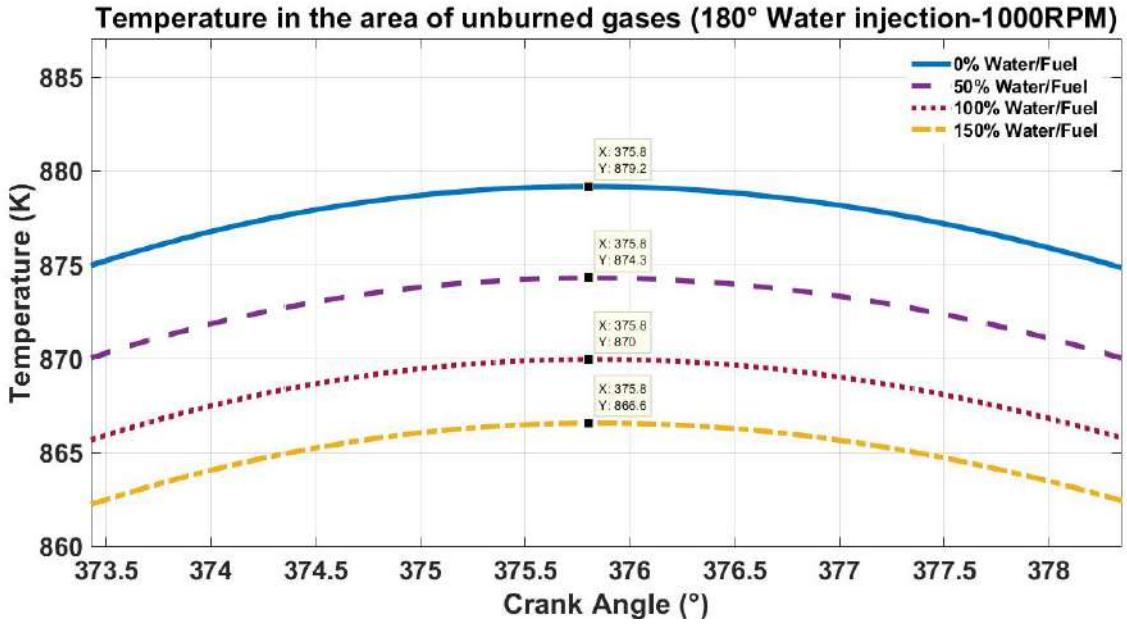

Fig. 4.30 – Temperature 180° water injection Unburned zone 1000 RPM. Detail (4).

When the water injection is made at 240° ATDC of Exhaust-Intake (Fig.4.31), the behavior of the maximum pressure inside the cylinder is similar to that observed when the water injection is made at 180° ATDC Exhaust-Intake. In this case the water injection takes place after the closing of the inlet valve and during the closed phase. Unlike the previous case, there is no back flow phenomenon.

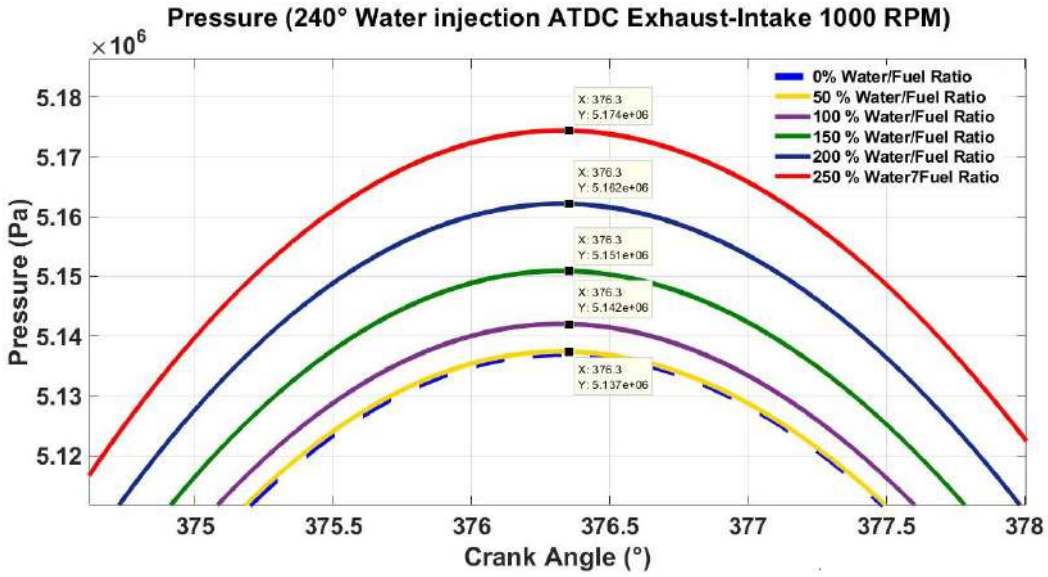

Fig. 4.31 – Pressure 240° 1000 RPM.

However for cases where the water injection is performed at 330° and 370° ATDC Exhaust-Intake, (Fig.4.32), (Fig.4.33) the pressure behavior is shown contrary to that observed when the injection is performed at 180° and 240° ATDC of Exhaust-Intake. This behaviour is due to the fact that while the water injection applied at 180° is carried out in the open phase, i.e. before the inlet valve closes, the water injections applied at 240°, 330° and 370° are all carried out in the closed phase, i.e. with the inlet and exhaust valves closed.

The water conditions in the injector are: 10 MPa pressure and 373.15 K temperature. When the water is injected at 180° ATDC Exhaust-Intake, the conditions in the cylinder are 86.57 KPa of pressure and 338.3 K of temperature, therefore, as the water is in liquid state when injected it remains in liquid state until the conditions of pressure and temperature inside the cylinder allow the liquid water to initiate the process of phase change, i.e. until the saturation point is reached. From then on, the water vapor generated by the saturation and the air/fuel mixture that enters the cylinder are homogenized during the compression phase, as a single gas, since the amount of heat that the water requires to absorb to change state only affects the temperature of the cylinder at the beginning of compression and until the liquid reaches the saturation state.

The influence of the process of injection and evaporation of water on the thermodynamic conditions inside the cylinder changes noticeably when the injection occurs during the closed

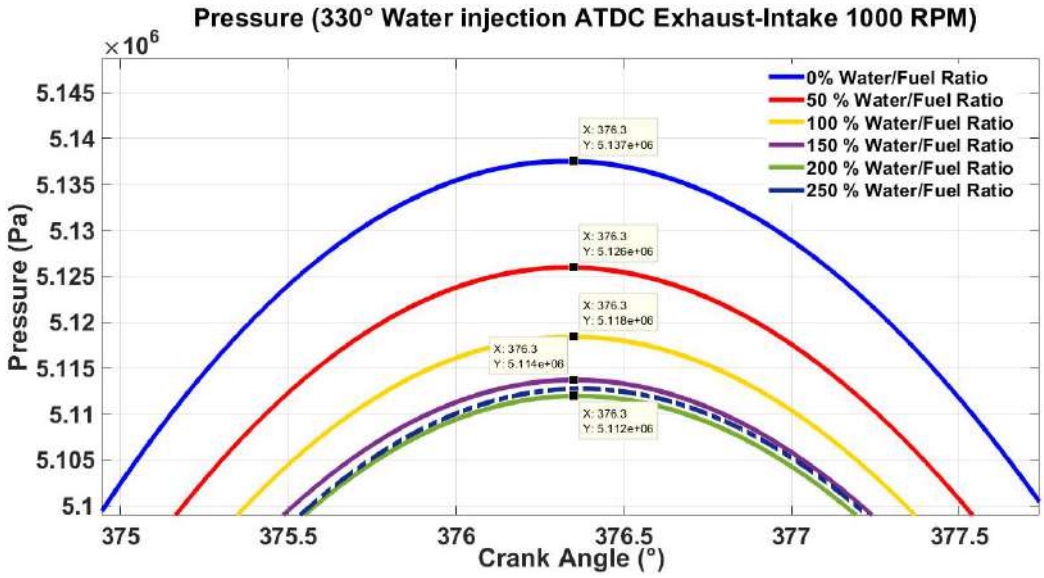

Fig. 4.32 – Pressure 330° 1000 RPM.

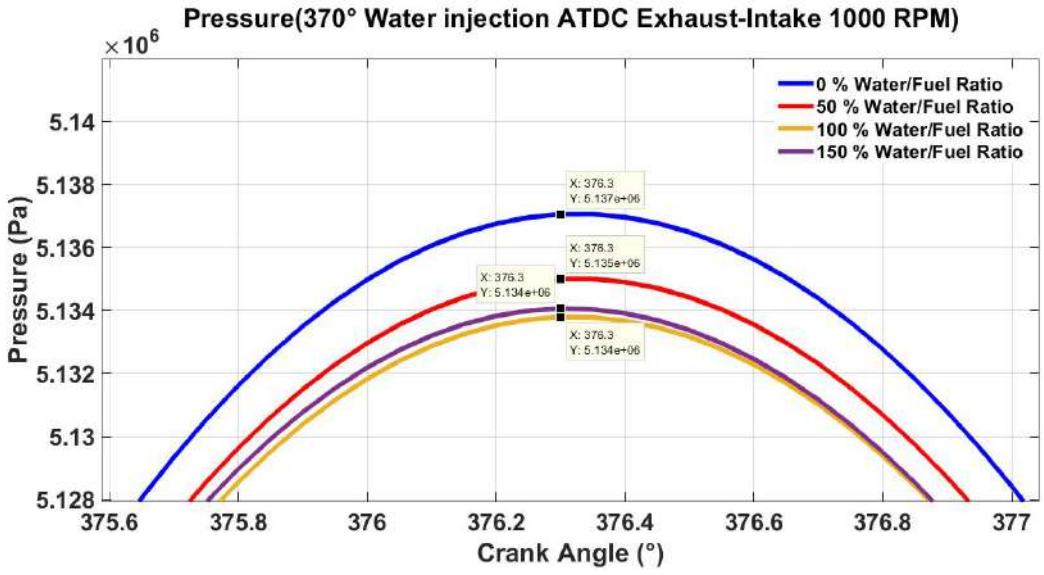

Fig. 4.33 – Pressure 370° 1000 RPM.

phase. When the injection is made in 240° ATDC Exhaust-Intake, the admission valve is already completely closed and both the pressure and the temperature inside the cylinder increase to a rate each time greater, the water injection enters in liquid state and it can absorb heat to reach the saturation condition more quickly than in the previous case, due to the higher temperature and pressure of the environment. However, this heat absorption affects the temperature of the cylinder and consequently also the pressure. But the time available to the steam generated by saturation and the air/fuel mixture to homogenize is significantly less than for the previous case, hence although the effect on the temperature is significant (Fig.4.34), (Fig.4.35) is not in the same proportion for the pressure (Fig.4.31). While the maximum temperature in the burned gas zone presents a difference of 379 K between the condition without water injection (2257 K) and the maximum water/fuel ratio (250% W/F, 1878 K) (Fig.4.35), the pressure increases by 37 KPa, which is the difference between the maximum pressure reached with a water/fuel ratio of 250% (5.174 MPa) and without water injection (5.137 MPa) (Fig.4.31).

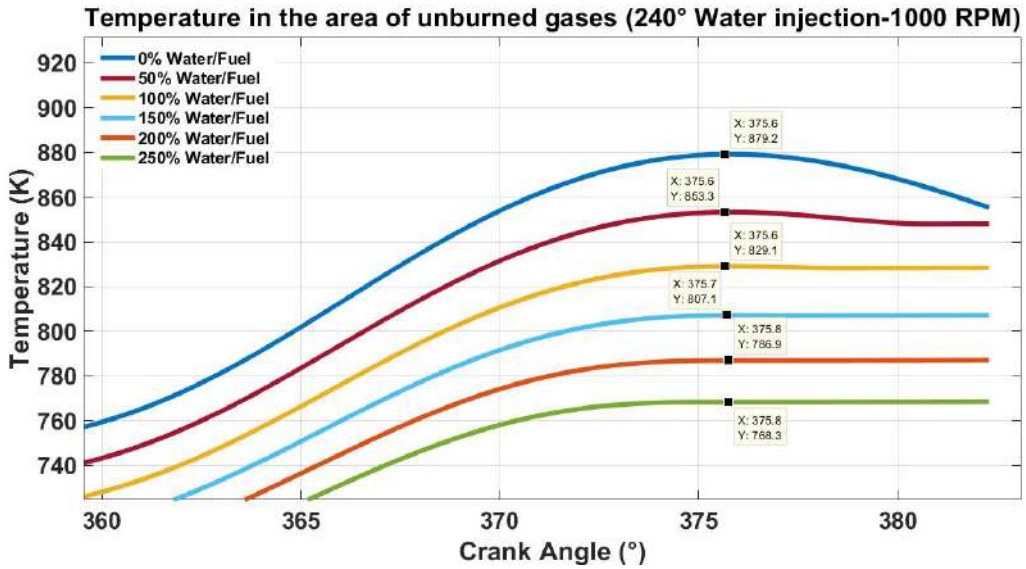

Fig. 4.34 – Temperature 240° 1000 RPM. Detail (1).

The behavior of the pressure when the injection of water is made in 330° ATDC Exhaust-Intake, presents a fall in the maximum values. Thus, the highest value of maximum pressure is reached for the condition without water injection (5.137 MPa) while for the maximum water/fuel ratio (250%) the maximum pressure reached in the compression TDC is 5.112 MPa (Fig.4.32). This pressure drop observed is consistent with the temperature behavior in the burned gas zone for the same water injection point (330°) (Fig.

As mentioned above this behavior is contrary to what is observed when the injection is made at 180° and 240° ATDC Exhaust-Intake. Yet again this is a consequence of the available time the liquid water to absorb the energy needed for the change phase. In this case the injection is made at a point (330°) very close to the ignition and the beginning of the combustion.

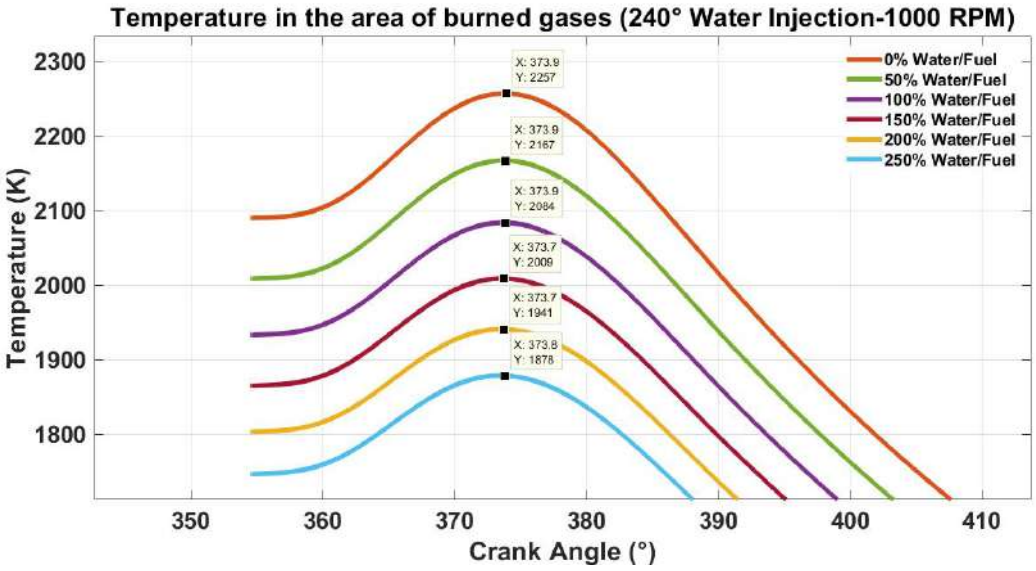

Fig. 4.35 – Temperature 240° 1000 RPM. Detail (2).

Although heat absorption takes place very quickly, decreasing the temperature considerably (Fig.4.36), the effect on the pressure is also noticeable, although the pressure drop is relatively slight (Fig.4.32), (5.137 MPa without water injection and 5.112 MPa with a 250% water/fuel ratio, the difference is 25 KPa).

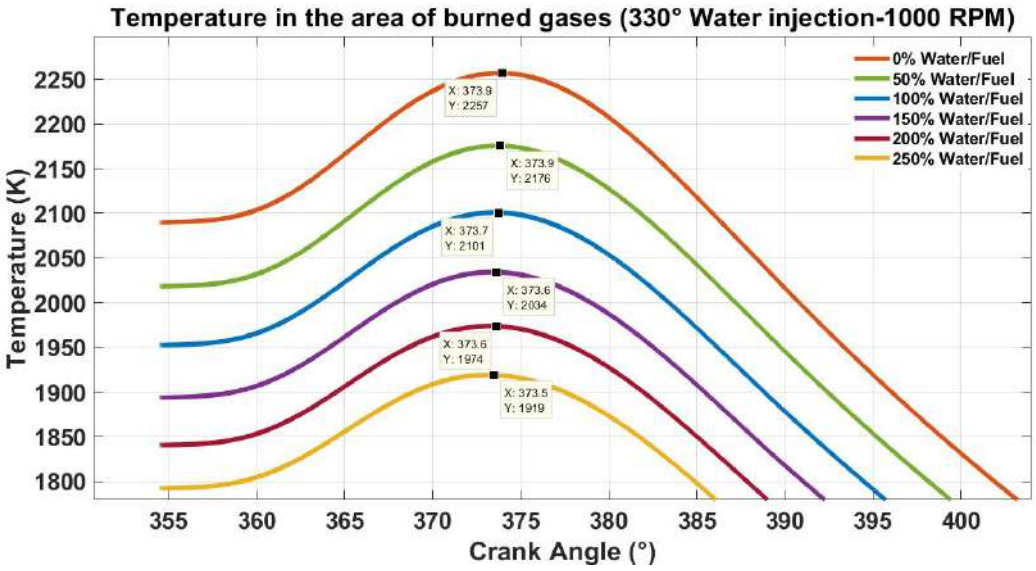

Fig. 4.36 – Temperature 330° 1000 RPM. Detail (2).

(Fig.4.37) to (Fig.4.39) show how the water evaporation process occurs. The dashed lines represent the amount of total mass inside the cylinder while the continuous lines represent the mass of gases (water vapor plus air/fuel mixture). It is observed how the mass of gases is slightly behind the total mass, until finally both masses are equal, this happens when all the

injected water evaporates. The horizontal distance between the two lines represents the time that the droplets of injection water takes to evaporate.

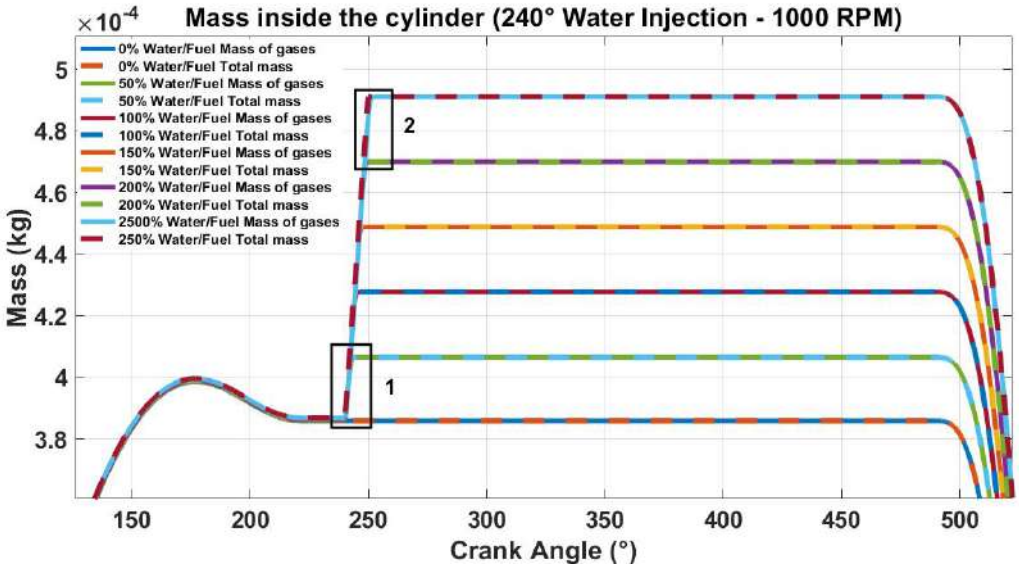

Fig. 4.37 – Mass In-Cylinder 240° 1000 RPM. .

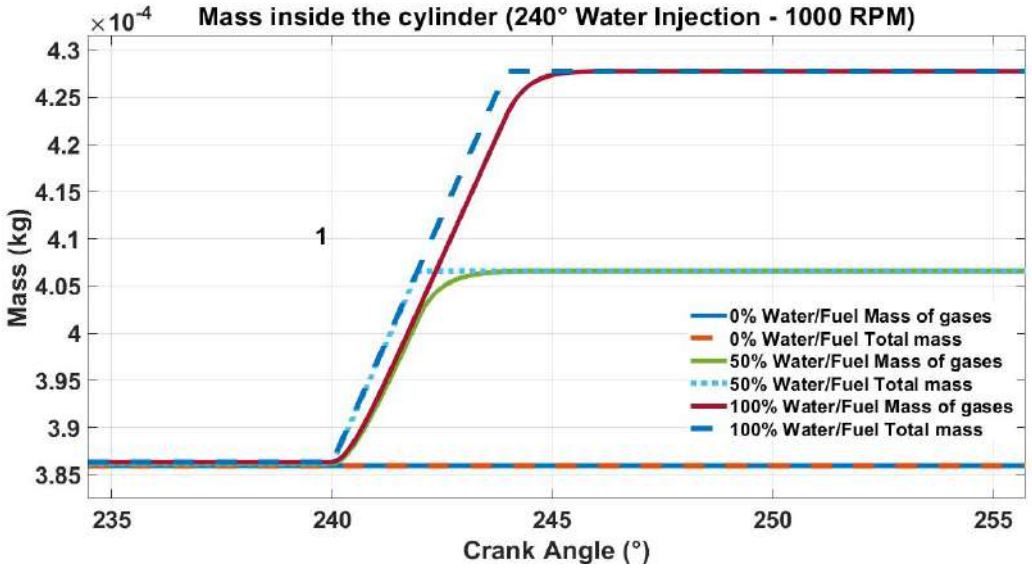

Fig. 4.38 – Mass In-Cylinder 240° 1000 RPM. Detail (1).

When the water injection is carried out at 370° (Closed phase but at the beginning of the power stroke stage) the pressure has a similar behaviour to the one observed when the injection is carried out at 330°. The pressure presents a drop in the maximum value reached (Fig.4.33). The maximum value when there is no water injection is 5.137 MPa while for the maximum water/fuel ratio used in this case, 150%, the maximum pressure value is 5.134 MPa. However, the difference between the two values is very small, 3KPa. In the case of the temperature of the

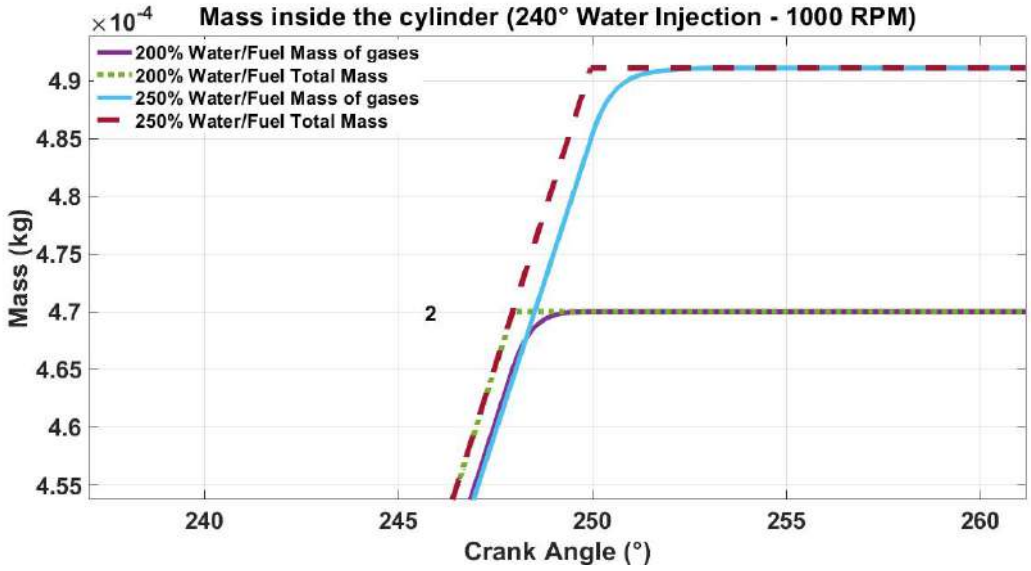

Fig. 4.39 – Mass In-Cylinder 240° 1000 RPM. Detail (2).

gases burned (Fig.4.40) two phenomena are observed: Initially it is shown that the maximum temperature value is the same for the three cases where water injection is applied (ratios of 50%, 100% and 150% water/fuel) and the maximum temperature value for the case without water injection is only 10 K higher (2247 K and 2257 K respectively) and these maximum values are located at different points (371.8° and 373.9° respectively), unlike what was observed in all the previous cases, when the injection is carried out at 180°, 240° and 330° ATDC Exhaust-Intake, where in all cases the maximum temperature in the burned gas zone was located at the same point of the cycle measured with respect to the crankshaft turning angle.

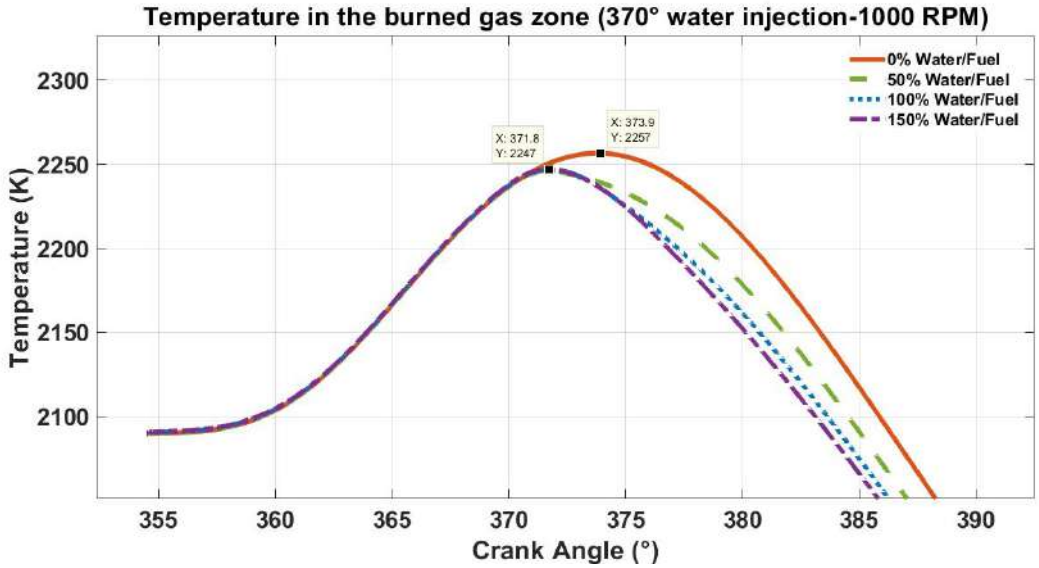

Fig. 4.40 – Temperature 370° 1000 RPM. Detail (2).

Both the observed temperature behavior and the pressure for this water injection condition (370° ATDC Exhaust-Intake) obeys the same phenomenology explained in the previous case (Water injection in 330° ATDC Exhaust-Intake). On the other hand, what has been observed so far shows that the injection of water after combustion has little influence on the variables measured in the cycle.

The second case that is analyzed corresponds to an engine rotation speed of 2000 RPM and the process of water injection is done 240° ATDC of Exhaust-Intake. At 2000 RPM the behavior perceived when injection is performed at 240° ATDC Exhaust-Intake (Fig.4.41) is very similar to that observed for the same water injection point but at 1000 RPM. In (Fig.4.31), the same behaviour can be seen. The rise in pressure between the condition without water injection (6.447 MPa) and the pressure reached with the highest ratio of fuel water used (150%, 6.454 MPa) is 7 KPa.

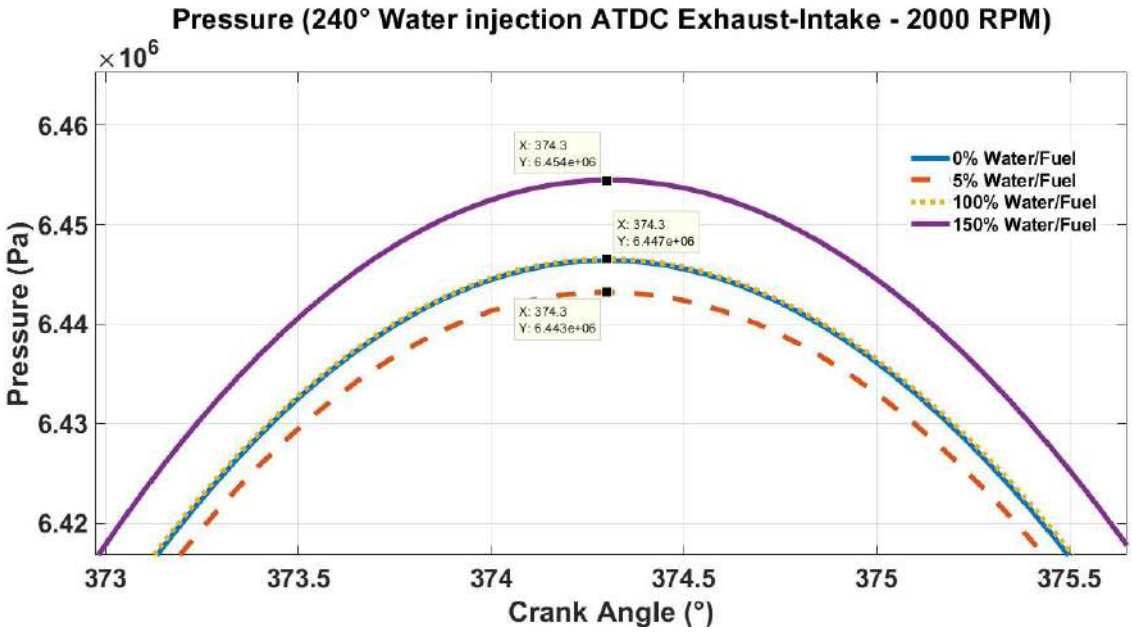

Fig. 4.41 – Comparison of Pressure in Cylinder 2000 RPM.

Likewise, the temperature curves of the unburned gases zone in the region where the maximum value is reached, the injection is made at 240° ATDC Exhaust-Intake and 2000 RPM, (Fig.4.42) show a behavior in the same trend for the same injection point at 1000 RPM (Fig.4.34) .

For 2000 RPM the temperature droplets between the maximum value reached in the burned gas zone without water injection (2312 K) and the maximum temperature value for the highest water/fuel ratio (150%, 2041 K) (Fig.4.43) is 271 K. The phenomenology of the process maintains the trend previously observed and explained (1000 RPM, 240° water injection (Fig.4.35)) . Both pressure and temperature have similar behaviors in terms of how water in-

jection affects engine behavior at these first two analyzed rotation speeds (1000 RPM and 2000 RPM).

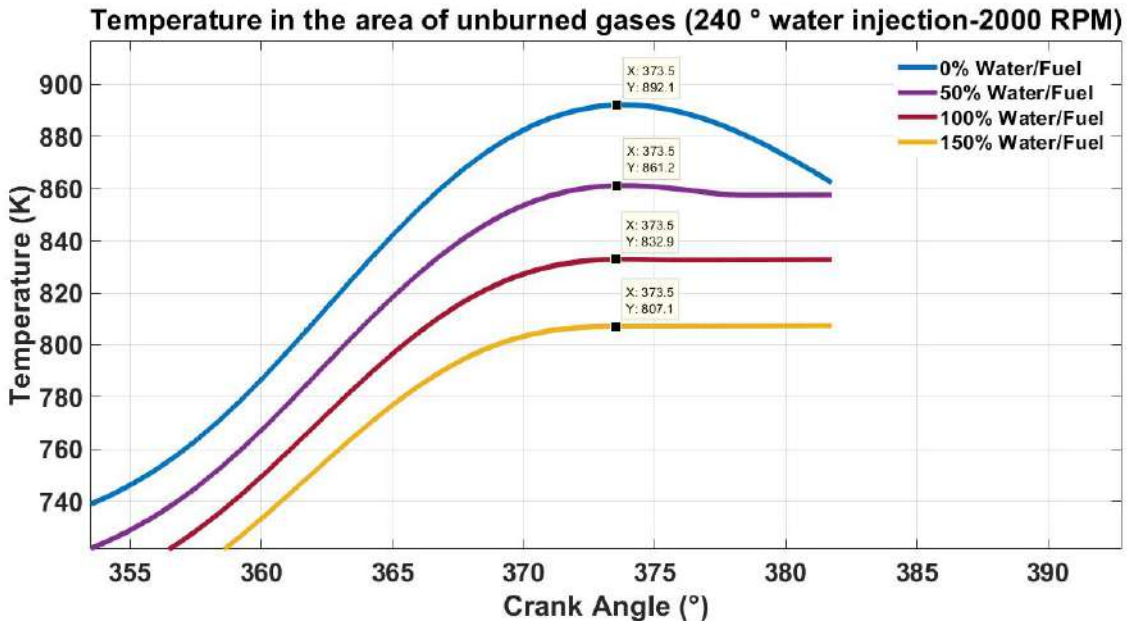

Fig. 4.42 – Temperature 240° water injection Unburned Zone 2000 RPM. Detail (1).

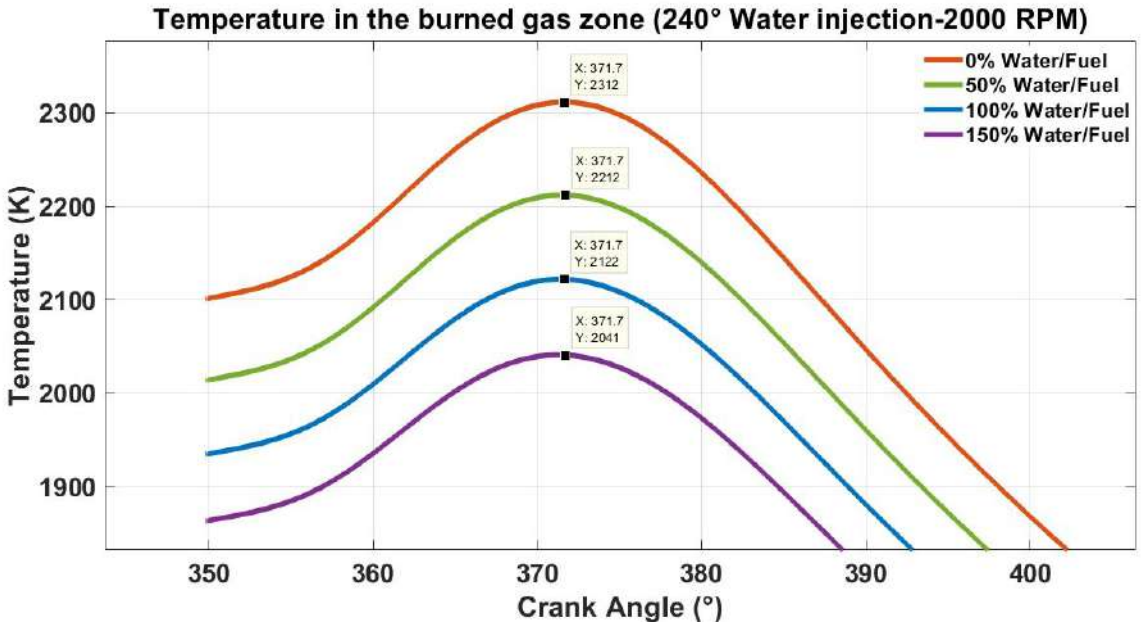

Fig. 4.43 – Temperature 240° water injection Burned Zone 2000 RPM. Detail (2).

(Fig.4.44) to (Fig.4.46) show the variation of the total mass and the mass of gases inside the cylinder. (Fig.4.45) and (Fig.4.46) in particular show the process of water injection and evaporation. The characteristic S-curve observed in the three water injection ratios (50%, 100% and 150% water/fuel) shows that the program correctly simulates the process.

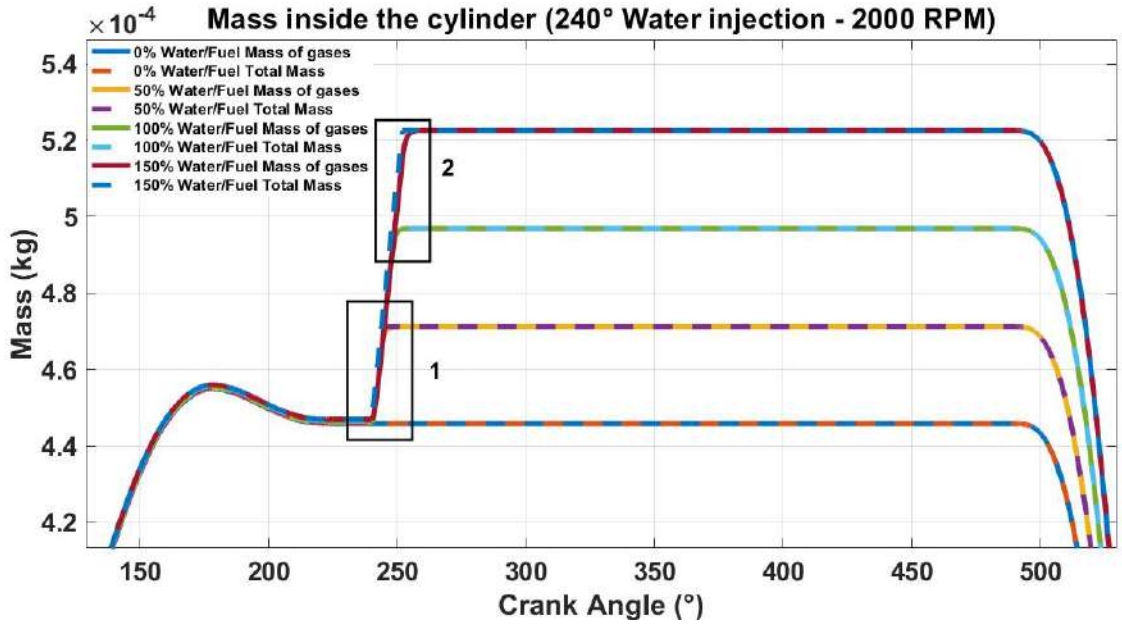

Fig. 4.44 – Mass In-Cylinder 240° water injection 2000 RPM.

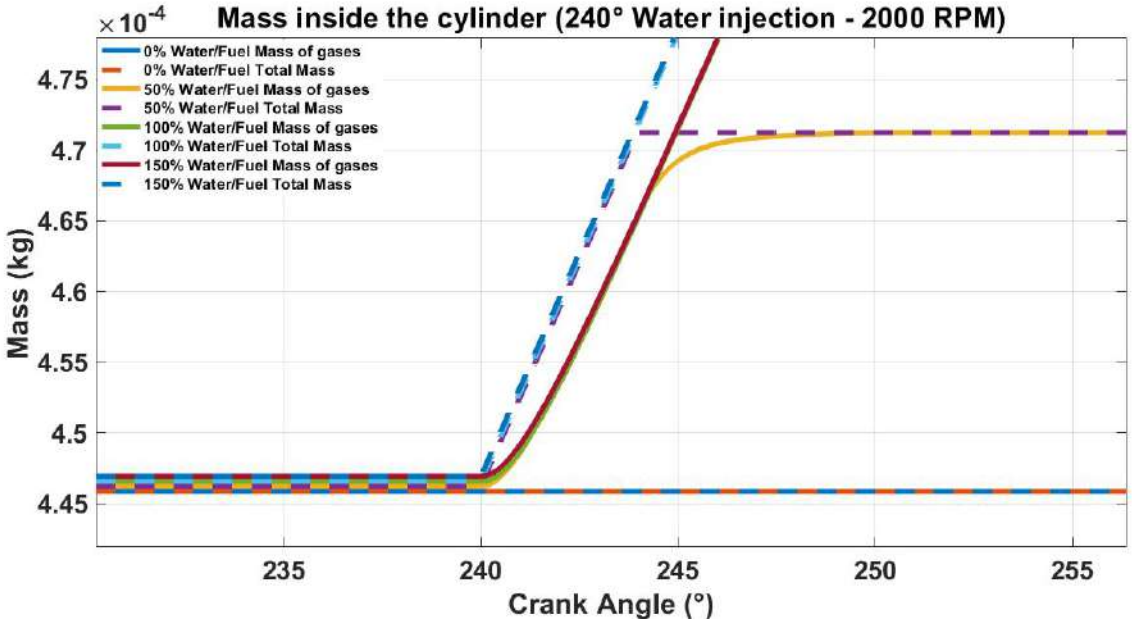

Fig. 4.45 – Mass In-Cylinder 240° water injection 2000 RPM. Detail (1)

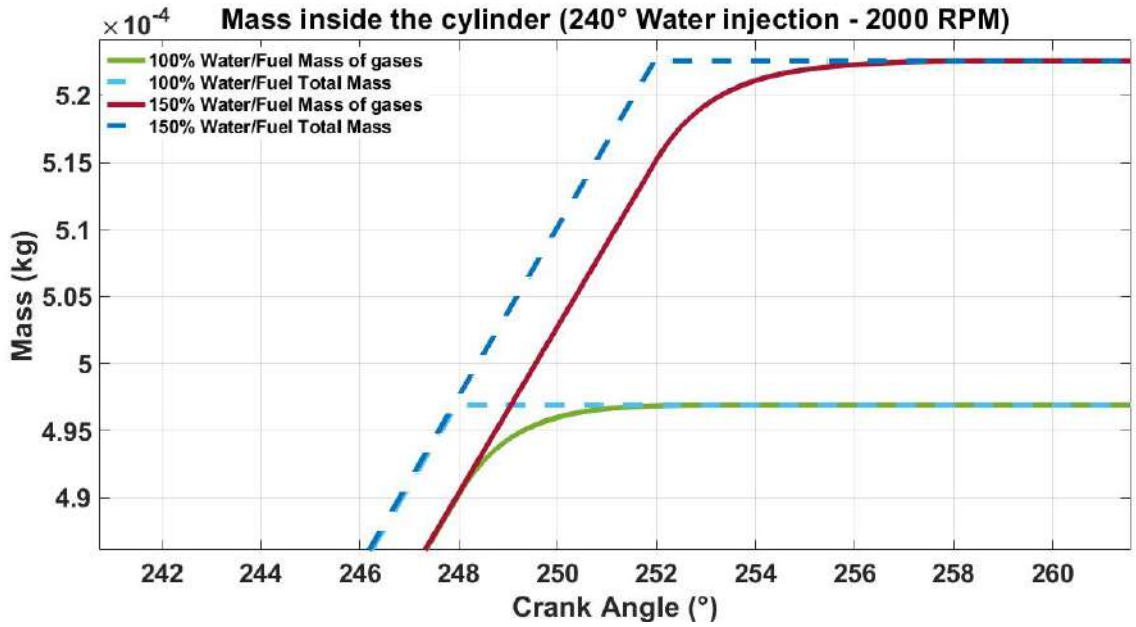

Fig. 4.46 – Mass In-Cylinder 240° water injection 2000 RPM. Detail (2)

In cases where the water injection is carried out at 330° and 370° (2000 RPM), the behavior of the three variables analyzed (pressure, temperature in the burned and unburned gas zones and the amount of mass inside the cylinder) maintain the trend observed at 1000 RPM, i.e. the maximum pressure values are obtained for cases without water injection and this value is proportional to the amount of water injected (Table 4.12), (Fig.4.47). For injection at 370° in a similar way, the pressure drop is very small (Fig.4.48); the difference between the condition without water injection (6.447 MPa) and the minimum pressure value (6.444 MPa) reached with water injection is 3 KPa. Very similar to that observed for 1000 RPM.

In relation to the temperature in the burned gas zone, again the trend in the maximum values and the behaviour of the graphs of the variations of this parameter (Fig.4.49) maintains the trend previously observed at 1000 RPM. There is a drop between the maximum temperatures without water injection (2312 K) and the maximum amount of water injected (150%, 2068 K). 244 K is the corresponding decrease in temperature when water is injected at 330° ATDC Exhaust-Intake.

At 370° (2000 RPM), water injection point, the maximum temperature value is the same for all water injection conditions, including the case where no water is injected (Fig.4.50). A little different from what was observed at 1000 RPM although it should be remembered that for here the maximum temperature difference is very small (10 K).

At 1000, 2000, 3000, 4000 and 5000 RPM, when the injection is made at 180° ATDC Exhaust-Intake, the pressure behavior is practically the same. (Fig.4.25, 1000 RPM), ((Fig.4.51), 2000 RPM), ((Fig.4.52), 3000 RPM), ((Fig.4.53), 4000 RPM) and ((Fig.4.54), 5000 RPM),

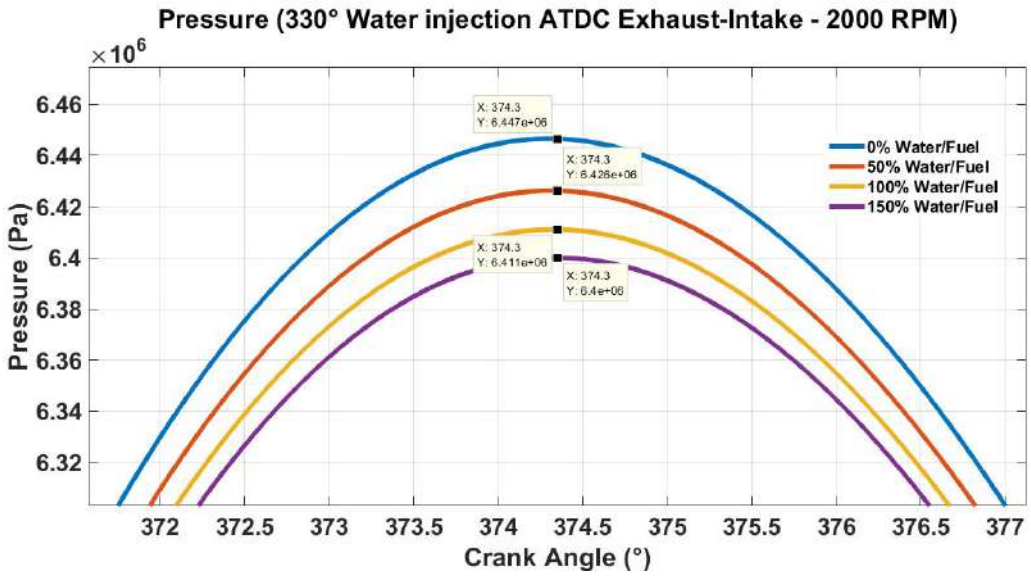

Fig. 4.47 – Pressure 330° 2000 RPM.

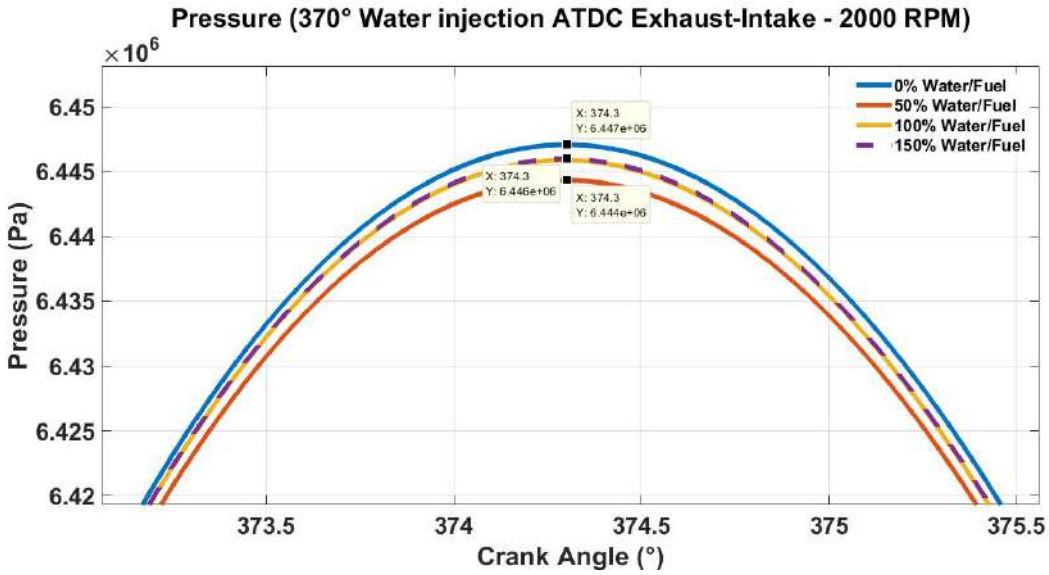

Fig. 4.48 – Pressure 370° 2000 RPM.

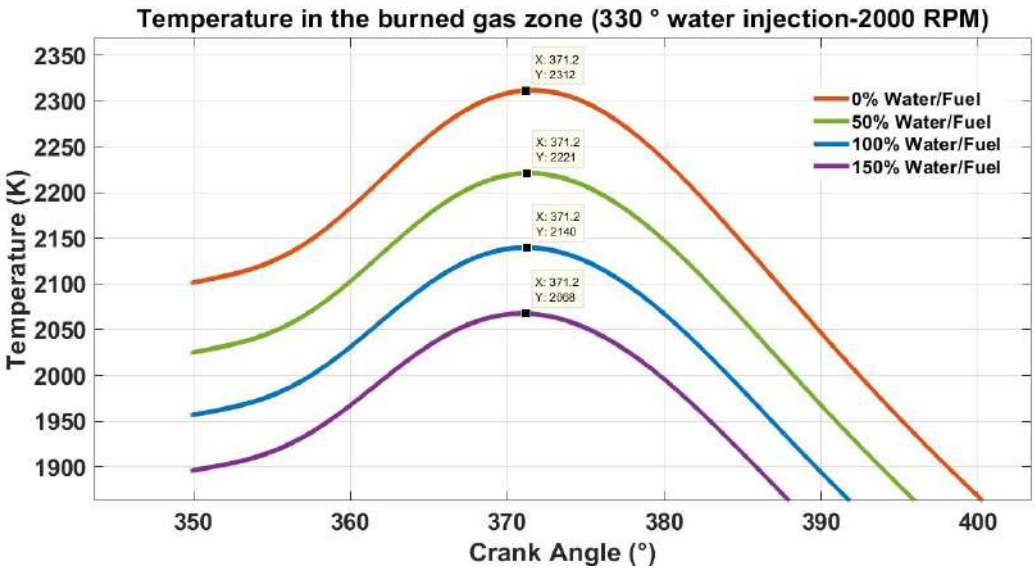

Fig. 4.49 – Temperature 330° Burned zone 2000 RPM. Detail (2).

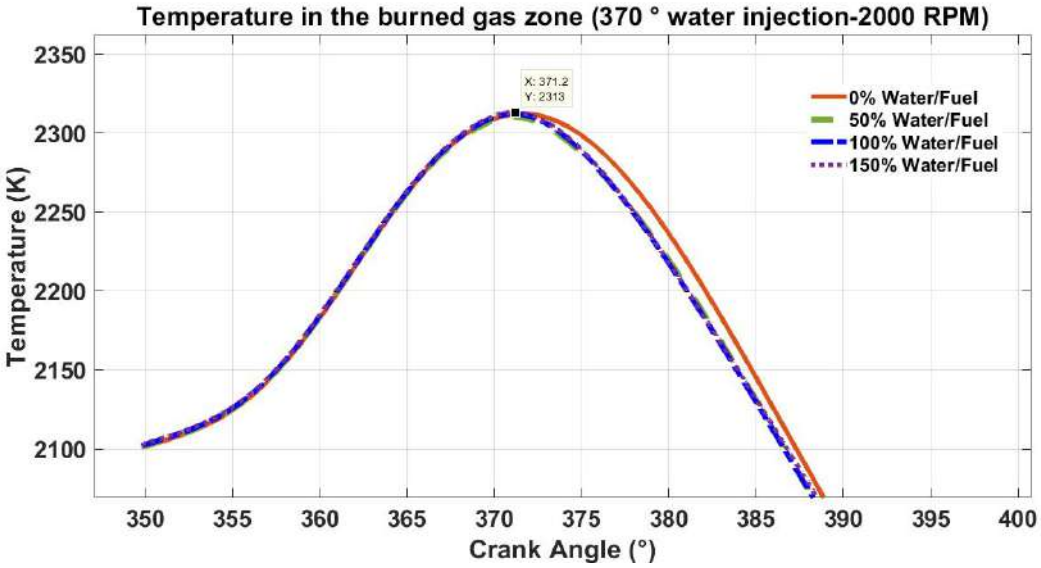

Fig. 4.50 – Temperature 370° Burned zone 2000 RPM. Detail (2).

show that the tendency to increase the pressure for the mentioned water injection condition is constant in all rotation speed regimes and for all amounts of water injection (Table 4.12).

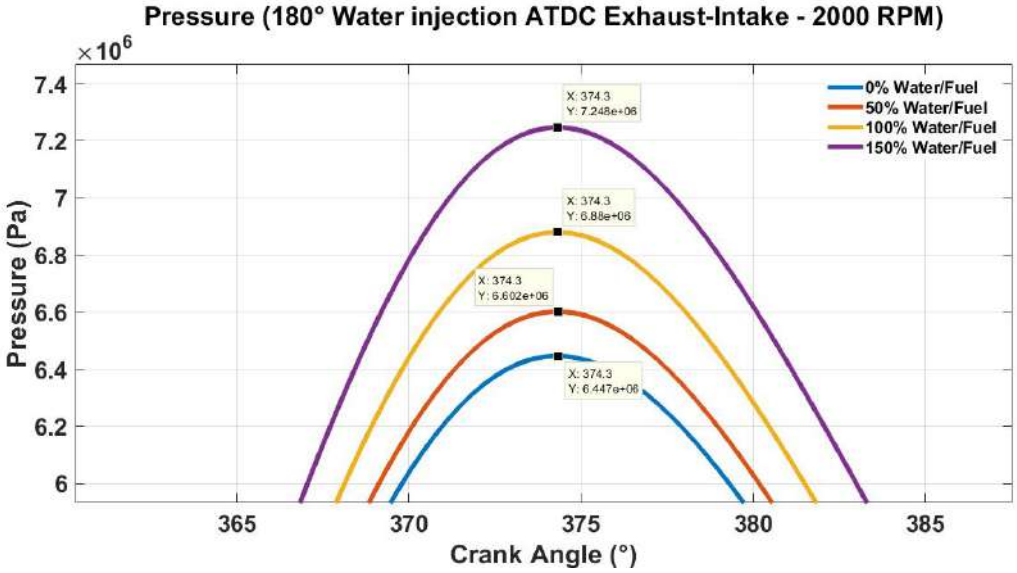

Fig. 4.51 – Pressure 180° 2000 RPM.

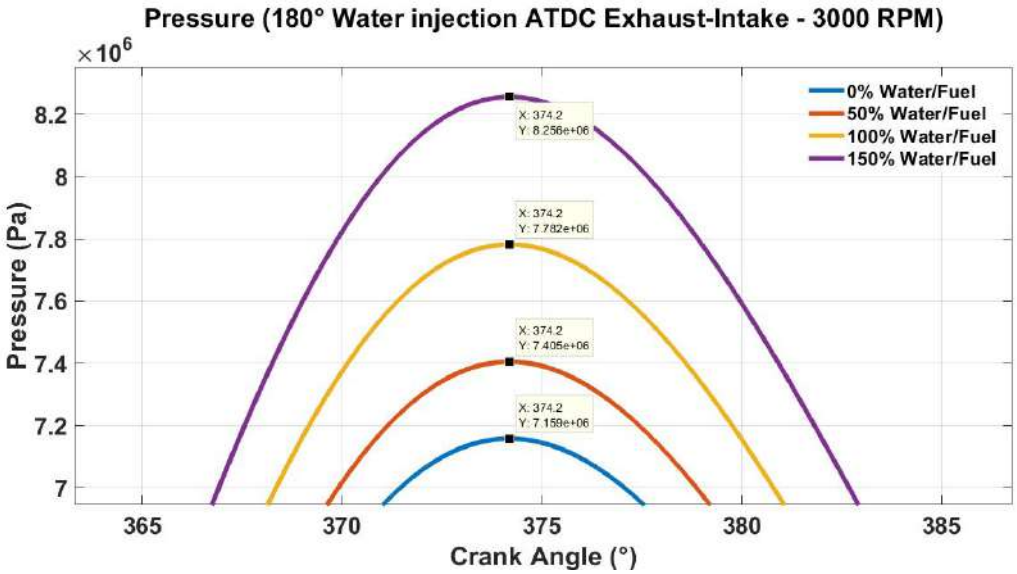

Fig. 4.52 – Pressure 180° 3000 RPM.

It was mentioned earlier that when the injection is performed 240° ATDC Exhaust-Intake, the behavior differs between what is observed in 1000 and 2000 RPM with respect to what is observed in 3000, 4000 and 5000 RPM. For the first two speeds of rotation ((Fig.4.31), 1000 RPM) the value of the maximum pressure inside the cylinder increases as a consequence of the addition of the mass of water injection while in 3000 RPM, 4000 RPM and 5000 RPM, the maximum pressure decreases in proportion to the amount of water injected ((Fig.4.55) 3000

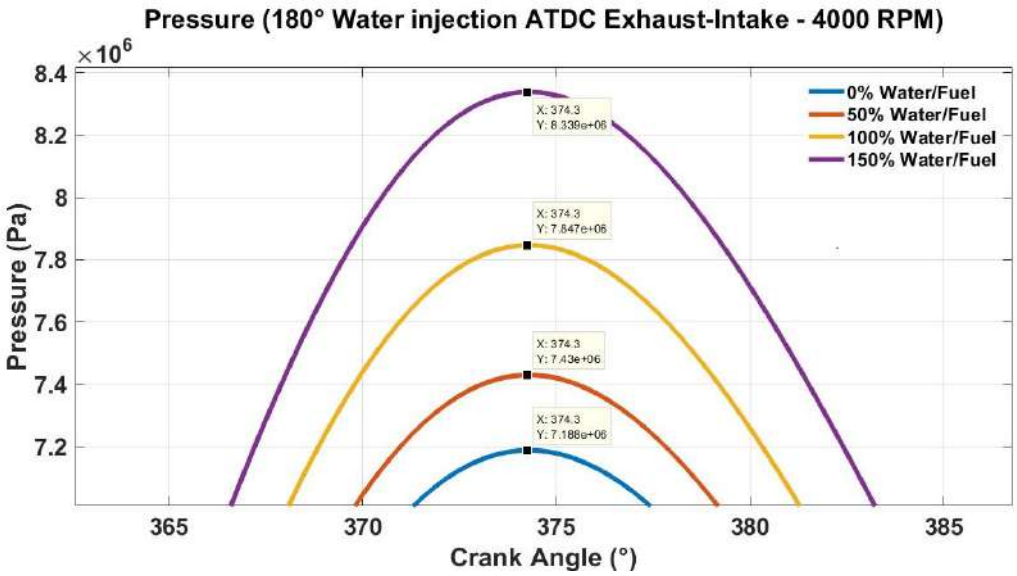

Fig. 4.53 – Pressure 180° 4000 RPM.

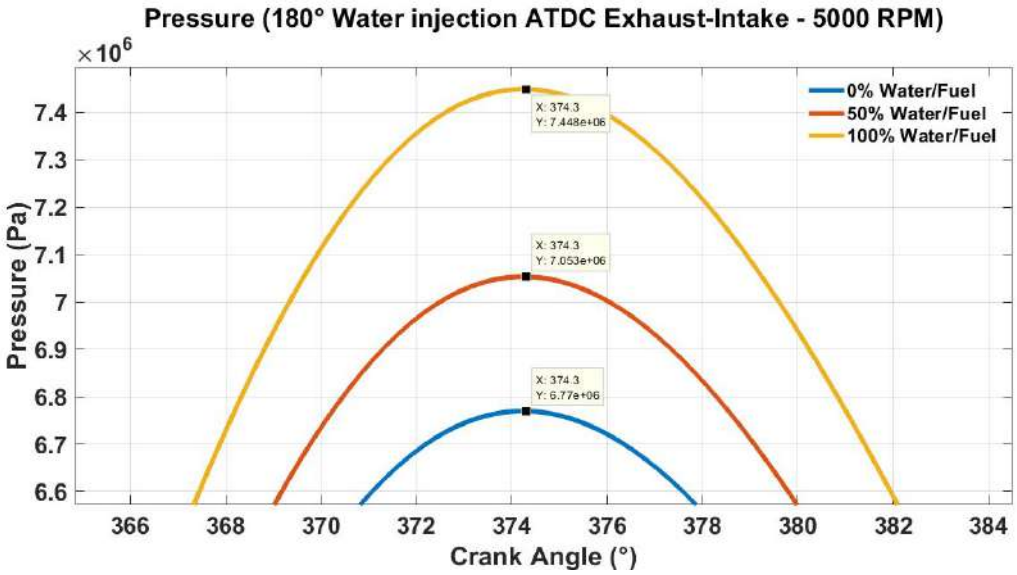

Fig. 4.54 – Pressure 180° 5000 RPM

RPM, (Fig.4.56) 4000 RPM and (Fig.4.57) 5000 RPM). These differences in pressure behavior for this water injection condition are related with the time available for the water vapor generated by the injection and evaporation process and the air/fuel mixture to become a homogeneous gas mixture. At 1000 and 2000 RPM there is more time available for this homogenization than at 3000, 4000 and 5000 RPM.

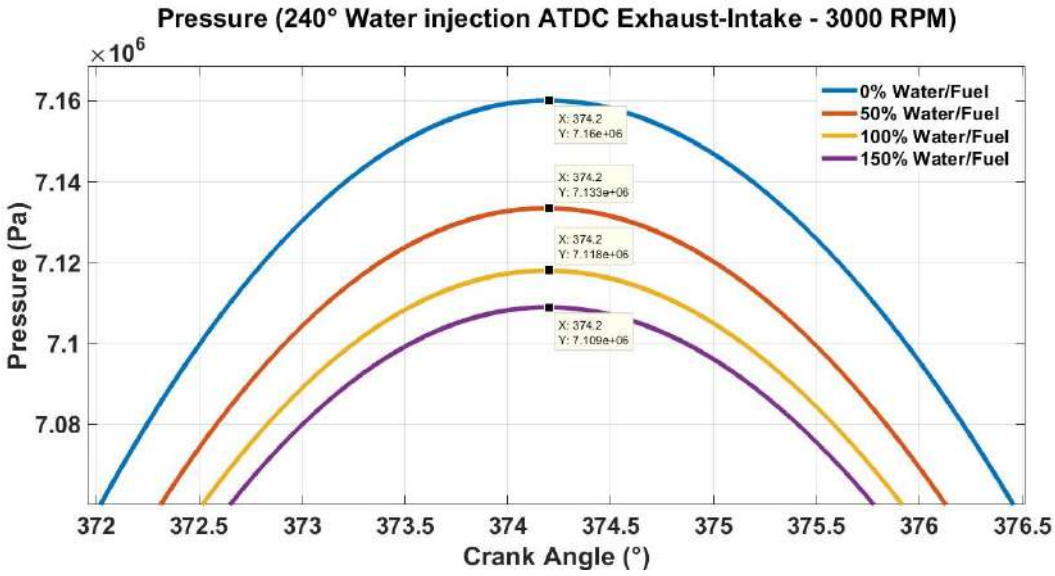

Fig. 4.55 – Pressure 240° 3000 RPM.

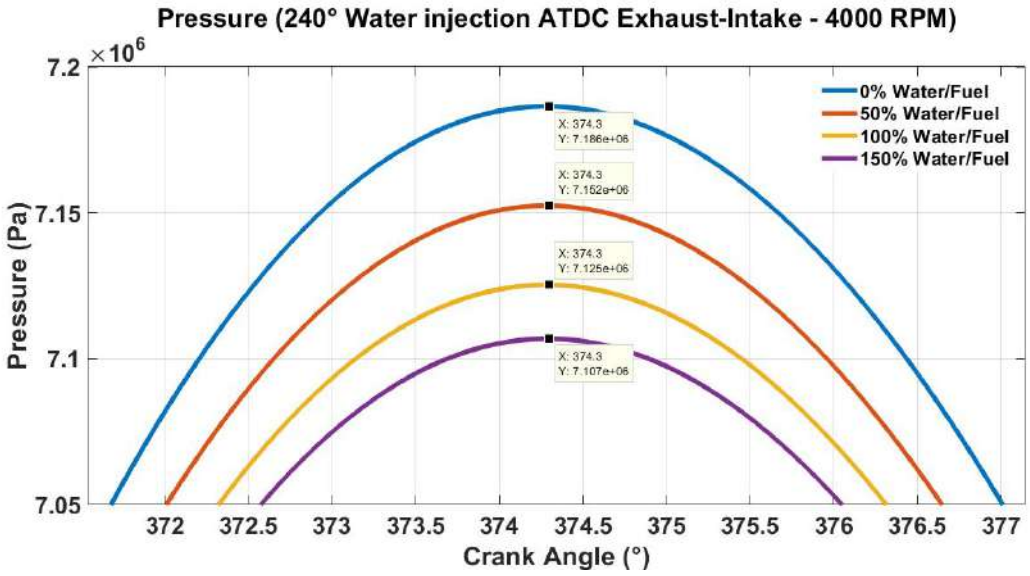

Fig. 4.56 – Pressure 240° 4000 RPM.

For the maximum temperature values in the burned gas zone when the injection is made in 180° ATDC Exhaust-Intake, it is observed that the temperature drop resulting from the injection of water is smaller as the rotation speed increases. In all rotations, the highest temperature

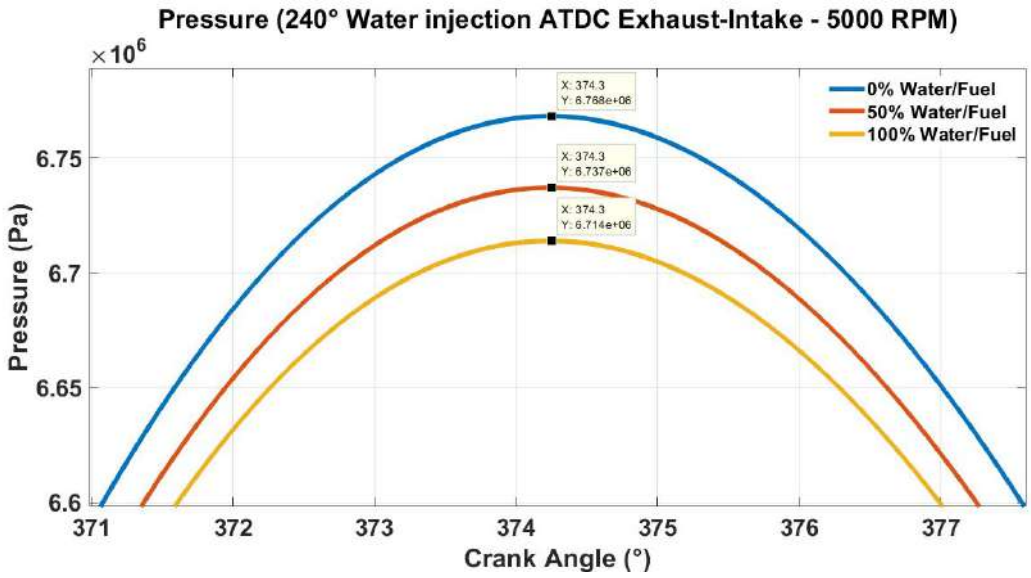

Fig. 4.57 – Pressure 240° 5000 RPM.

values in this area are reached for the connection without water injection, and these values are decreasing in direct proportion to the amount of water injected, but it is also observed that as the speed of rotation increases the difference between the maximum temperature values between the condition without injection and the maximum temperature reached for the largest amount of water injected (150% water/fuel, table 4.12) becomes smaller and smaller (12 K at 1000 RPM (Fig.4.28), 6 K at 2000 RPM (Fig.4.58), 5 K at 3000 RPM (Fig.4.59), 5 K at 4000 RPM (Fig.4.60) and 4 K at 5000 RPM, (Fig.4.61).

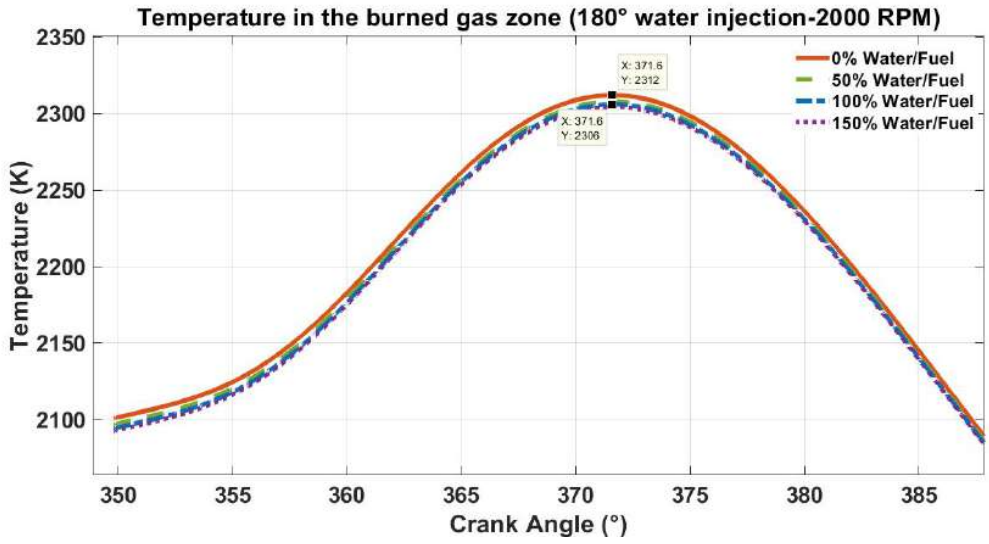

Fig. 4.58 – Temperature 180° Burned zone 2000 RPM. Detail (2).

It is observed that the influence of water injection when performed at 240° ATDC Exhaust-Intake is very similar in all rotation speed regimes. In all cases there is a drop between

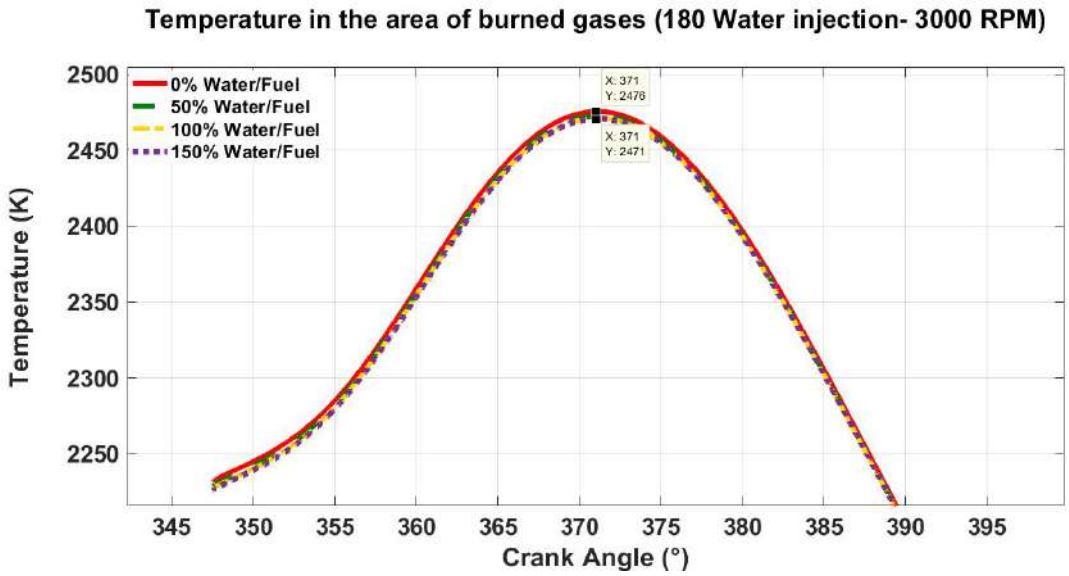

Fig. 4.59 – Temperature 180° Burned zone 3000 RPM. Detail (2).

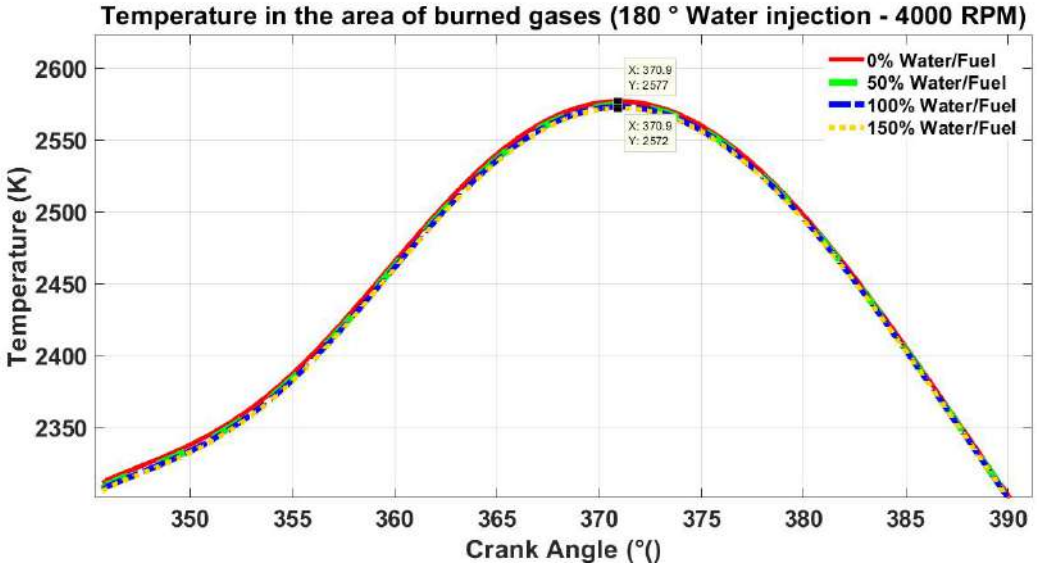

Fig. 4.60 – Temperature 180° Burned zone 4000 RPM. Detail (2).

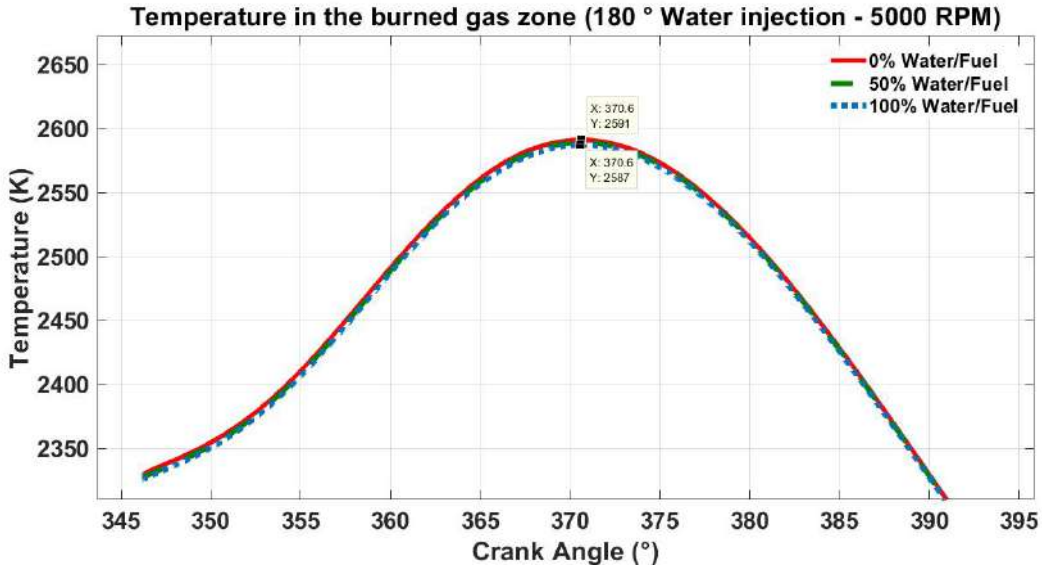

Fig. 4.61 – Temperature 180° Burned zone 5000 RPM. Detail (2).

the maximum temperature reached by the condition without water injection and the maximum amount of water injected (150% water/fuel, Table 4.12). At 1000 RPM the temperature drop is 248 K (Fig.4.62), at 2000 RPM, as mentioned above, the drop is 271 K (Fig.4.43).

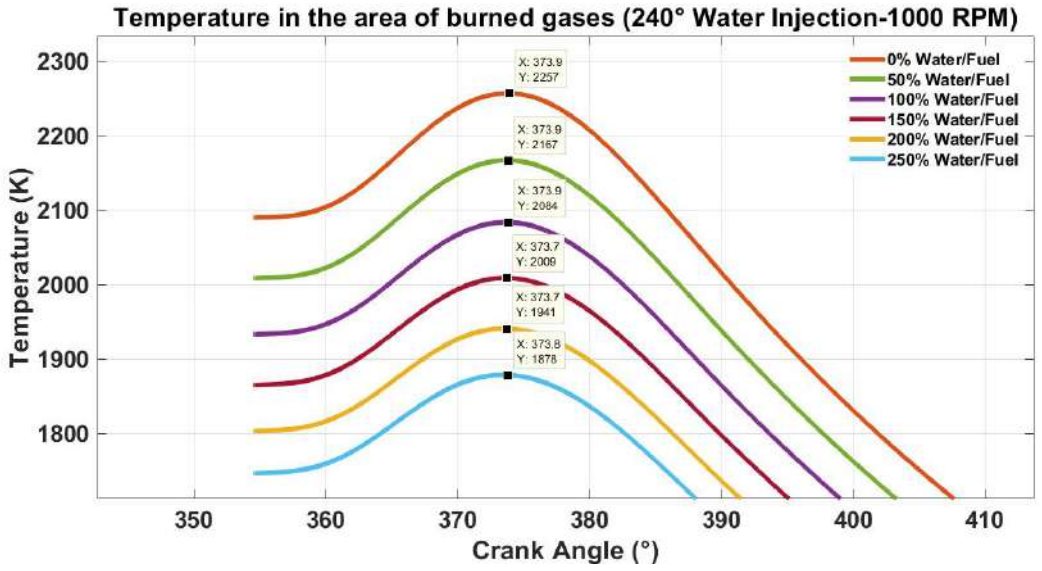

Fig. 4.62 – Temperature 240° 1000 RPM. Detail (2).

For 3000 RPM the temperature drop is 297 K (Fig.4.63), for 4000 RPM the temperature has to decrease by 316 K (Fig.4.64). Finally at 5000 RPM the drop is 229 K (0% water/fuel, 100% water/fuel, (Fig.4.65)).

If the injection is made in 330° ATDC Exhaust-Intake, the maximum pressure values for all the proposed cases (from 0% water/fuel to 150% water/fuel) decrease in a similar way. The

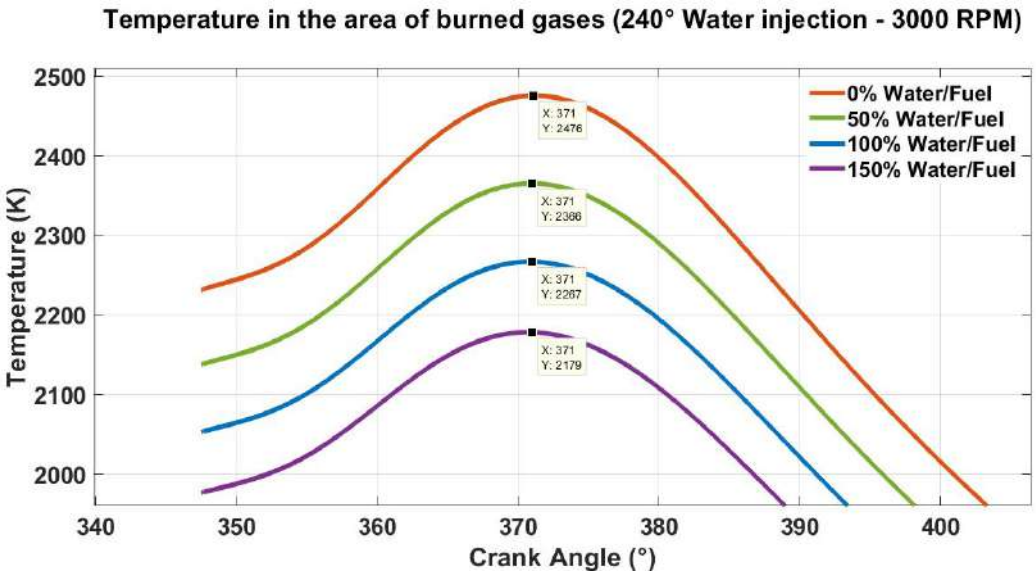

Fig. 4.63 – Temperature 240° Burned zone 3000 RPM. Detail (2).

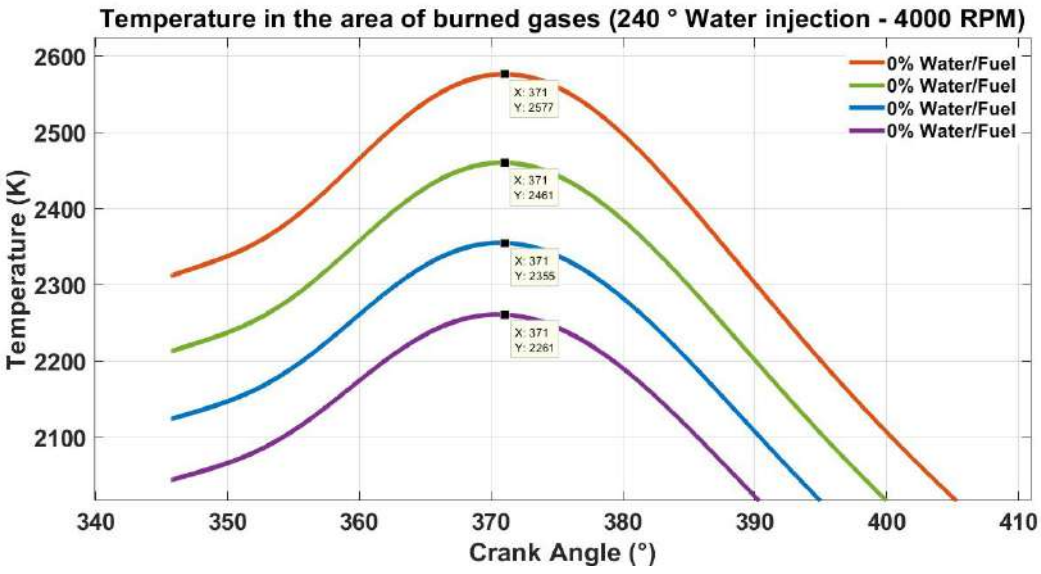

Fig. 4.64 – Temperature 240° Burned zone 4000 RPM. Detail (2).

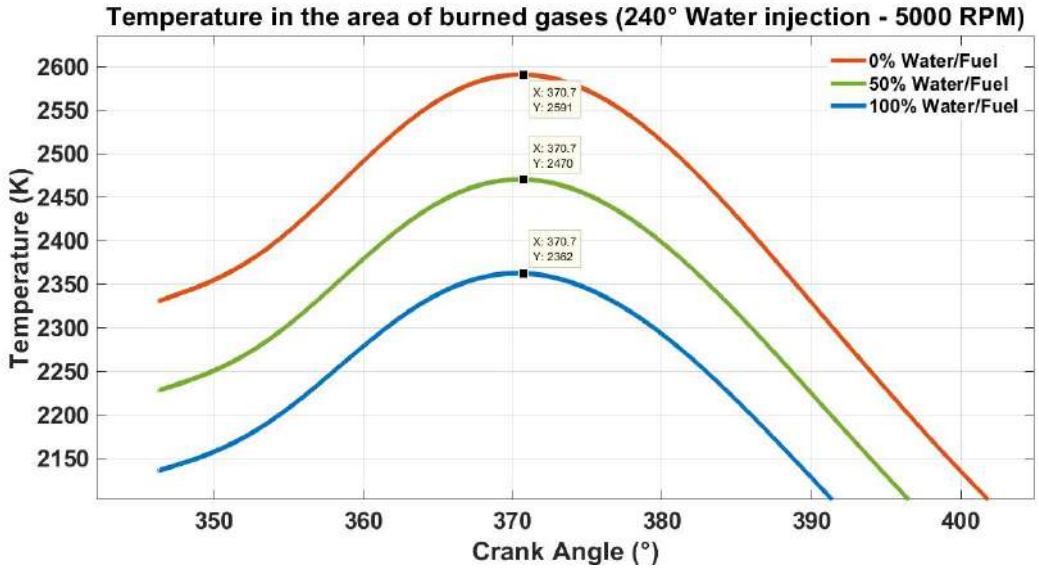

Fig. 4.65 – Temperature 240° Burned zone 5000 RPM. Detail (2).

maximum pressure falls in proportion to the amount of water injected (Table 4.12).

Table 4.13 – Comparison of the maximum pressures reached for water injection at 330° and 370° ATDC Exhaust-Intake.

		1000 RPM		2000 RPM		3000 RPM		4000 RPM		5000 RPM	
Water injection start point	**Water/Fuel Ratio**	**Maximum pressure reached (MPa)**	**Maximum pressure position (°)**	**Maximum pressure reached (MPa)**	**Maximum pressure position (°)**	**Maximum pressure reached (MPa)**	**Maximum pressure position (°)**	**Maximum pressure reached (MPa)**	**Maximum pressure position (°)**	**Maximum pressure reached (MPa)**	**Maximum pressure position (°)**
330° Water injection	***0***	5.137	376.3	6.447	374.3	7.159	374.2	7.187	374.3	6.77	374.3
	50	5.126	376.3	6.426	374.3	7.116	374.2	7.133	374.3	6.719	374.3
	100	5.118	376.3	6.411	374.3	7.081	374.2	7.085	374.3	6.68	374.3
	150	5.114	376.3	6.4	374.3	7.05	374.2	7.057	374.3		
	200	5.112	376.3								
	250	5.114	376.3								
370° Water injection	***0***	5.137	376.3	6.447	374.3	7.159	374.2	7.187	374.3	6.77	374.3
	50	5.135	376.3	6.444	374.3	7.158	374.2	7.189	374.3	6.77	374.3
	100	5.134	376.3	6.446	374.3	7.157	374.2	7.19	374.3	6.77	374.3
	150	5.134	376.3	6.446	374.3	7.157	374.2	7.19	374.3		

Table 4.13 shows the maximum values reached by the pressure inside the cylinder for the different quantities of water injected and for the injection points 330° and 370° ATDC Exhaust-Intake. It is observed how the values of the maximum pressure decrease as the amount of injection water increases, when the latter is done at 330° ATDC Exhaust-Intake ((Fig.4.66) 1000 RPM, (Fig.4.47) 2000 RPM, (Fig.4.67) 3000 RPM, (Fig.4.68) 4000 RPM, (Fig.4.69) 5000 RPM).

While in the case of injection at 370° no significant changes are observed in the maximum pressure values ((Fig.4.70) 1000 RPM, (Fig.4.71) 2000 RPM, (Fig.4.72) 3000 RPM, (Fig.4.73) 4000 RPM and (Fig.4.74) 5000 RPM.

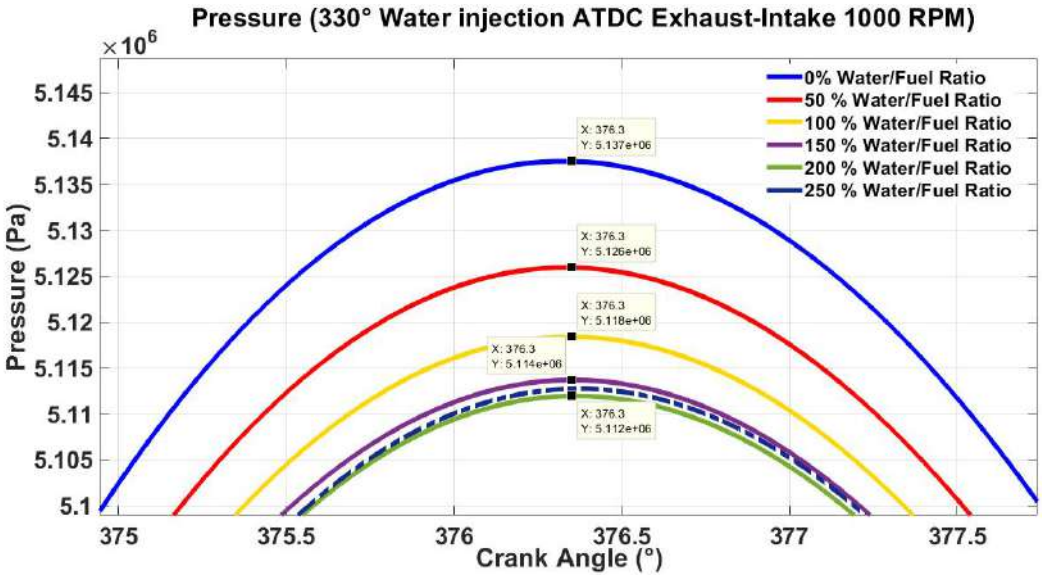

Fig. 4.66 – Pressure 330° 1000 RPM.

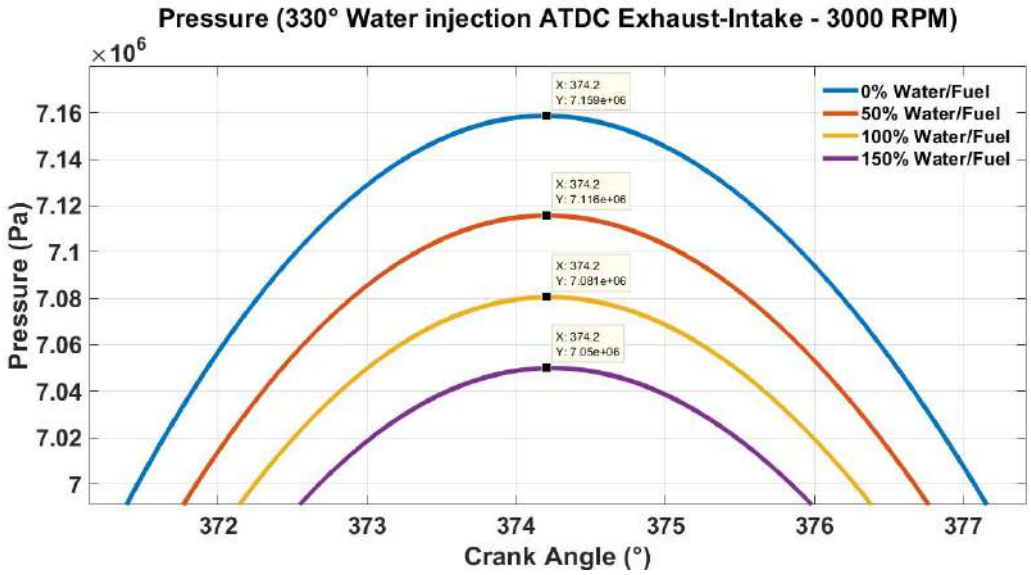

Fig. 4.67 – Pressure 330° 3000 RPM.

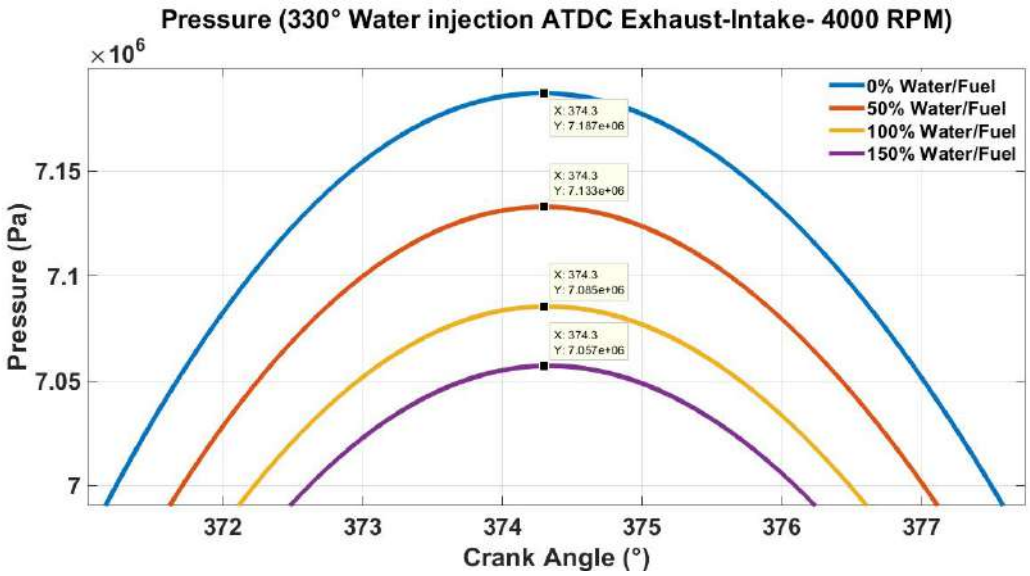

Fig. 4.68 – Pressure 330° 4000 RPM.

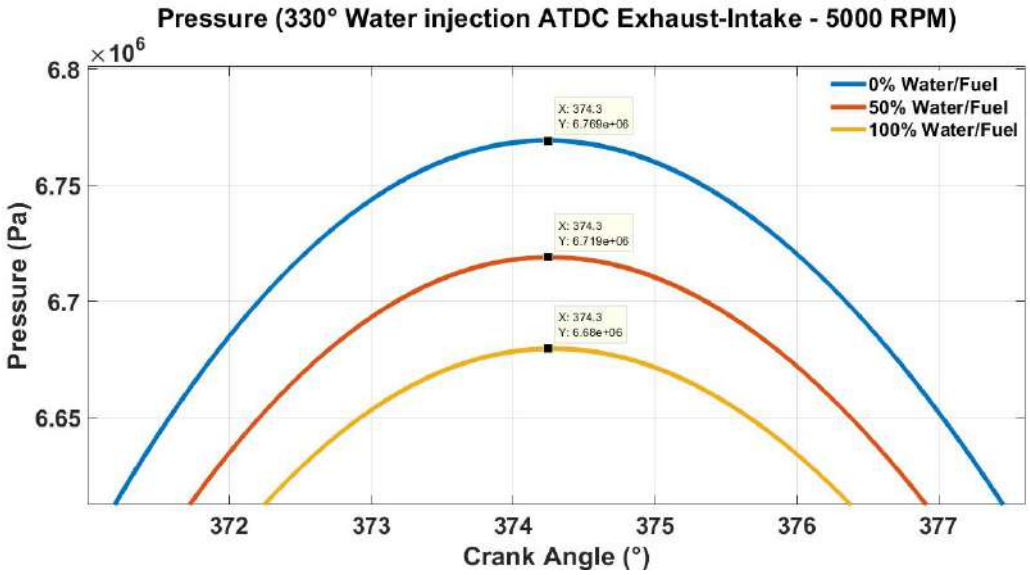

Fig. 4.69 – Pressure 330° 5000 RPM.

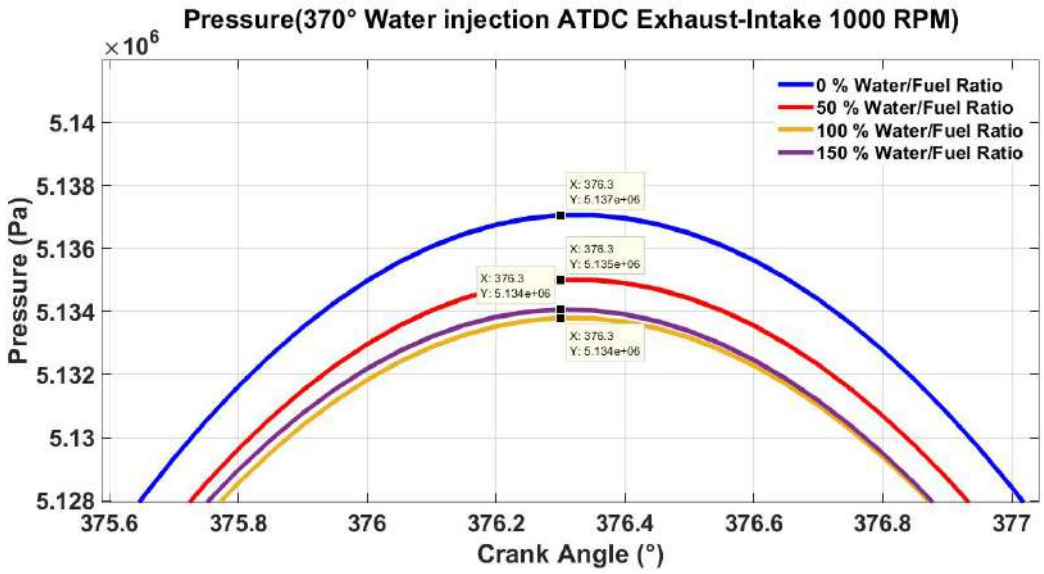

Fig. 4.70 – Pressure 370° 1000 RPM.

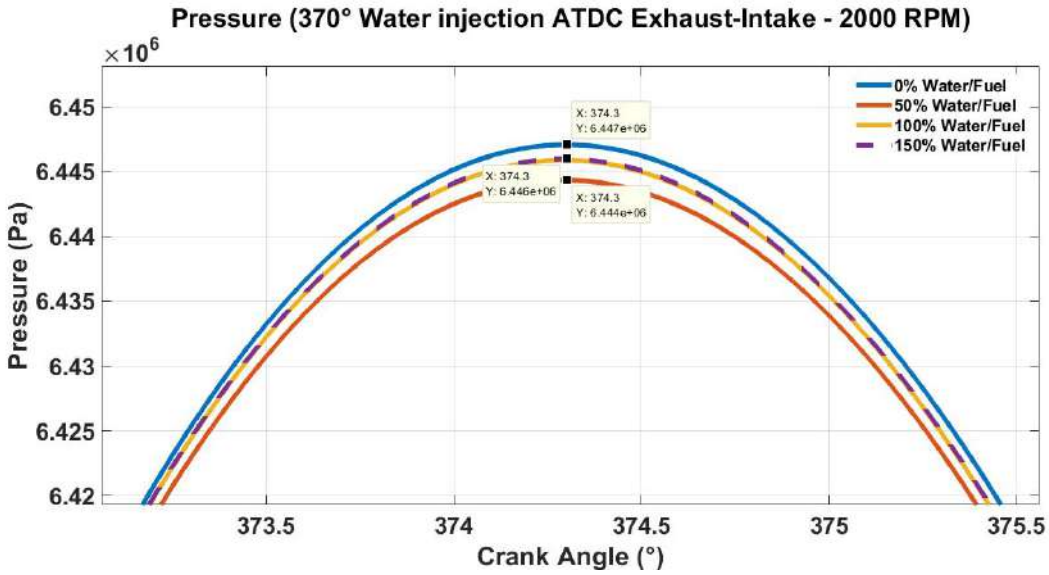

Fig. 4.71 – Pressure 370° 2000 RPM.

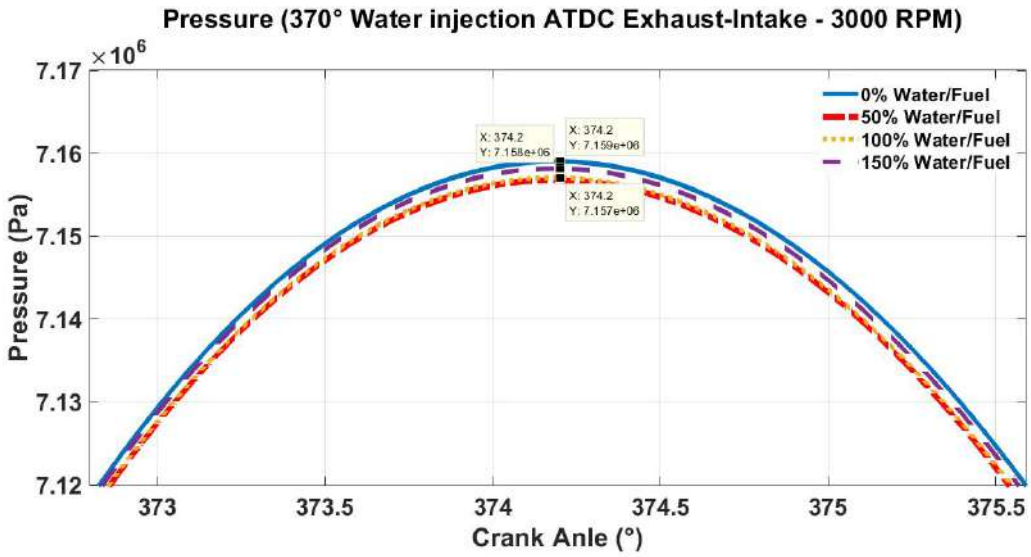

Fig. 4.72 – Pressure 370° 3000 RPM.

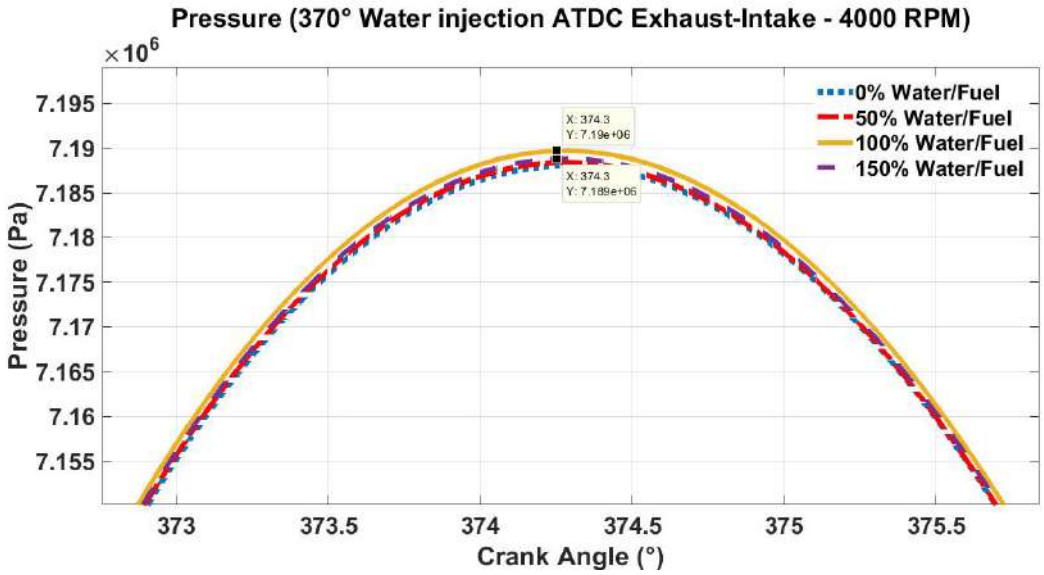

Fig. 4.73 – Pressure 370° 4000 RPM.

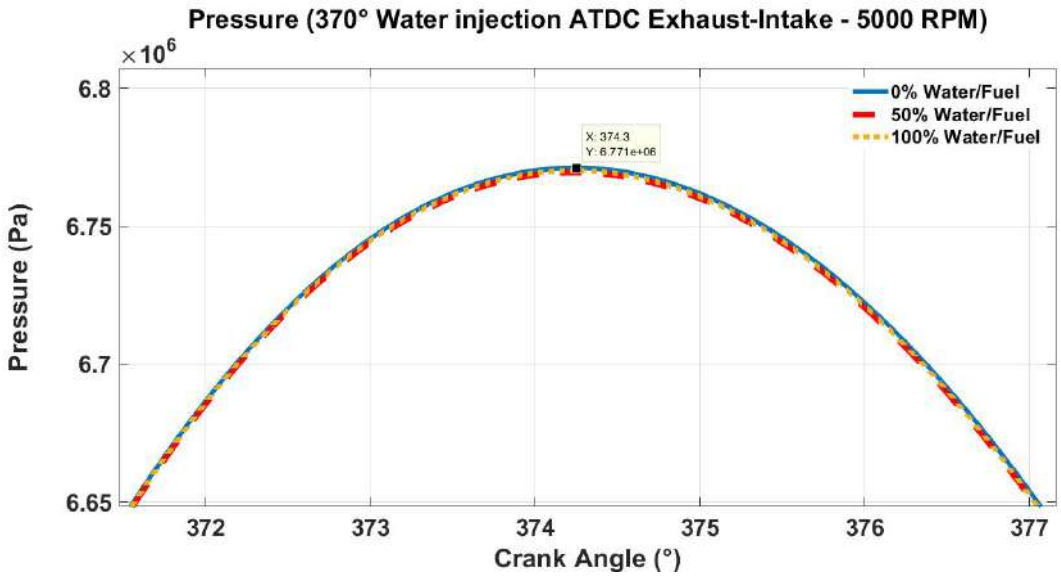

Fig. 4.74 – Pressure 370° 5000 RPM.

Table 4.14 – Comparison between the maximum temperatures reached inside the cylinder, for the burned gas zone (water injection at 330° and 370° ATDC Exhaust-Intake)

		1000 RPM		2000 RPM		3000 RPM		4000 RPM		5000 RPM	
Water injection start point	**Water/Fuel Ratio**	**Maximum temperature burned gases (K)**	**Position Maximum temperature burned gases Tb (°)**	**Maximum temperature burned gases (K)**	**Position Maximum temperature burned gases Tb (°)**	**Maximum temperature burned gases (K)**	**Position Maximum temperature burned gases Tb (°)**	**Maximum temperature burned gases (K)**	**Position Maximum temperature burned gases Tb (°)**	**Maximum temperature burned gases (K)**	**Position Maximum temperature burned gases Tb (°)**
330° Water injection	***0***	2257	373.9	2312	371.2	2476	371.0	2577	371	2591	370.6
	50	2176	373.9	2221	371.2	2375	371.0	2469	371	2480	370.6
	100	2101	373.9	2140	371.2	2287	370.8	2374	371	2384	370.6
	150	2034	373.9	2068	371.2	2207	370.6	2293	371		
	200	1974	373.9								
	250	1919	373.9								
370° Water injection	***0***	2257	373.9	2313	371.2	2476	370.9	2577	370.8	2591	370.5
	50	2247	371.8	2313	371.2	2478	370.9	2580	370.8	2593	370.5
	100	2247	371.8	2313	371.2	2478	370.9	2580	370.8	2593	370.5
	150	2247	371.8	2313	371.2	2478	370.9	2580	370.8		

Table 4.14 presents the comparison between the maximum temperatures reached in the burned gas zone when the water injection is performed at 330° and 370° ATDC Exhaust-Intake and for the proposed water quantities (0%, 50%, 100% and 150% water/fuel). It is observed a similar behavior to that seen in the pressure. When the injection is done at 330° ATDC Exhaust-Intake, the temperatures decrease in direct proportion to the quantities of water injected at all the rotation speeds selected for the simulations ((Fig.4.75) 1000 RPM, (Fig.4.76) 2000 RPM, (Fig.4.77) 3000 RPM (Fig.4.78) 4000 RPM and (Fig.4.79) 5000 RPM.

When water is injected at 370° ATDC Exhaust-Intake, the temperature decrease is very small. Only at 1000 RPM it reaches 10 K while at other engine speeds it does not exceed 3 K. ((Fig.4.80) 1000 RPM, (Fig.4.81) 2000 RPM, (Fig.4.82) 3000 RPM, (Fig.4.83) 4000 RPM and

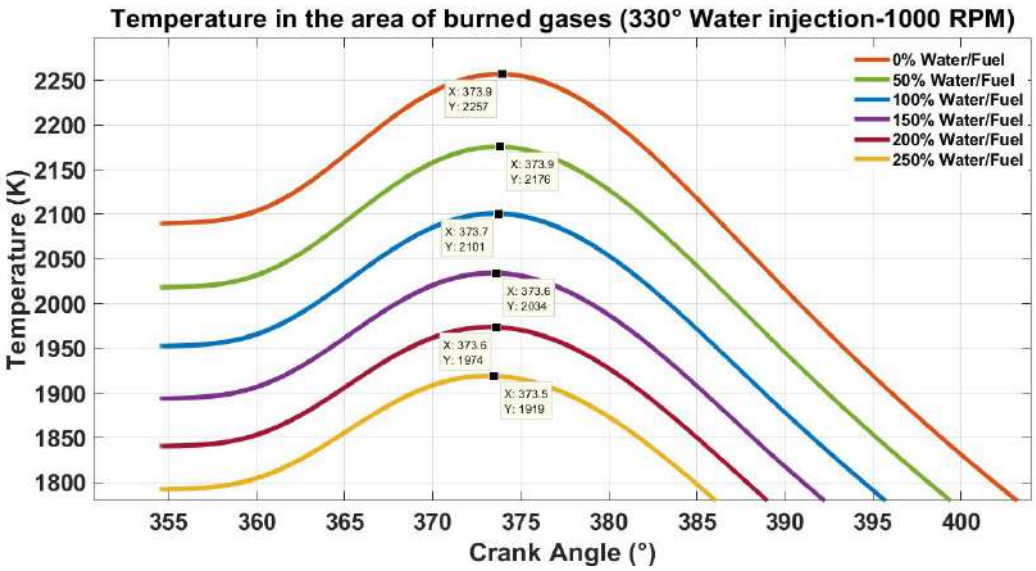

Fig. 4.75 – Temperature 330° 1000 RPM. Detail (2).

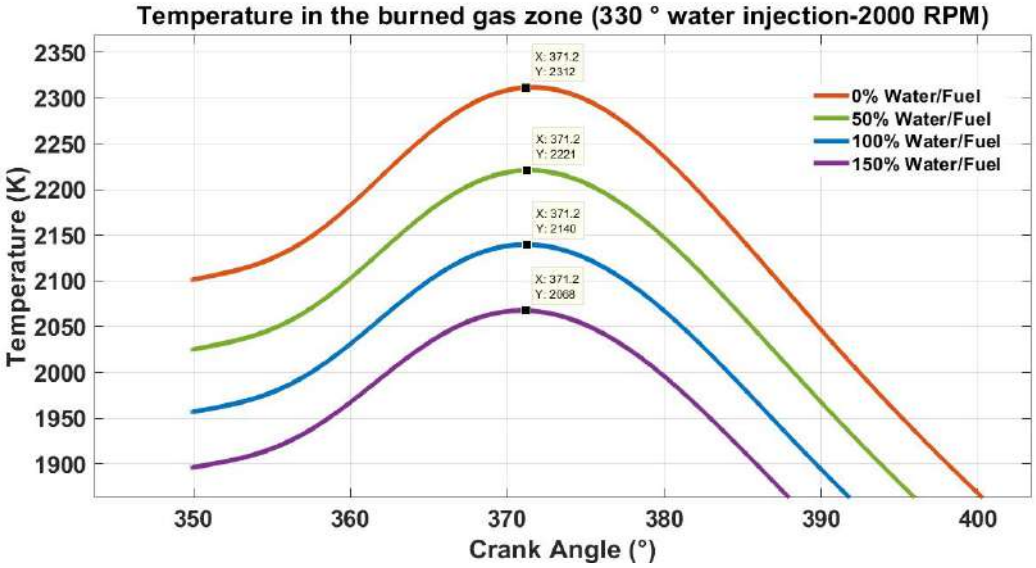

Fig. 4.76 – Temperature 330° Burned zone 2000 RPM. Detail (2).

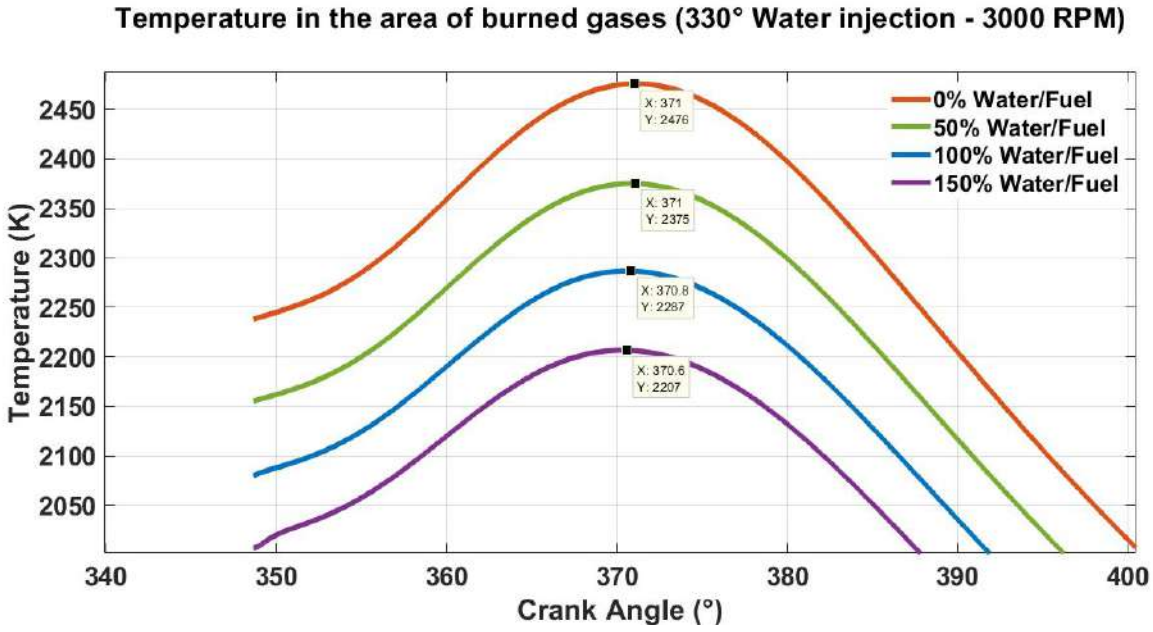

Fig. 4.77 – Temperature 330° water injection Burned Zone 3000 RPM. Detail (2).

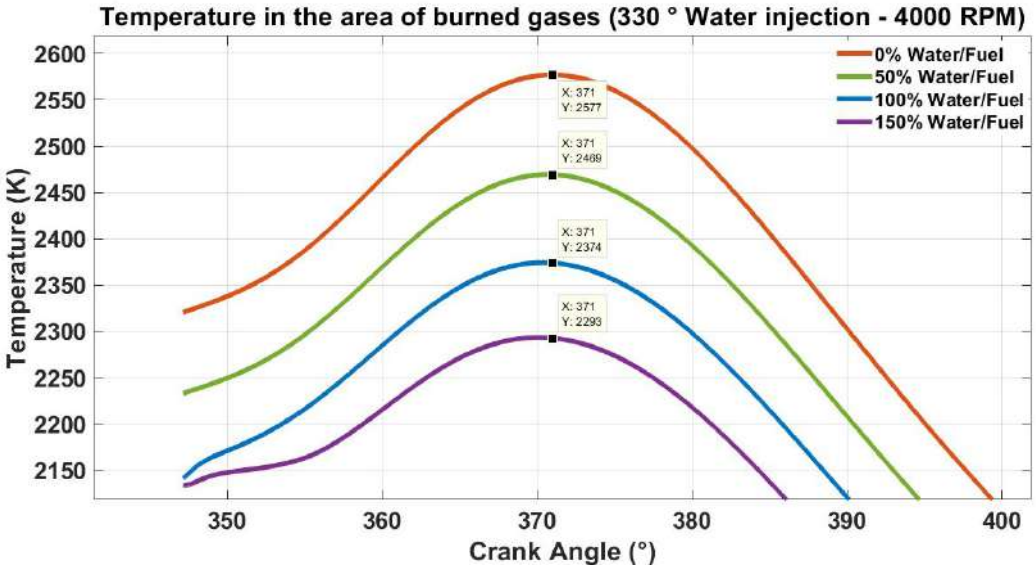

Fig. 4.78 – Temperature 330° Burned zone 4000 RPM. Detail (2).

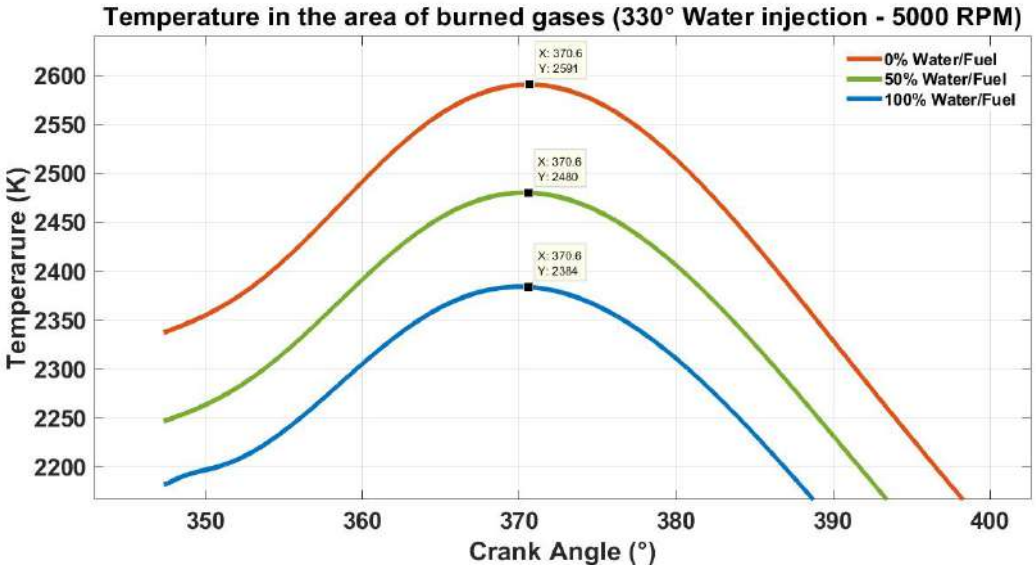

Fig. 4.79 – Temperature 330° Burned zone 5000 RPM. Detail (2).

(Fig.4.84) 5000 RPM.

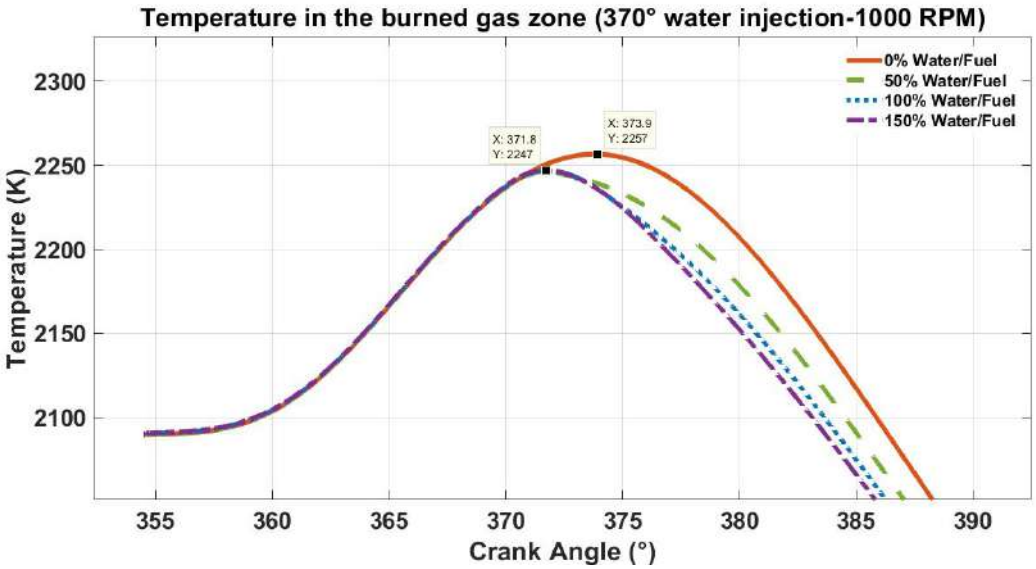

Fig. 4.80 – Temperature 370° 1000 RPM. Detail (2).

With respect to the variation of the amount of total mass and mass of gases inside the cylinder over the combustion cycle, (Fig.4.85) to (Fig.4.87), present the behavior of this variable when the injection of water is made in 330° ATDC Exhaust-Intake in 3000 RPM.

It is observed that the characteristic curve in S seen previously in other cases of water injection, confirm the correct interpretation by the simulation program of the thermodynamic conditions inside the cylinder and its influence on the process of evaporation of the water injection and as a result, how evaporation influences the conditions in the cylinder.

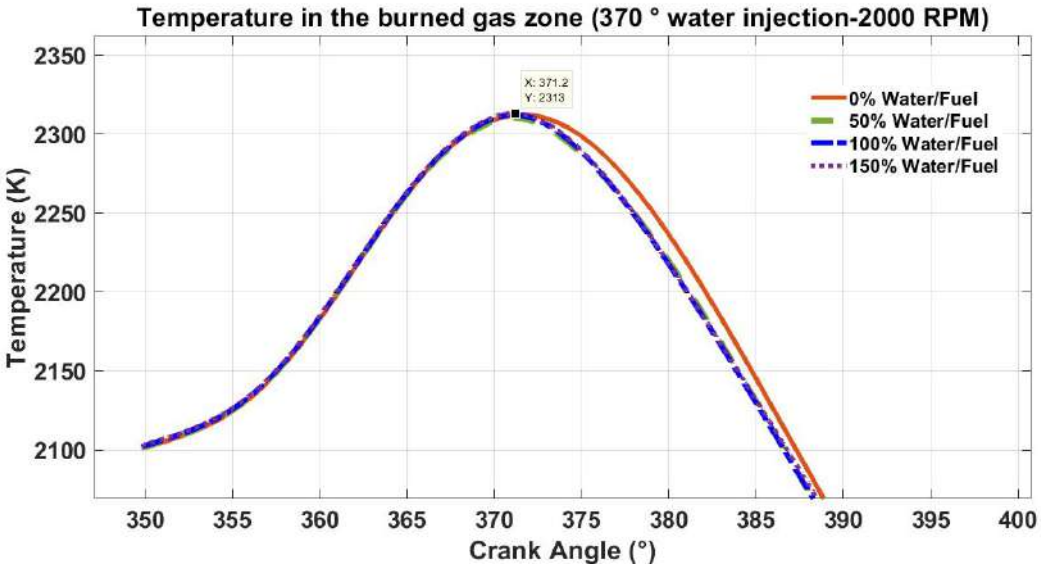

Fig. 4.81 – Temperature 370° Burned zone 2000 RPM. Detail (2).

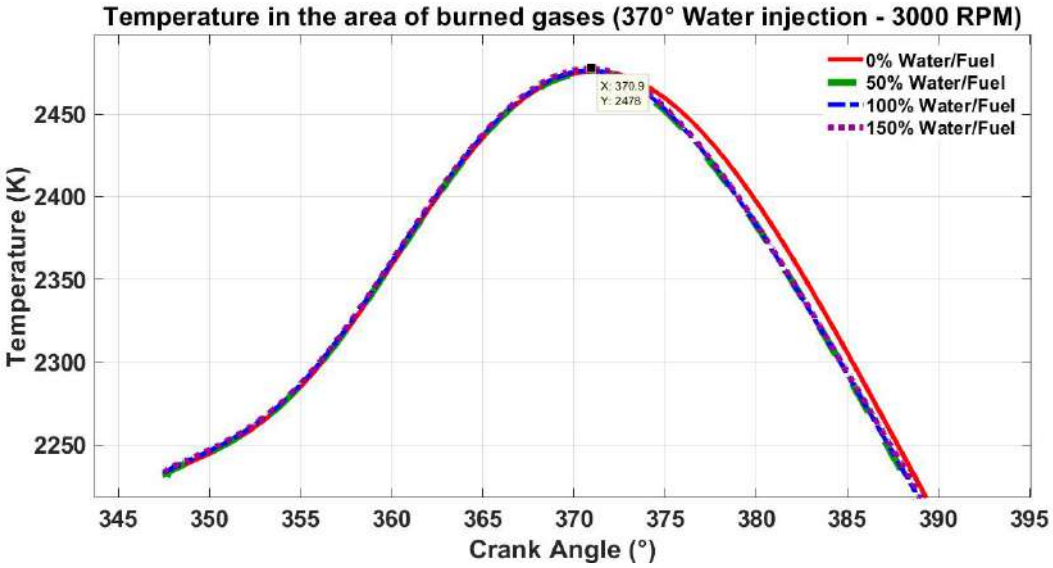

Fig. 4.82 – Temperature 370° Burned zone 3000 RPM. Detail (2).

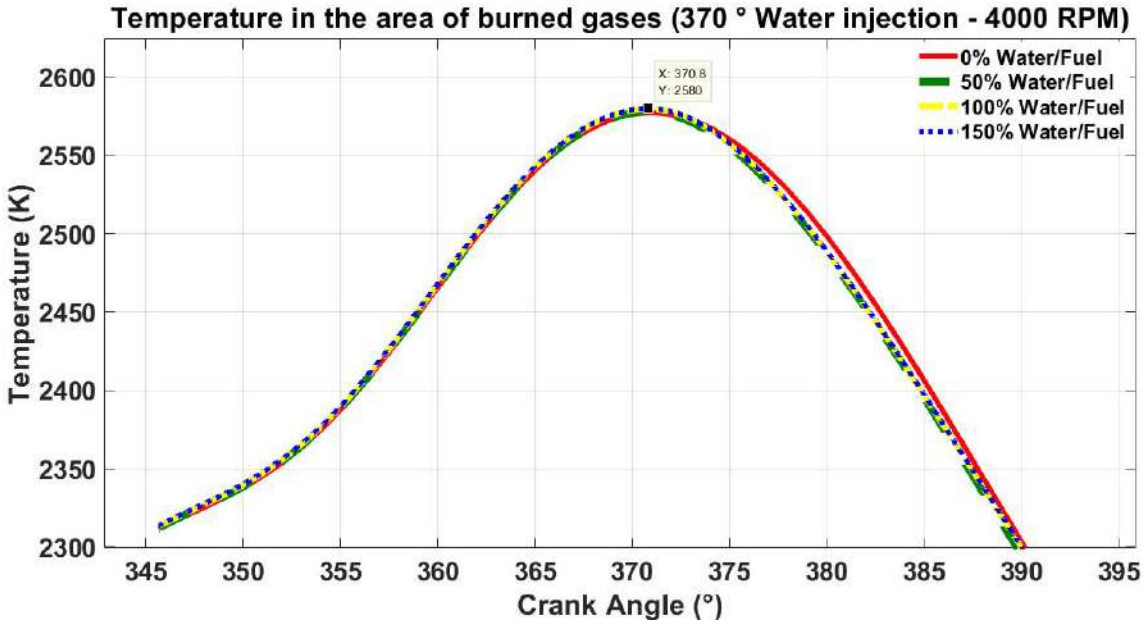

Fig. 4.83 – Temperature 370° water injection Burned Zone 4000 RPM. Detail (2).

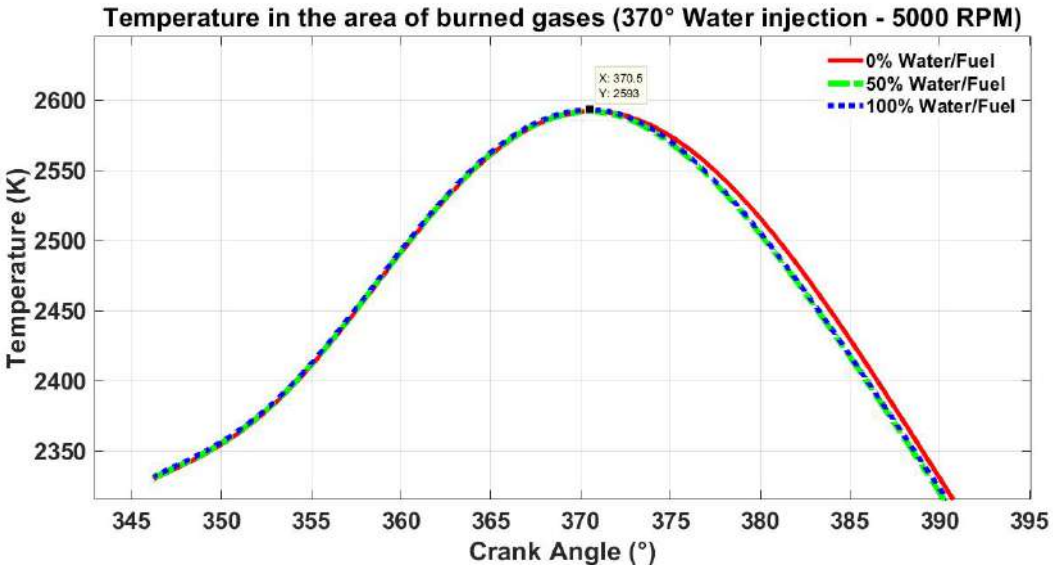

Fig. 4.84 – Temperature 370° Burned zone 5000 RPM. Detail (2).

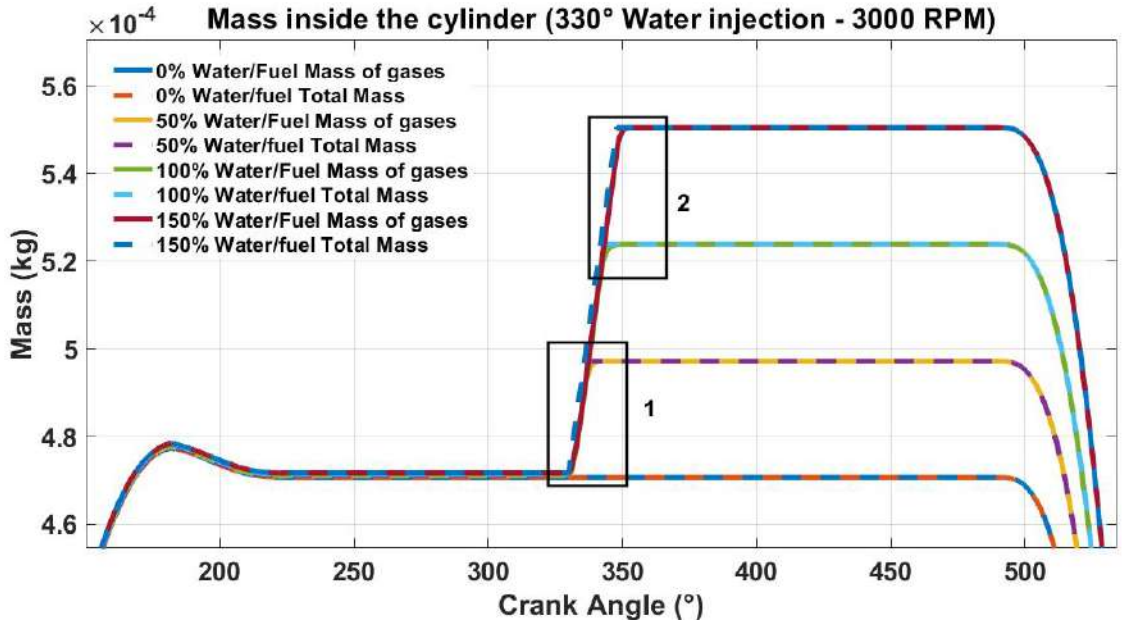

Fig. 4.85 – Mass In-Cylinder 330° water injection 3000 RPM.

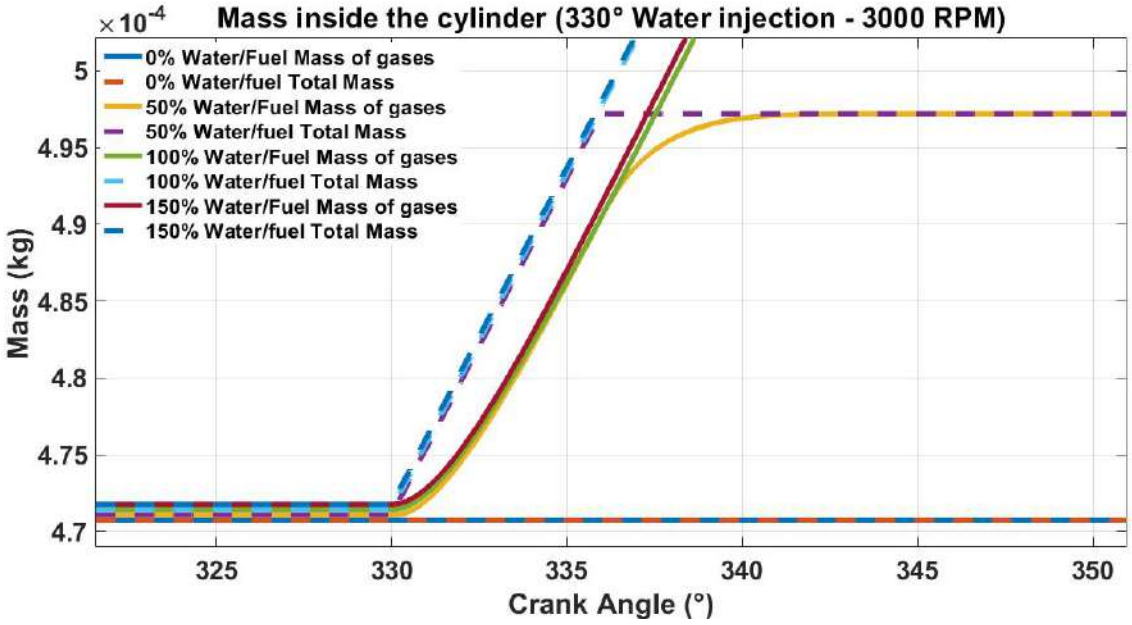

Fig. 4.86 – Mass In-Cylinder 330° water injection 3000 RPM. Detail (1)

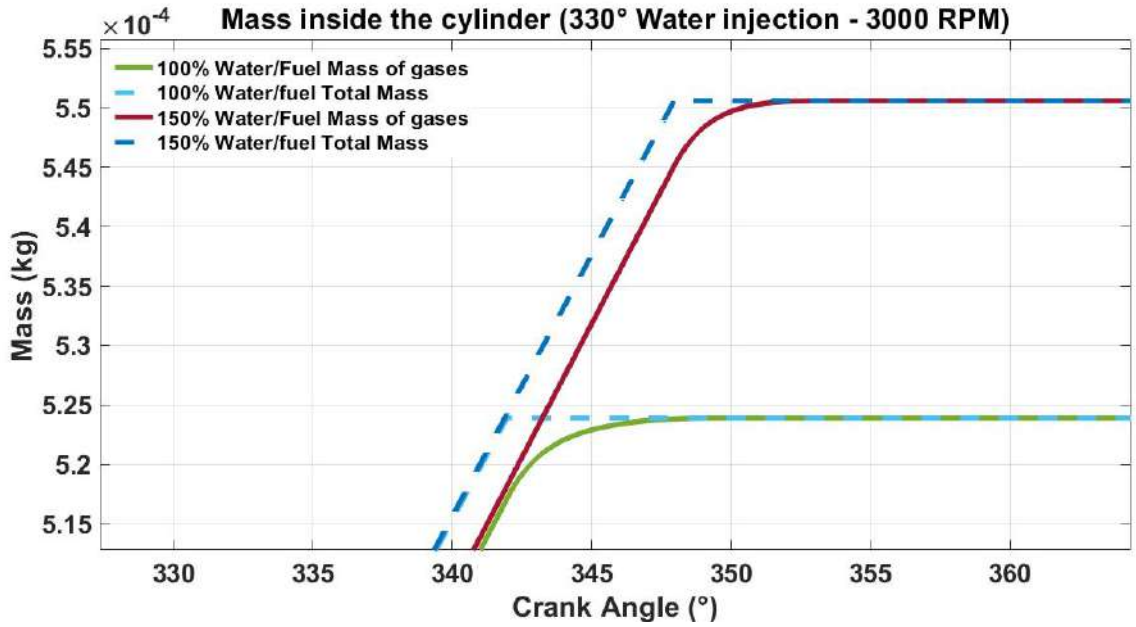

Fig. 4.87 – Mass In-Cylinder 330° water injection 3000 RPM. Detail (2)

The last case presented corresponds to the injection of water at 370°, i.e. after the start of combustion and 10° ATDC compression and 4000 RPM. (Fig.4.73) shows the behaviour of the pressure and the maximum values reached for the waterless condition and the three proposed quantities of water for injection (50%, 100% and 150% water/fuel). The variation of the maximum pressure is very small, around 1 KPa, which shows the little influence that the injection of water has on this variable when the injection is made on the zone of burned gases.

A similar behaviour for the maximum temperature in the burned gas zone was observed. (Fig.4.83) shows the temperature behaviour for the same water injection conditions mentioned above. No variation is observed in the value of the maximum temperature, however a little further on, towards the 374° ATDC of compression, it can be appreciated that the lines of temperature corresponding to the three conditions of water injection, are slightly separated from the line that corresponds to the condition without water injection.

This separation has a duration approximately equal to the angular interval that delays the injection of water which, for this particular case, is 24° when the greatest amount of water is injected (Table 4.12). Therefore, it is possible to affirm that the separation between the temperature lines in the burned gas zone corresponds to the influence of the evaporation process during the combustion cycle of the engine.

(Fig.4.88) to (Fig.4.90) show the variation of total mass and gases inside the cylinder for the aforementioned water injection condition. It is appreciated that the time that passes between the entrance of the water to the chamber of combustion and the evaporation of this one is very small. The process of evaporation is practically instantaneous when the water is injected in the

zone of burned gases, where the temperatures of the gaseous medium exceed 2000 K. This same behaviour is observed in all the rotational speed regimes analyzed, when the injection is carried out in 370° ATDC Exhaust-Intake, always in the burned gas zone.

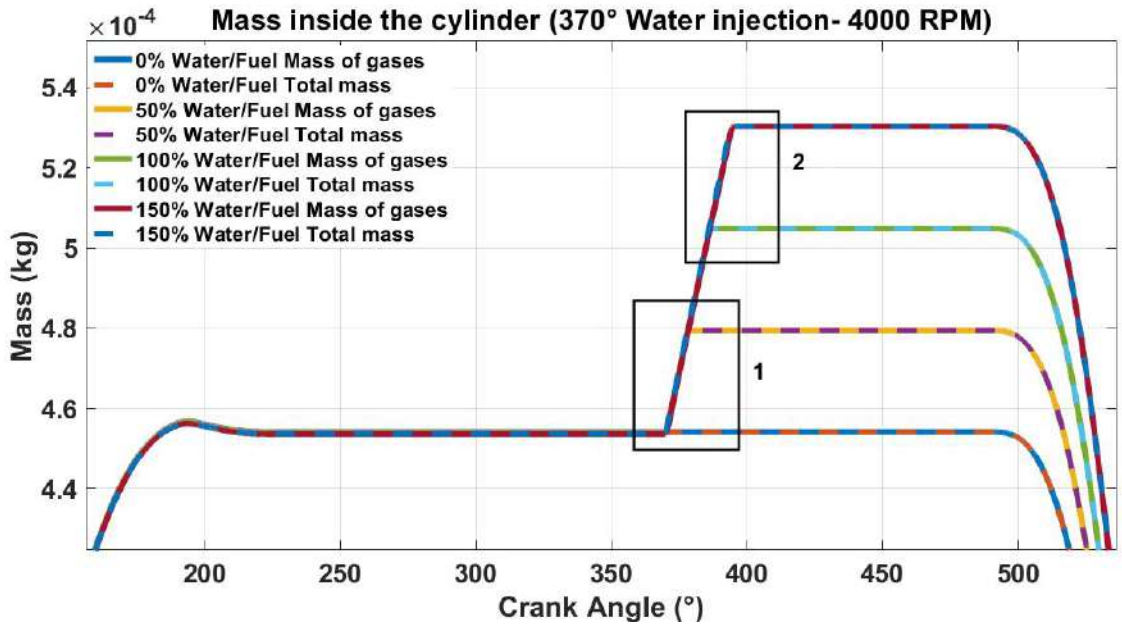

Fig. 4.88 – Mass In-Cylinder 370° water injection 4000 RPM.

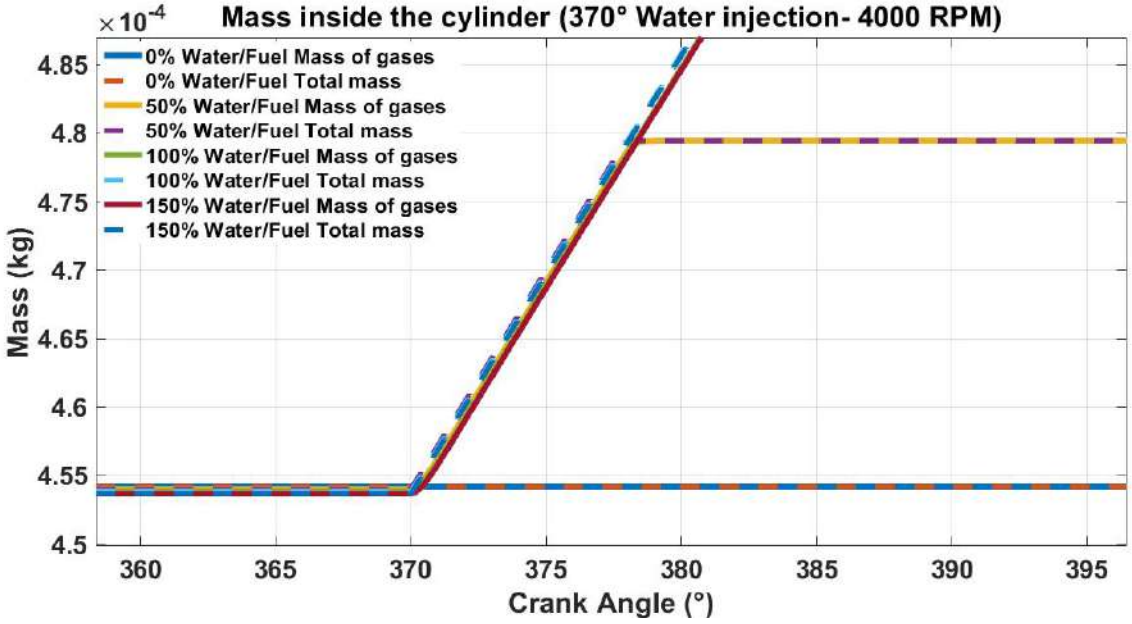

Fig. 4.89 – Mass In-Cylinder 370° water injection 4000 RPM. Detail (1)

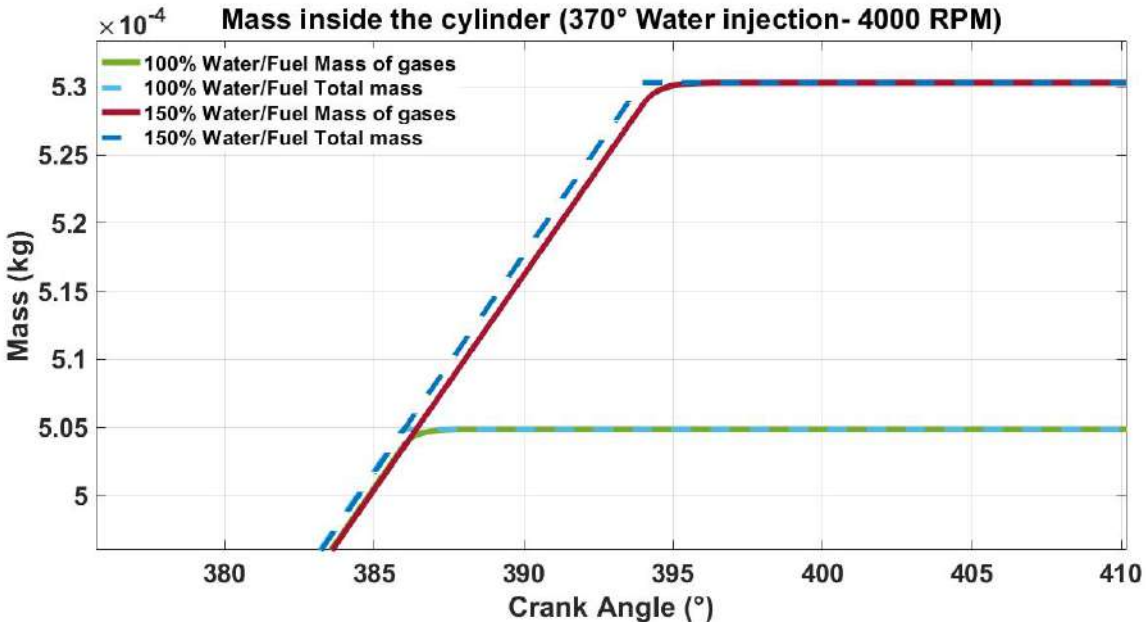

Fig. 4.90 – Mass In-Cylinder 370° water injection 4000 RPM. Detail (2)

4.3.1 ANALYSIS OF ENGINE PERFORMANCE VARIABLES WITH DIRECT WATER INJECTION (SIMULATION).

Below there is a comparison about the behavior of the ethanol engine performance variables studied in section 4.2.2. from the results of the simulations presented in section 4.3. The performance variables selected for this comparison correspond to those mentioned in tables B.1 to B.10 in B Appendix. In addition to power, thermal efficiency and specific fuel consumption, the impact of the process of water injection and evaporation on detonation and NOx emissions is also analyzed.

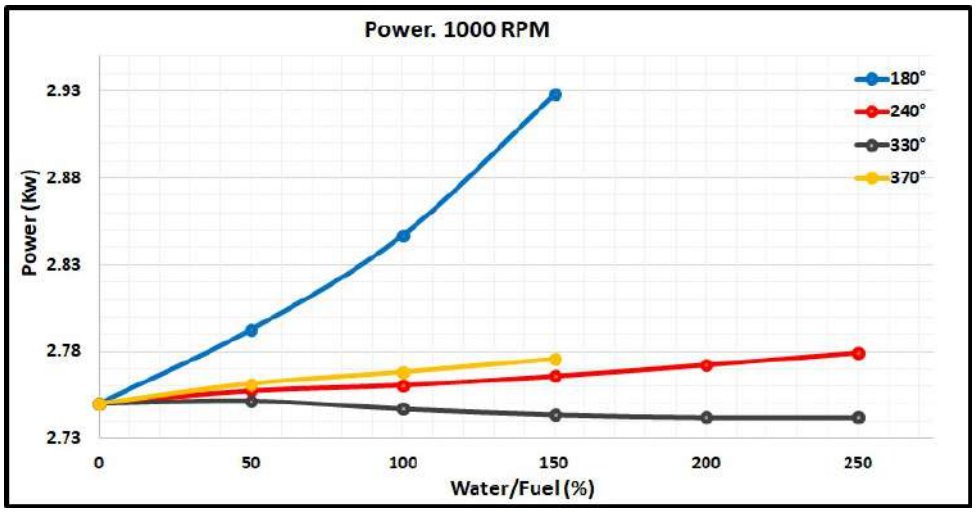

Fig. 4.91 – Power 1000 RPM.

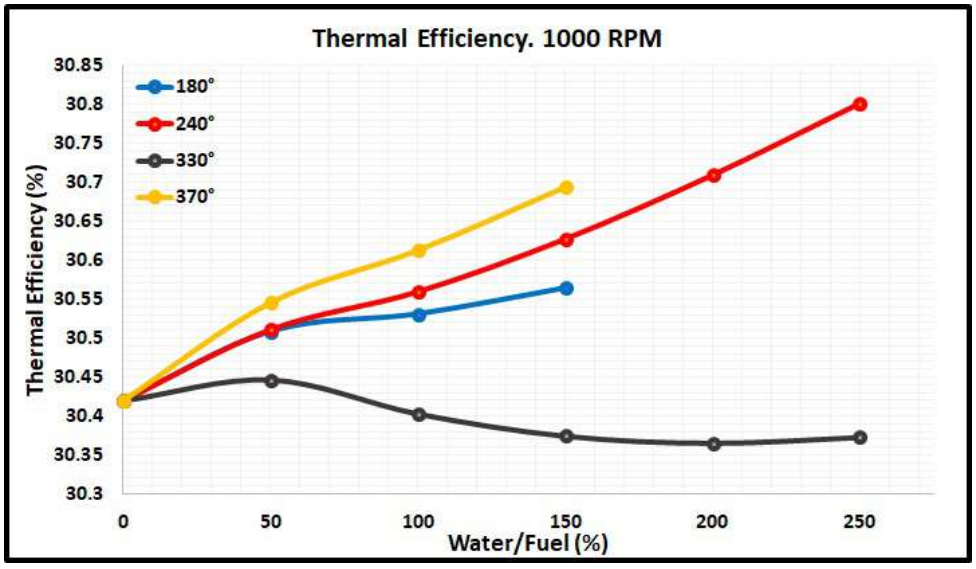

Fig. 4.92 – Thermal Efficiency 1000 RPM.

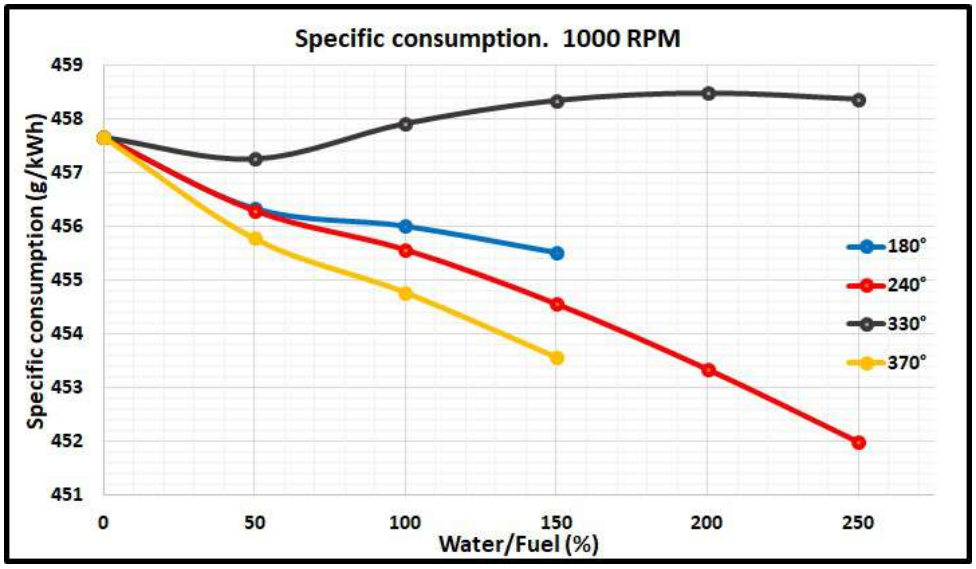

Fig. 4.93 – Specific Consumption 1000 RPM.

(Fig.4.91), (Fig.4.92) and (Fig.4.93) show variations in power, thermal efficiency and specific fuel consumption, respectively, for an engine rotational speed regime of 1000 RPM. The best power curve is obtained when the water is injected at 180° ATDC Exhaust-Intake, i.e. during the open phase. It was already explained in section 4.3 that this injection condition increases the amount of mass inside the cylinder for all quantities of water injected, which increases the pressure significantly. The increase in power is 0.18 Kw, or 6.5%.

In this rotation condition, the injection of water has little influence on the maximum temperature reached in the burned gas zone (Fig.4.28). It is observed that the thermal efficiency improves slightly and the specific fuel consumption decreases in a low proportion. Of the three water injection conditions carried out in the closed phase, the one with the best performance

in the power curve, with a slight increase, corresponds to the injection made in 240° ATDC Exhaust-Intake. A similar behaviour is observed regarding to thermal efficiency and specific fuel consumption, it also decreases in a slightly better proportion than in the previous case. For the injection in 370° ATDC Exhaust-Intake shows a behavior close to that observed in the previous case (240° ATDC Exhaust-Intake). However, when the injection is made at 330° ATDC Exhaust-Intake, the power drops slightly in reference to that obtained without water injection. The thermal efficiency is also the worst of all the quantities of water injected, this is a logical effect if we take into account that the injection is made near the moment of ignition and the beginning of combustion and as it can be seen in (Fig.4.92), the process of water injection and evaporation has a strong effect on the maximum temperature in the burned gas zone, decreasing it by 338 K from the condition without water injection and the condition of the maximum amount of water injected (250% water/fuel Table 4.12).

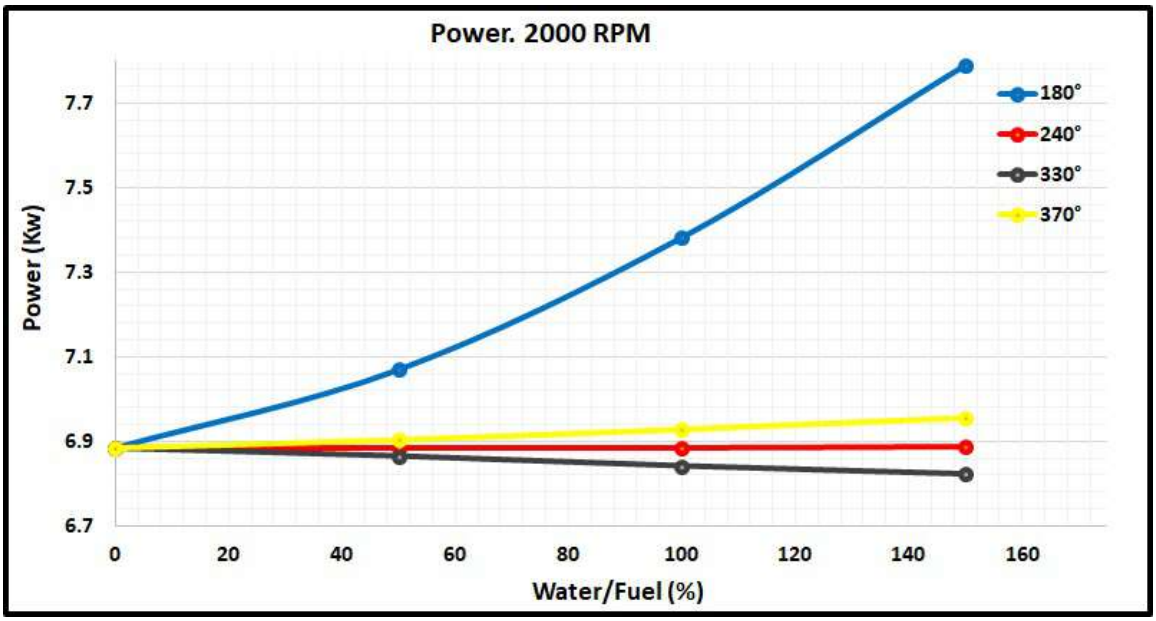

Fig. 4.94 – Power 2000 RPM.

(Fig.4.94), (Fig.4.95) and (Fig.4.96), present the behavior of the same variables mentioned above (Power, thermal efficiency and specific fuel consumption, respectively) for the different injection conditions but for a rotation speed of 2000 RPM. The power shows the same tendency observed in (Fig.4.91), that is, when the water injection is carried out in 180° ATDC Exhaust-Intake, the power values increase in proportion to the amount of water injected, confirming the phenomenology explained regarding the influence of the injection and evaporation of water in this condition (13% increase). Likewise, when the injection is performed at 240°, 330° and 370° ATDC Exhaust-Intake, the observed behavior maintains the trend previously obtained at 1000 RPM. The worst thermal efficiency corresponds to water injection at 330° ATDC Exhaust-Intake (2000 RPM) while for the other two injection conditions (240° and 370° ATDC Exhaust-Intake) a slight improvement is observed. With regard to specific fuel consumption, the behaviour is similar to that described for thermal efficiency.

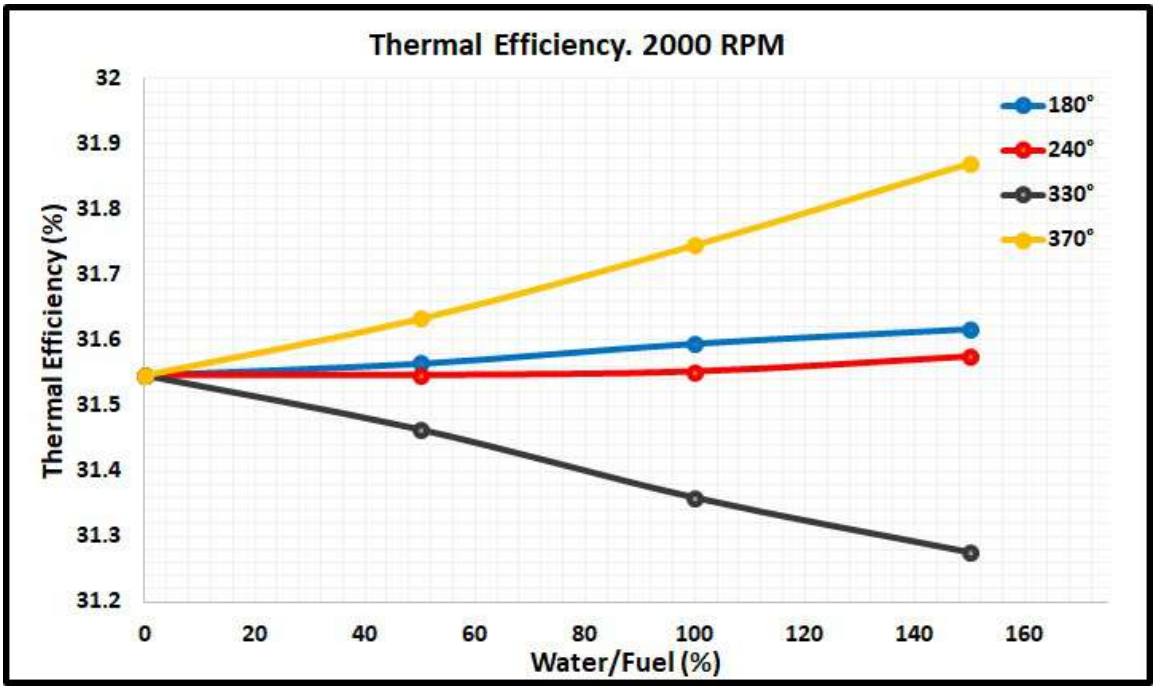

Fig. 4.95 – Thermal Efficiency 2000 RPM.

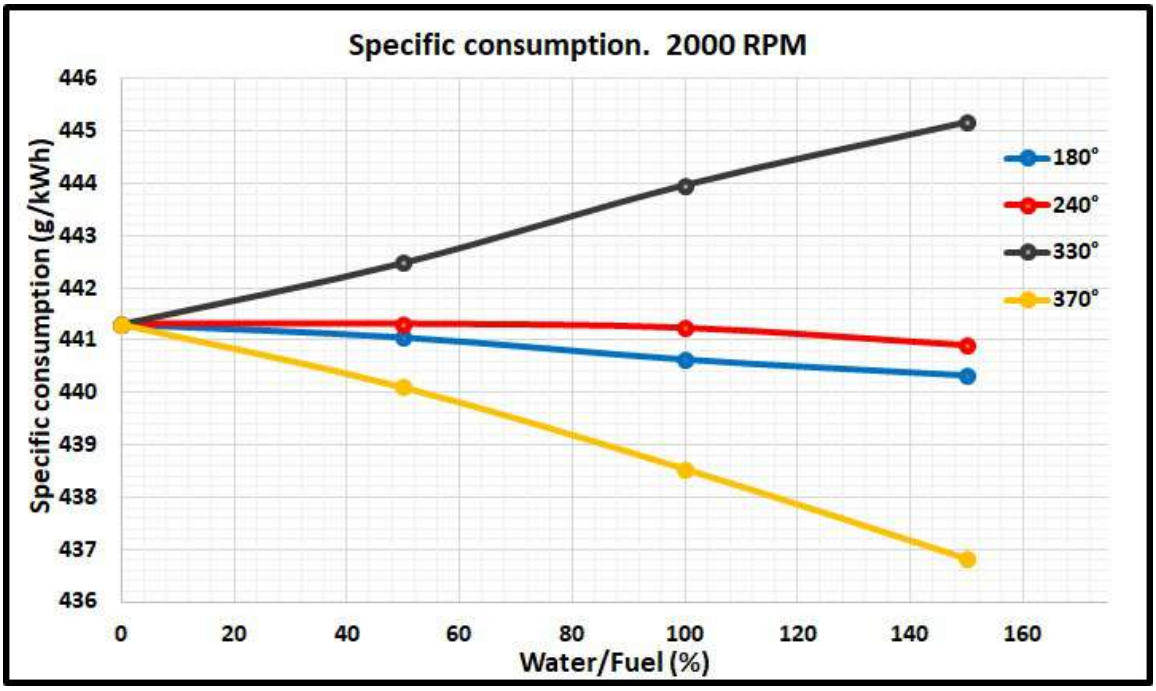

Fig. 4.96 – Specific Consumption 2000 RPM.

For the other rotational speeds analyzed (3000, 4000 and 5000 RPM) the power, thermal efficiency and specific fuel consumption show the same trend in their behavior observed in 2000 RPM for all water injection conditions ((Fig.4.97 to (Fig.4.105)). The coherence in the interpretation by the simulation program of the conditions inside the cylinder is demonstrated again, both without water injection and with the injection in the different points where it is carried out. At 3000 RPM a 15.87% increase in power is observed when the injection is made at 180° ATDC Exhaust-Intake, 16.62% increase in power at 4000 RPM, maintaining an observed trend from 1000 RPM.

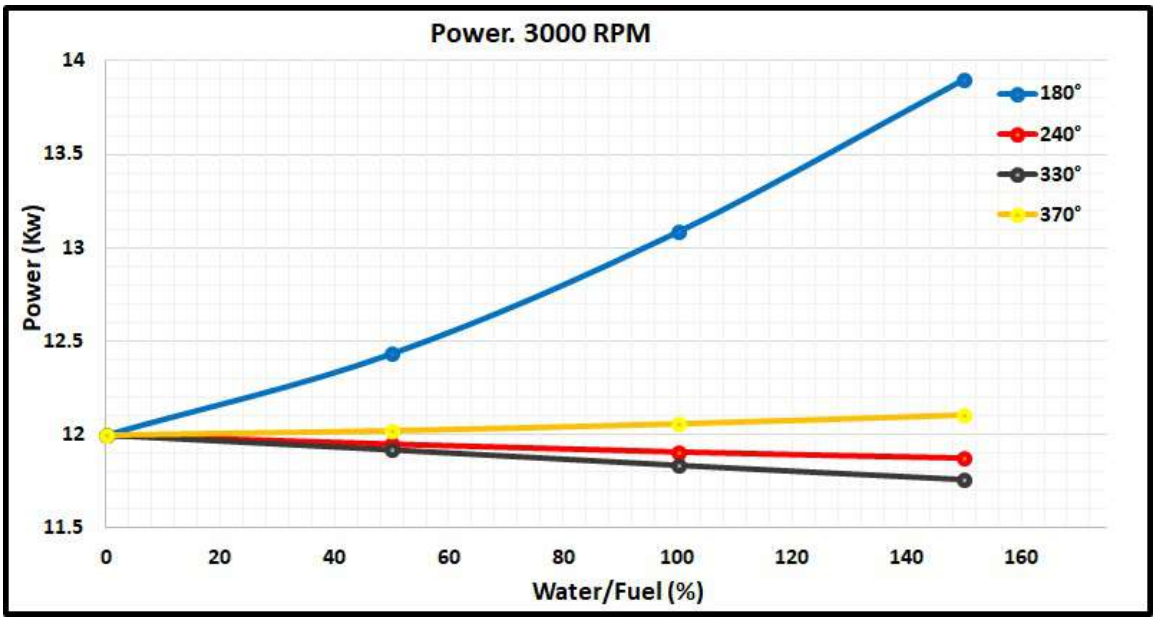

Fig. 4.97 – Power 3000 RPM.

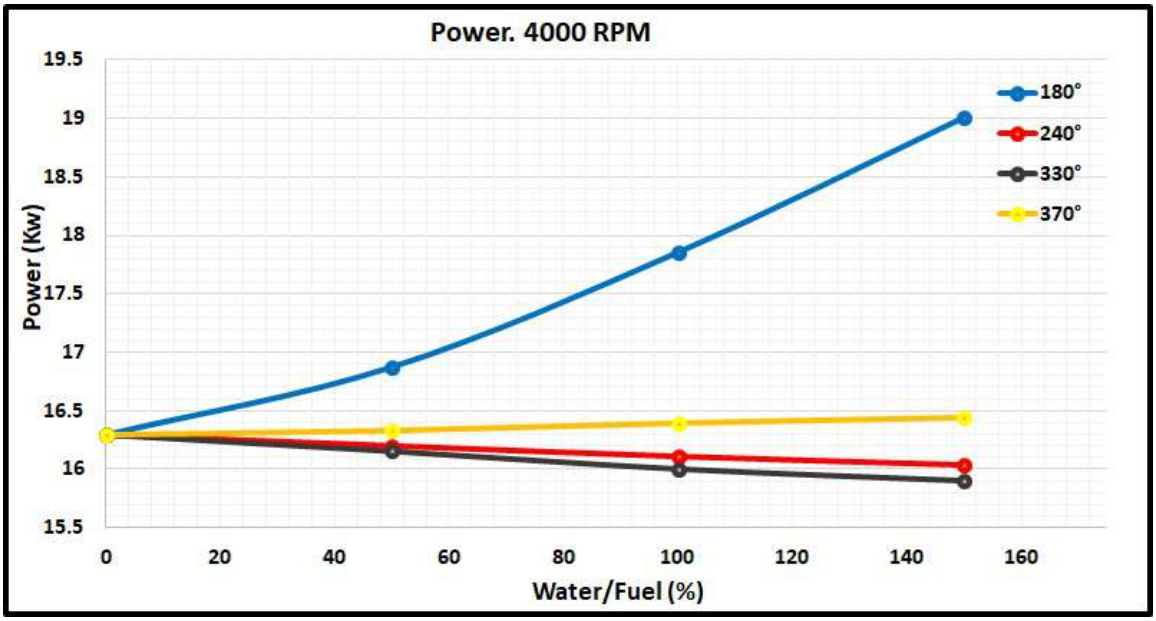

Fig. 4.98 – Power 4000 RPM.

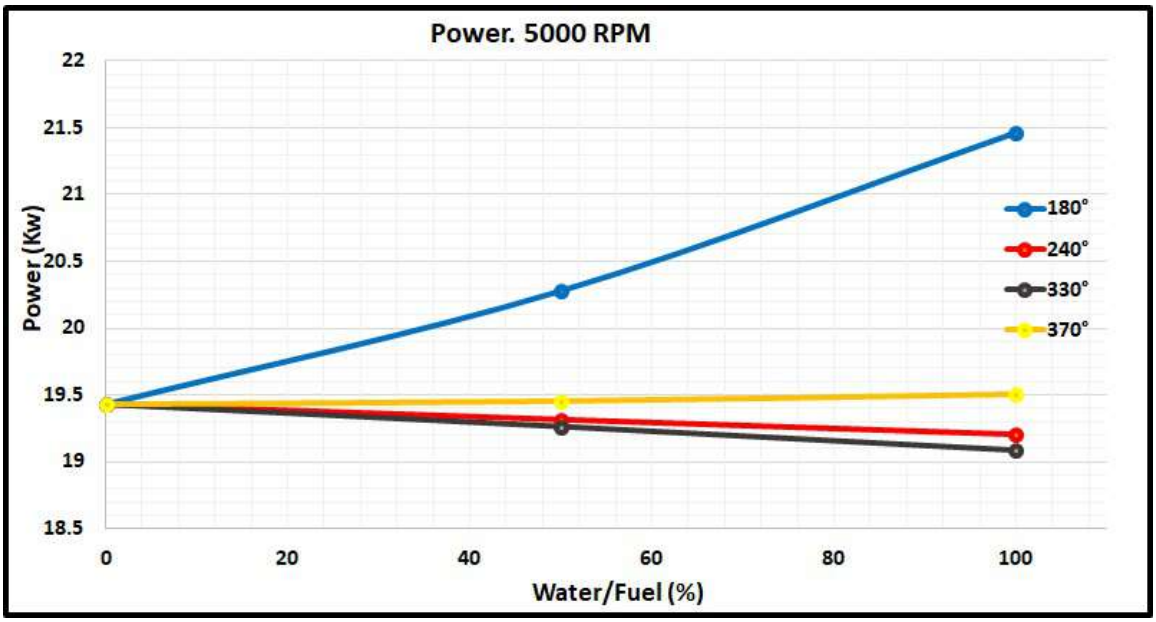

Fig. 4.99 – Power 5000 RPM.

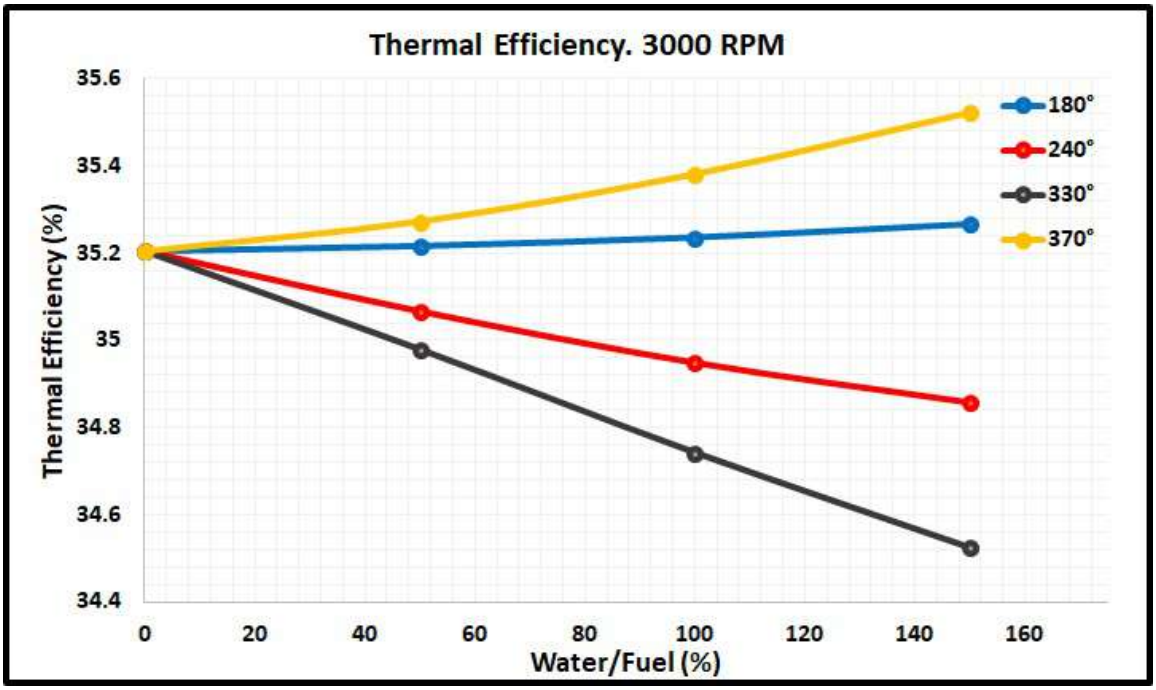

Fig. 4.100 – Thermal Efficiency 3000 RPM.

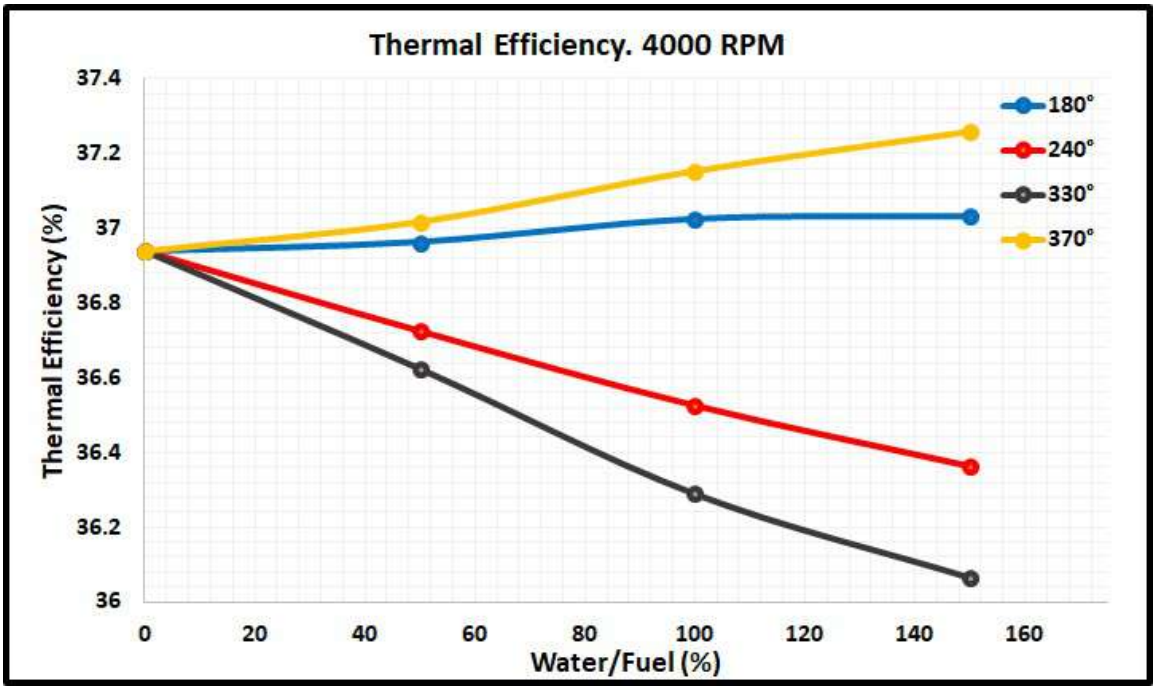

Fig. 4.101 – Thermal Efficiency 4000 RPM.

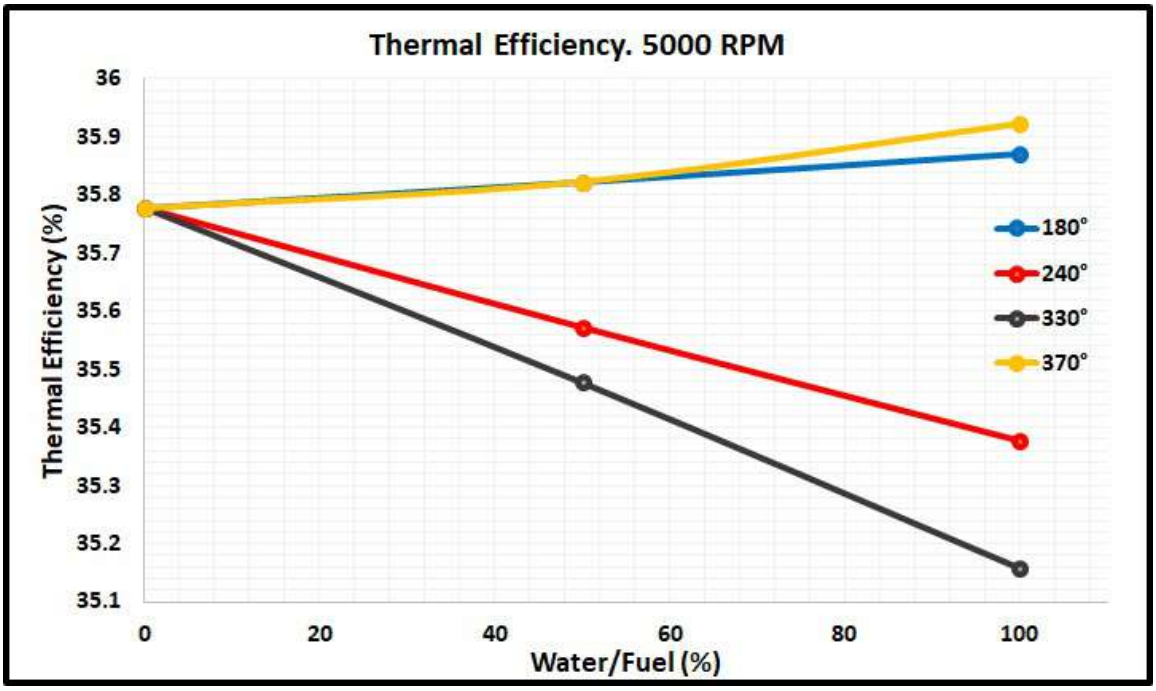

Fig. 4.102 – Thermal Efficiency 5000 RPM.

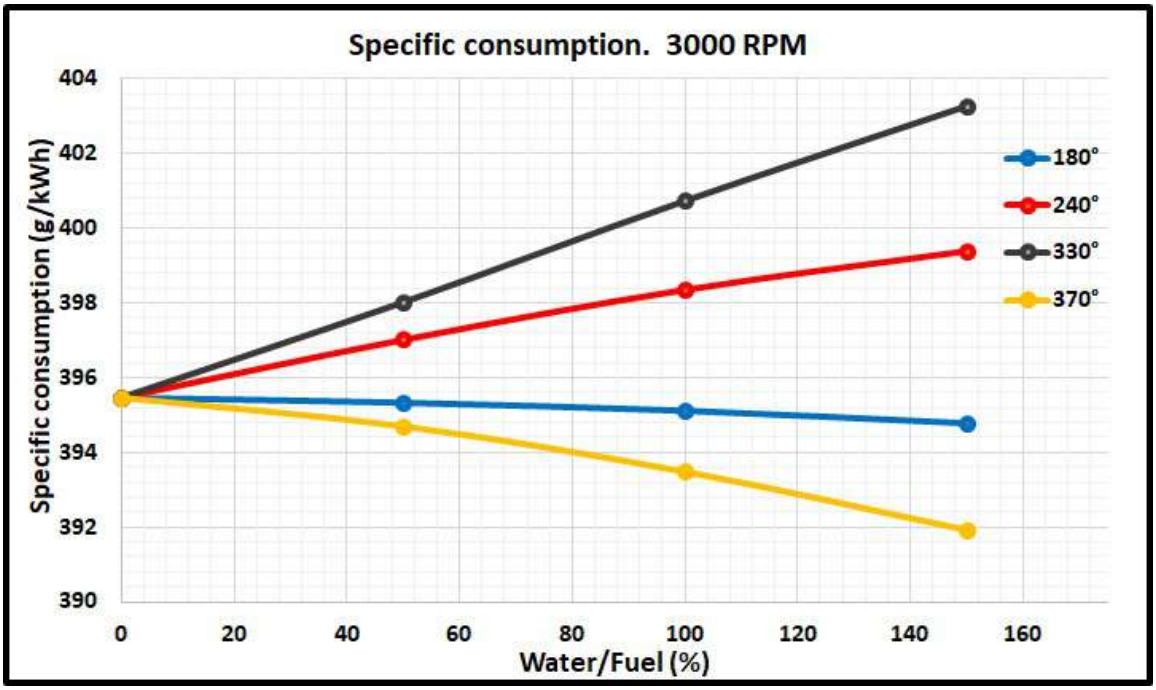

Fig. 4.103 – Specific Consumption 3000 RPM.

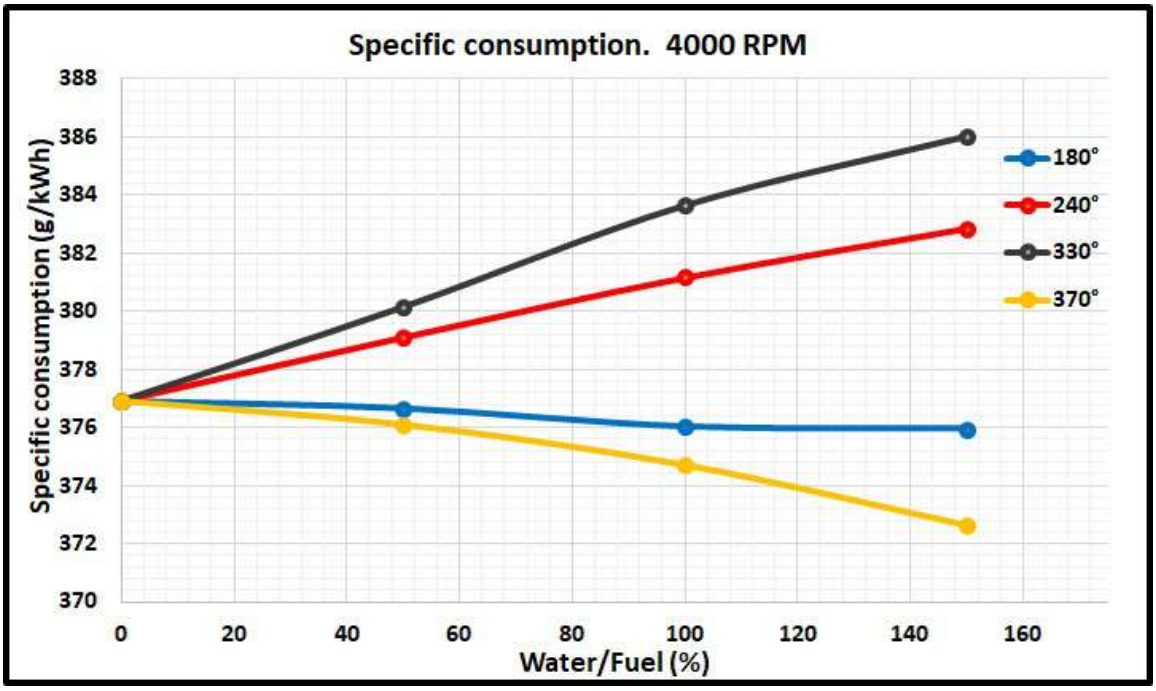

Fig. 4.104 – Specific Consumption 4000 RPM.

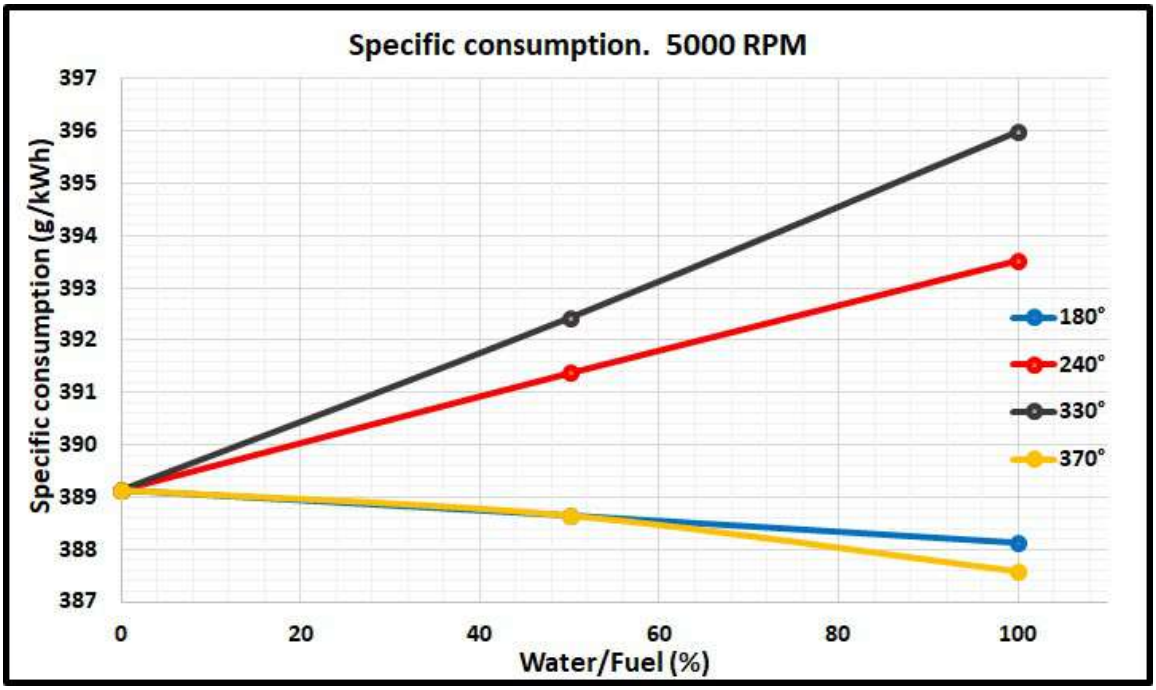

Fig. 4.105 – Specific Consumption 5000 RPM.

4.3.2 ANALYSIS OF THE INFLUENCE OF DIRECT WATER INJECTION ON DETONATION AND NOX EMISSIONS (SIMULATION).

One of the main reasons why water injection is used in combustion engines is because of the effectiveness that this technique has shown to control the knocking phenomenon and the control of NOx emissions. Tables 7.6 to 7.10 of Annex B show the capacity that the simulation program that incorporates the process of injection and evaporation of water proposed here, shows how this technique controls the phenomenon of detonation, particularly when the engine operates at full load and low revolutions (1000 and 2000 RPM) as well as its influence on the reduction of NOx emissions. The graphs presented below provide a more precise idea of how the simulation of the operation of the engine with water injection affects the appearance of blows and polluting emissions. To calculate the detonation index is used the model proposed by (JÚNIOR, 2017) which calculates a number which if it is less than 1, indicates that there is no knocking and if it is greater than 1 indicates the appearance of knocking.

(Fig.4.106) and (Fig.4.107) show how water injection and location of the moment of application of water within the cycle affect knocking. At 1000 RPM (Fig.4.106) it is observed how applying the water injection at 180° increases the probability of the appearance of the detonation regardless of the amount of water injected. In 240° and 330° to greater amount of water injection the detonation index decreases significantly, so that 240° requires a relationship of 250% between the mass of water and the mass of fuel for the detonation index is less than 1. However for the injection in 330° requires a water/fuel ratio greater than 250%.

(Fig.4.106), where the behavior of the detonation index is observed when the engine

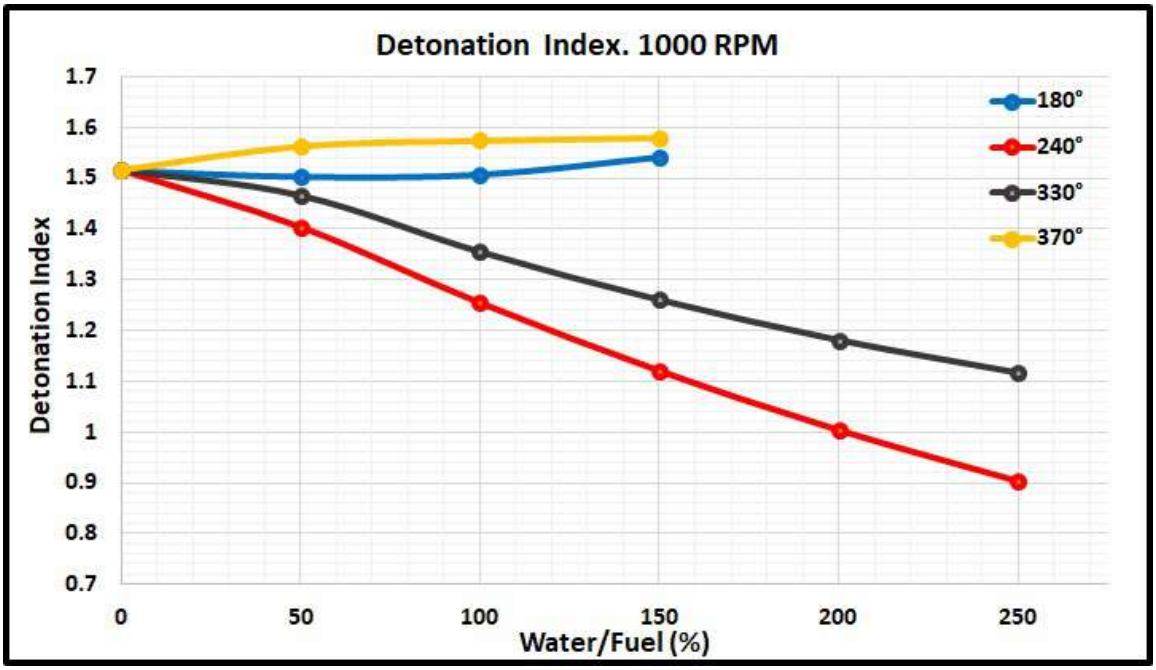

Fig. 4.106 – Detonation Index 1000 RPM.

works at 1000 RPM, shows that when the water injection is carried out at 180° ATDC Exhaust-Intake, the value of the detonation index does not decrease proportionally to the amount of water injected, on the contrary, when the ratio of water mass/fuel mass is 150%, the value of this detonation index increases when compared with the value of the immediately preceding index (Water/Fuel 100%). A possible explanation for this phenomenon can be found in the moment of water injection. When the injection is carried out in 180° ATDC Exhaust-Intake, the work cycle is still in the open phase for the selected engine (Fig.4.16). (Fig.4.107) shows the temperature behaviour in the area of unburned gases at the precise moment the water injection is carried out up to the moment the intake valve is closed (225° ATDC Exhaust-Intake).

It is observed that the temperature decreases around 12 K comparing the condition without water injection (blue line) and the temperature for the maximum water/fuel ratio (yellow line). This decrease in temperature remains constant throughout the burned gas zone ((Fig.4.29) and (Fig.4.30)). The above shows that the impact of the decrease in temperature resulting from the injection of liquid water is not effective for this water injection point (180° ATDC Exhaust-Intake 1000 RPM) as it is for other water injection points (240° and 330°) as observed in (Fig.4.106).

The water that enters when the injection is made at 180° ATDC Exhaust-Intake, remains liquid until the conditions of pressure and temperature inside the cylinder are favorable to change to gaseous phase, which occurs a little later during the cycle of work (Fig.4.108). Due to the fact that the water evaporates before the closing of the intake valve, the impact on the temperature that the evaporation of water has on the air/fuel mixture, dissipates with the advance of the cycle, therefore during the compression phase the water vapour generated is already mixed

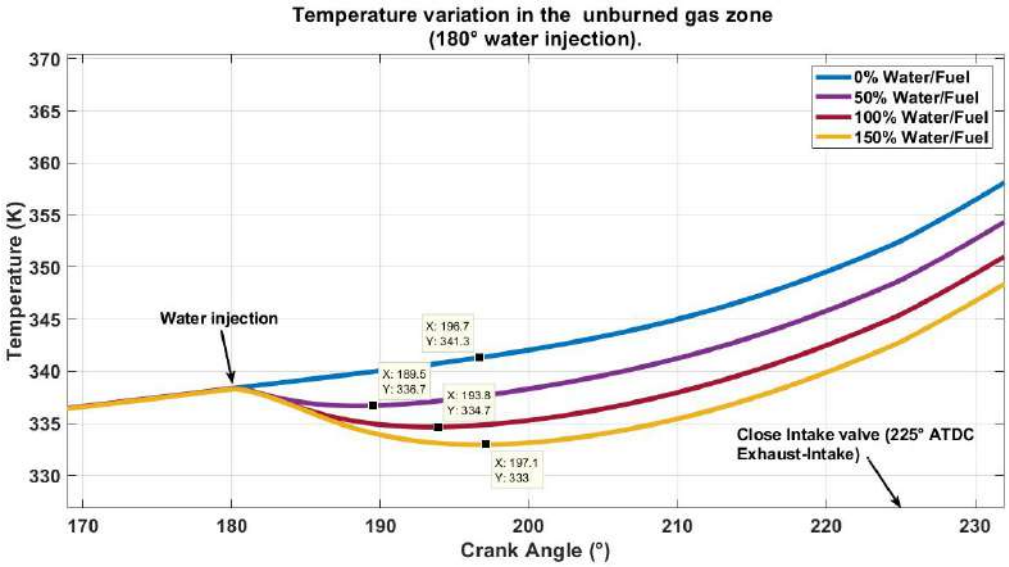

Fig. 4.107 – Temperature 180° 1000RPM Injection Point.

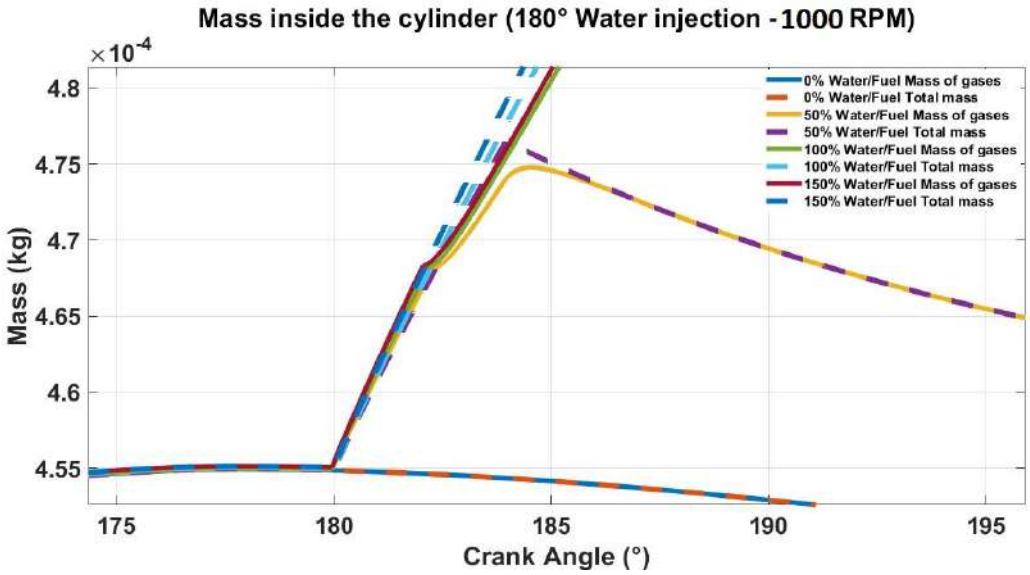

Fig. 4.108 – Mass In-Cylinder 180° 1000 RPM. Detail (1)

with the unburned gases and the piston compresses all this mixture whose conditions of pressure and temperature are practically homogeneous.

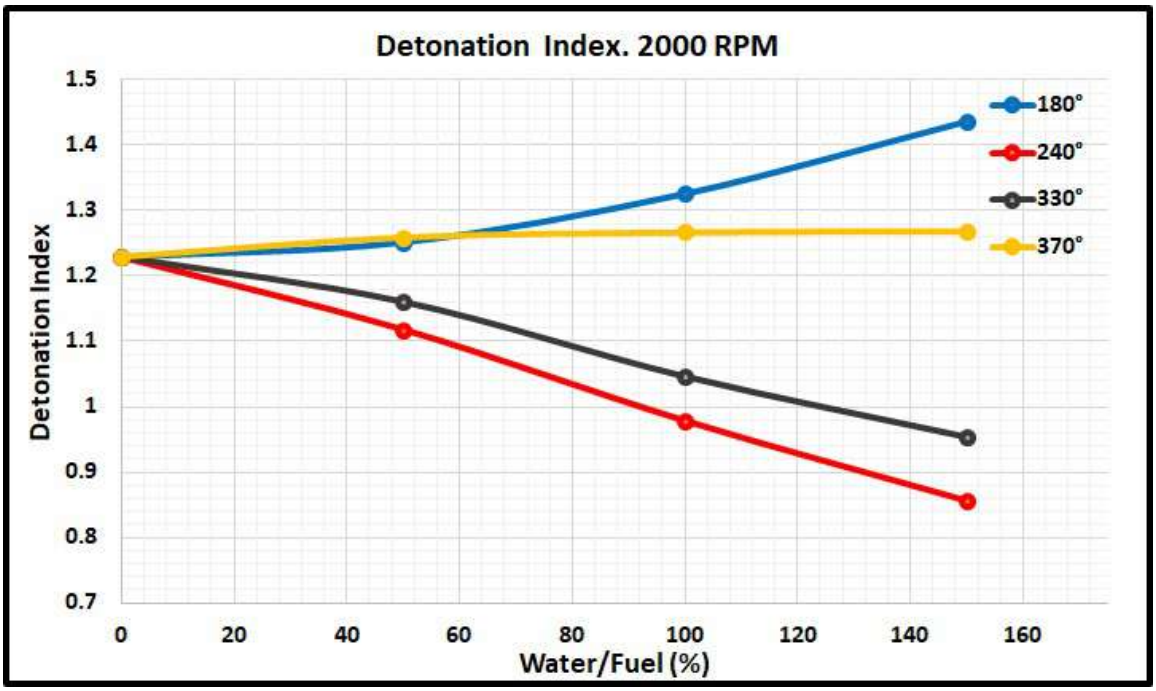

Fig. 4.109 – Detonation Index 2000 RPM.

(Fig.4.109) presents the behavior of the knock index for all water injection conditions with a rotation speed of 2000 RPM. It is again observed that the water injection carried out in 180° ATDC Exhaust-Intake does not have a favorable effect and on the contrary the detonation index increases in the same proportion as the amount of water injected. For the 240° and 330° ATDC Exhaust-Intake injection the effect of the water injection is favorable, since the detonation index decreases as the amount of water injected increases, being the best option the injection at 240°. At 370° ATDC Exhaust-Intake the water injection does not show any influence on the detonation index at this rotation speed.

The trend observed by the behavior of the detonation index in 2000 RPM is maintained for 3000, 4000 and 5000 RPM ((Fig.4.110), (Fig.4.111) and (Fig.4.112)). The best water injection option for detonation control in the cases proposed for simulation is 240° ATDC Exhaust-Intake. (Fig.4.34, 1000 RPM), (Fig.4.42, 2000 RPM), are observed, corresponding to the maximum temperatures in the unburned gas zone, it is observed that the temperature always decreased proportionally to the amount of water injected, with the exception of 370° where the water injection does not influence the maximum temperature reached in this zone.

Regarding the control of NOx emissions, at all simulated rotational speeds (1000, 2000 3000, 4000 and 5000 RPM) the water injection showed a reduction in NOx emissions, for all quantities of water injected (Table 4.12) and at all injection instants of proposed (180°, 240°, 330° and 370° ATDC Exhaust-Intake).

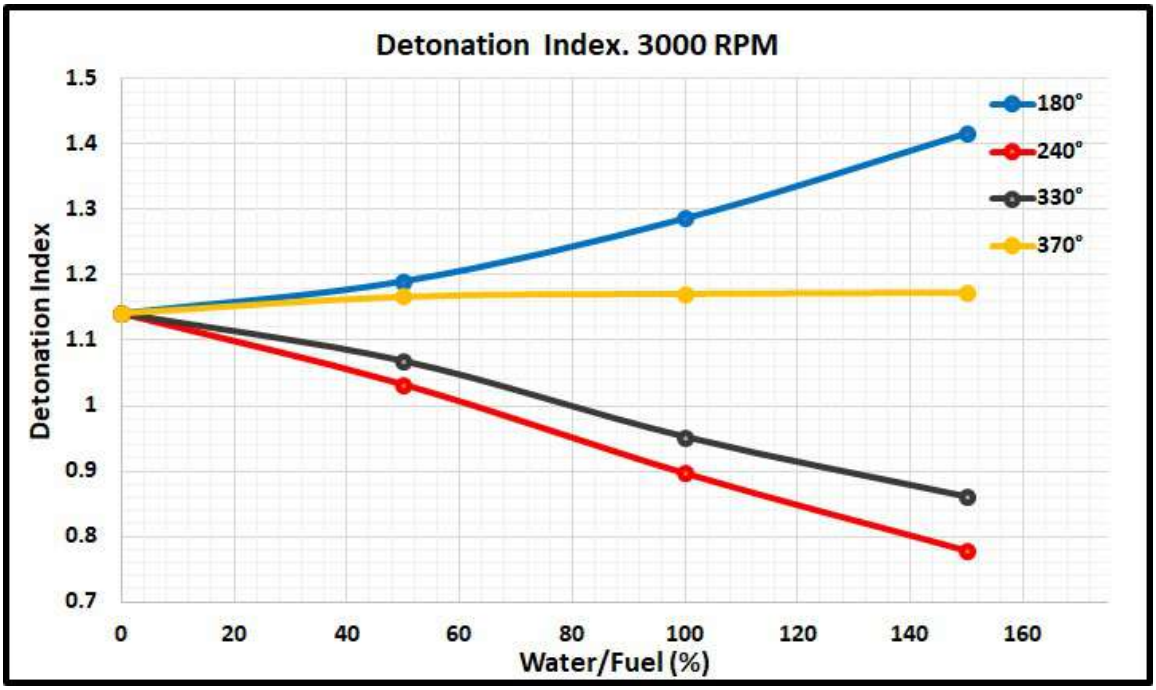

Fig. 4.110 – Detonation Index 3000 RPM.

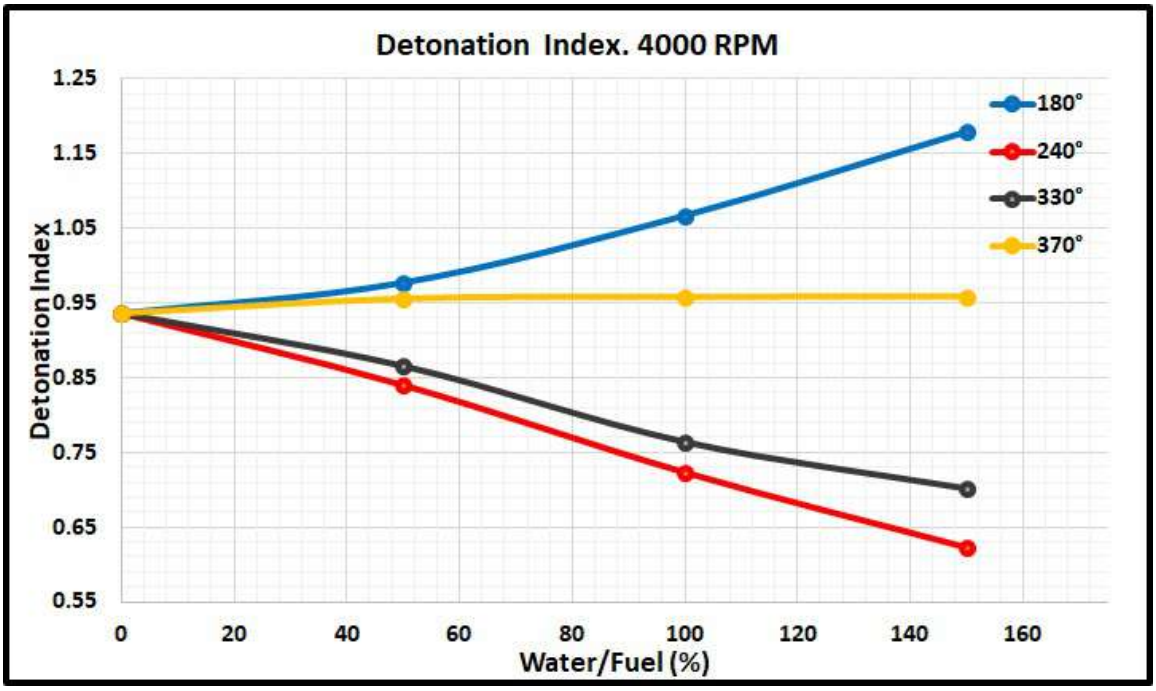

Fig. 4.111 – Detonation Index 4000 RPM.

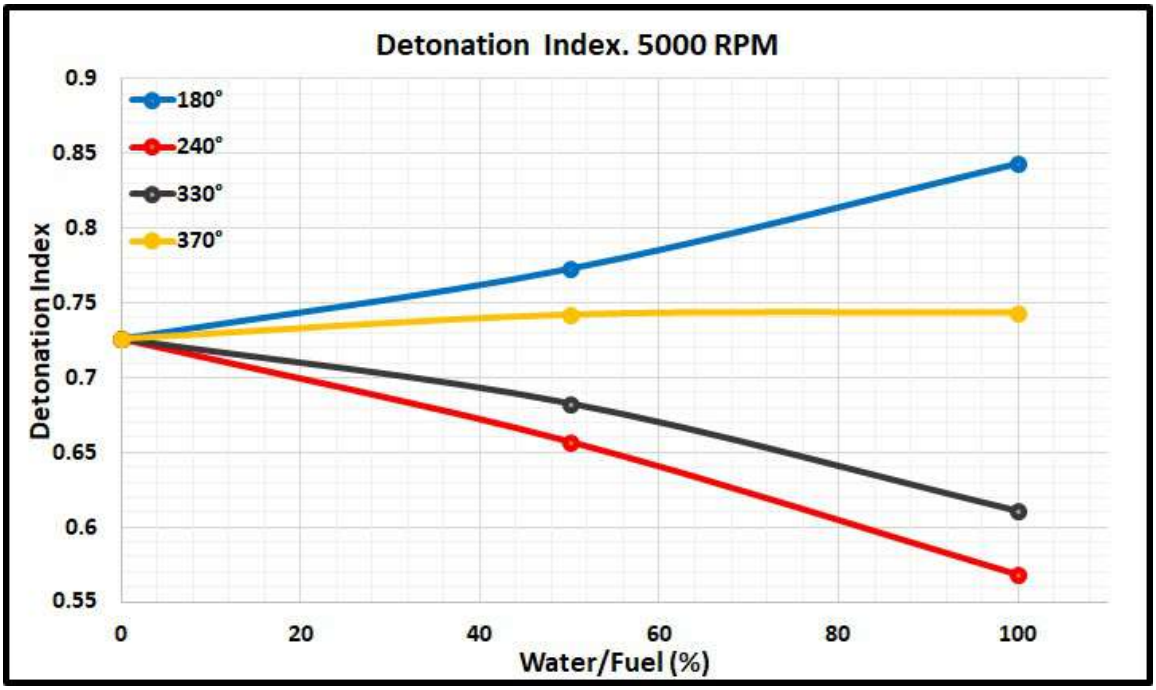

Fig. 4.112 – Detonation Index 5000 RPM.

Observing (Fig.4.113), (Fig.4.114) and (Fig.4.115) show that direct water injection evidently has a positive influence on the reduction of NOx emissions, particularly when the injection is made at 240° and 330° ATDC Exhaust-Intake. All the graphs referring to NOx emissions show that the best injection condition corresponds to 240° ATDC Exhaust-Intake, in a similar way to that observed in the analysis of the knock index. Again this reduction in emissions due to the injection of water is related to the way this process of injection and evaporation of water influences the maximum temperatures in the area of gases burned (Fig.4.28), (Fig.4.43), (Fig.4.77) and (Fig.4.83), where reductions of up to 300 K are observed as a result of water injection and evaporation.

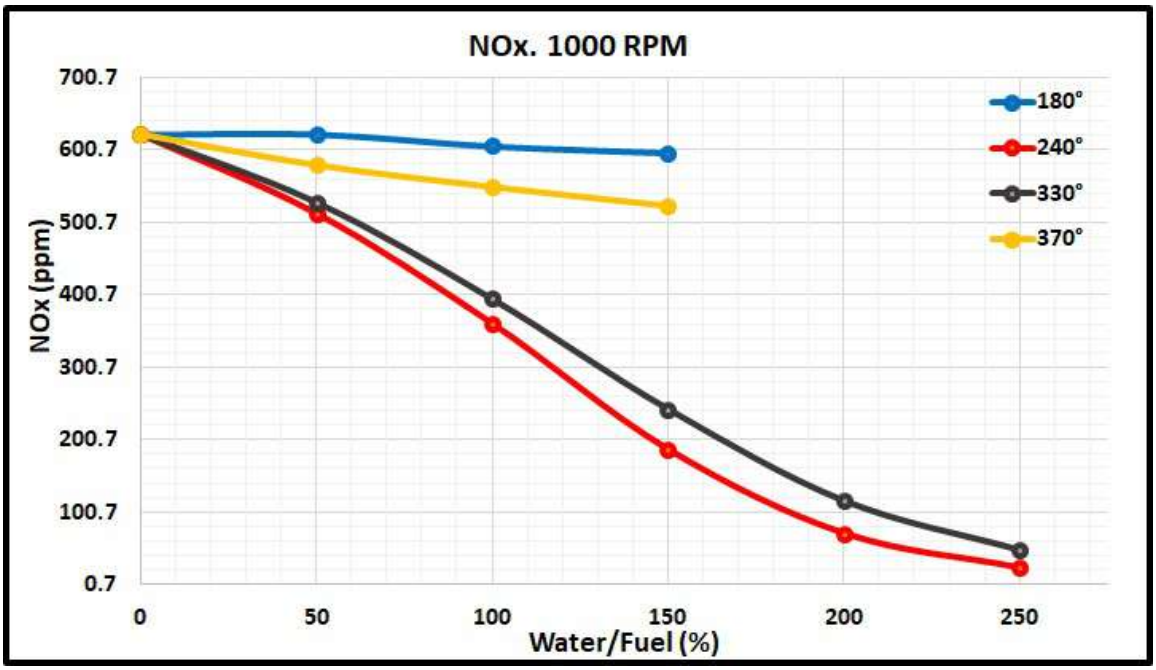

Fig. 4.113 – NOx emissions 1000 RPM.

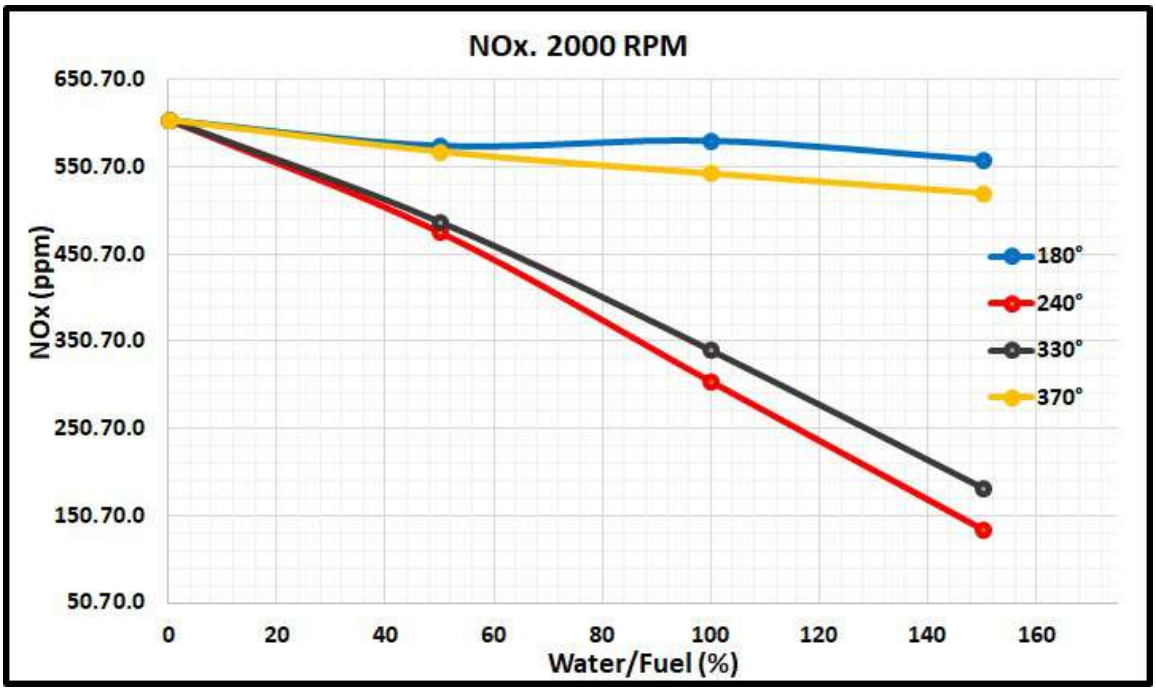

Fig. 4.114 – NOx emissions 2000 RPM.

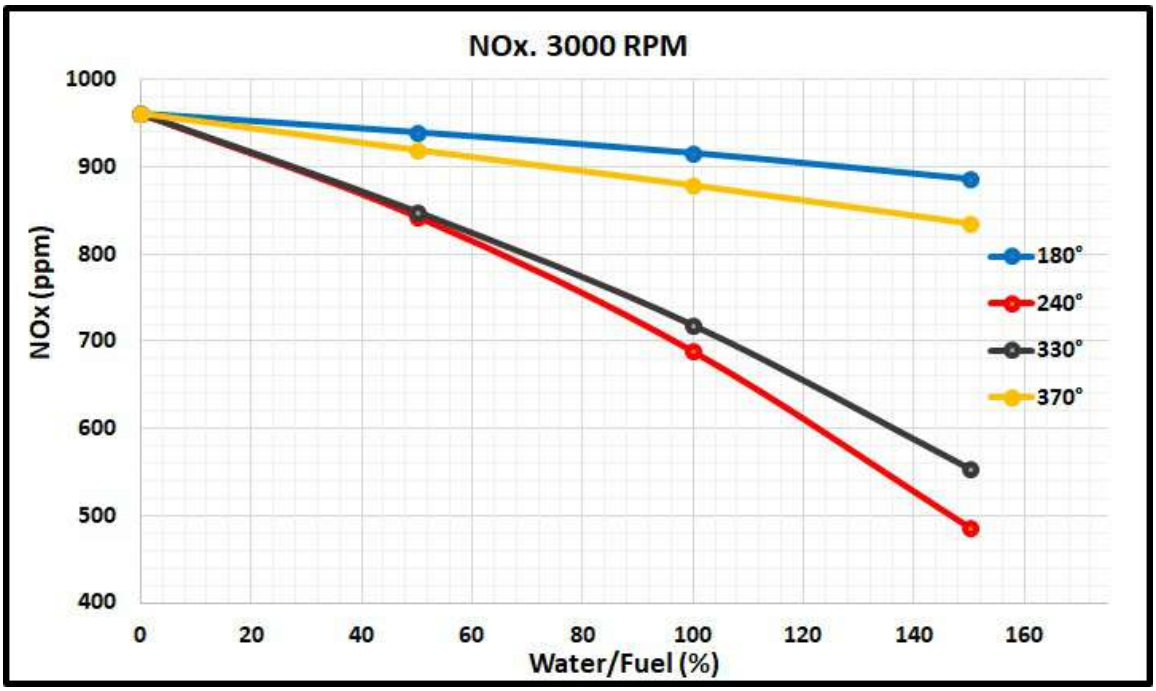

Fig. 4.115 – NOx emissions 3000 RPM.

5 CONCLUSION

Using mathematical models of water injection combined with thermodynamic models of combustion and computational simulation it was possible to demonstrate that it is possible to predict through numerical simulation the performance of an internal combustion engine with water injection.

The proposed thermodynamic model fits the phenomenology of the process of injecting water directly into the combustion chamber. When comparing the results provided by the simulation of the model with respect to the behaviour of the pressure inside the cylinder during the closed phase, with the experimental data taken from (KIM *et al.*, 2016) for the case of the gasoline engine and with the data provided by the ethanol engine tests located at the MAUA Institute of Technology, it is observed that the relative margin of error is less than 2.5% for the data of the maximum pressures reached inside the cylinder. This shows that the proposed simulation model is an accurate interpretation, as it can correctly simulate the operating conditions and engine geometry, showing simulated results very close to those delivered by the experimental tests.

Regarding the fraction of mass burned, the comparison between the experimental results ((KIM *et al.*, 2016)) and those delivered by the simulation model, present margins of error between 9 and 13%. The reason for this discrepancy could be due to the transfer of heat between the walls of the cylinder and the gases contained in it, especially in the phase before the start of combustion. The approach used in the simulation model for heat transfer corresponds to that proposed by Hohenberg (HOHENBERG, 1979). However, we do not have enough information to clearly define how adequate this approach is to describe the phenomenology of the experiment. On the other hand, the trend in the behavior of the fraction of mass burned, between the experimental and simulated curves, which is observed in (Fig.4.5), (Fig.4.7) and (Fig.4.9) is very close, what would demonstrate again, that the simulation model interprets coherently the operating conditions of the test engine.

The drop evaporation model presents a behavior according to the variations of pressure and temperature inside the cylinder. The slope of the line that describes the variation of the diameter as a function of time, changes in proportion to the increase in temperature and pressure during the interval from the injection of water to the total evaporation of the drop (Fig.4.2). This shows that the assumptions from which the model was built correspond to the phenomenology of the evaporation process.

The assumption of air as a gaseous medium where the drop of water evaporates, proved to be equally adequate. This condition is assumed due to the impossibility of knowing the value of the diffusivity of the water in the air/fuel mixture. However, when comparing the results of

the behavior of the pressure and the tendency shown by the temperature, it is observed that this assumption does not significantly affect the phenomenology of the process.

Finally, the comparison made between the experimental data and those delivered by the simulation, for the fuel specific brake consumption variables (BSFC, Table 4.4) and the NOx emissions, (Table 4.5 and (Fig.4.15)) demonstrate again that the simulation it has a behavior with the same tendency as that shown by the experimental data. This reinforces the claim that the simulation model interprets the phenomenology of the process in an appropriate way.

The injection of water directly into the combustion chamber proves to be an effective alternative for the control of detonation when the engine works at high load and low revolutions (1000, 1200 and 2000 RPM).

Likewise, direct water injection significantly reduces NOx emissions by reducing the maximum combustion temperature.

Water injection does not negatively affect performance parameters such as power and torque, except when water is injected at 330° ATDC Exhaust-Intake, where a slight decrease in power is observed in ethanol engine simulations. The variations observed in the data delivered by the simulation do not exceed 1%. Therefore, direct water injection manages detonation and NO emissions without affecting engine performance.

Of the four points chosen for water injection, the one that shows the best results on the model is when the water injection 240° is performed after the top dead center of the exhaust air intake (TDC). The analysis of the effects on the control of detonation and NOx emissions shows that injection at this point (240° ATDC Exhaust-Intake) is the best choice within the proposed set of water injection points, to achieve even small improvements in parameters such as power and torque.

Performing water injection after the start of combustion has no advantage in terms of emission control or detonation control. Nor in terms of engine performance. The results of the direct injection made 370° ATDC Exhaust-Intake show this.

However, it is important to mention that when the water injection is performed at 180° ATDC Exhaust-Intake, the increase in power is significant, exceeding 10% as is the case in 4000 and 5000 RPM, ((Fig.4.98) and (Fig.4.99) Annex A). Although according to the simulation model the 180° ATDC Exhaust-Intake injection is not effective in preventing detonation when the engine is running at full load and low revolutions (Fig.4.106) and (Fig.4.107).

5.1 FUTURE WORK

As future work, it is proposed to perform the same type of analysis with data from a turbocharged engine and direct fuel injection. The implementation of turbocharging and the use of direct injection is the current trend in the development and application of ICE SI. The analyzes with this type of engines would provide information that would allow the simulation model to be improved, which in turn would allow the spectrum of use and updating of the model to be expanded.

Now that the models of water injection and evaporation and engine simulation have been validated for the case where gasoline is used as fuel through experimental work is shown in (KIM *et al.*, 2016) and for an ethanol engine without water injection, with data supplied by MAUA. The model was used to explore the effects of water injection in an aspirated ethanol engine. These models will be used to study the effect of direct water injection on turbo-ethanol and gasoline engines.

In addition, it is also proposed to compare the results obtained with the implementation of direct water injection in the combustion chamber, with data obtained using recirculated exhaust gas (EGR) systems, particularly to determine the influence on NOx and HC.

Finally, it is proposed to implement within the simulator, more precise water evaporation models than the one used (Clausius-Clapeyron). In this way it is possible to evaluate the influence on the response of the evaporation time of the droplets and how the temperature and pressure values inside the combustion chamber are affected.

REFERENCES

AL-BAGHDADI, M. A. S. A simulation model for a single cylinder four-stroke spark ignition engine fueled with alternative fuels. **Turkish Journal of Engineering and Environmental Sciences**, The Scientific and Technological Research Council of Turkey, v. 30, n. 6, p. 331–350, 2007.

ALLA, G. A. *et al.* Combustion quasi-two zone predictive model for dual fuel engines. **Energy Conversion and Management**, Elsevier, v. 42, n. 12, p. 1477–1498, 2001.

ALTIN, I.; BILGIN, A. Quasi-dimensional modeling of a fast-burn combustion dual-plug spark-ignition engine with complex combustion chamber geometries. **Applied Thermal Engineering**, Elsevier, v. 87, p. 678–687, 2015.

ANNAND, W. *et al.* Heat transfer in the cylinders of reciprocating internal combustion engines. **Proceedings of the Institution of Mechanical Engineers**, SAGE Publications, v. 177, n. 1, p. 973–996, 1963.

ASHGRIZ, N. **Handbook of atomization and sprays: theory and applications**. [S.l.]: Springer Science & Business Media, 2011.

AYALA, F. A.; HEYWOOD, J. B. **Lean SI engines: the role of combustion variability in defining lean limits**. [S.l.], 2007.

BABINSKY, E.; SOJKA, P. Modeling drop size distributions. **Progress in energy and combustion science**, Elsevier, v. 28, n. 4, p. 303–329, 2002.

BALABEL, A.; WILSON, S. A theoretical model for predicting the mean droplet diameter in spray based on the linear stability analysis. **INTERNATIONAL JOURNAL OF CONTROL, AUTOMATION AND SYSTEMS**, 2013.

BARTON, R.; LESTZ, S. S.; MEYER, W. E. **An empirical model for correlating cycle-by-cycle cylinder gas motion and combustion variations of a spark ignition engine**. [S.l.], 1971.

BELL, A. H. Continuous use of internal cooling to suppress knock in aircraft engines cruising at high power. 1944.

BENSON W. J. D. ANNAND, P. C. B. R. S. A simulation model including intake and exhaust system for a single cylinder four-stroke cycle spark ignitionngine. **International Journal of Mechanical Engineering**, 1975.

BERGMAN, T. L.; INCROPERA, F. P. **Fundamentals of heat and mass transfer**. [S.l.]: John Wiley & Sons, 2011.

BERNI, F. *et al.* Numerical investigation on the effects of water/methanol injection as knock suppressor to increase the fuel efficiency of a highly downsized gdi engine. In: **SAE Technical Paper**. SAE International, 2015. Disponível em: <https://doi.org/10.4271/2015-24-2499>.

BLAIR, G. P. Design and simulation of four-stroke engines. **Technology**, v. 2011, p. 10–18, 1999.

BLUMBERG, P. N.; LAVOIE, G. A.; TABACZYNSKI, R. J. Phenomenological models for reciprocating internal combustion engines. **Progress in Energy and Combustion Science**, Elsevier, v. 5, n. 2, p. 123–167, 1979.

BORETTI, A. Water injection in directly injected turbocharged spark ignition engines. **Applied Thermal Engineering**, Elsevier, v. 52, n. 1, p. 62–68, 2013.

BOZZA, F. *et al.* **Validation of a fractal combustion model through flame imaging**. [S.l.], 2005.

BRUSCA, S.; LANZAFAME, R. Water injection in ic - si engines to control detonation and to reduce pollutant emissions. In: **SAE Technical Paper**. SAE International, 2003. Disponível em: <http://dx.doi.org/10.4271/2003-01-1912>.

BUTTSWORTH, D. R. **Spark ignition internal combustion engine modelling using Matlab**. [S.l.]: Faculty of Engineering & Surveying, University of Southern Queensland, 2002.

CARPENTER, M.; RAMOS, J. Mathematical modelling of spark-ignition engines. **Applied mathematical modelling**, Elsevier, v. 9, n. 1, p. 40–52, 1985.

CHAN, S. H.; ZHU, J. Modelling of engine in-cylinder thermodynamics under high values of ignition retard. **International journal of thermal sciences**, Elsevier, v. 40, n. 1, p. 94–103, 2001.

CHASE, M. W. *et al.* Janaf thermochemical tables, 1975 supplement. **Journal of Physical and Chemical Reference Data**, v. 4, n. 1, p. 1–176, 1975. Disponível em: <https://doi.org/10.1063/1.555517>.

CHIANG, C.; RAJU, M.; SIRIGNANO, W. Numerical analysis of convecting, vaporizing fuel droplet with variable properties. **International Journal of Heat and Mass Transfer**, v. 35, n. 5, p. 1307 – 1324, 1992. ISSN 0017-9310. Disponível em: <http://www.sciencedirect.com/science/article/pii/001793109290186V>.

CRÓ, N. P. R. *et al.* **Computational Modeling of Internal Combustion Engines: Influence of Compression Ratio in the Indicated Performance Curves**. [S.l.], 2013.

CRUZ, I. W. S. L. *et al.* Zero-dimensional mathematical model of the torch ignited engine. **Applied Thermal Engineering**, Elsevier, v. 103, p. 1237–1250, 2016.

CUDDIHY, J. L. **A User-Friendly, Two-Zone Heat Release Model for Predicting Spark-Ignition Engine Performance and Emissions**. Dissertação (Mestrado) — College of Graduate Studies University of Idaho, 2014.

DEPCIK, C. **Open-ended thermodynamic cycle simulation**. 2000.

DOUAUD, A.; EYZAT, P. Four-octane-number method for predicting the anti-knock behavior of fuels and engines. **SAE Transactions**, JSTOR, p. 294–308, 1978.

DRYER, F. Water addition to practical combustion systems—concepts and applications. In: ELSEVIER. **Symposium (international) on combustion**. [S.l.], 1977. v. 16, n. 1, p. 279–295.

FERGUSON, C. R.; KIRKPATRICK, A. T. **Internal combustion engines: applied thermosciences**. [S.l.]: John Wiley & Sons, 2001.

GALLO, W. L. R. **Analise Exergetica de Motores a Gasolina e Alcool**. Tese (Doutorado) — University of Campinas, 1990.

GORDON, S.; MCBRIDE, B. J. **Computer program for calculation of complex chemical equilibrium compositions, rocket performance, incident and reflected shocks, and Chapman-Jouguet detonations**. [S.l.], 1976.

GREEVES, G.; KHAN, I.; ONION, G. Effects of water introduction on diesel engine combustion and emissions. In: ELSEVIER. **Symposium (International) on Combustion**. [S.l.], 1977. v. 16, n. 1, p. 321–336.

GUEZENNEC, Y. G.; HAMAMA, W. **Two-zone heat release analysis of combustion data and calibration of heat transfer correlation in an IC engine**. [S.l.], 1999.

HAMRIN, D. A.; HEYWOOD, J. B. **Modeling of engine-out hydrocarbon emissions for prototype production engines**. [S.l.], 1995.

HARTESVELDT, C. H. V. **Temperature control apparatus for a mold**. [S.l.]: Google Patents, 1959. US Patent 2,907,070.

HEYWOOD, J. B. *et al.* Internal combustion engine fundamentals. Mcgraw-hill New York, v. 930, 1988.

HOHENBERG, G. F. **Advanced approaches for heat transfer calculations**. [S.l.], 1979.

HOLDER, G. **Evaporation of a Droplet**. 2012. Heat and Mass Transport.

HOPKINSON, B. A new method of cooling gas-engines. **Journal of the Royal Society of Arts**, Royal Society for the Encouragement of Arts, Manufactures and Commerce, v. 61, n. 3168, p. 867–872, 1913. ISSN 00359114. Disponível em: <http://www.jstor.org/stable/41340767>.

HOPKINSON, B. A method of measuring the pressure produced in the detonation of high explosives or by the impact of bullets. **Philosophical Transactions of the Royal Society of London. Series A, Containing Papers of a Mathematical or Physical Character**, The Royal Society, v. 213, n. 497-508, p. 437–456, 1914.

JERZEMBECK, S. *et al.* Laminar burning velocities at high pressure for primary reference fuels and gasoline: Experimental and numerical investigation. **Combustion and Flame**, Elsevier, v. 156, n. 2, p. 292–301, 2009.

JÚNIOR, F. R. d. S. **Estudo de um modelo computacional para prever a ocorrência da detonação em um motor avançado a etanol.** Dissertação (Mestrado) — Universidade Estadual de Campinas, Faculdade de Engenharia Mecânica, Campinas,, 2017.

KEE, R. J.; RUPLEY, F. M.; MILLER, J. A. The chemkin thermodynamic data base. **Sandia National Labs., Albuquerque, NM**, v. 1, 1990.

KIM, J. *et al.* Effects of water direct injection on the torque enhancement and fuel consumption reduction of a gasoline engine under high-load conditions. **International Journal of Engine Research**, SAGE Publications Sage UK: London, England, v. 17, n. 7, p. 795–808, 2016.

KLAPATCH, R.; KOBLISH, T. Nitric oxide control with water injection in gas turbines. **Am. Soc. Mech. Eng. Paper No. 71-WA/GT-9**, 1971.

KLAPATCH, R.; KOBLISH, T. R. Nitrogen oxide control with water injection in gas turbines. In: ASME. [S.l.], 1971.

KLEIN, M. **A specific heat ratio model and compression ratio estimation**. [S.l.]: Division of Vehicular Systems, Department of Electrical Engineering, Linköping University, 2004.

KODAH, Z. *et al.* Combustion in a spark-ignition engine. **Applied Energy**, Elsevier, v. 66, n. 3, p. 237–250, 2000.

KOENIG, R. J.; HEISER, G. Effect of water injection on cooling characteristics of pratt and whitney, r2800 engine. **NACA ARR**, n. 3-K09, 1943.

KOPA, R. D.; HOLLANDER, B. R.; KIMURA, H. **Combustion Temperature, Pressure, and Products at Chemical Equilibrium**. [S.l.], 1963.

KUHRING, M. Water and water-alcohol injection in a supercharged jaguar aircraft engine. **Canadian Journal of Research**, NRC Research Press, v. 16, n. 8, p. 149–176, 1938.

KULMALA, M. *et al.* Mass transfer from a drop—ii. theoretical analysis of temperature dependent mass flux correlation. **International journal of heat and mass transfer**, Elsevier, v. 38, n. 9, p. 1705–1708, 1995.

LANZAFAME, R. Water injection effects in a single-cylinder cfr engine. In: **SAE Technical Paper**. SAE International, 1999. Disponível em: <http://dx.doi.org/10.4271/1999-01-0568>.

LASHERAS, J.; FERNANDEZ-PELLO, A.; DRYER, F. Initial observations on the free droplet combustion characteristics of water-in-fuel emulsions. **Combustion Science and Technology**, Taylor & Francis, v. 21, n. 1-2, p. 1–14, 1979.

LEFEBVRE, A. H.; MCDONELL, V. G. **Atomization and sprays**. [S.l.]: CRC press, 2017.

LEVEQUE, R. J.; YEE, H. C. A study of numerical methods for hyperbolic conservation laws with stiff source terms. **Journal of computational physics**, Elsevier, v. 86, n. 1, p. 187–210, 1990.

LEVICH, V. G. **Physicochemical hydrodynamics**. [S.l.]: Prentice hall, 1962.

LIMA, A. J. T. B. d. *et al.* **Pollutant formation simulation models (CO, NOx and UHC) for Ethanol-fueled engines= Modelos de simulação de formação de poluentes (CO, NOx e UHC) em motores a etanol**. Dissertação (Mestrado) — Universidade Estadual de Campinas,, 2017.

LIU, H. *et al.* Dual-fuel spark ignition (dfsi) combustion fuelled with different alcohols and gasoline for fuel efficiency. **Fuel**, Elsevier, v. 157, p. 255–260, 2015.

LOAIZA, J. **First Scientific Report. Study of Internal Combustion Engine Operation, Powered by Ethanol Indirect Injection and Water Direct Injection into the Combustion Chamber.** [S.l.], 2016.

MATTAVI, J. N. **Combustion modeling in reciprocating engines**. [S.l.]: Plenum Publishing Corporation, 1980.

MIDGLEY, T.; BOYD, T. The chemical control of gaseous detonation with particular reference to the internal-combustion engine. **Industrial & Engineering Chemistry**, ACS Publications, v. 14, n. 10, p. 894–898, 1922.

MIGITA, H. *et al.* The new 1.3-liter 2-plug engine for the 2002 honda fit. **JSAE review**, Elsevier, v. 23, n. 4, p. 507–511, 2002.

MINGRUI, W. *et al.* Water injection for higher engine performance and lower emissions. **Journal of the Energy Institute**, Elsevier BV, jan 2016. Disponível em: <http://dx.doi.org/10.1016/j.joei.2015.12.003>.

MOREA-ROY, J.; MUÑOZ, M.; MORENO, F. Simulación numérica del ciclo operativo de un motor de encendido provocado. **Revista internacional de métodos numéricos**, Universitat Politècnica de Catalunya, 1999.

MOREL, T.; KERIBAR, R. **A model for predicting spatially and time resolved convective heat transfer in bowl-in-piston combustion chambers**. [S.l.], 1985.

NELSON, A. Exhaust emission characteristics of aircraft gas turbine engines. In: AMERICAN SOCIETY OF MECHANICAL ENGINEERS. **ASME 1972 International Gas Turbine and Fluids Engineering Conference and Products Show**. [S.l.], 1972. p. V001T01A074–V001T01A074.

NI, P. A fuel droplet vaporization model in a hot air stream. **Applied Mathematical Modelling**, v. 34, n. 9, p. 2370 – 2376, 2010. ISSN 0307-904X. Disponível em: <http://www.sciencedirect.com/science/article/pii/S0307904X09003758>.

NICHOLLS, J.; EI-MESSIRI, I.; NEWHALI, H. **Inlet manifold water injection for control of nitrogen oxides—theory and experiment**. [S.l.], 1969.

OLIKARA, C.; BORMAN, G. L. **A computer program for calculating properties of equilibrium combustion products with some applications to IC engines**. [S.l.], 1975.

PETERS, B. D.; STEBAR, R. F. **Water-gasoline fuels-their effect on spark ignition engine emissions and performance**. [S.l.], 1976.

PUCHER, H.; SPERLING, E. n-butanol-diesel mixture as alternative fuel for diesel motors. **Erdol & Kohle Erdgas Petrochemie**, URBAN-VERLAG GMBH PO BOX 70 16 06, D-22016 HAMBURG, GERMANY, v. 39, n. 8, p. 353–356, 1986.

RAKOPOULOS, C.; RAKOPOULOS, D.; KYRITSIS, D. Development and validation of a comprehensive two-zone model for combustion and emissions formation in a di diesel engine. **International journal of energy research**, Wiley Online Library, v. 27, n. 14, p. 1221–1249, 2003.

RAMACHANDRAN, S. Rapid thermodynamic simulation model of an internal combustion engine on alternate fuels. In: **Proceedings of the International MultiConference of Engineers and Computer Scientists**. [S.l.: s.n.], 2009. v. 2, p. 18–20.

REID, R. C.; PRAUSNITZ, J. M.; POLING, B. E. The properties of gases and liquids. McGraw Hill Book Co., New York, NY, 1987.

REITZ, R.; BRACCO, F. Mechanism of atomization of a liquid jet. **The Physics of Fluids**, AIP, v. 25, n. 10, p. 1730–1742, 1982.

RENKSIZBULUT, M.; YUEN, M. C. Experimental study of droplet evaporation in a high-temperature air stream. **Journal of Heat Transfer**, ASME, v. 105, n. 2, p. 384–388, maio 1983. ISSN 0022-1481. Disponível em: <http://dx.doi.org/10.1115/1.3245590>.

REYES, M. **Modelos Cuasi-Estacionarion**. [S.l.]: CEC, COMET, Programme, 1993.

RICARDO, H. R. The high-speed internal-combustion engine. Blackie, 1953.

RUFINO, C. H. Adjustable stroke length and compression ratio engine. **Acta Mechanìca et Mobilitatem**, v. 2, n. 3, p. 1–11, 2017.

SAZHIN, S. **Droplets and Sprays**. [S.l.]: Springer, 2014. 97-117 p.

SEZER, I.; BILGIN, A. Exergy analysis of si engines. **International Journal of Exergy**, Inderscience Publishers, v. 5, n. 2, p. 204–217, 2008.

STEFAN, J. Ueber die theorie der eisbildung, insbesondere über die eisbildung im polarmeere. **Annalen der Physik**, v. 278, n. 2, p. 269–286, 1891. Disponível em: <https://onlinelibrary.wiley.com/doi/abs/10.1002/andp.18912780206>.

STONE, R. Introduction to internal combustion engines. Springer, 1999.

STULL D R ; PROPHET, H. **JANAF Thermochemical Tables. Second Edition,**. [S.l.], 1971.

SUBRAMANIAN, V.; MALLIKARJUNA, J.; RAMESH, A. Effect of water injection and spark timing on the nitric oxide emission and combustion parameters of a hydrogen fuelled spark ignition engine. **International Journal of Hydrogen Energy**, Elsevier BV, v. 32, n. 9, p. 1159–1173, jun 2007. Disponível em: <http://dx.doi.org/10.1016/j.ijhydene.2006.07.022>.

THEWES, M. *et al.* Water injection for gasoline combustion systems. **MTZ worldwide**, Springer, v. 76, n. 2, p. 10–15, 2015.

TURNER, D. W.; SIEGMUND, C.; ANDREWS, R. Influence of combustion modification and fuel nitrogen content on nitrogen oxides emissions from fuel oil combustion. **Combustion**, COMBUSTION PUBL CO 277 PARK AVE, NEW YORK, NY 10017, v. 44, n. 2, p. 21, 1972.

TURNS, S. R. **An introduction to combustion**. [S.l.]: McGraw-Hill New York, 1996. v. 499.

URBACH, H. B. *et al.* **The reduction of NOx emissions from marine power plants**. [S.l.], 1997.

VERHELST, S.; SHEPPARD, C. Multi-zone thermodynamic modelling of spark-ignition engine combustion – an overview. **Energy Conversion and Management**, Elsevier BV, v. 50, n. 5, p. 1326–1335, may 2009. Disponível em: <http://dx.doi.org/10.1016/j.enconman.2009.01.002>.

WEISS, M. E.; RUDD, B. E. **Automotive Engineer**. [S.l.], 1959.

WOSCHNI, G. **A universally applicable equation for the instantaneous heat transfer coefficient in the internal combustion engine**. [S.l.], 1967.

WU, H. **Study of spark ignition engine combustion model for the analysis of cyclic variation and combustion stability at lean operating conditions**. Dissertação (Mestrado) — MICHIGAN TECHNOLOGICAL UNIVERSITY, 2013.

ZACHARIAS, F. **Analytical representation of the thermodynamic properties of combustion gases**. [S.l.], 1967.

ZELDOVICH, Y. B.; SADOVNIKOV, P. Y.; FRANK-KAMENETSKII, D. Nitrogen oxidation in combustion. **Izd. Akad. Nauk SSSR, Moscow**, 1947.

A APPENDIX

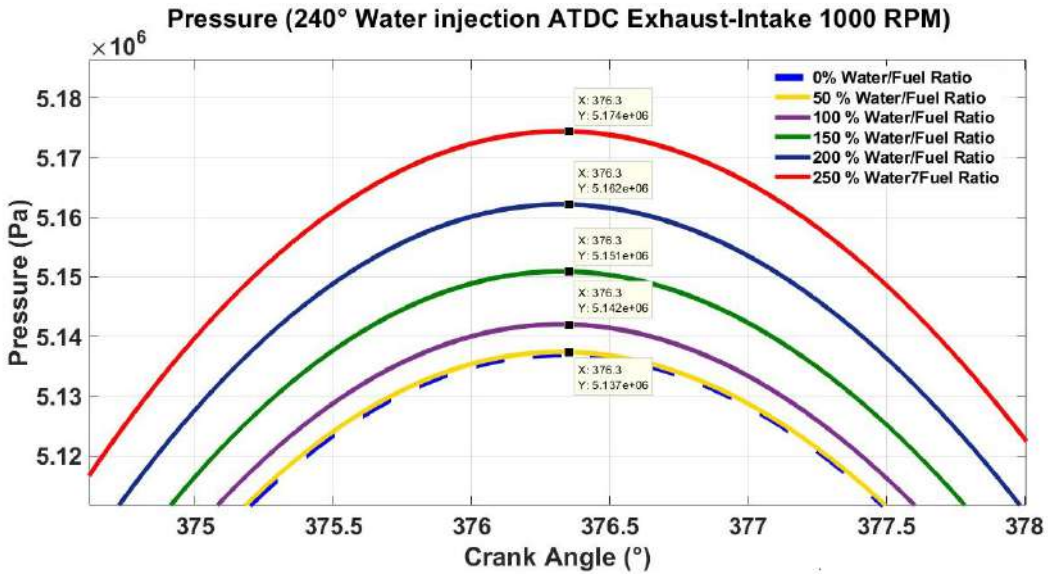

Fig. A.1 – Pressure 240° 1000 RPM.

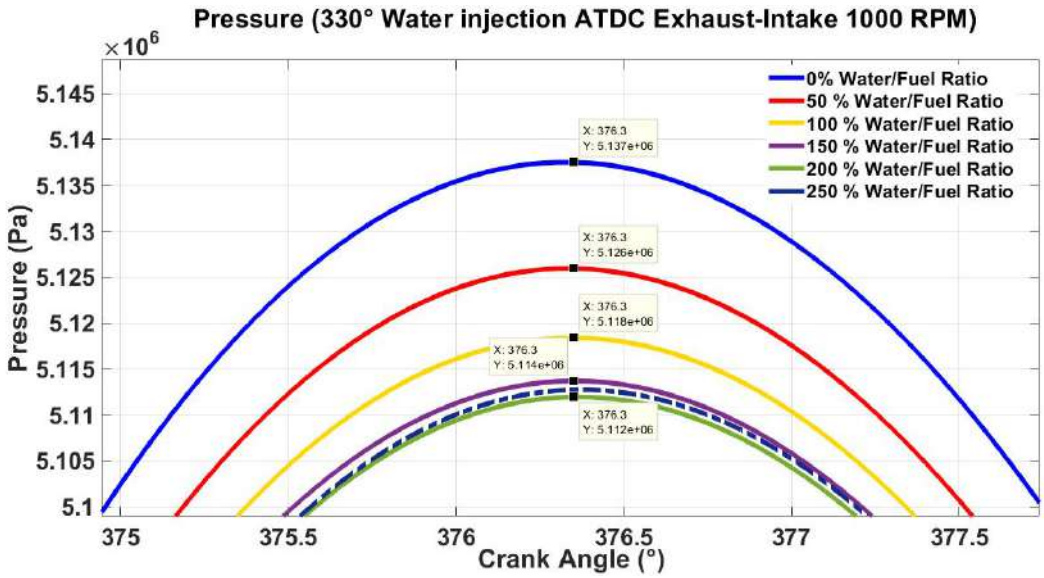

Fig. A.2 – Pressure 330° 1000 RPM.

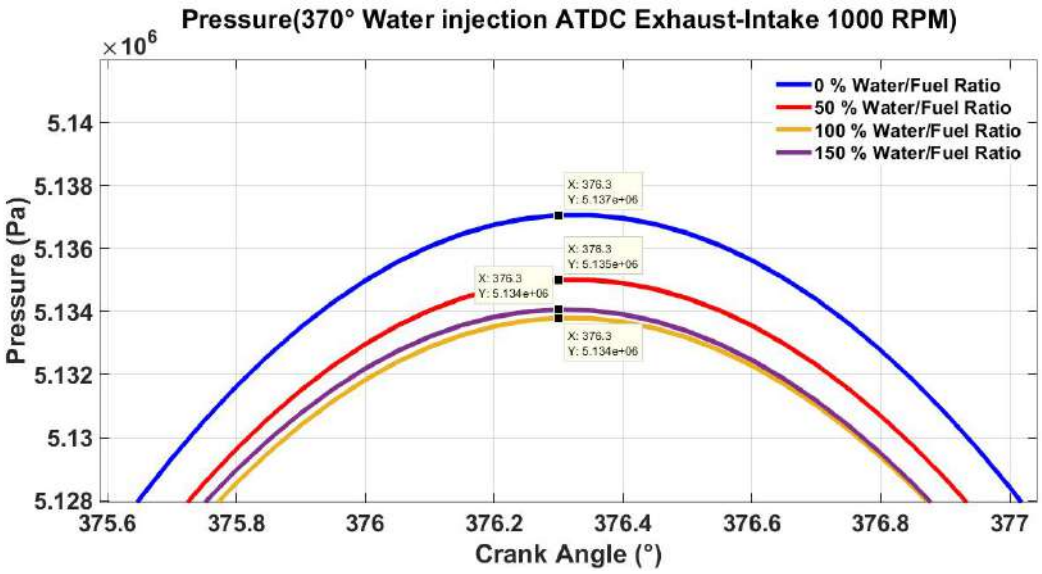

Fig. A.3 – Pressure 370° 1000 RPM.

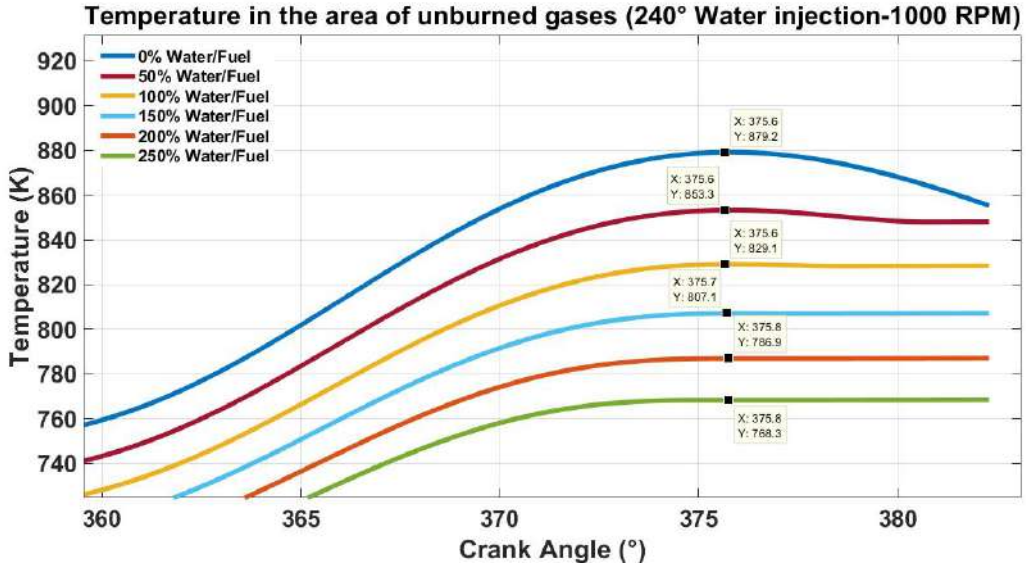

Fig. A.4 – Temperature 240° 1000 RPM. Detail (1).

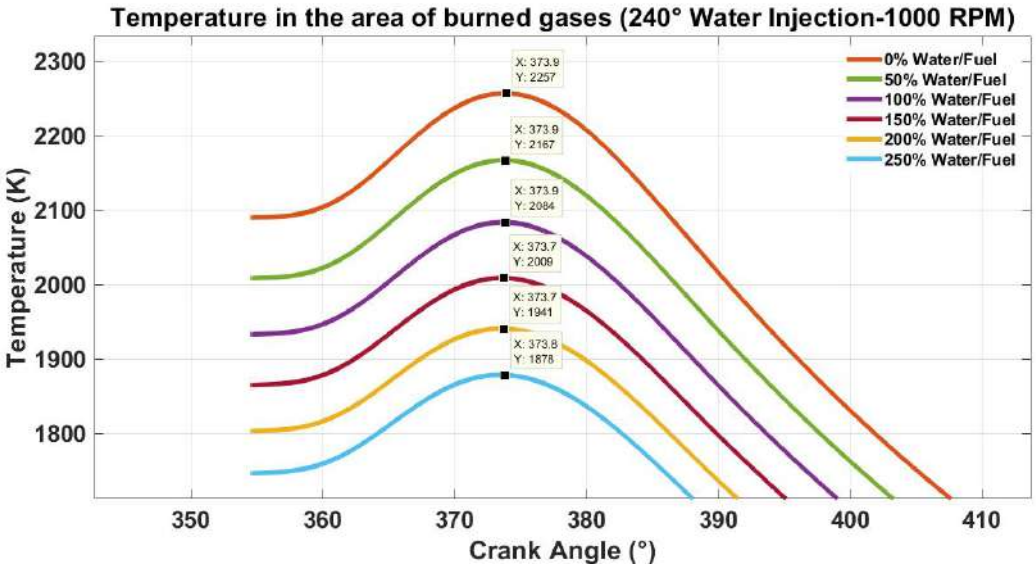

Fig. A.5 – Temperature 240° 1000 RPM. Detail (2).

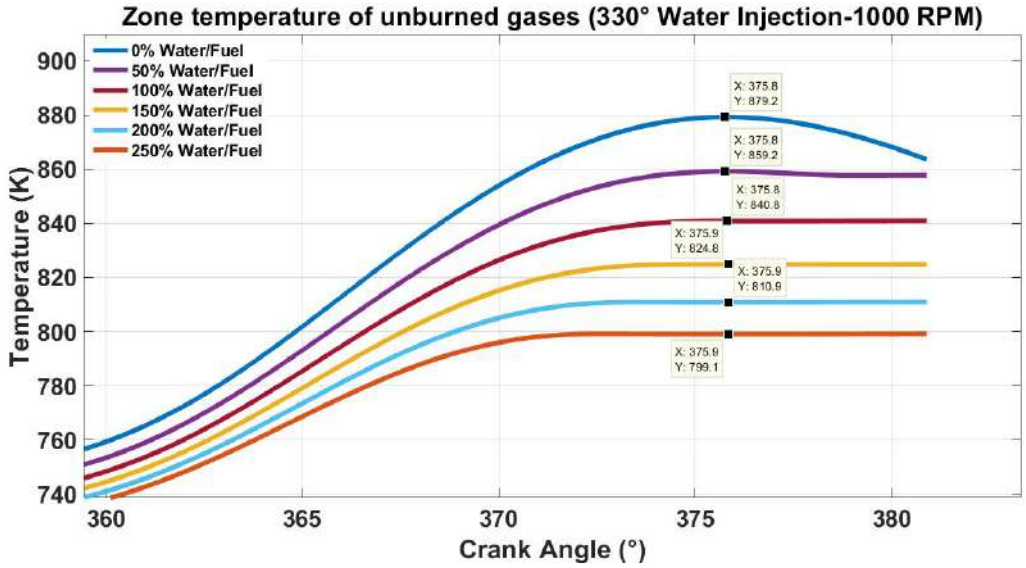

Fig. A.6 – Temperature 330° 1000 RPM. Detail (1).

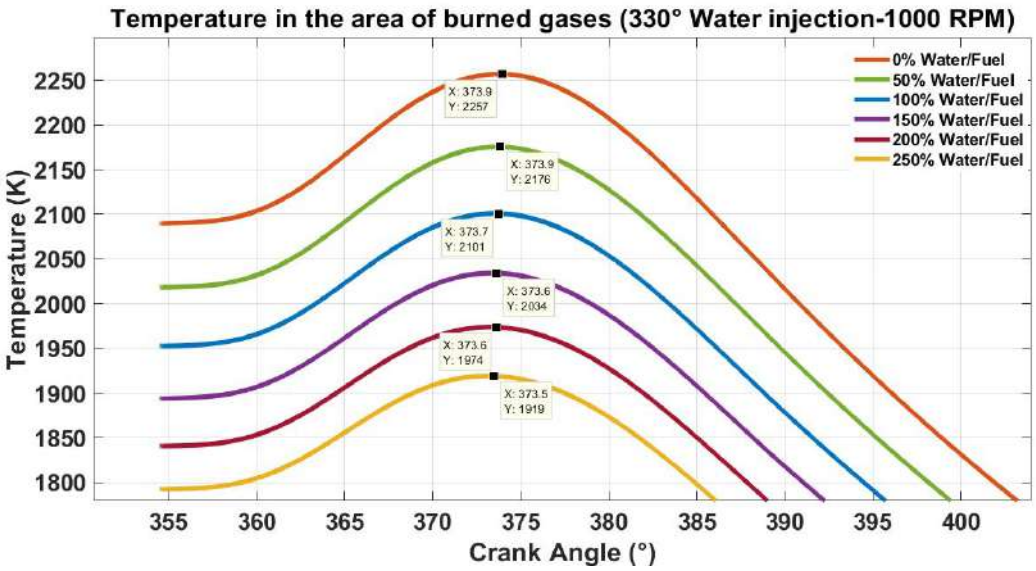

Fig. A.7 – Temperature 330° 1000 RPM. Detail (2).

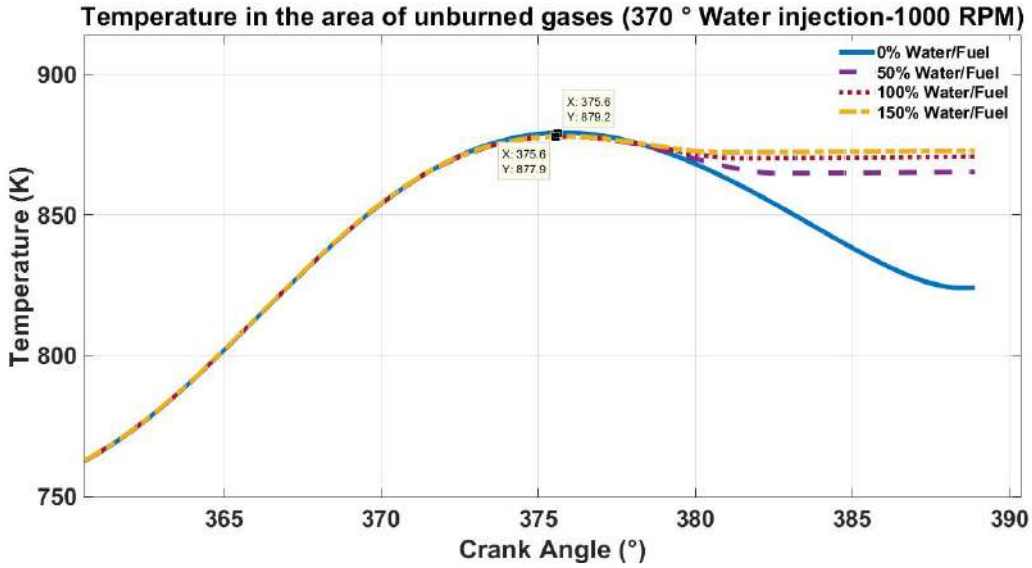

Fig. A.8 – Temperature 370° 1000 RPM. Detail (1).

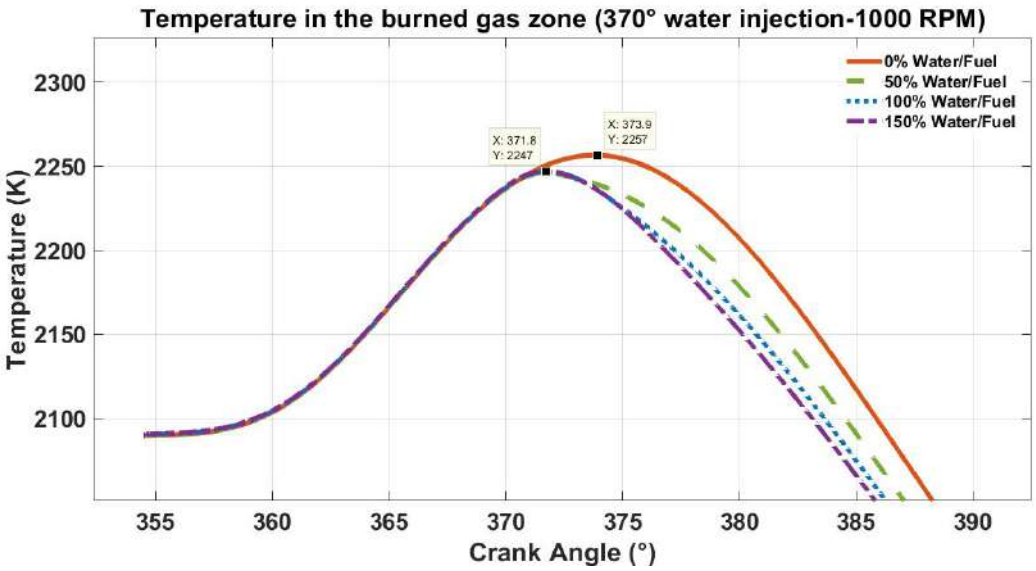

Fig. A.9 – Temperature 370° 1000 RPM. Detail (2).

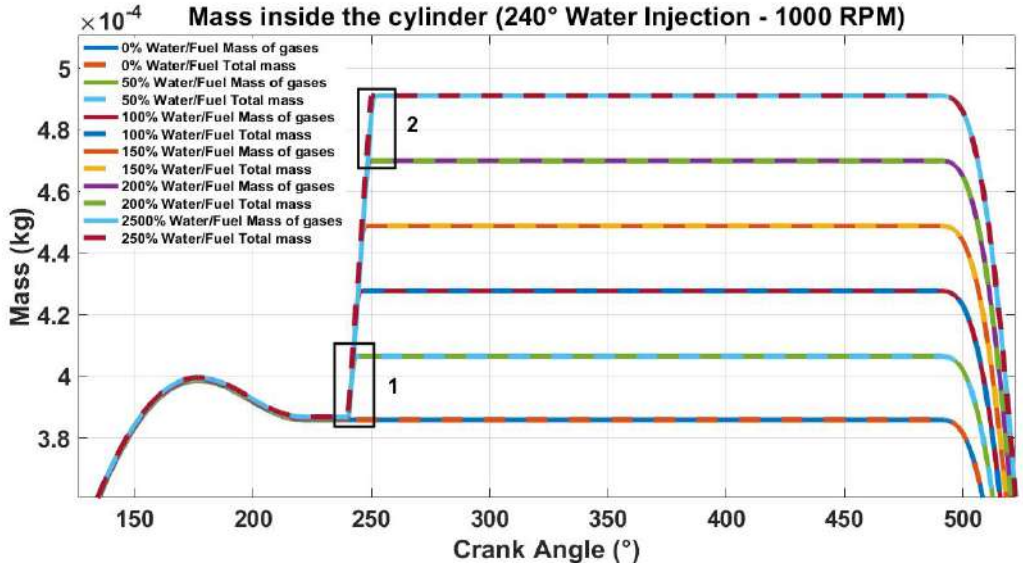

Fig. A.10 – Mass In-Cylinder 240° 1000 RPM. .

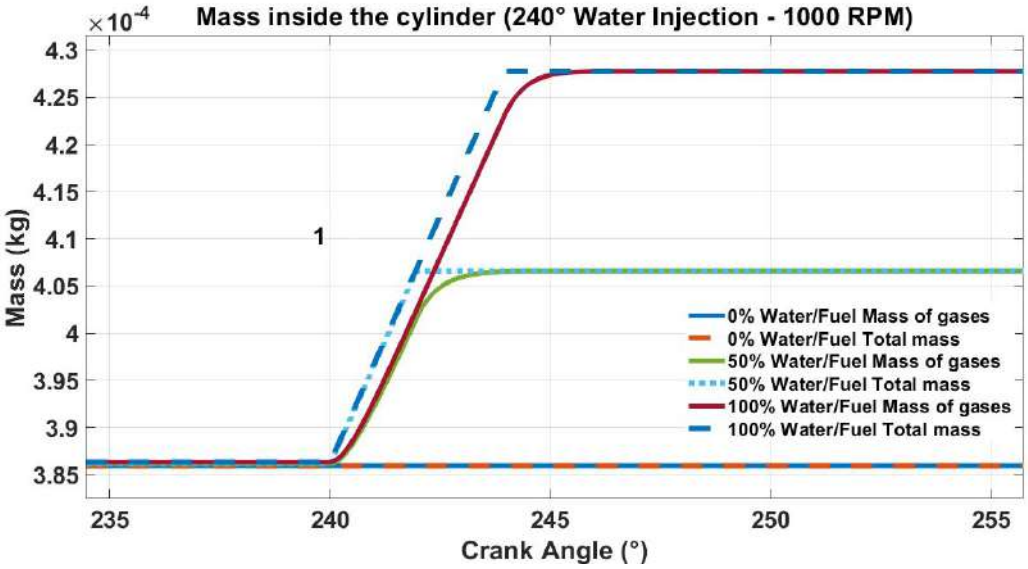

Fig. A.11 – Mass In-Cylinder 240° 1000 RPM. Detail (1).

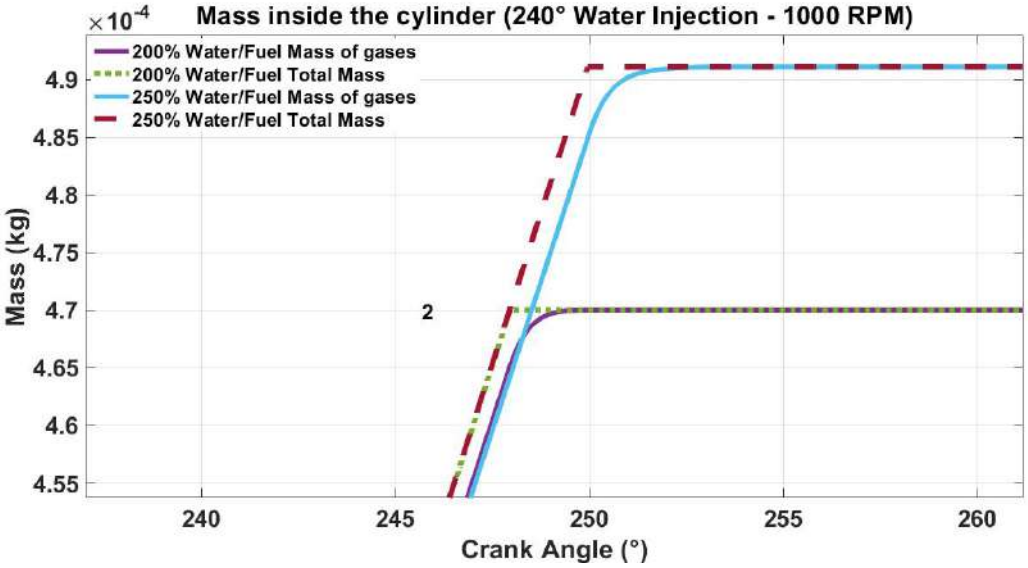

Fig. A.12 – Mass In-Cylinder 240° 1000 RPM. Detail (2).

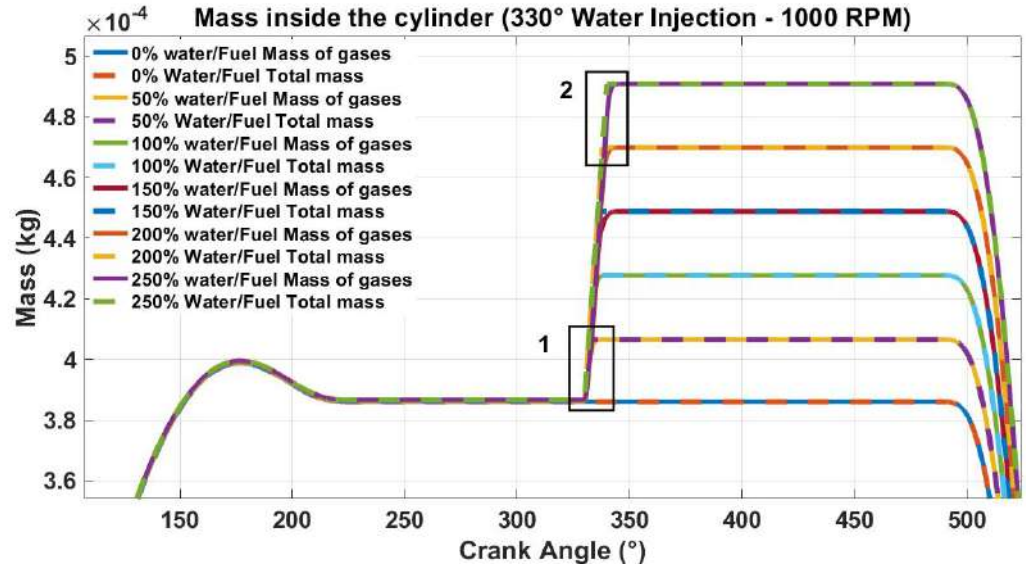

Fig. A.13 – Mass In-Cylinder 330° 1000 RPM.

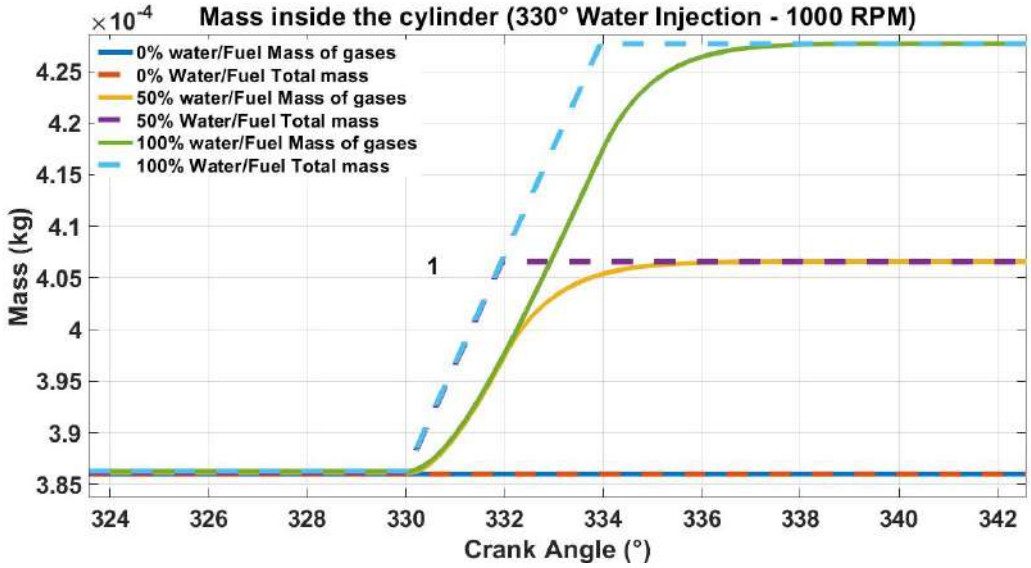

Fig. A.14 – Mass In-Cylinder 330° 1000 RPM. Detail (1).

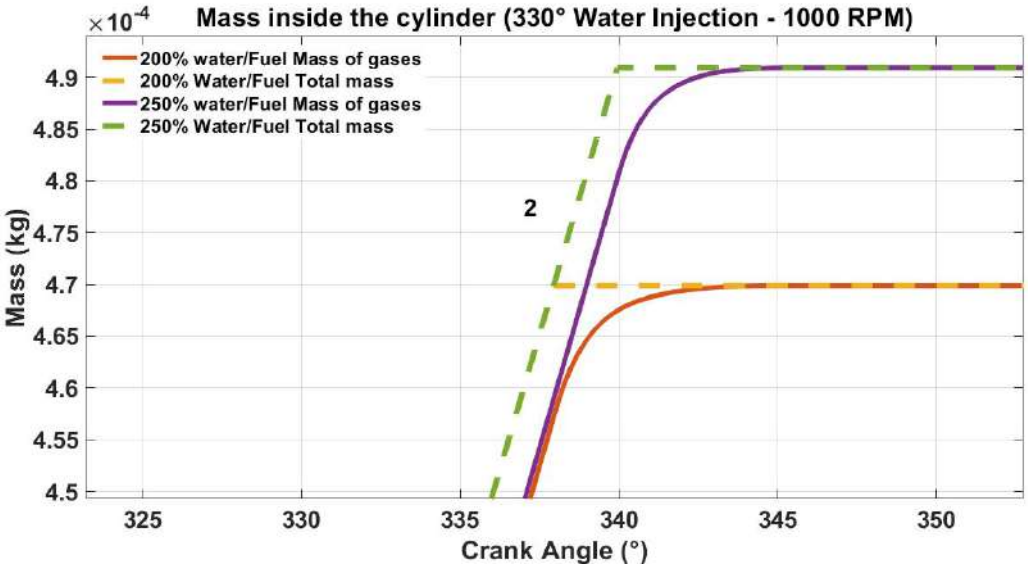

Fig. A.15 – Mass In-Cylinder 330° 1000 RPM. Detail (2).

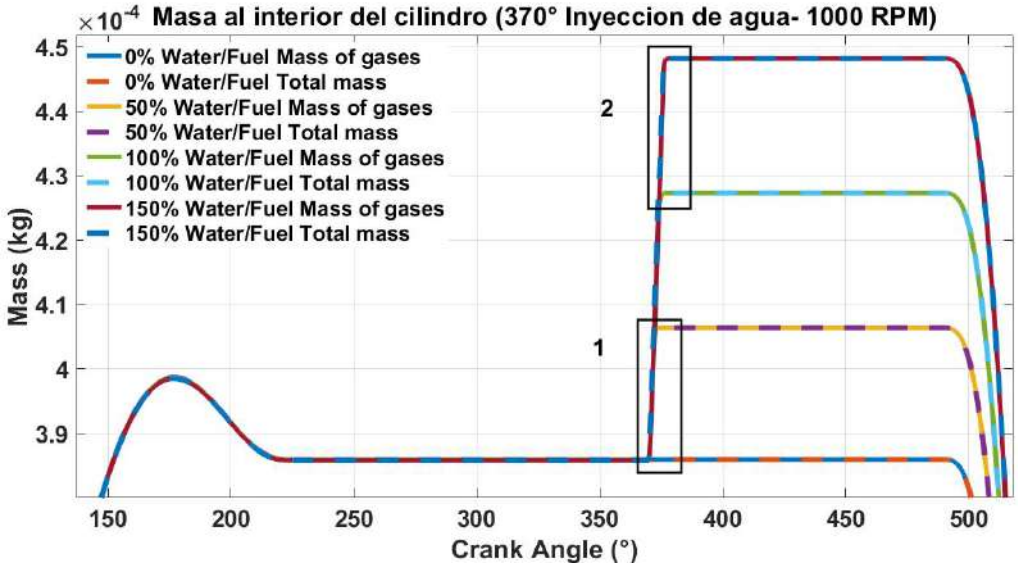

Fig. A.16 – Mass In-Cylinder 370° 1000 RPM.

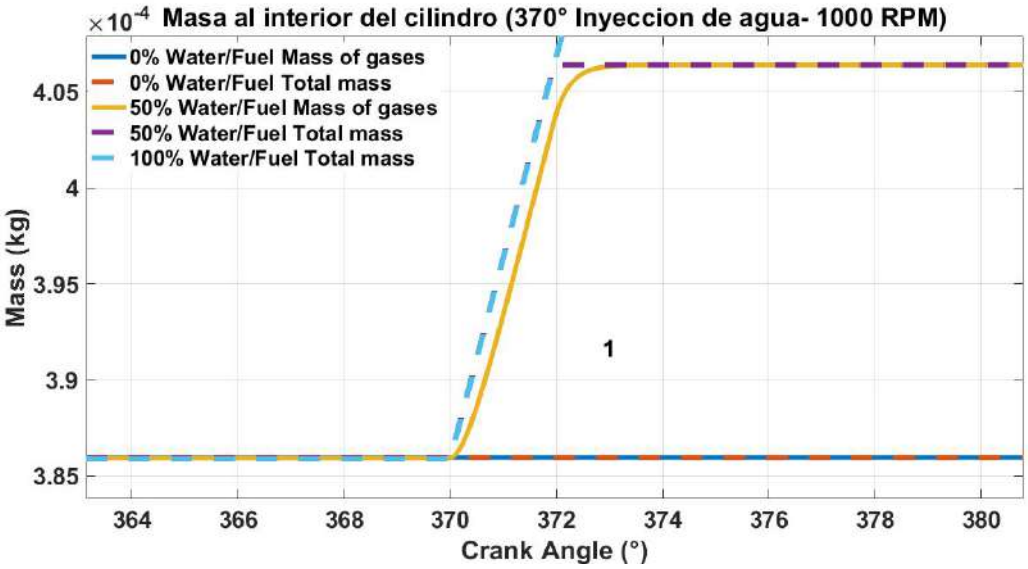

Fig. A.17 – Mass In-Cylinder 370° 1000 RPM. Detail (1).

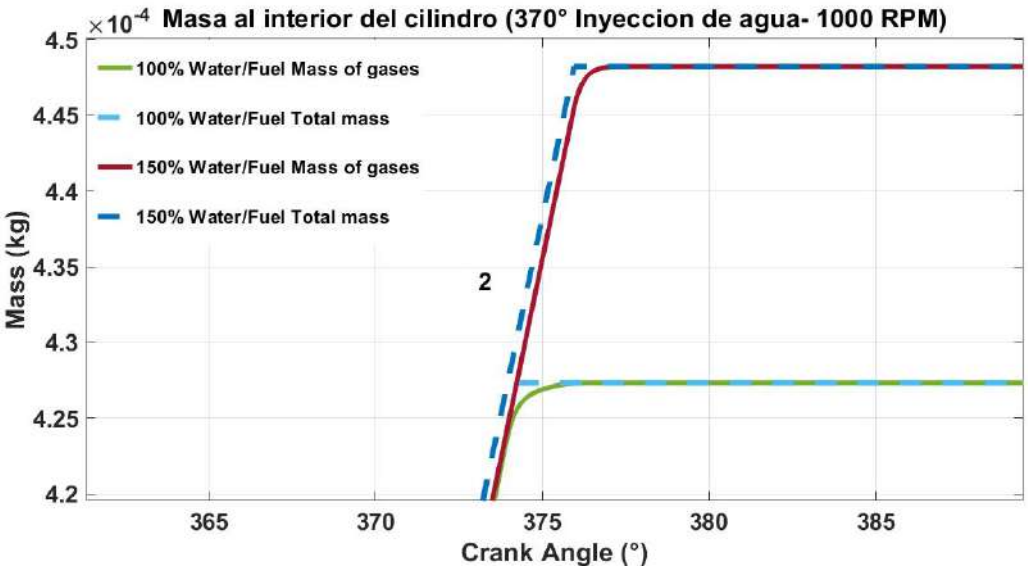

Fig. A.18 – Mass In-Cylinder 370° 1000 RPM. Detail (2).

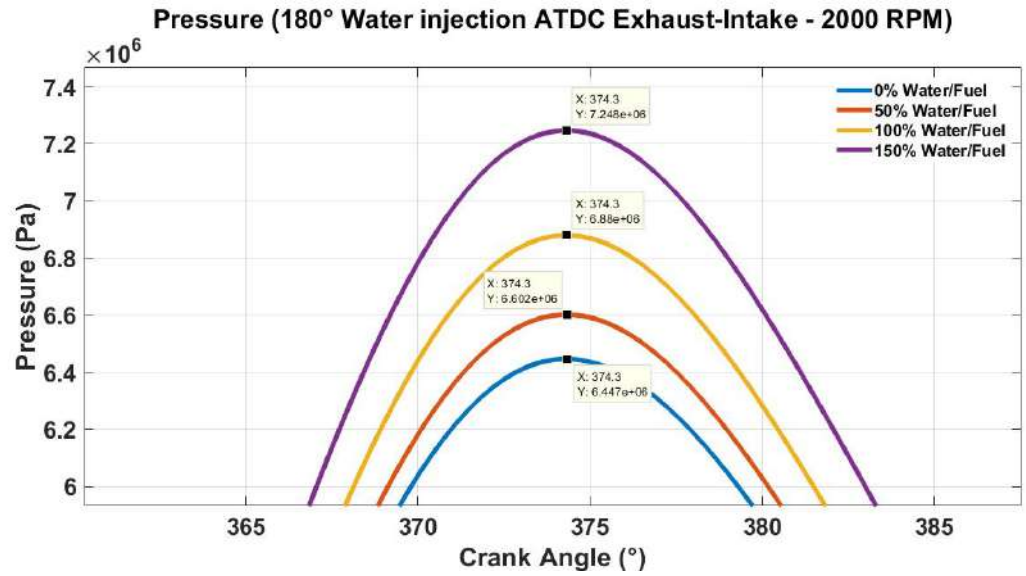

Fig. A.19 – Pressure 180° 2000 RPM.

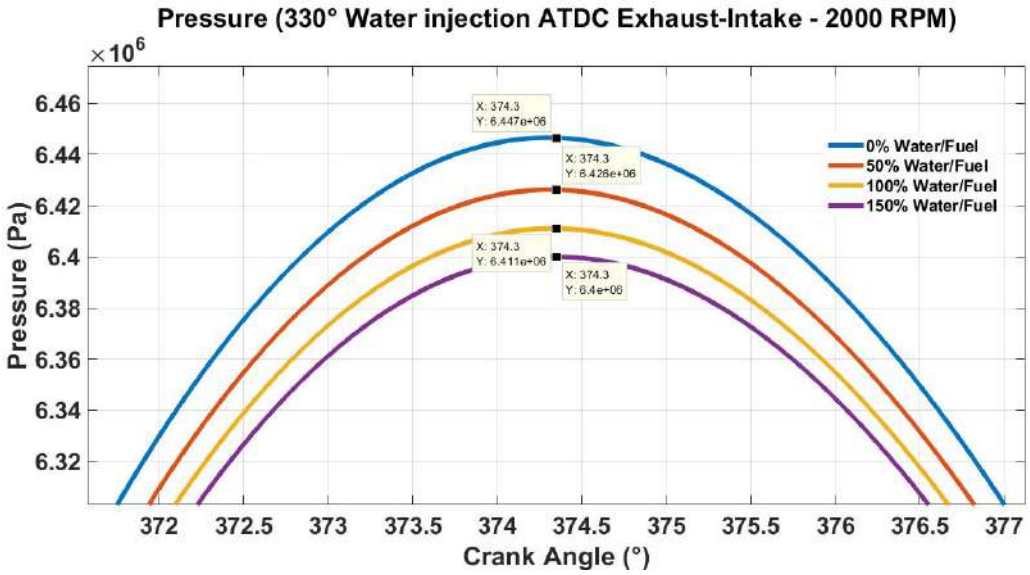

Fig. A.20 – Pressure 330° 2000 RPM.

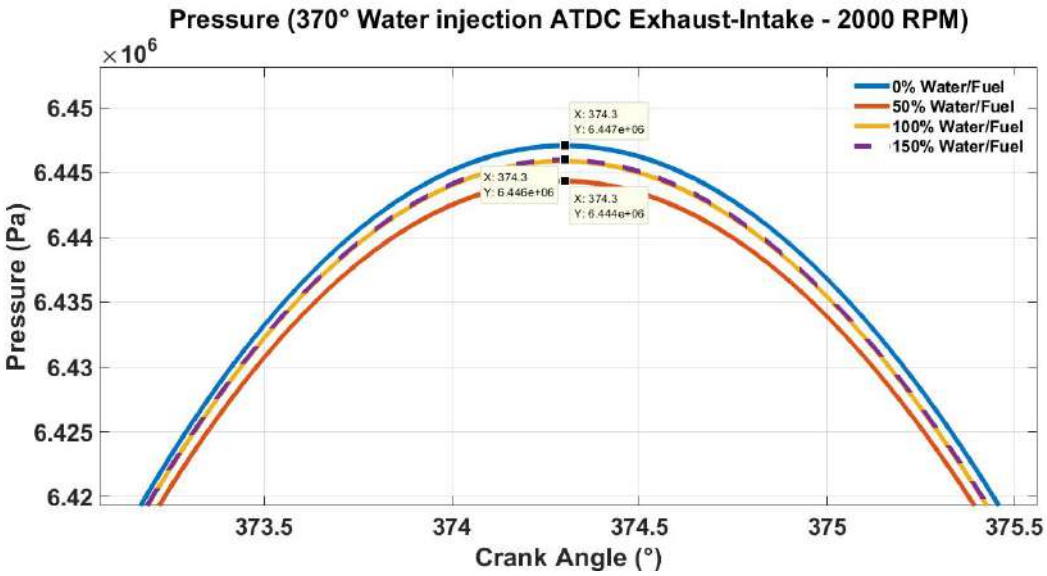

Fig. A.21 – Pressure 370° 2000 RPM.

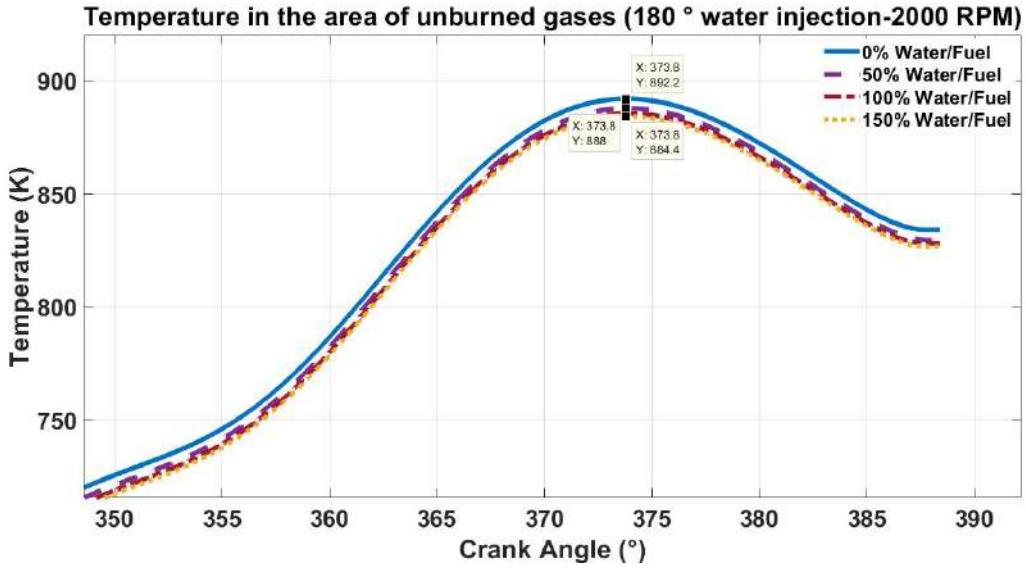

Fig. A.22 – Temperature 180° Unburned zone 2000 RPM. Detail (1).

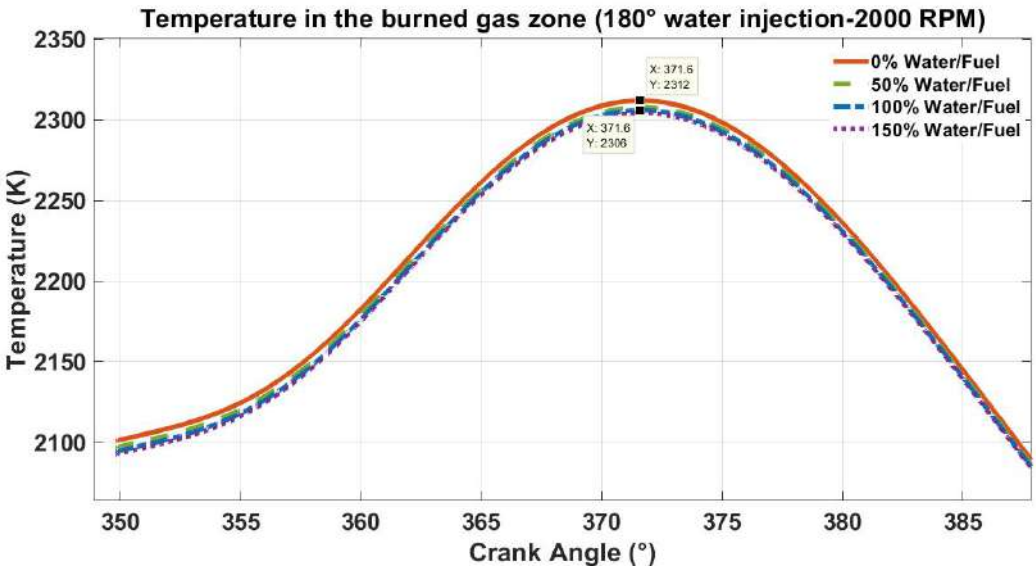

Fig. A.23 – Temperature 180° Burned zone 2000 RPM. Detail (2).

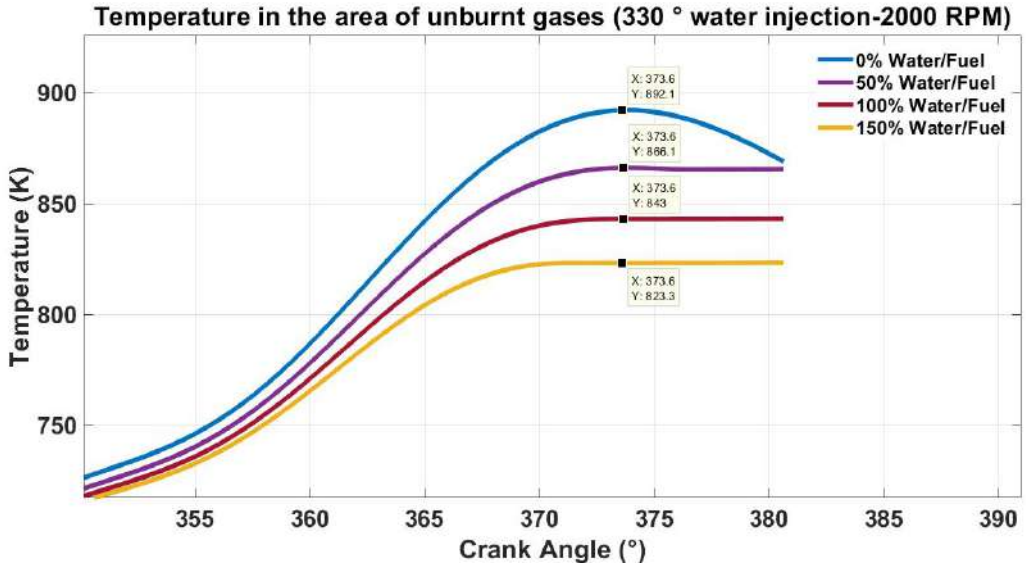

Fig. A.24 – Temperature 330° Unburned zone 2000 RPM. Detail (1).

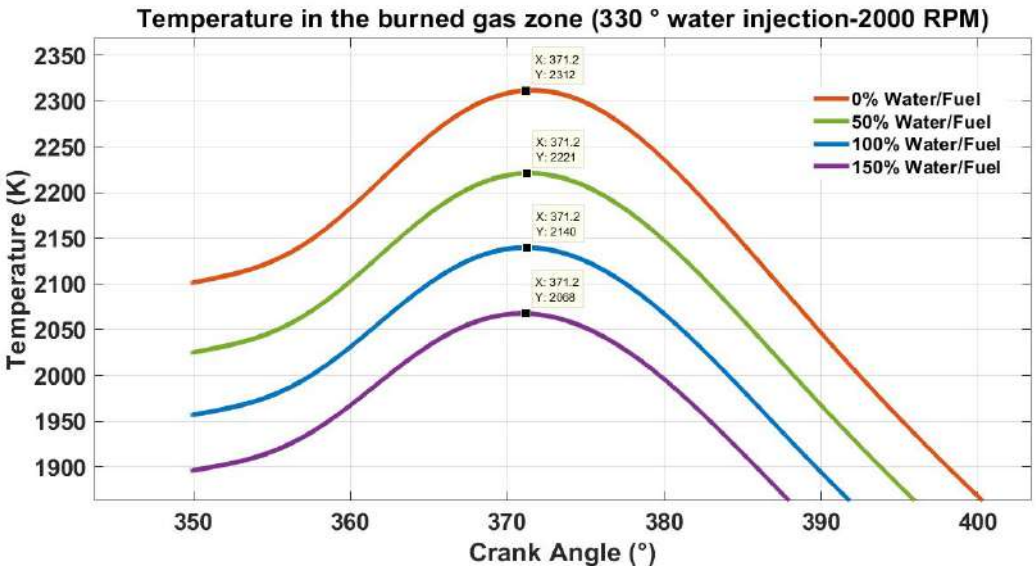

Fig. A.25 – Temperature 330° Burned zone 2000 RPM. Detail (2).

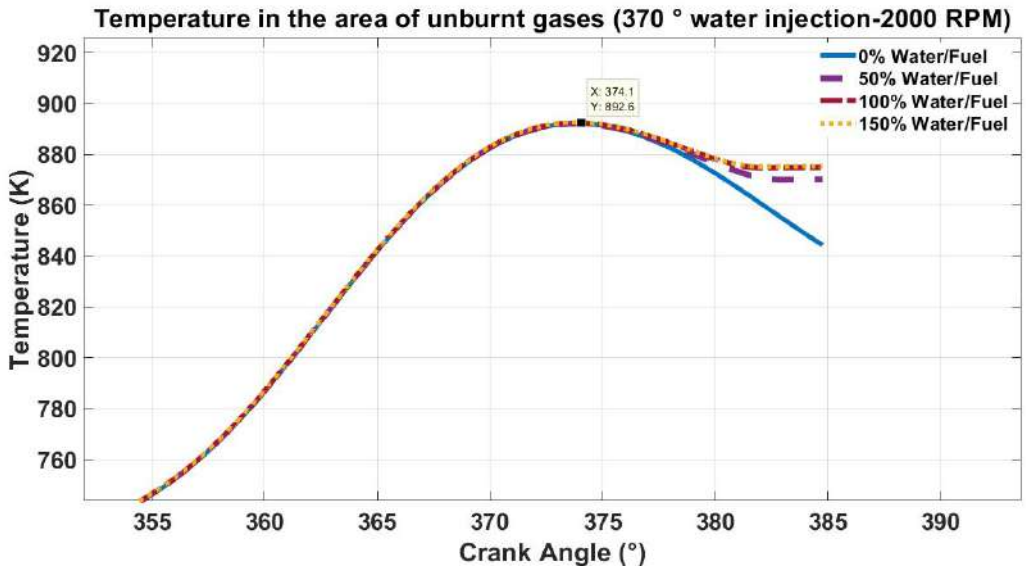

Fig. A.26 – Temperature 370° Unburned zone 2000 RPM. Detail (1).

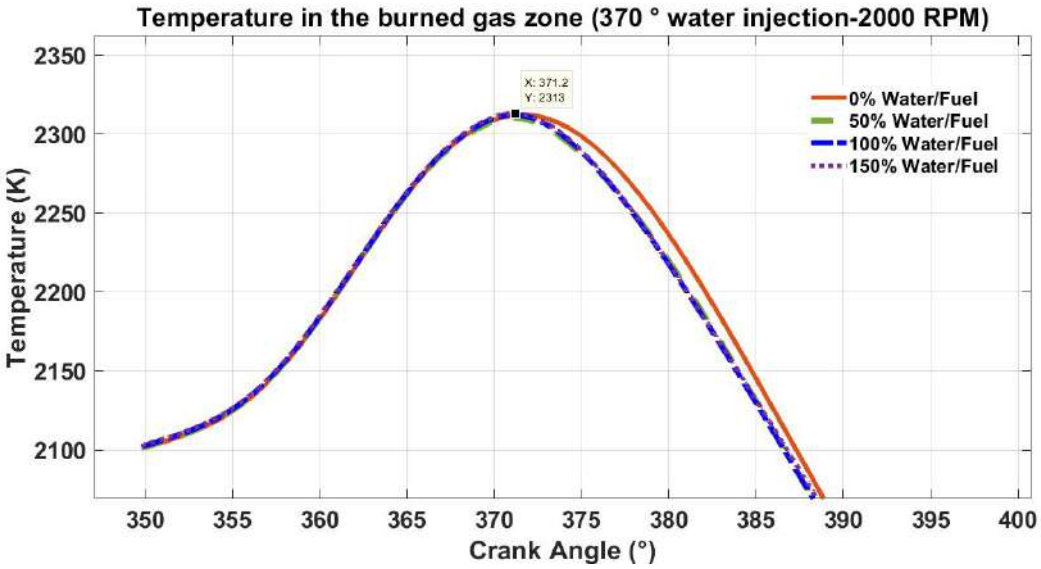

Fig. A.27 – Temperature 370° Burned zone 2000 RPM. Detail (2).

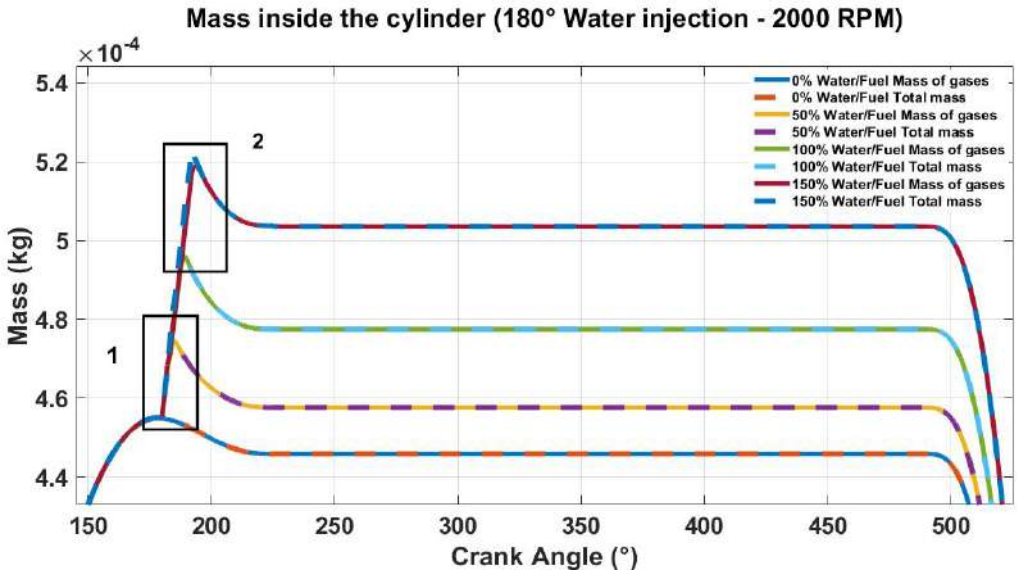

Fig. A.28 – Mass In-Cylinder 180° 2000 RPM.

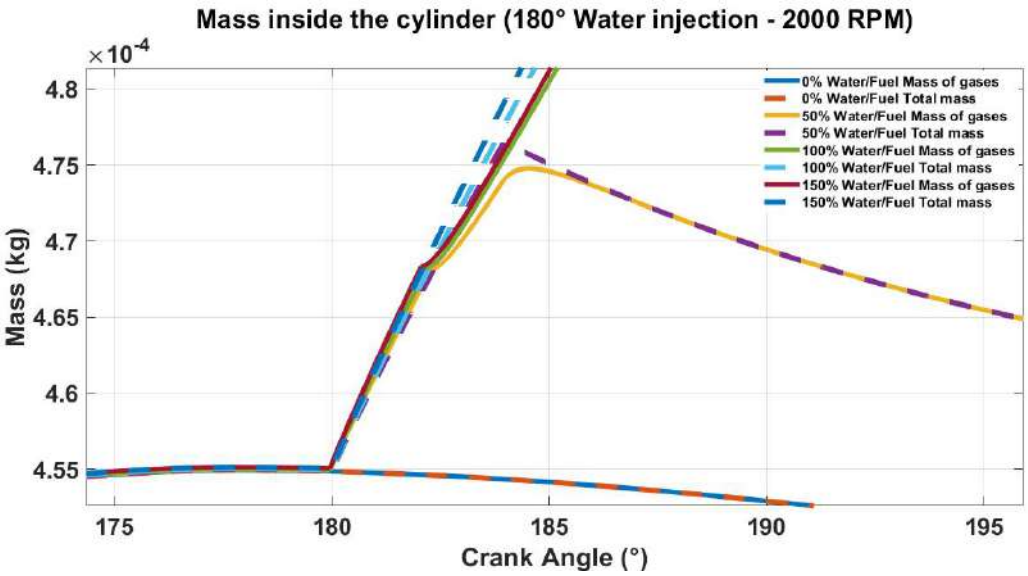

Fig. A.29 – Mass In-Cylinder 180° 2000 RPM. Detail (1)

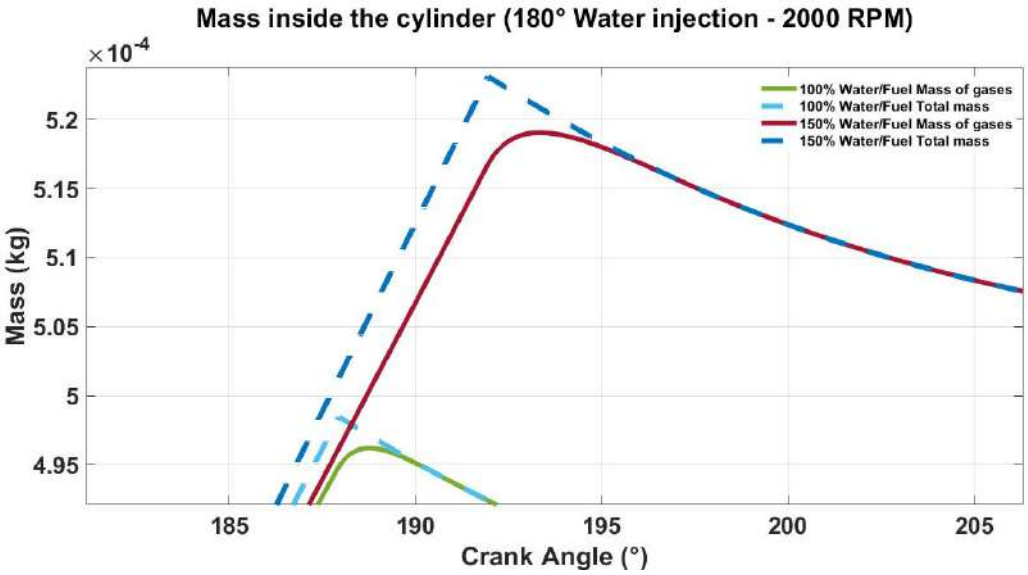

Fig. A.30 – Mass In-Cylinder 180° 2000 RPM. Detail (2)

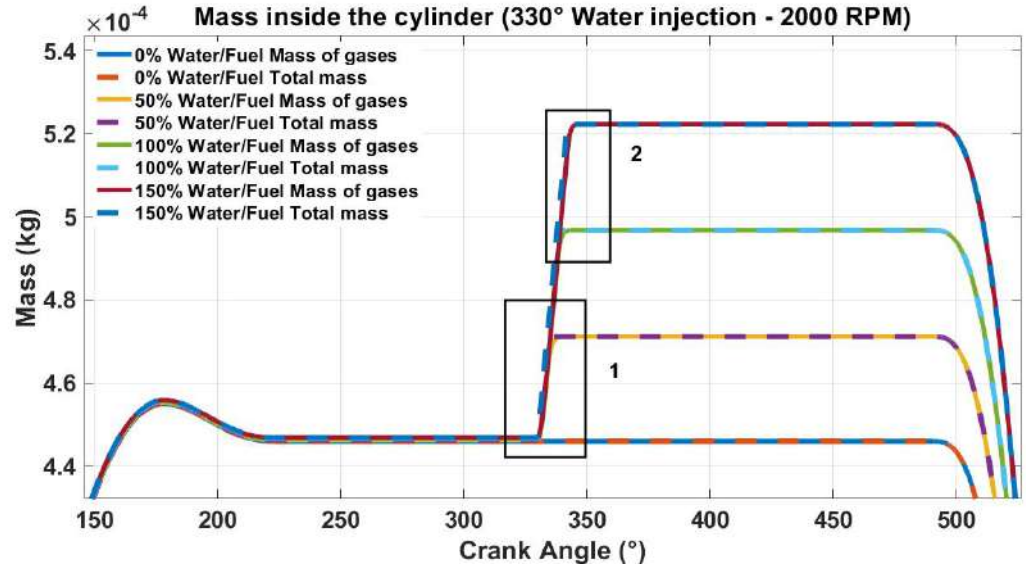

Fig. A.31 – Mass In-Cylinder 330° 2000 RPM.

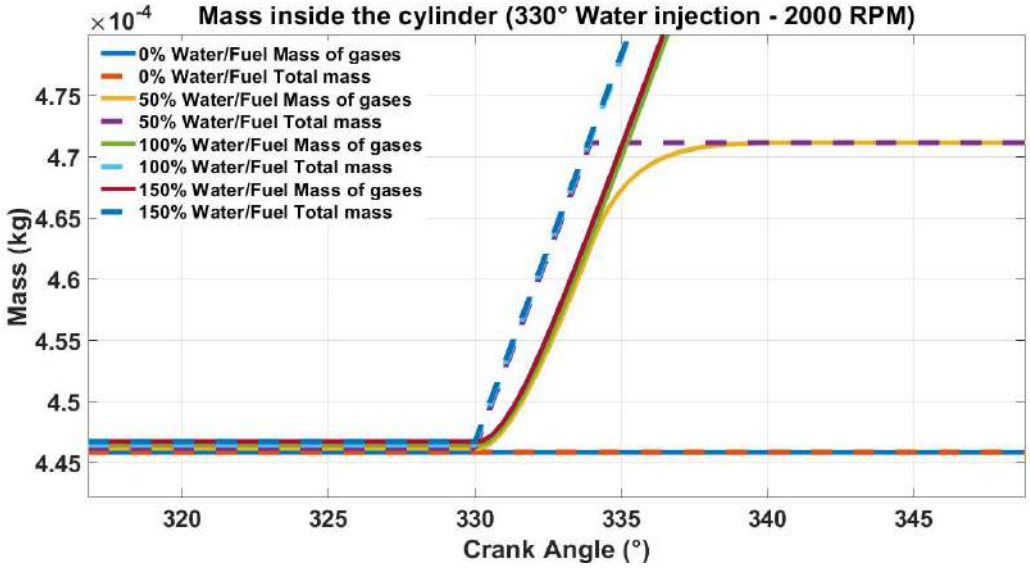

Fig. A.32 – Mass In-Cylinder 330° 2000 RPM. Detail (1)

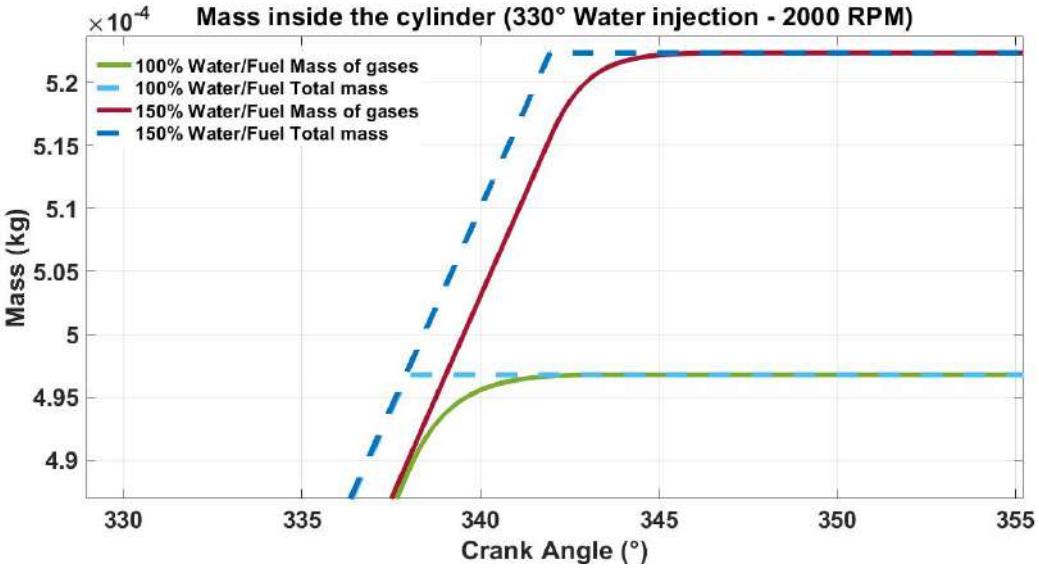

Fig. A.33 – Mass In-Cylinder 330° 2000 RPM. Detail (2)

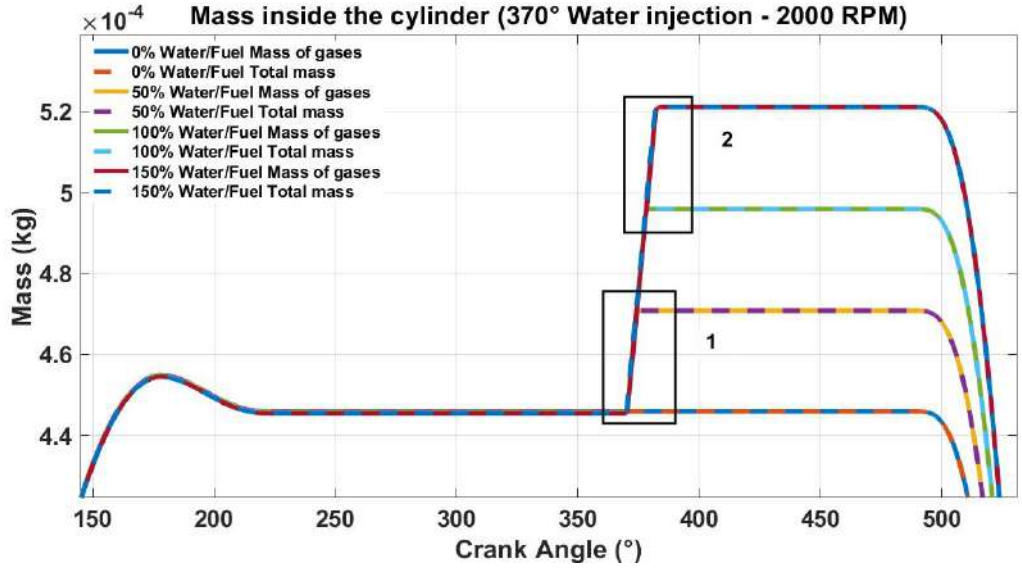

Fig. A.34 – Mass In-Cylinder 370° 2000 RPM.

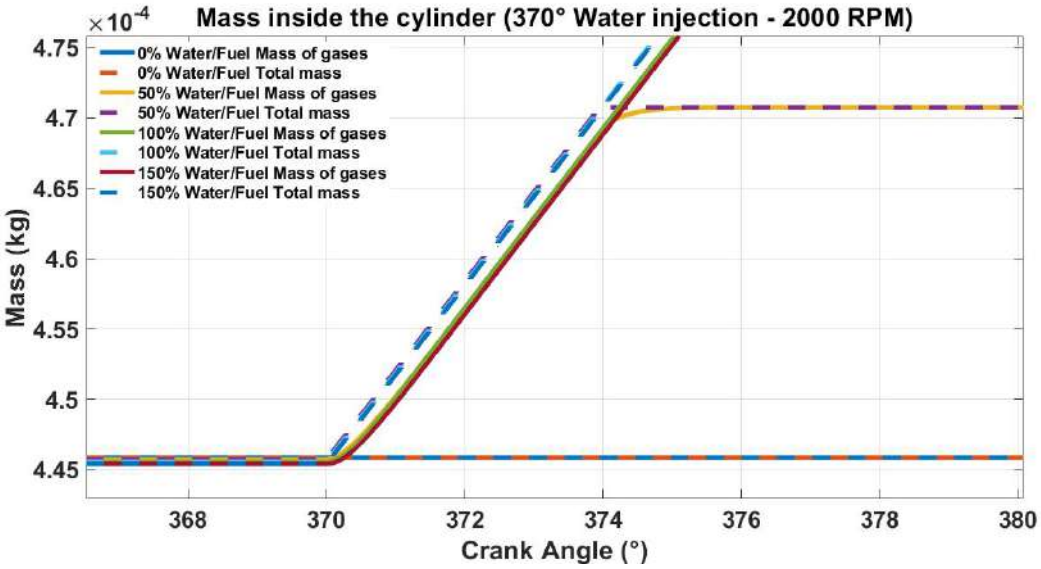

Fig. A.35 – Mass In-Cylinder 370° 2000 RPM. Detail (1)

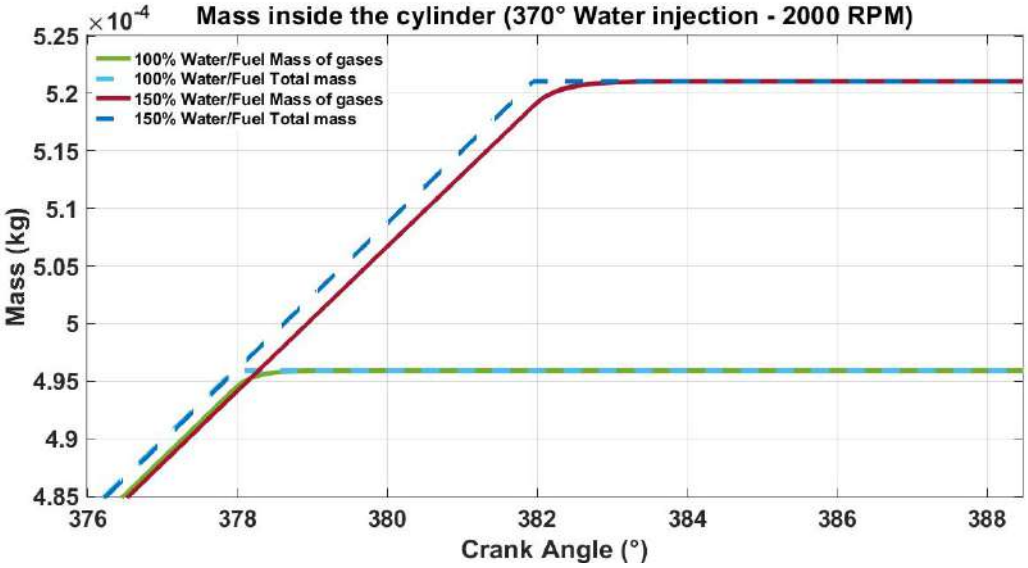

Fig. A.36 – Mass In-Cylinder 370° 2000 RPM. Detail (2)

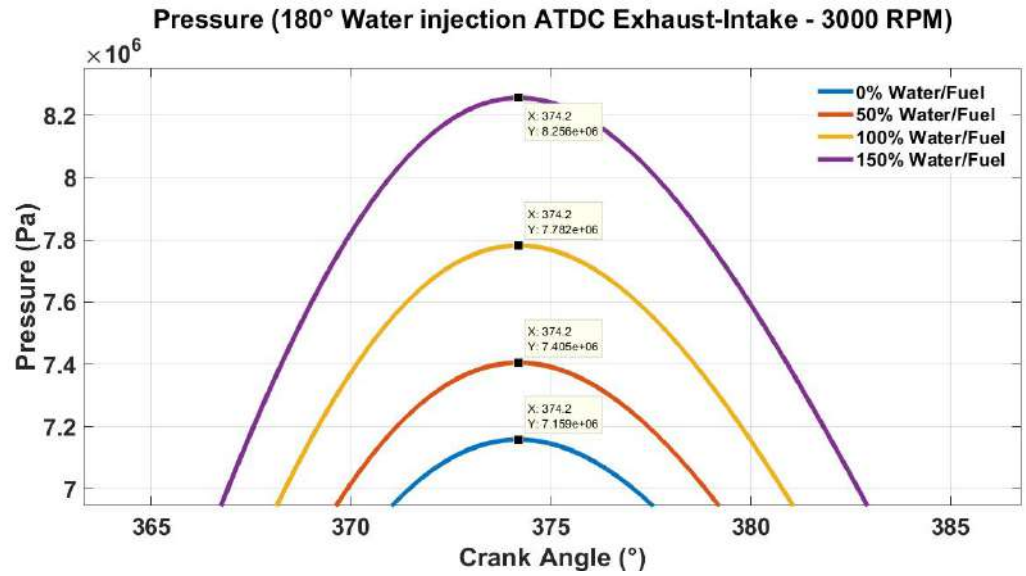

Fig. A.37 – Pressure 180° 3000 RPM.

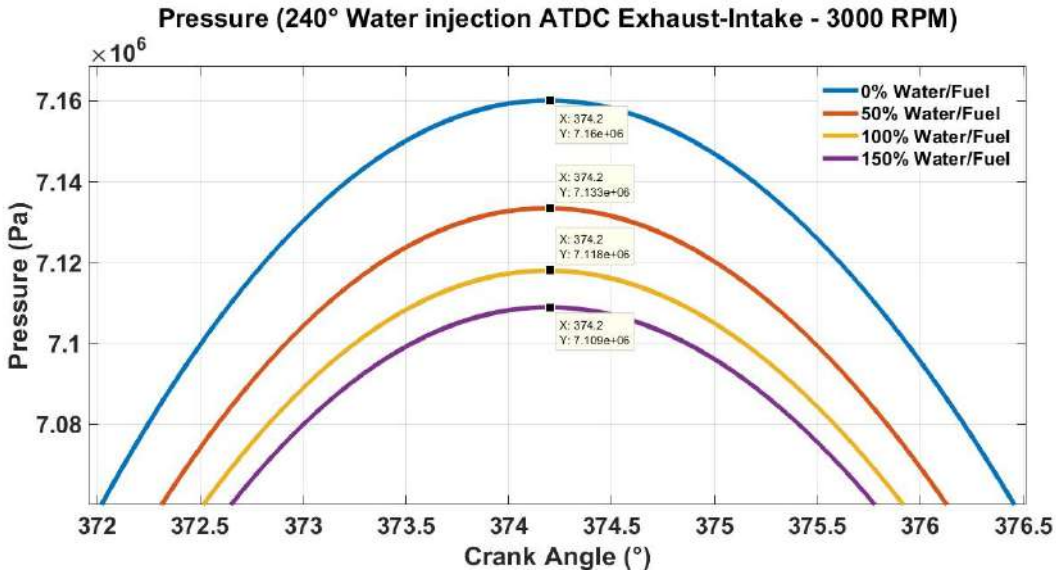

Fig. A.38 – Pressure 240° 3000 RPM.

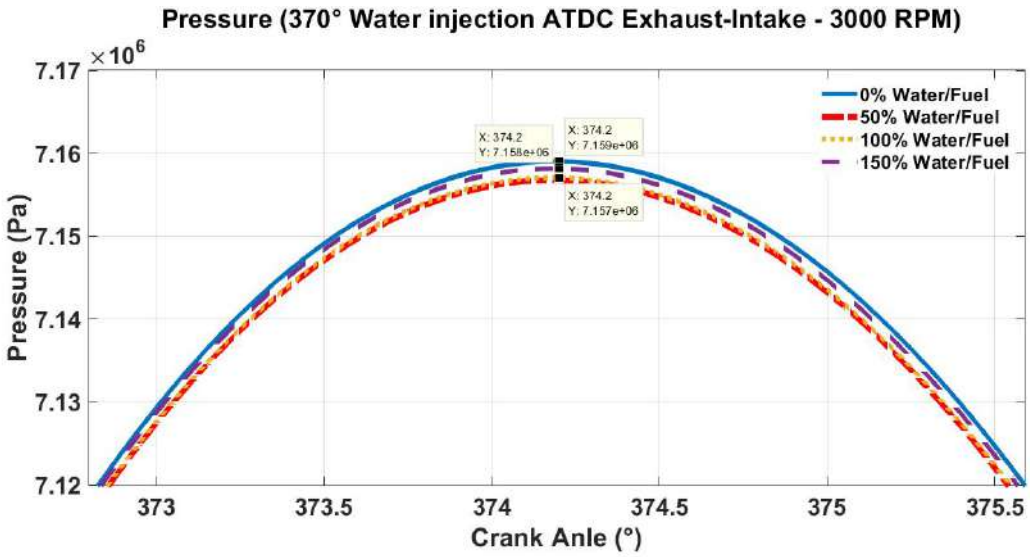

Fig. A.39 – Pressure 370° 3000 RPM.

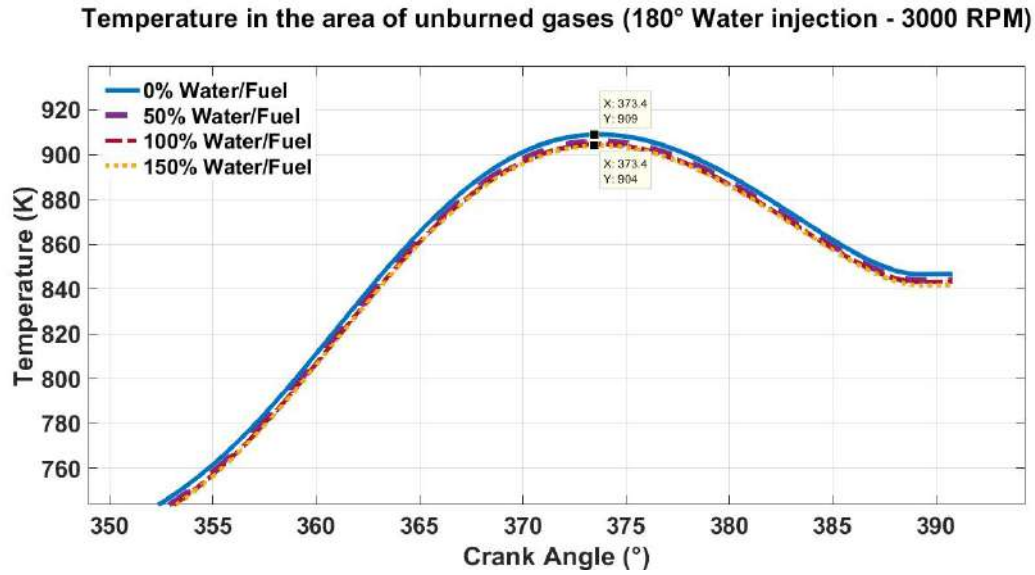

Fig. A.40 – Temperature 180° Unburned zone 3000 RPM. Detail (1).

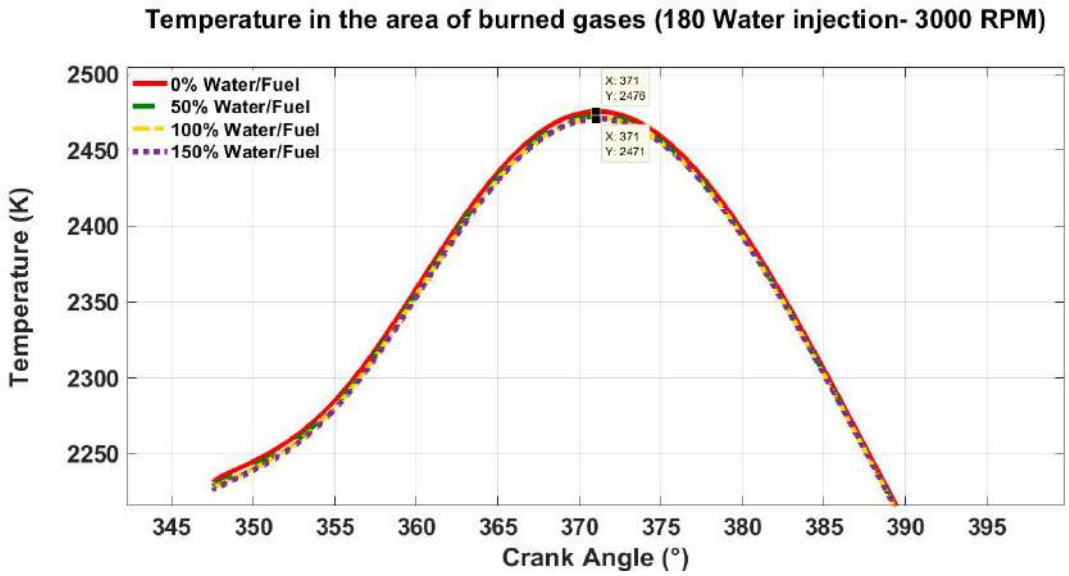

Fig. A.41 – Temperature 180° Burned zone 3000 RPM. Detail (2).

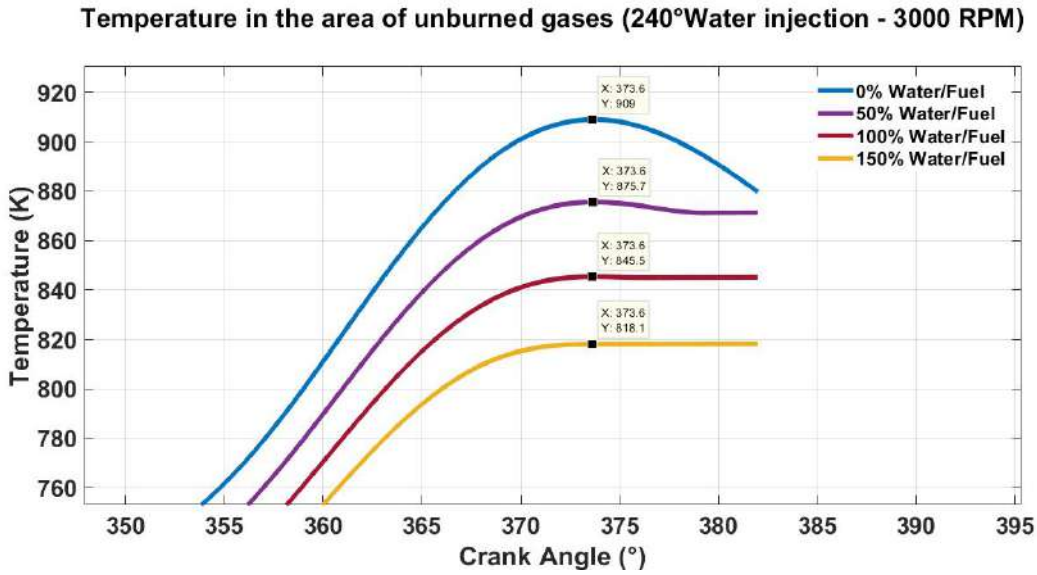

Fig. A.42 – Temperature 240° Unburned zone 3000 RPM. Detail (1).

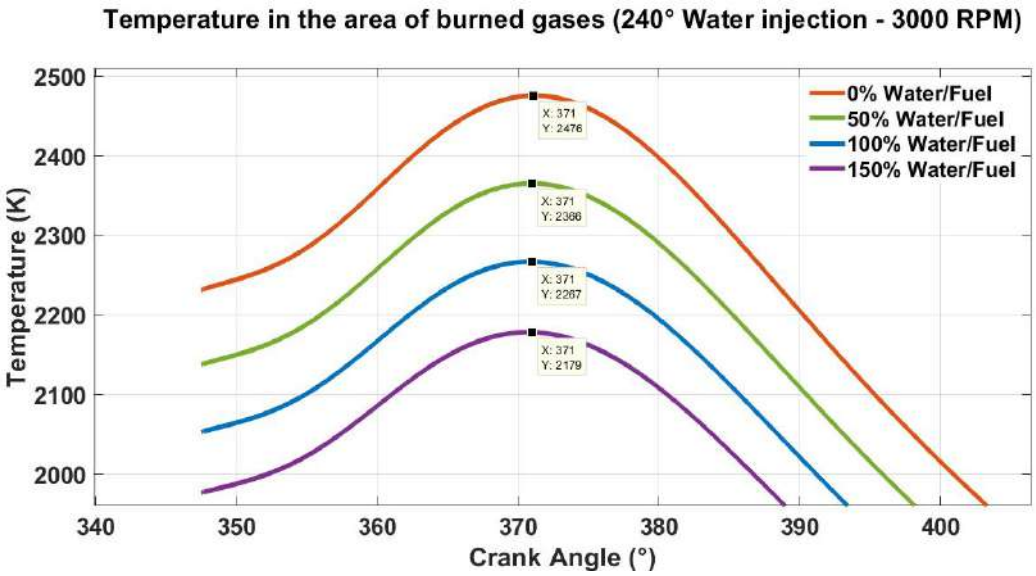

Fig. A.43 – Temperature 240° Burned zone 3000 RPM. Detail (2).

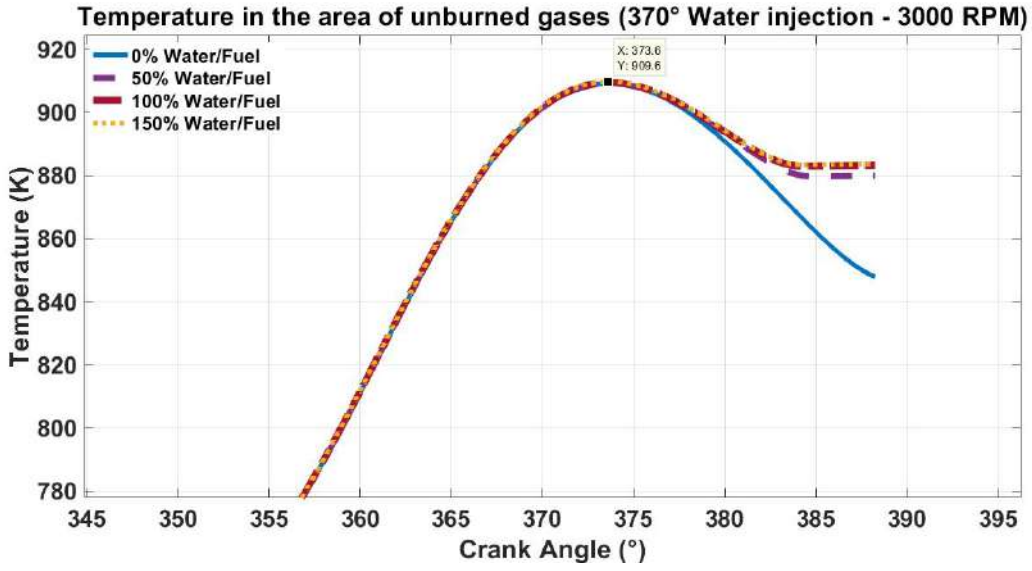

Fig. A.44 – Temperature 370° Unburned zone 3000 RPM. Detail (1).

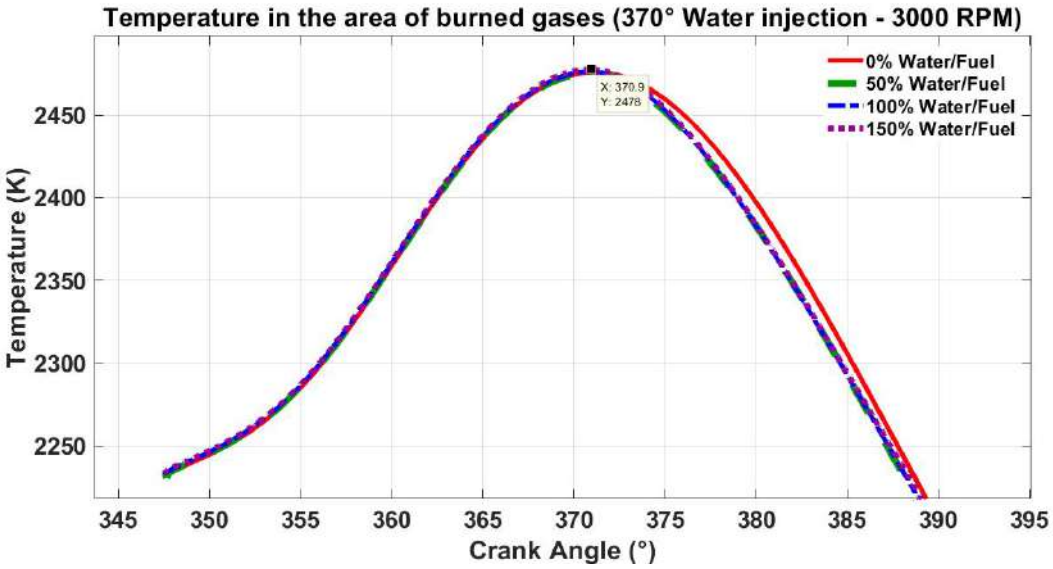

Fig. A.45 – Temperature 370° Burned zone 3000 RPM. Detail (2).

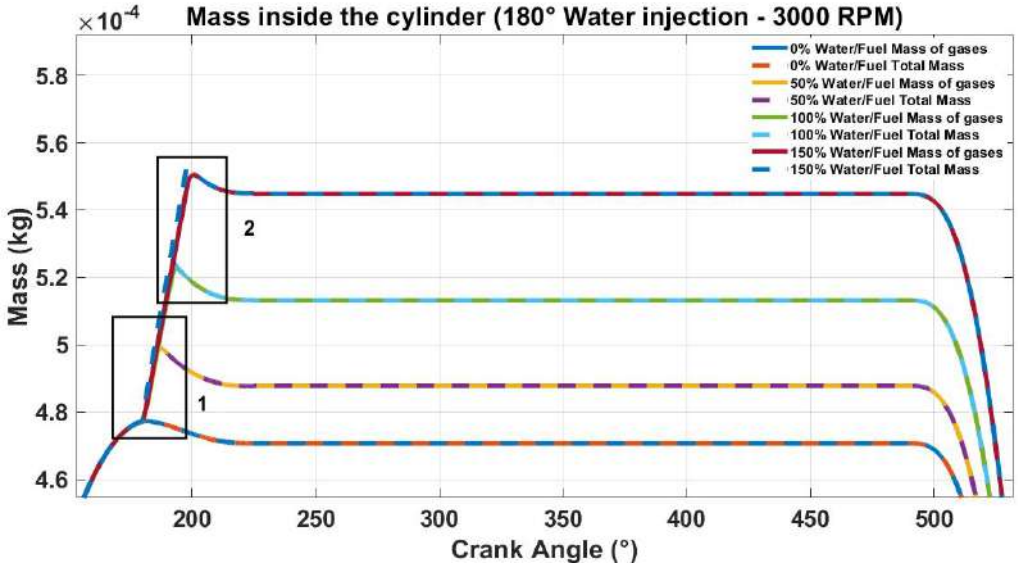

Fig. A.46 – Mass In-Cylinder 180° 3000 RPM.

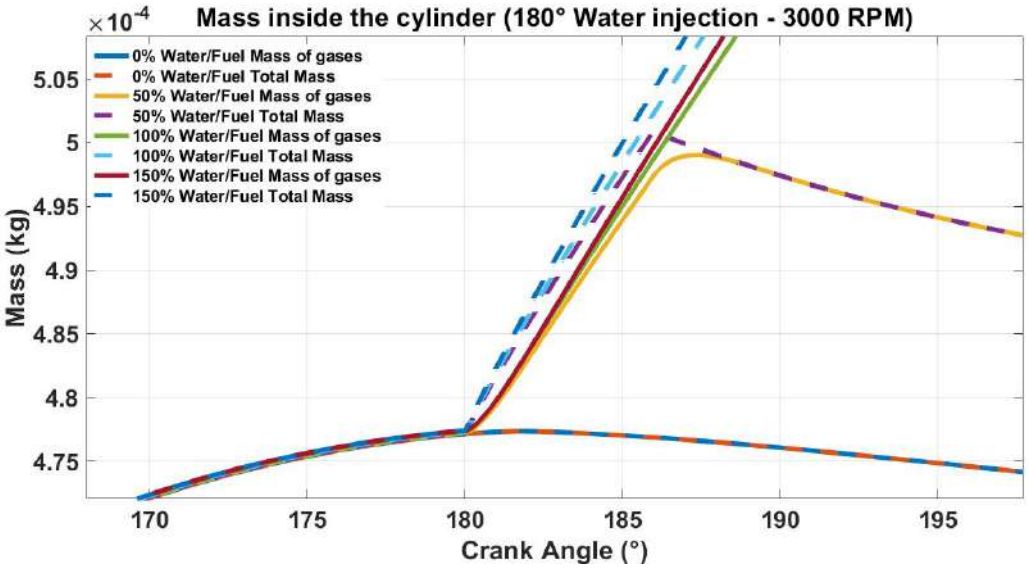

Fig. A.47 – Mass In-Cylinder 180° 3000 RPM. Detail (1)

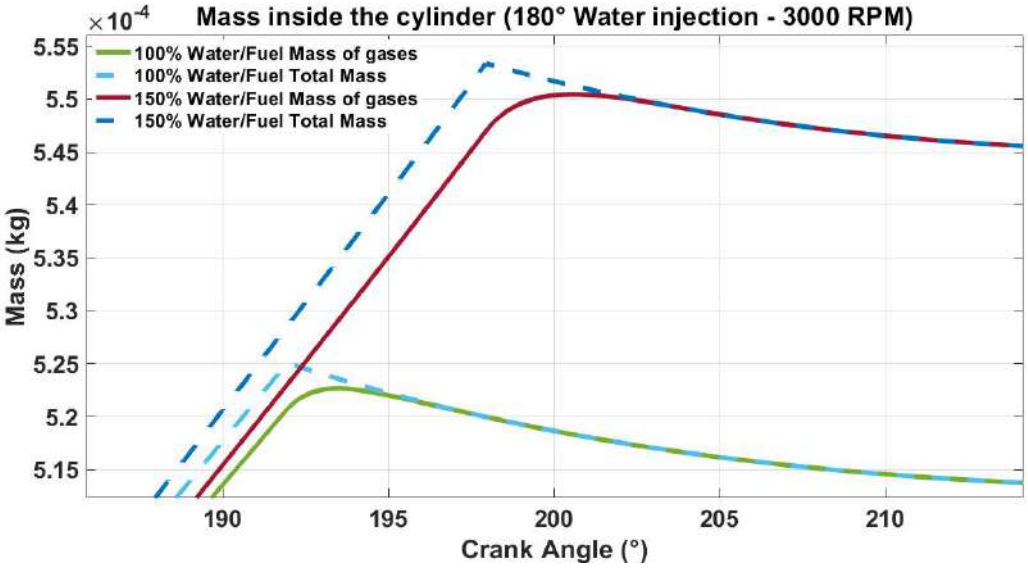

Fig. A.48 – Mass In-Cylinder 180° 3000 RPM. Detail (2)

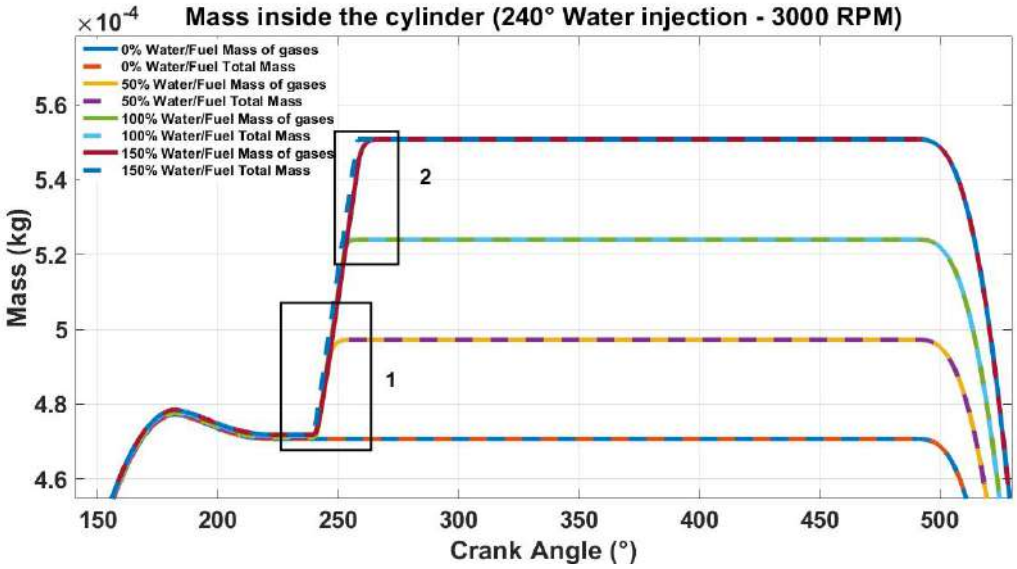

Fig. A.49 – Mass In-Cylinder 240° 3000 RPM.

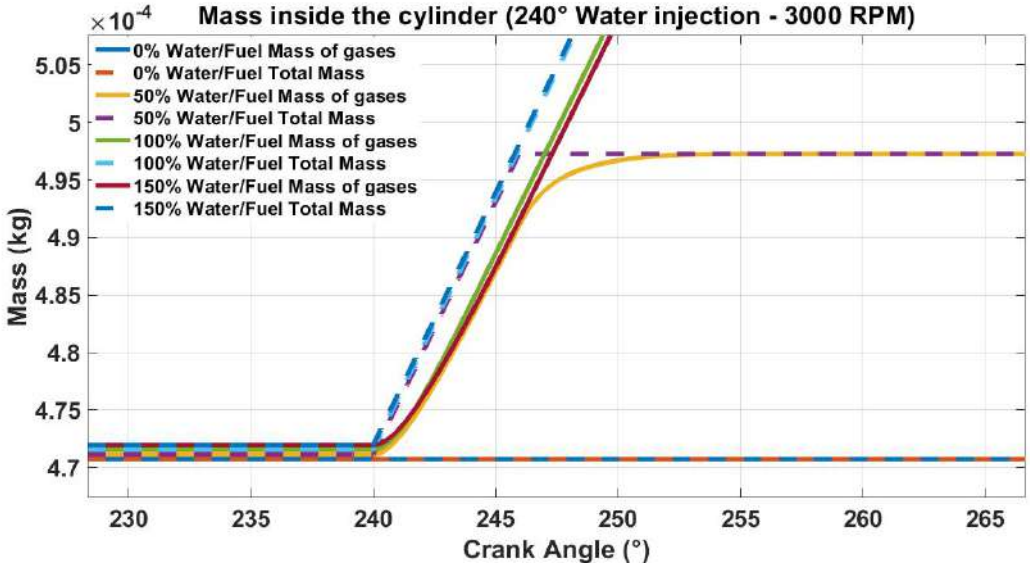

Fig. A.50 – Mass In-Cylinder 240° 3000 RPM. Detail (1)

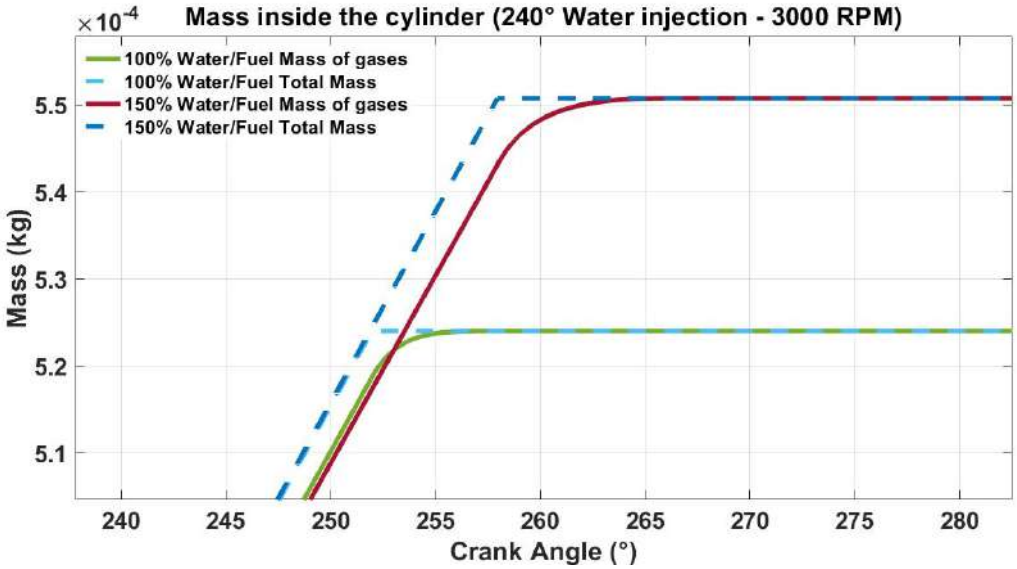

Fig. A.51 – Mass In-Cylinder 240° 3000 RPM. Detail (2)

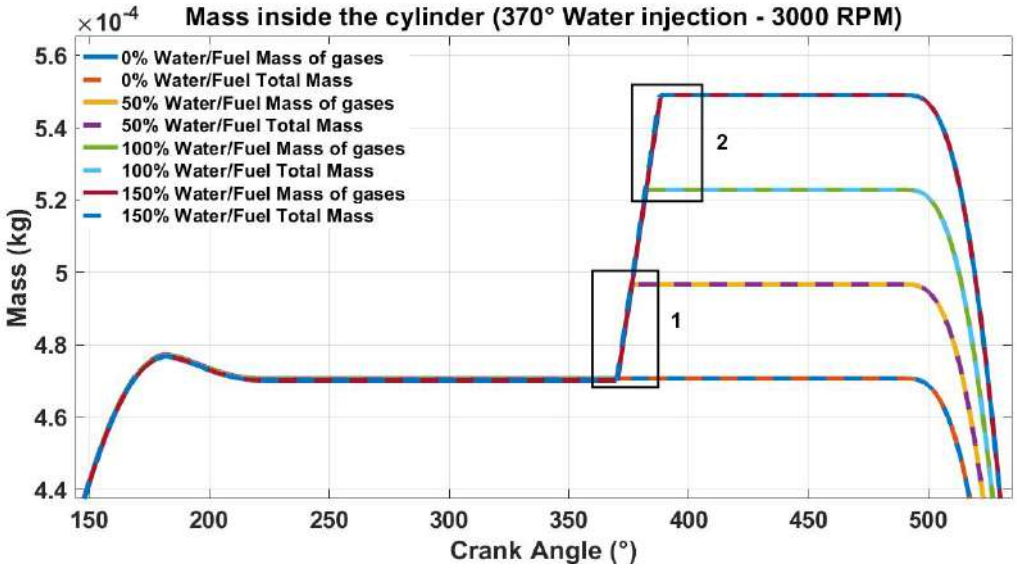

Fig. A.52 – Mass In-Cylinder 370° 3000 RPM.

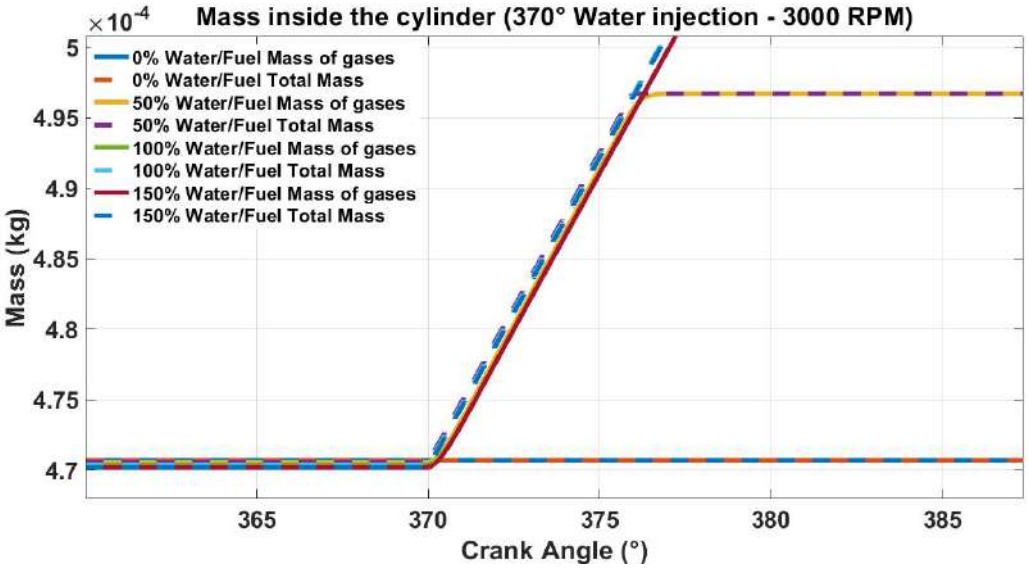

Fig. A.53 – Mass In-Cylinder 370° 3000 RPM. Detail (1)

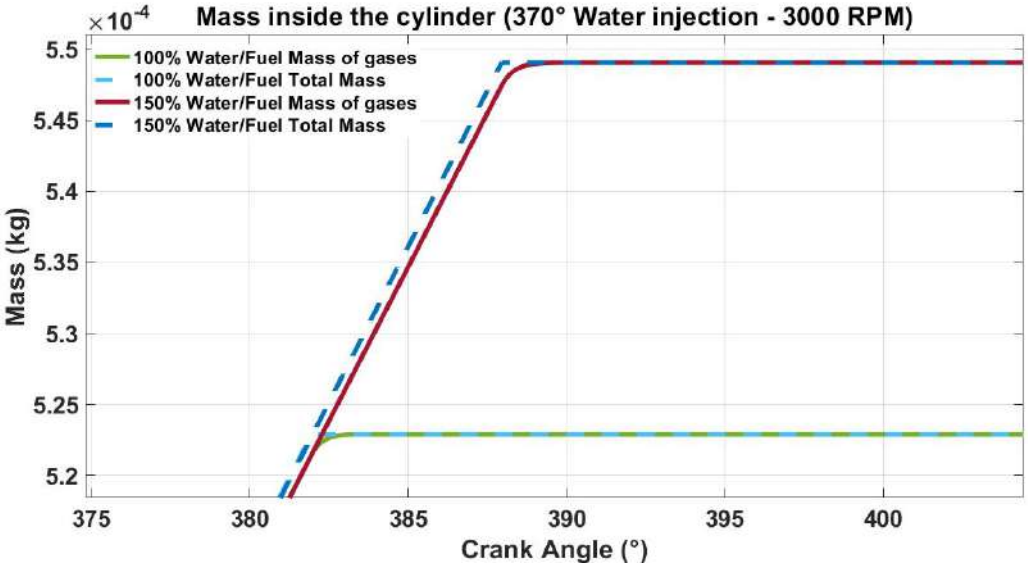

Fig. A.54 – Mass In-Cylinder 370° 3000 RPM. Detail (2)

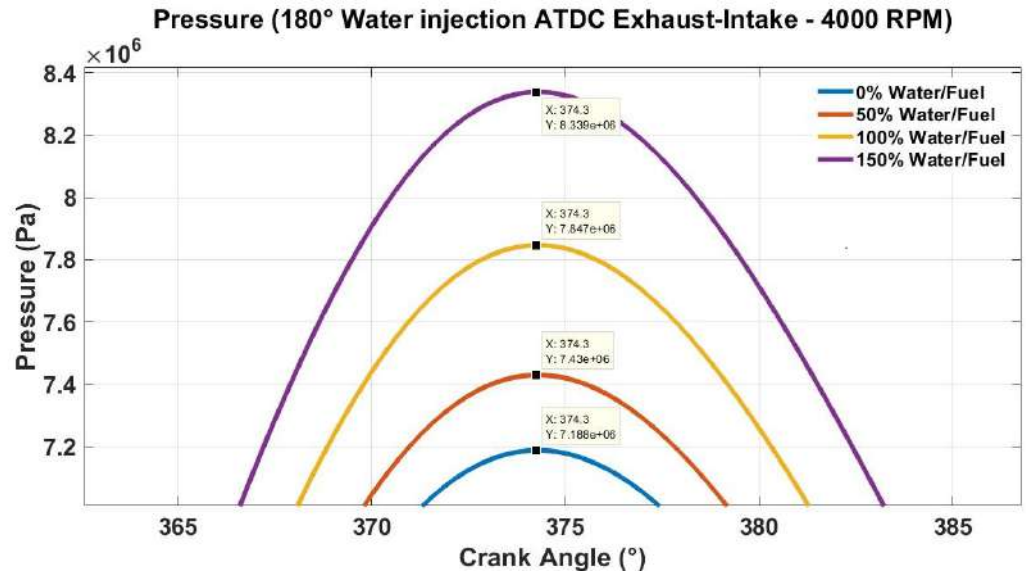

Fig. A.55 – Pressure 180° 4000 RPM.

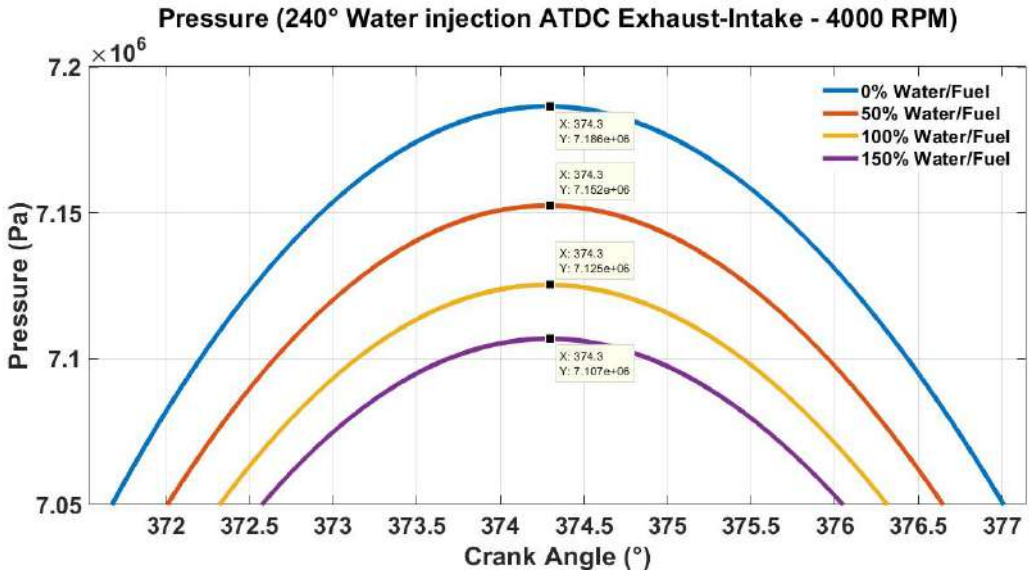

Fig. A.56 – Pressure 240° 4000 RPM.

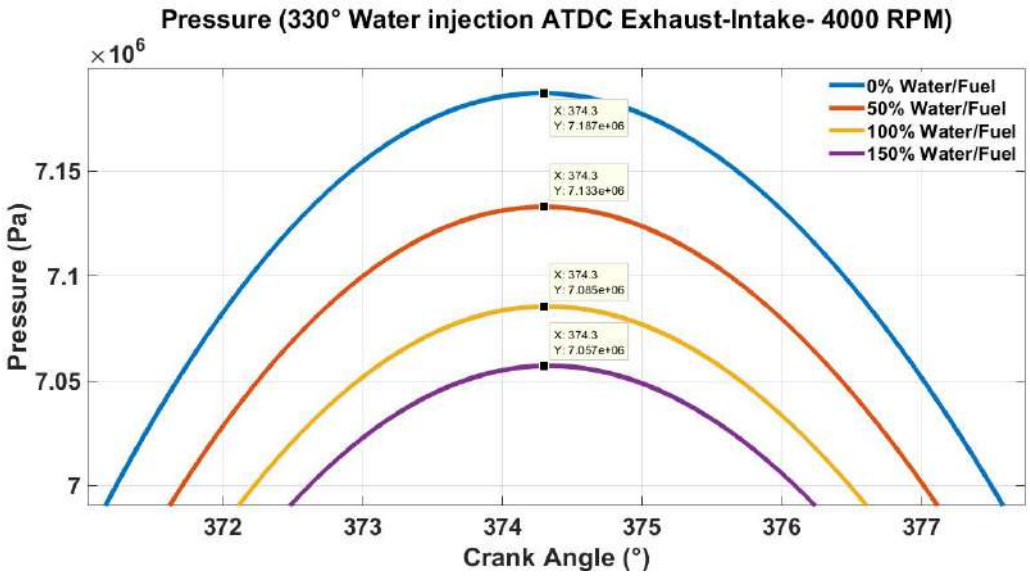

Fig. A.57 – Pressure 330° 4000 RPM.

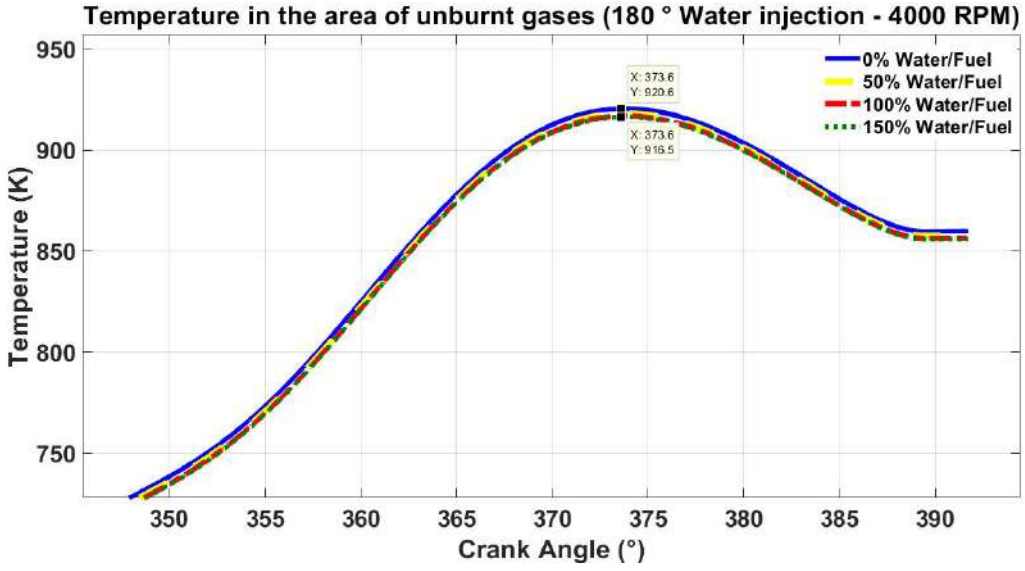

Fig. A.58 – Temperature 180° Unburned zone 4000 RPM. Detail (1).

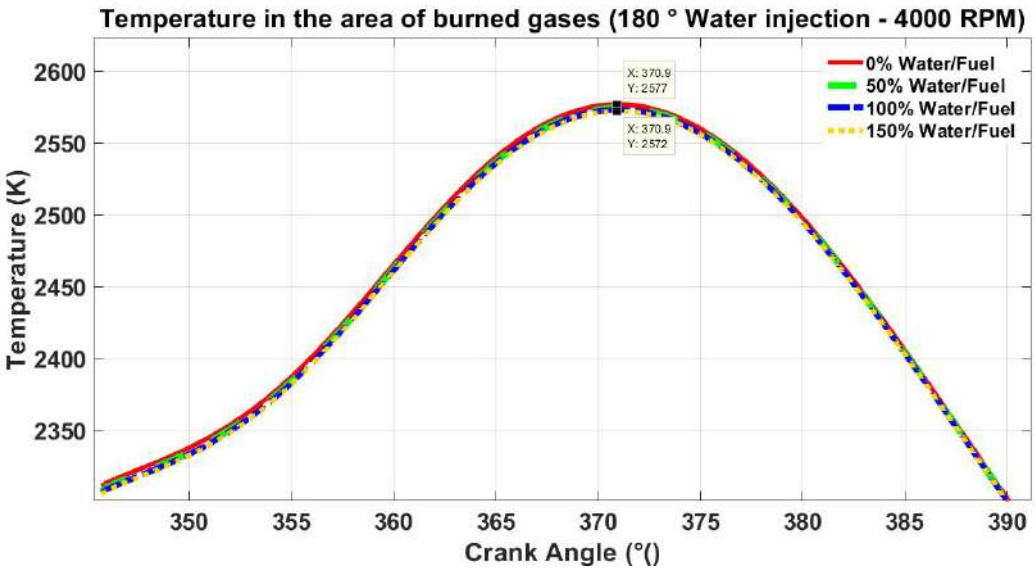

Fig. A.59 – Temperature 180° Burned zone 4000 RPM. Detail (2).

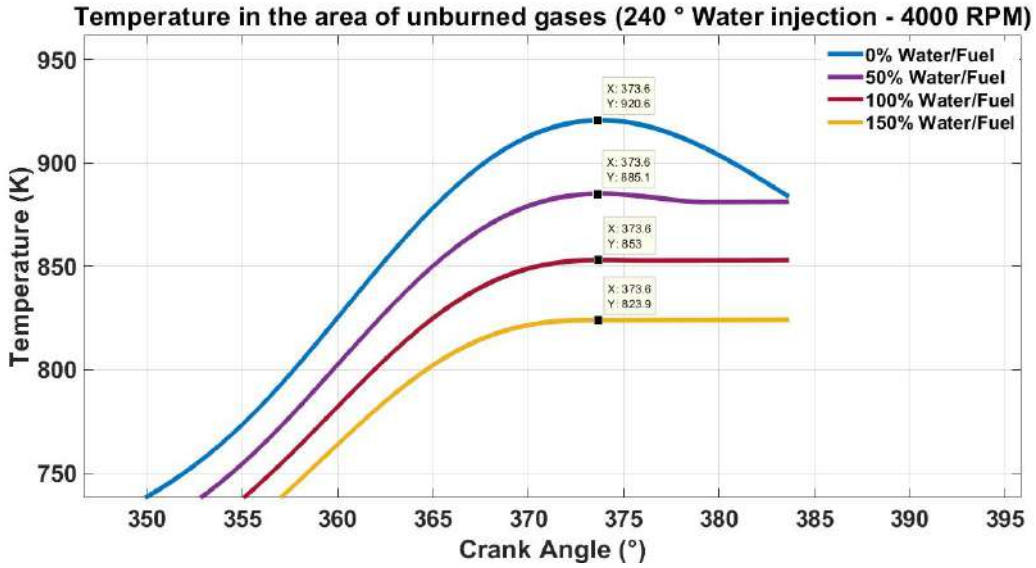

Fig. A.60 – Temperature 240° Unburned zone 4000 RPM. Detail (1).

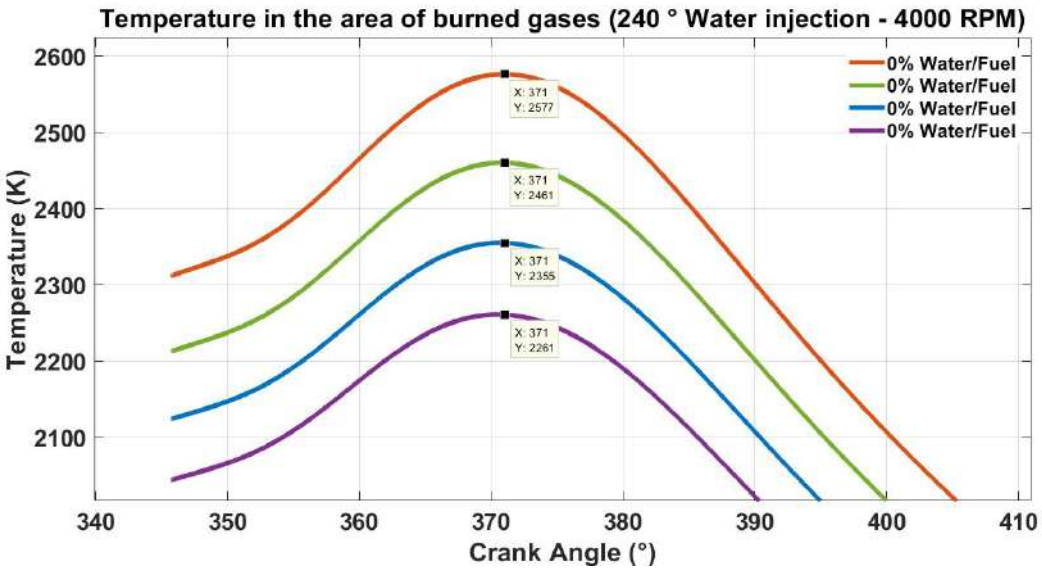

Fig. A.61 – Temperature 240° Burned zone 4000 RPM. Detail (2).

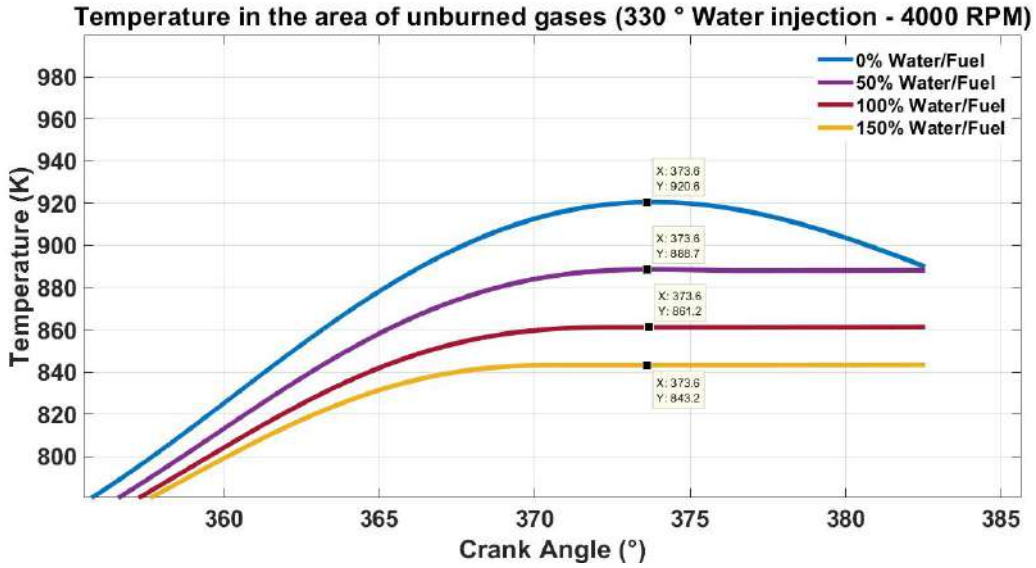

Fig. A.62 – Temperature 330° Unburned zone 4000 RPM. Detail (1).

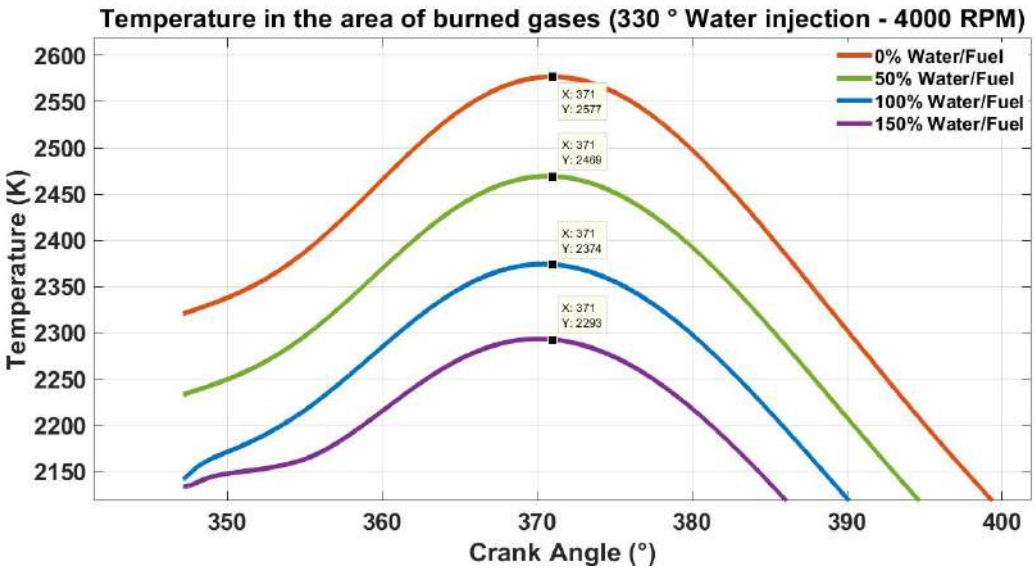

Fig. A.63 – Temperature 330° Burned zone 4000 RPM. Detail (2).

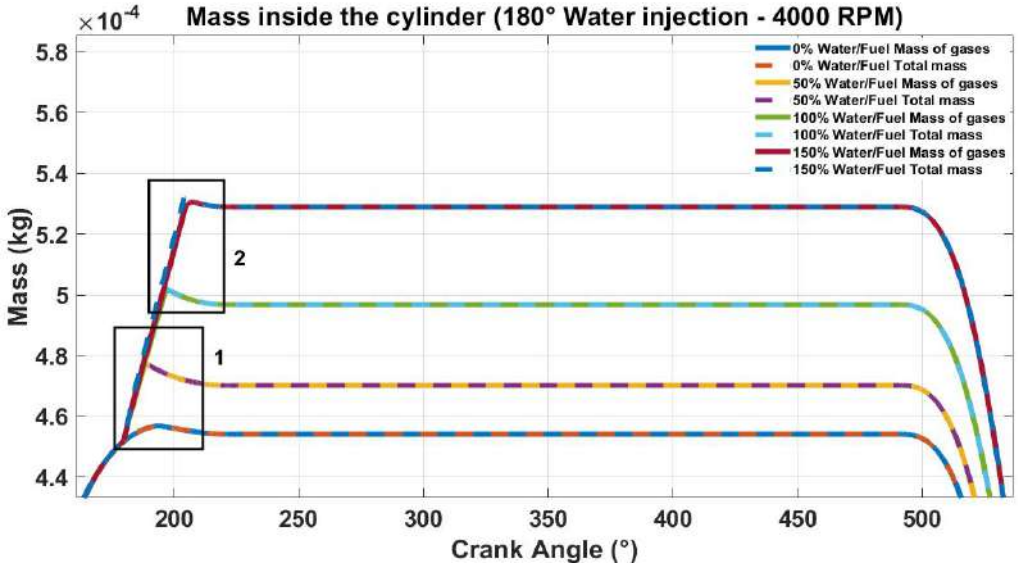

Fig. A.64 – Mass In-Cylinder 180° 4000 RPM.

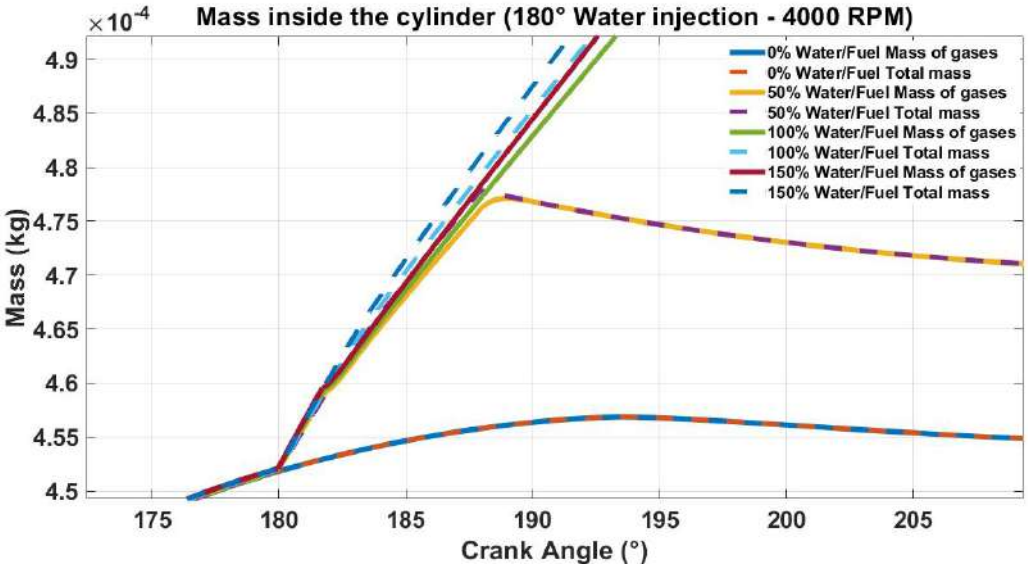

Fig. A.65 – Mass In-Cylinder 180° 4000 RPM. Detail (1)

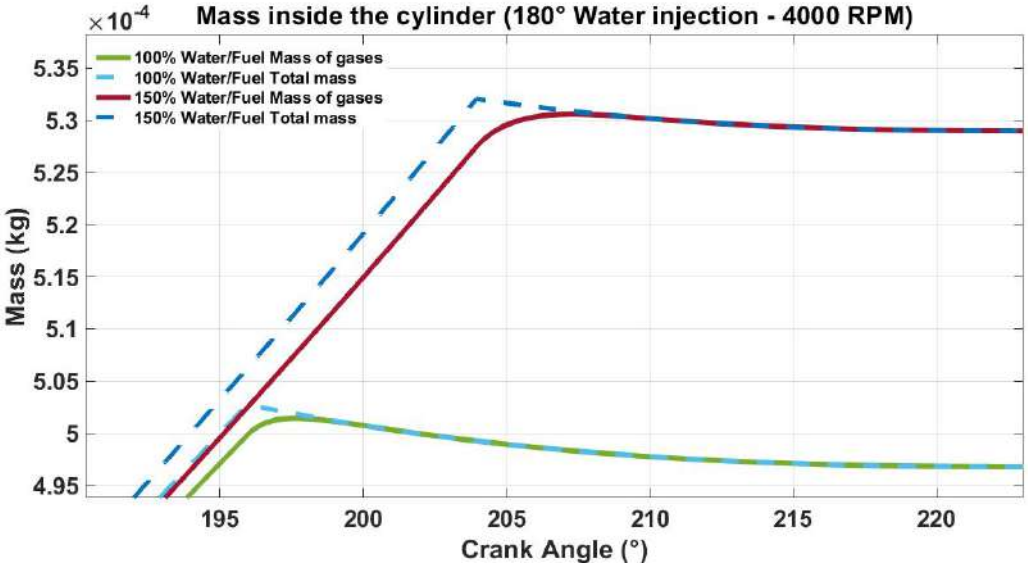

Fig. A.66 – Mass In-Cylinder 180° 4000 RPM. Detail (2).

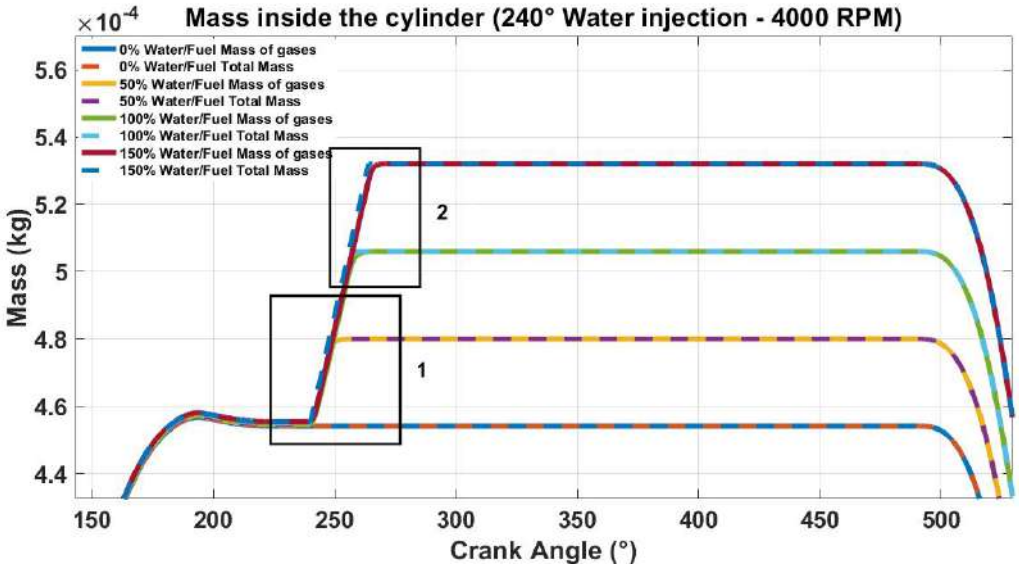

Fig. A.67 – Mass In-Cylinder 240° 4000 RPM.

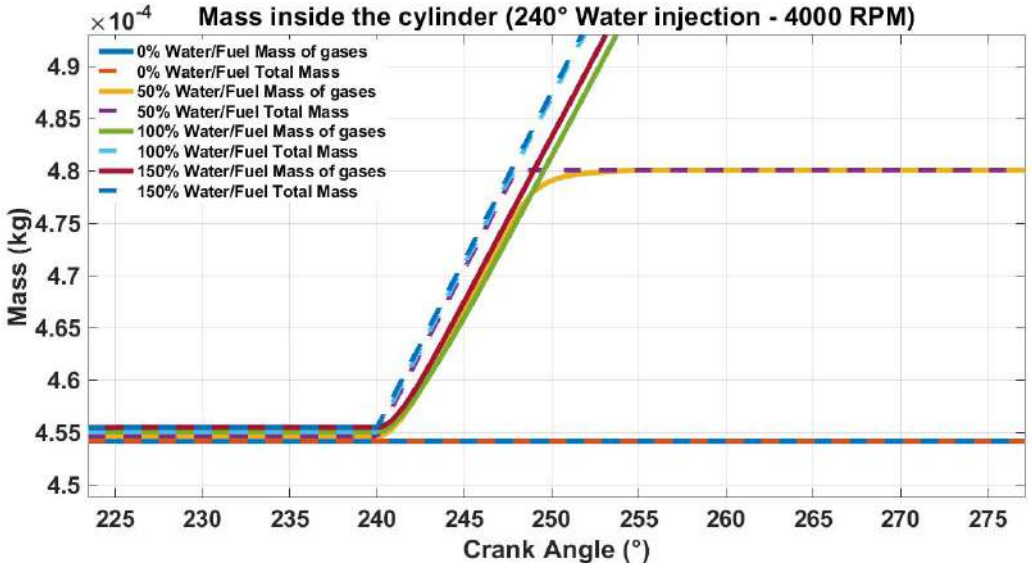

Fig. A.68 – Mass In-Cylinder 240° 4000 RPM. Detail (1).

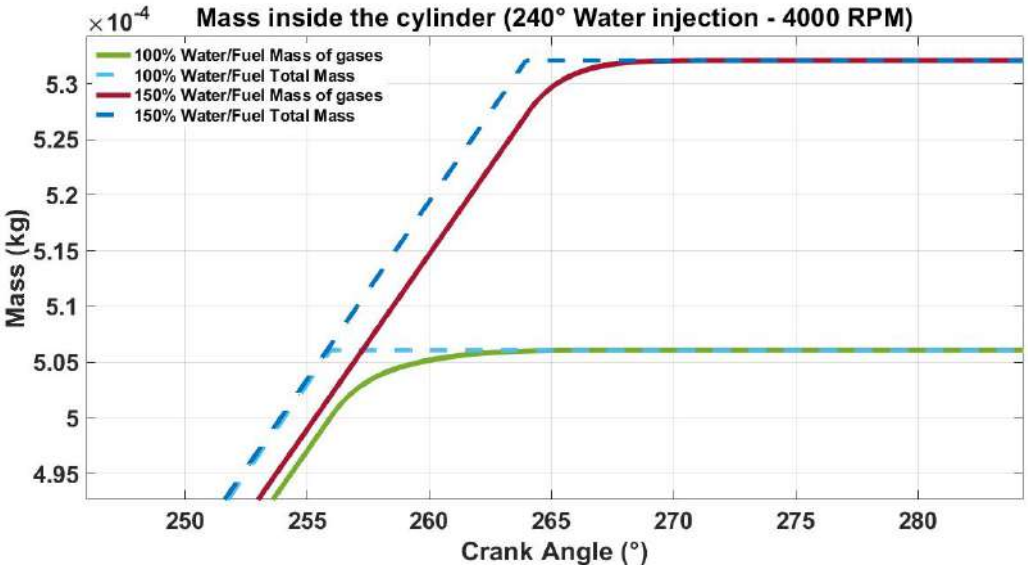

Fig. A.69 – Mass In-Cylinder 240° 4000 RPM. Detail (2).

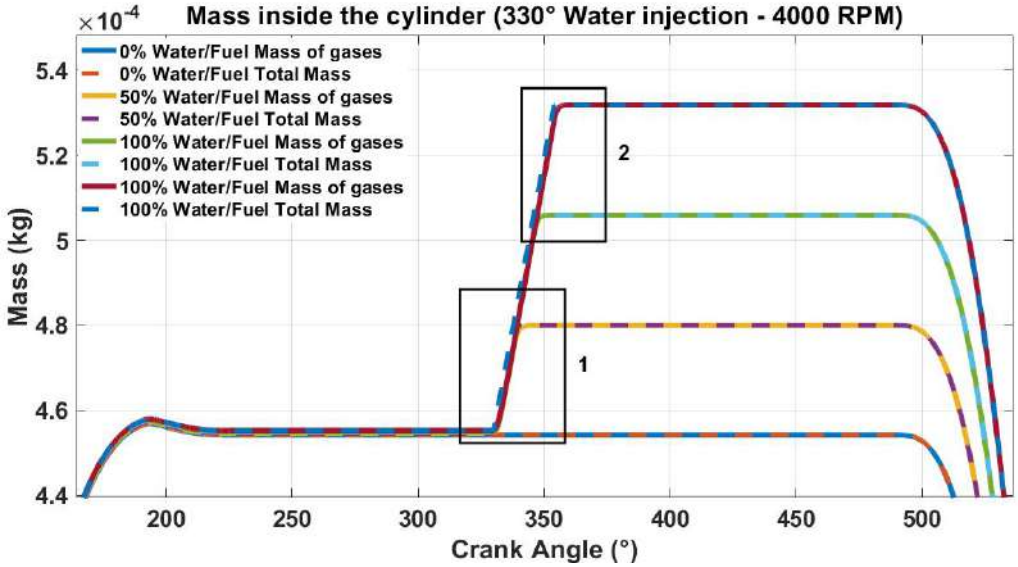

Fig. A.70 – Mass In-Cylinder 330° 4000 RPM.

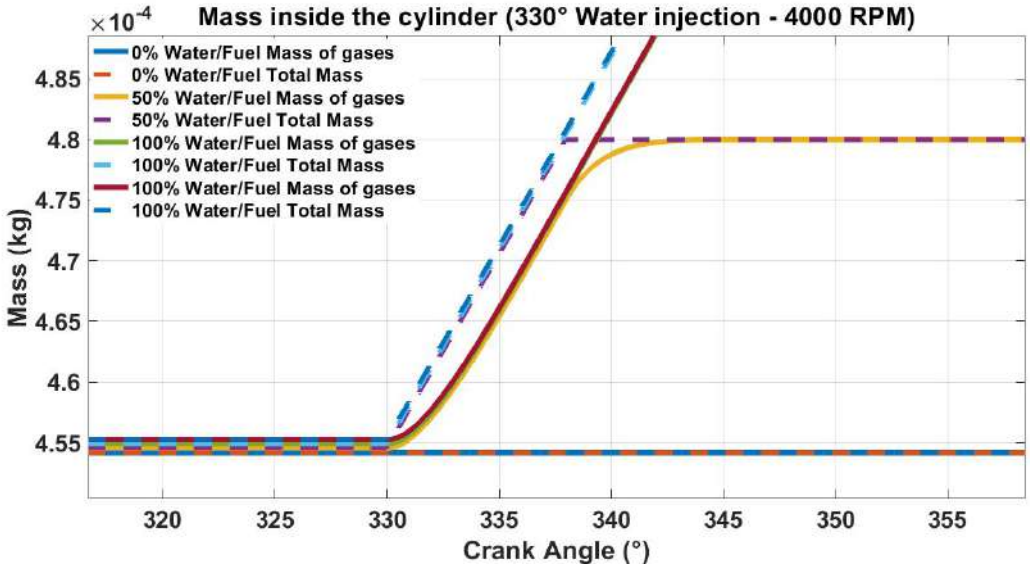

Fig. A.71 – Mass In-Cylinder 330° 4000 RPM. Detail (1).

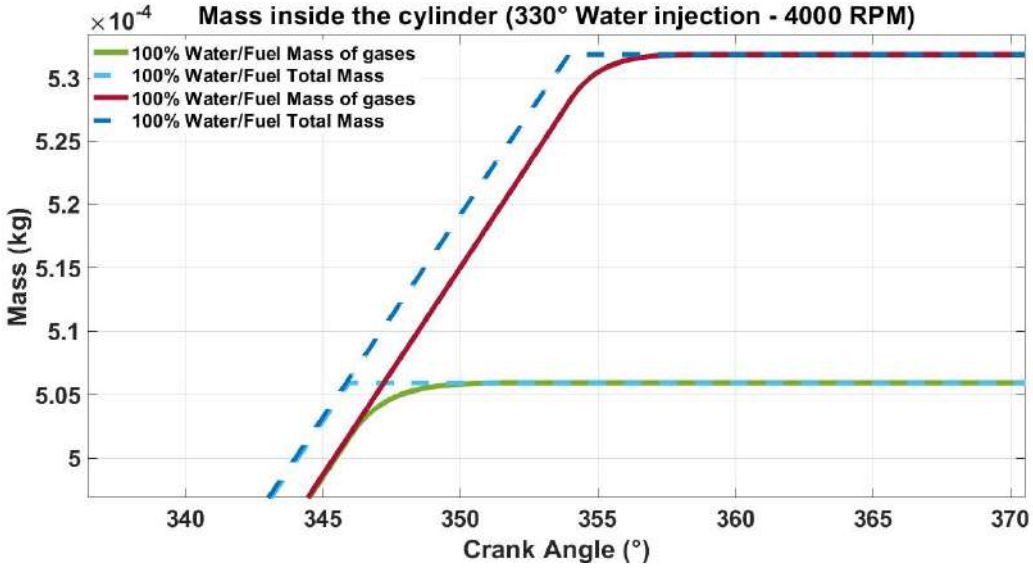

Fig. A.72 – Mass In-Cylinder 330° 4000 RPM. Detail (2).

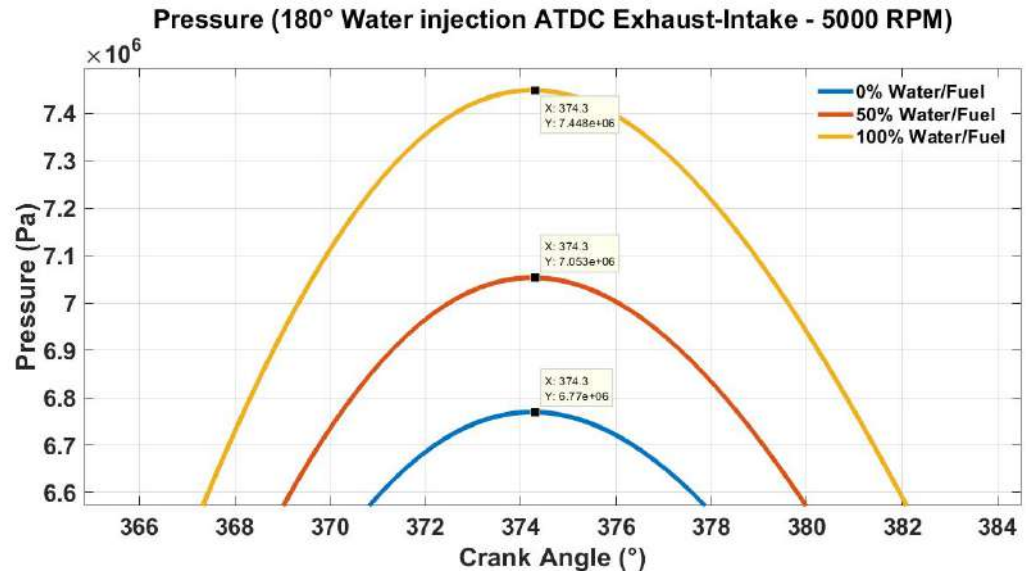

Fig. A.73 – Pressure 180° 5000 RPM

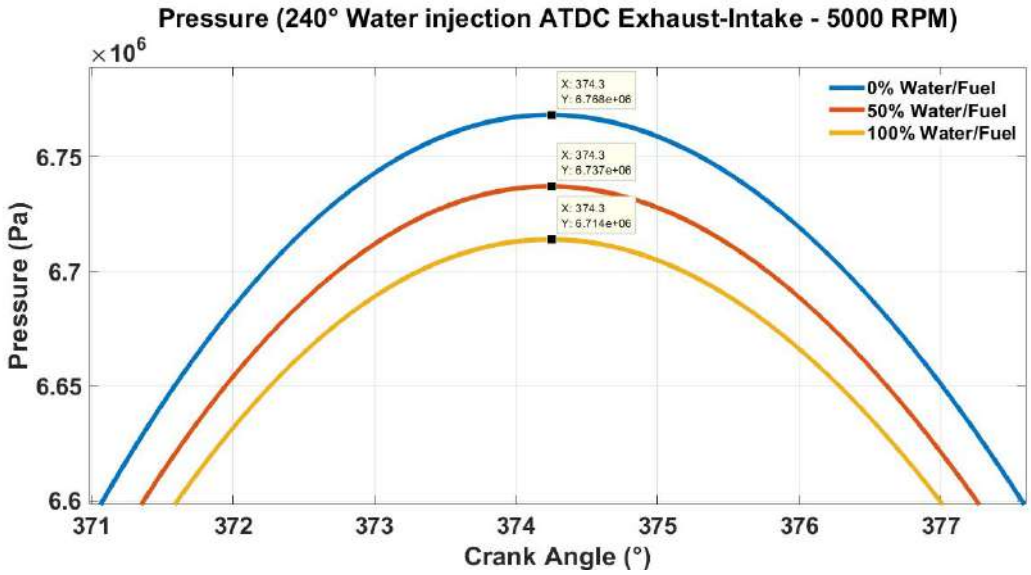

Fig. A.74 – Pressure 240° 5000 RPM.

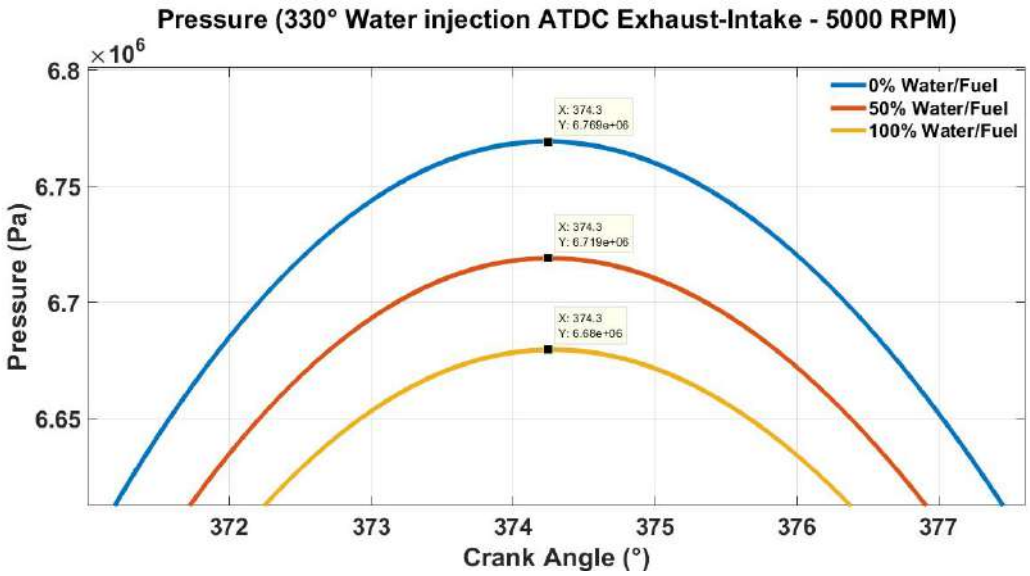

Fig. A.75 – Pressure 330° 5000 RPM.

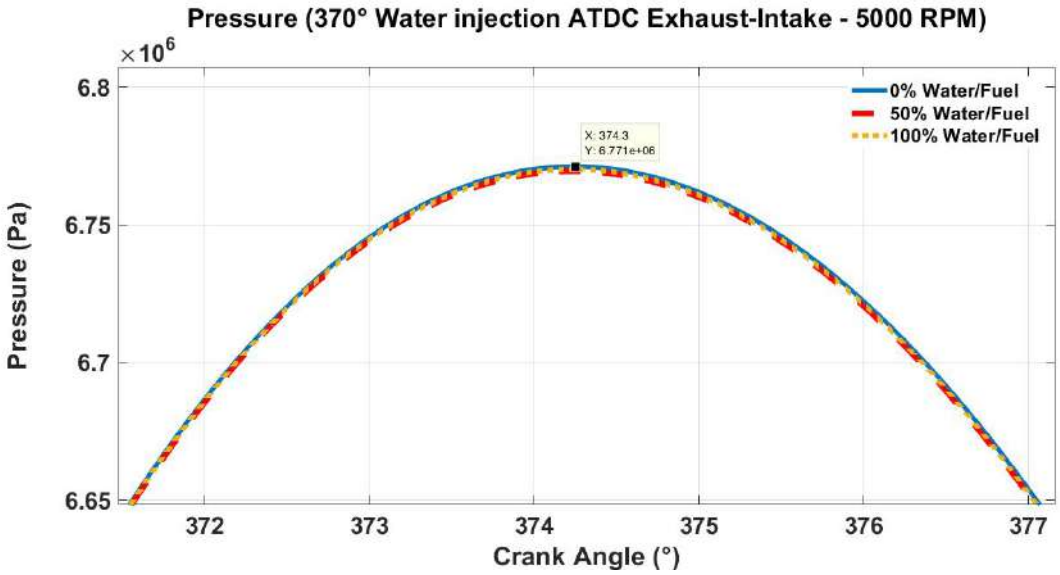

Fig. A.76 – Pressure 370° 5000 RPM.

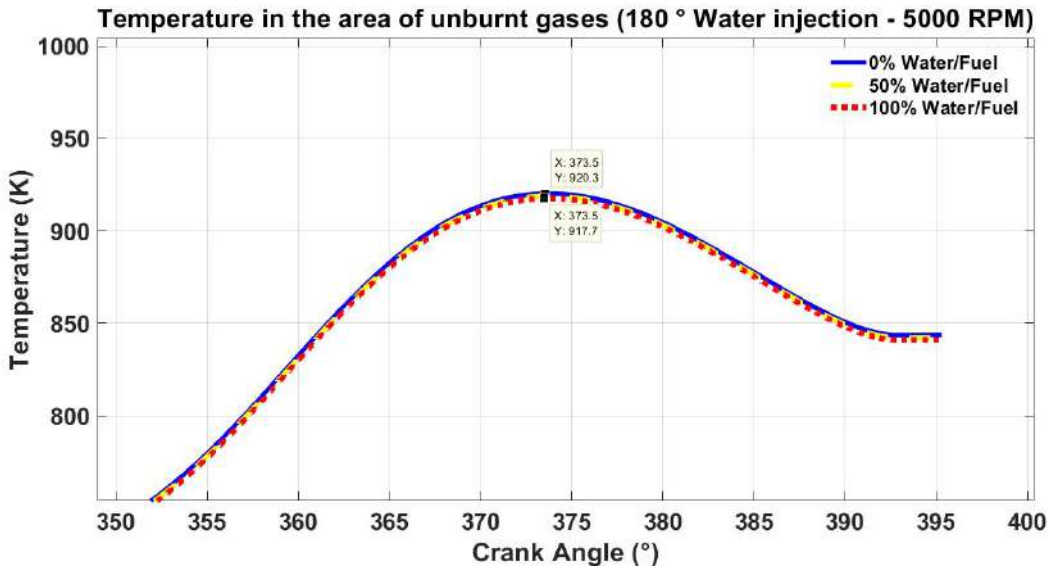

Fig. A.77 – Temperature 180° Unburned zone 5000 RPM. Detail (1).

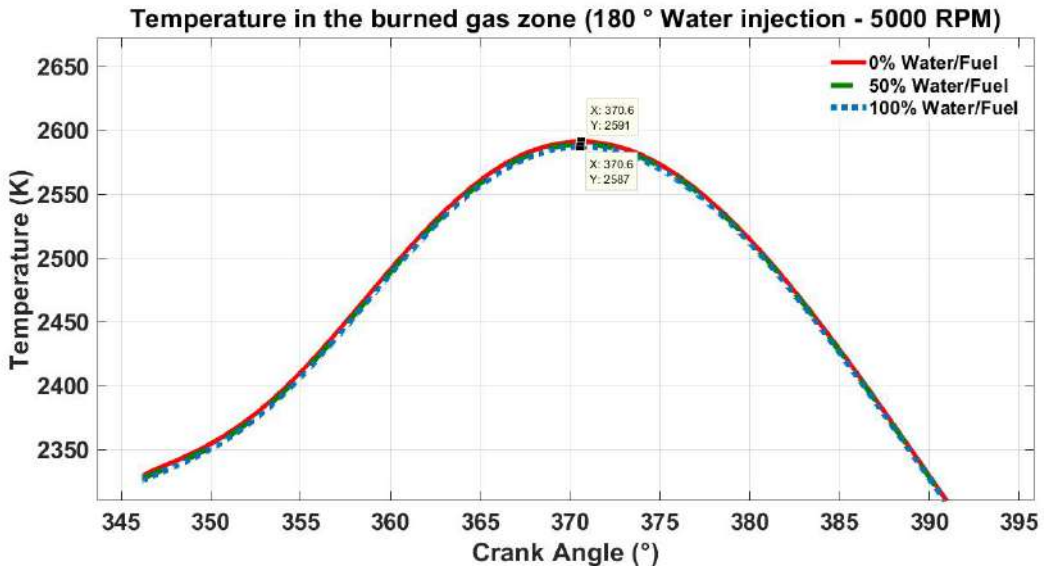

Fig. A.78 – Temperature 180° Burned zone 5000 RPM. Detail (2).

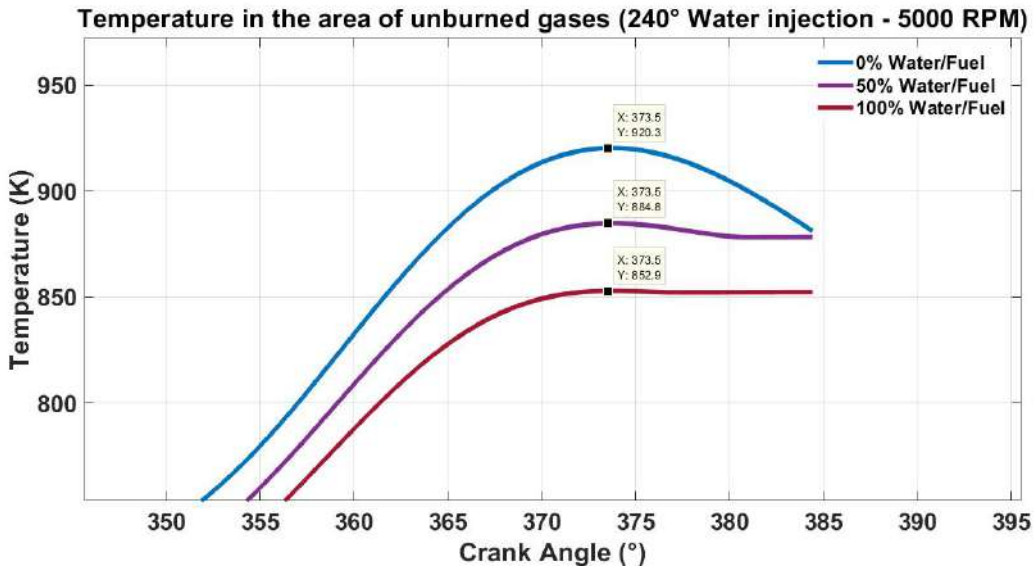

Fig. A.79 – Temperature 240° Unburned zone 5000 RPM. Detail (1).

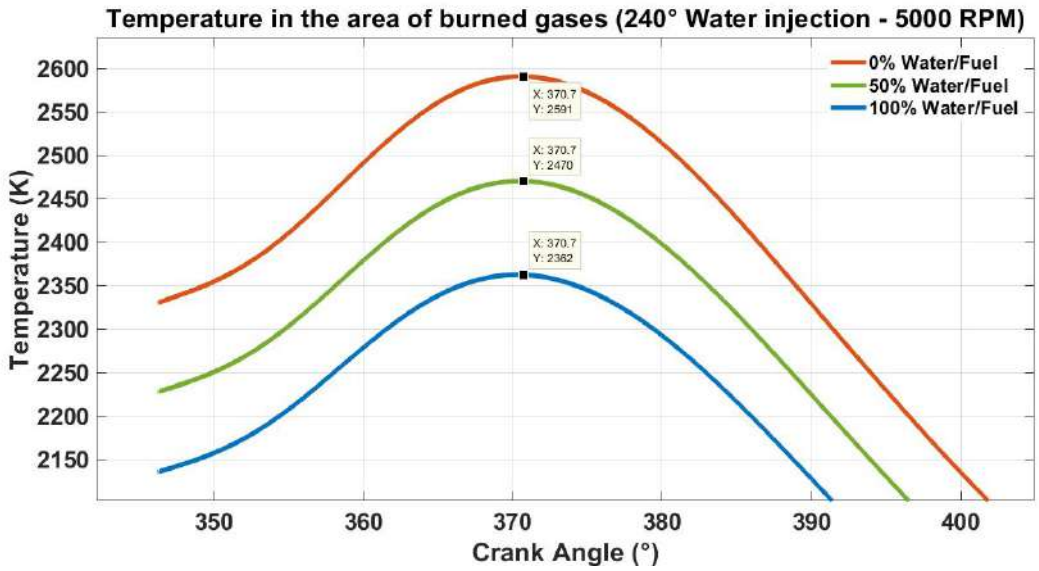

Fig. A.80 – Temperature 240° Burned zone 5000 RPM. Detail (2).

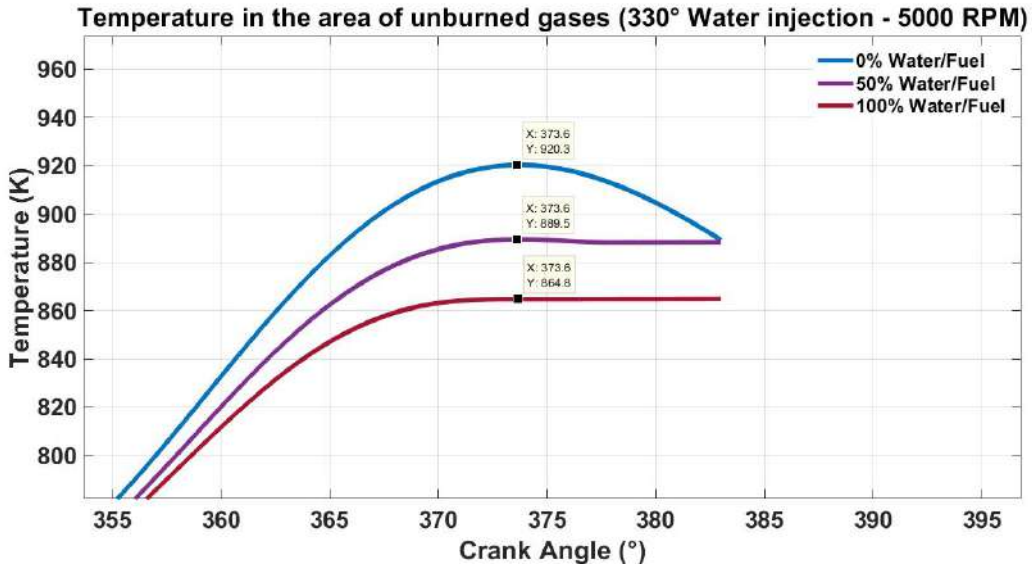

Fig. A.81 – Temperature 330° Unburned zone 5000 RPM. Detail (1).

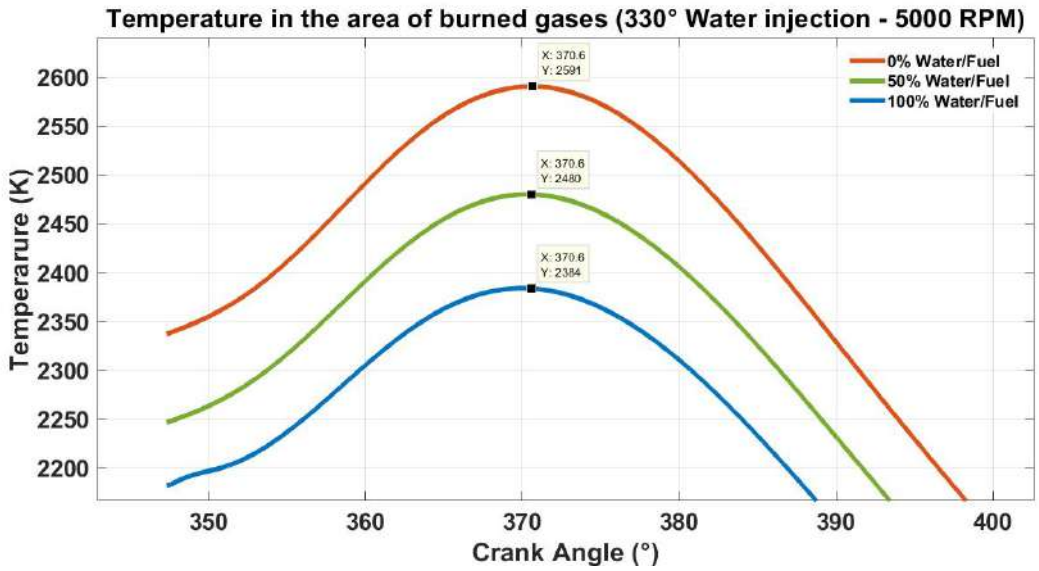

Fig. A.82 – Temperature 330° Burned zone 5000 RPM. Detail (2).

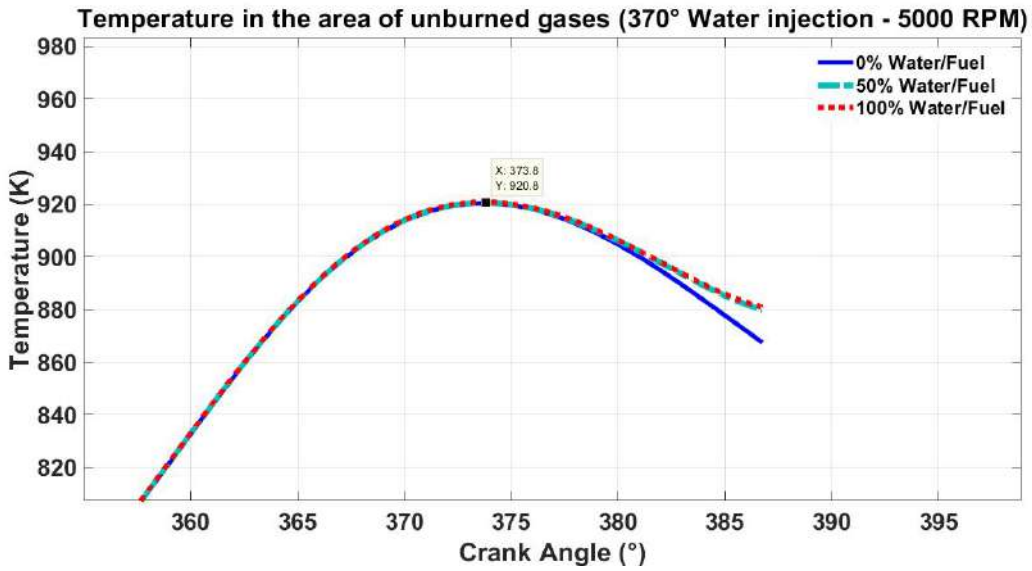

Fig. A.83 – Temperature 370° Unburned zone 5000 RPM. Detail (1).

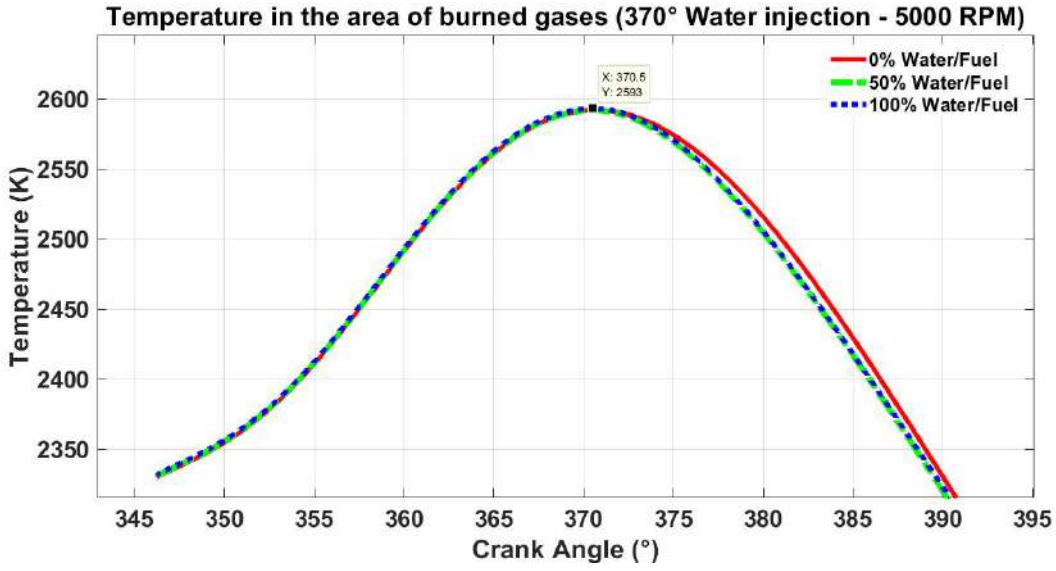

Fig. A.84 – Temperature 370° Burned zone 5000 RPM. Detail (2).

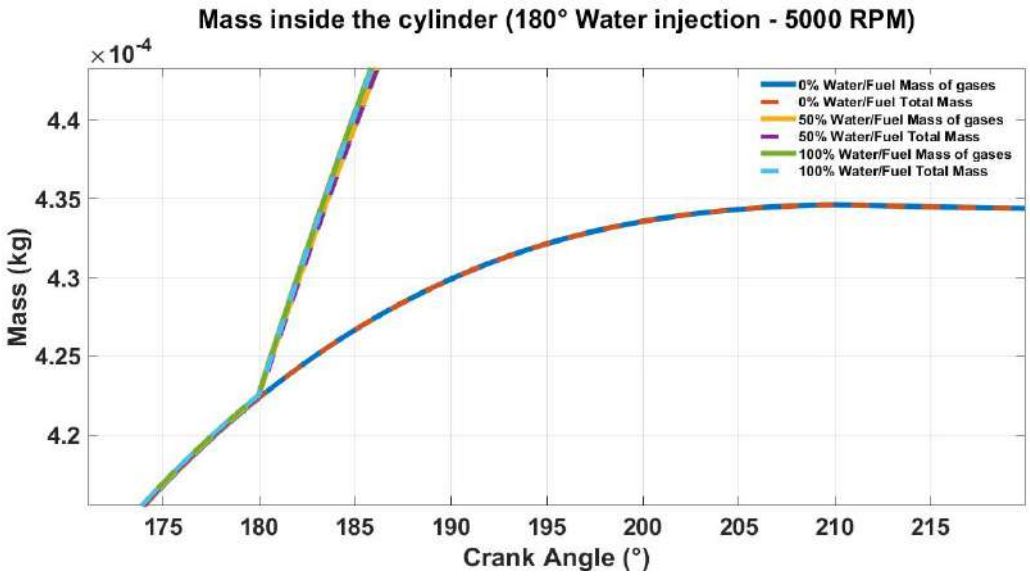

Fig. A.85 – Mass In-Cylinder 180° 5000 RPM. Detail (1).

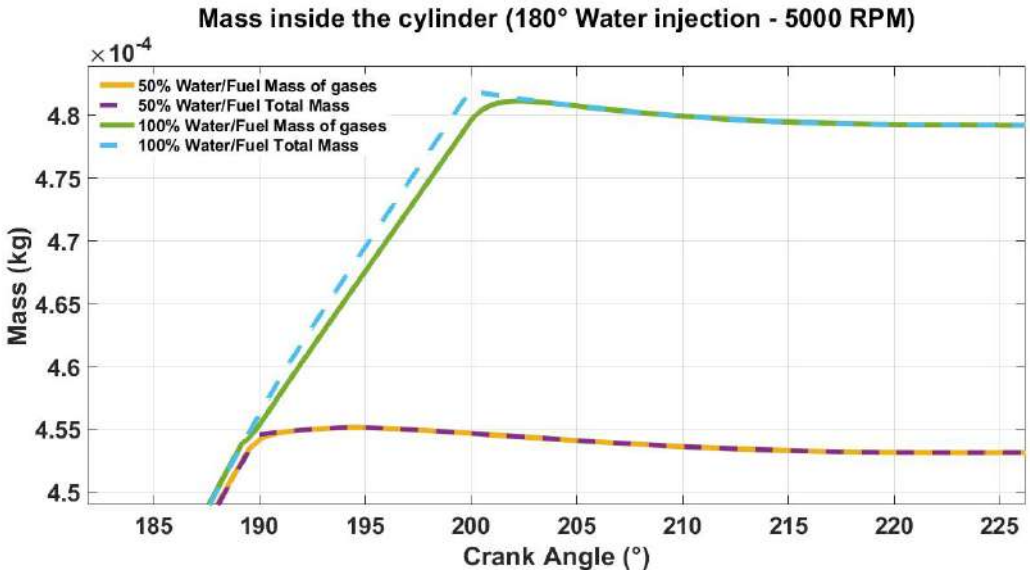

Fig. A.86 – Mass In-Cylinder 180° 5000 RPM. Detail (2).

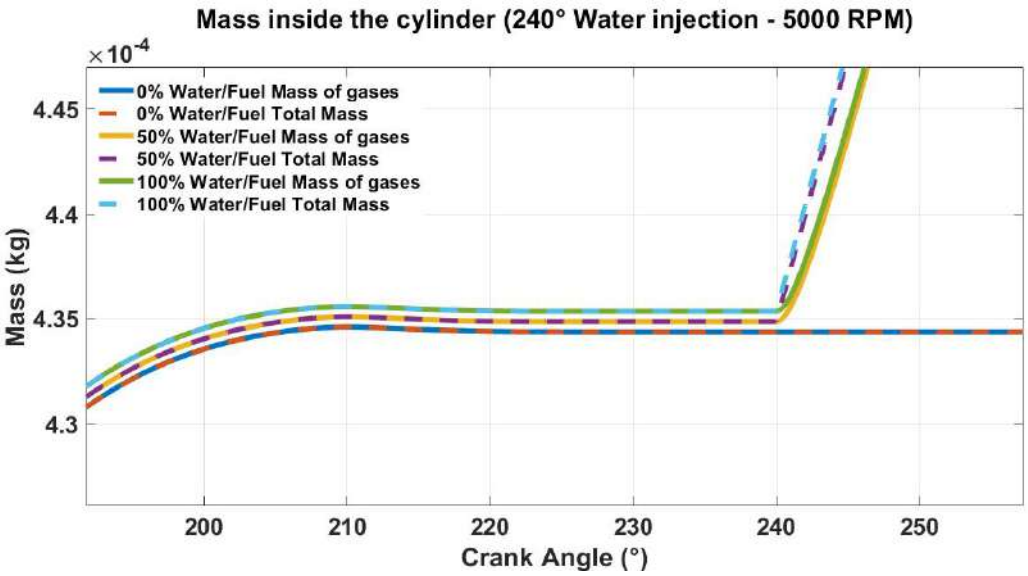

Fig. A.87 – Mass In-Cylinder 240° 5000 RPM. Detail (1).

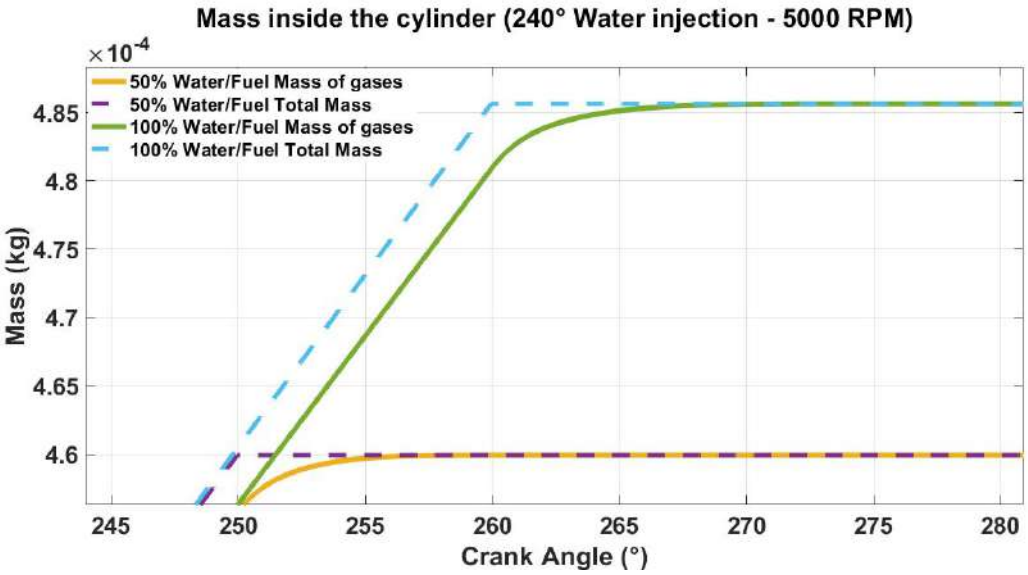

Fig. A.88 – Mass In-Cylinder 240° 5000 RPM. Detail (2).

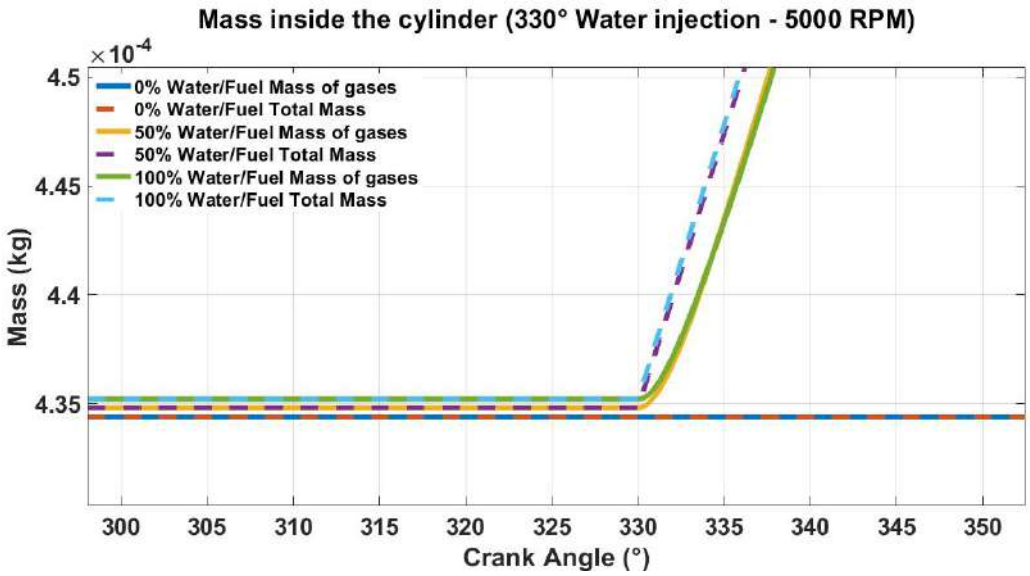

Fig. A.89 – Mass In-Cylinder 330° 5000 RPM. Detail (1).

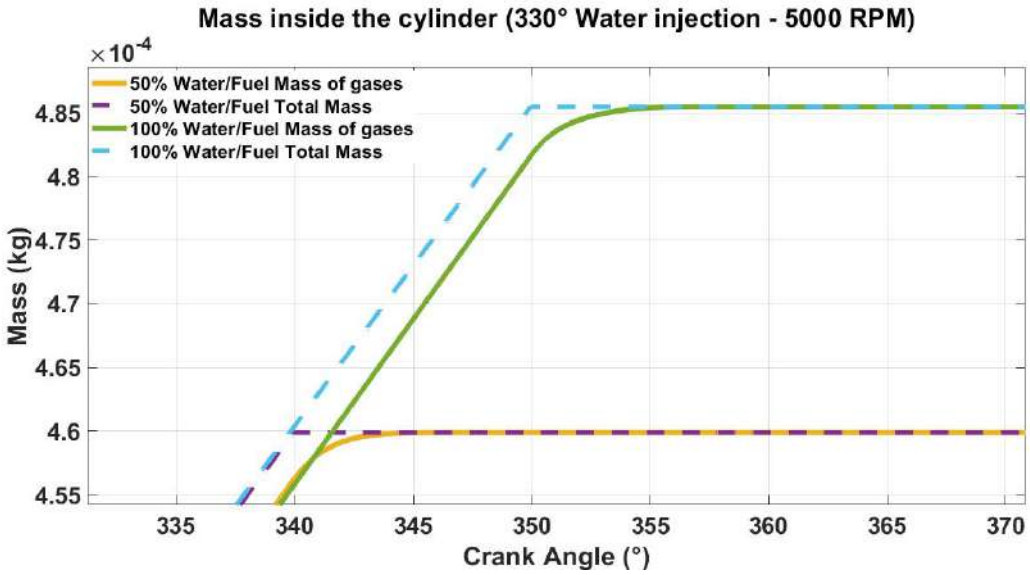

Fig. A.90 – Mass In-Cylinder 330° 5000 RPM. Detail (2).

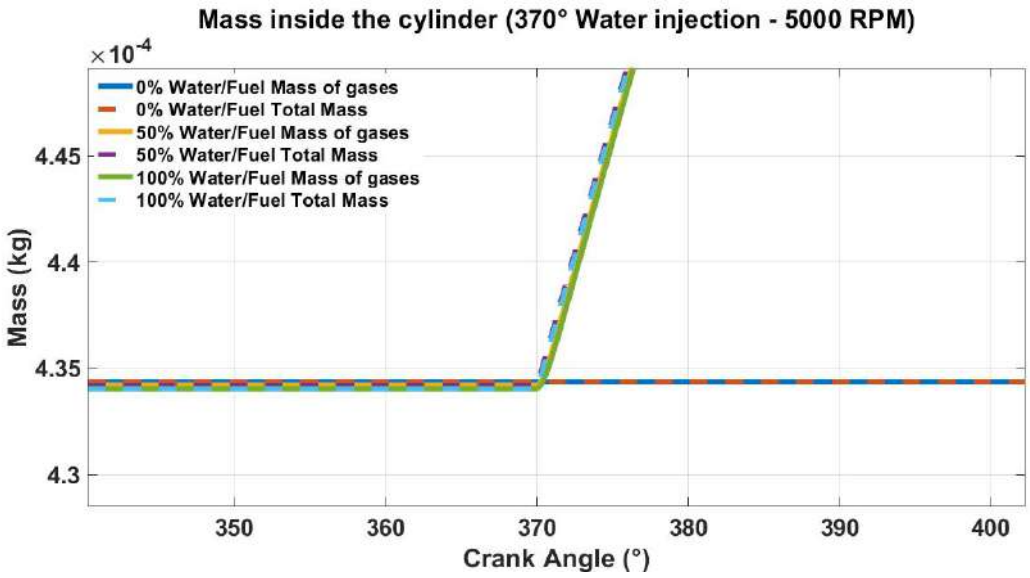

Fig. A.91 – Mass In-Cylinder 370° 5000 RPM. Detail (1).

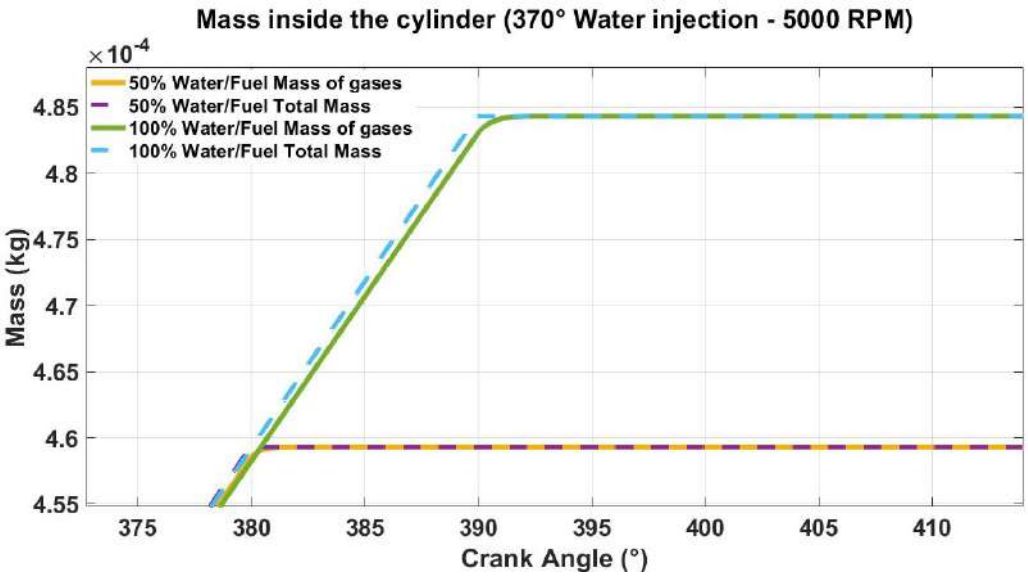

Fig. A.92 – Mass In-Cylinder 370° 5000 RPM. Detail (2).

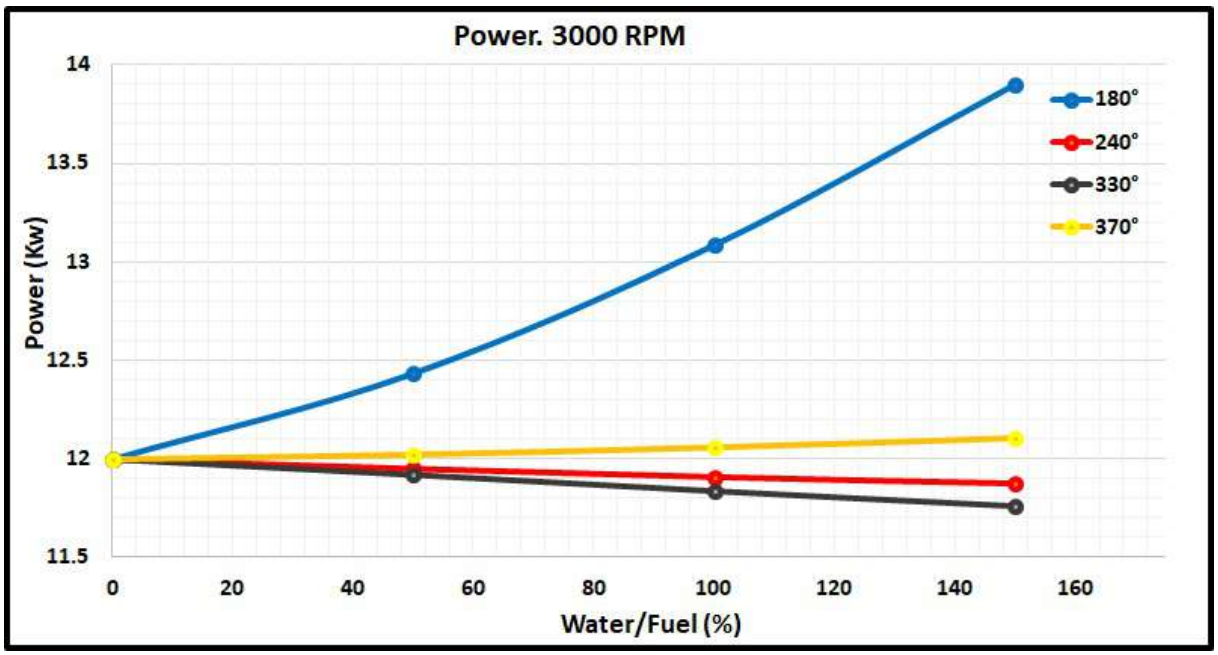

Fig. A.93 – Power 3000 RPM.

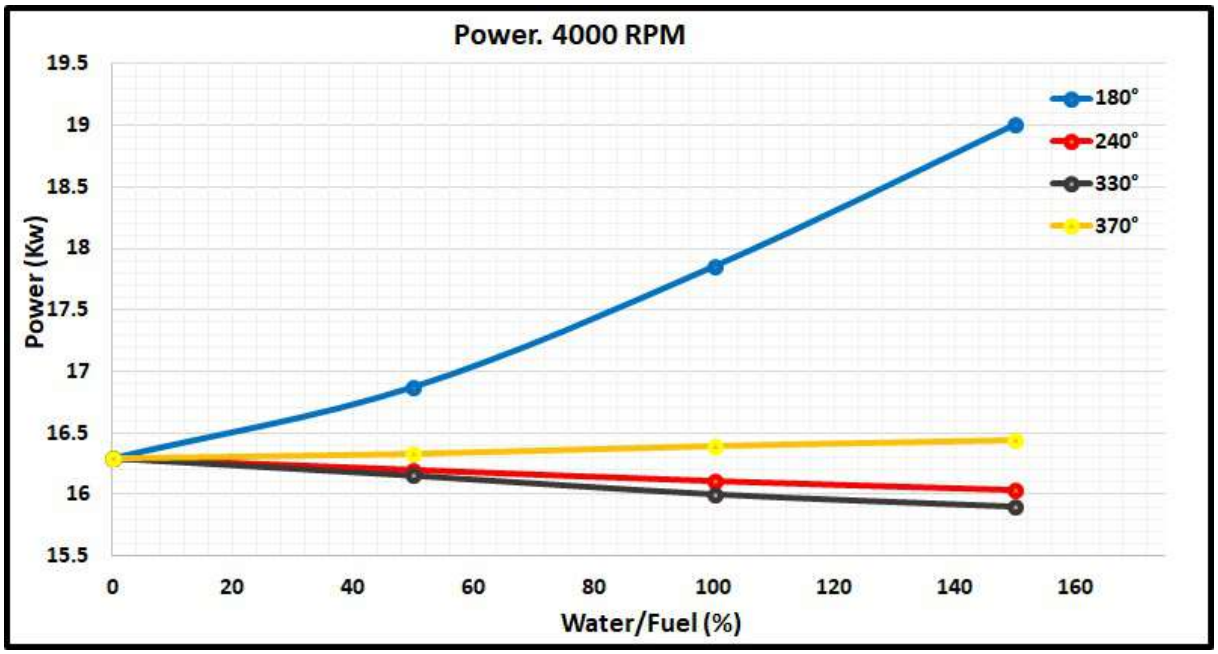

Fig. A.94 – Power 4000 RPM.

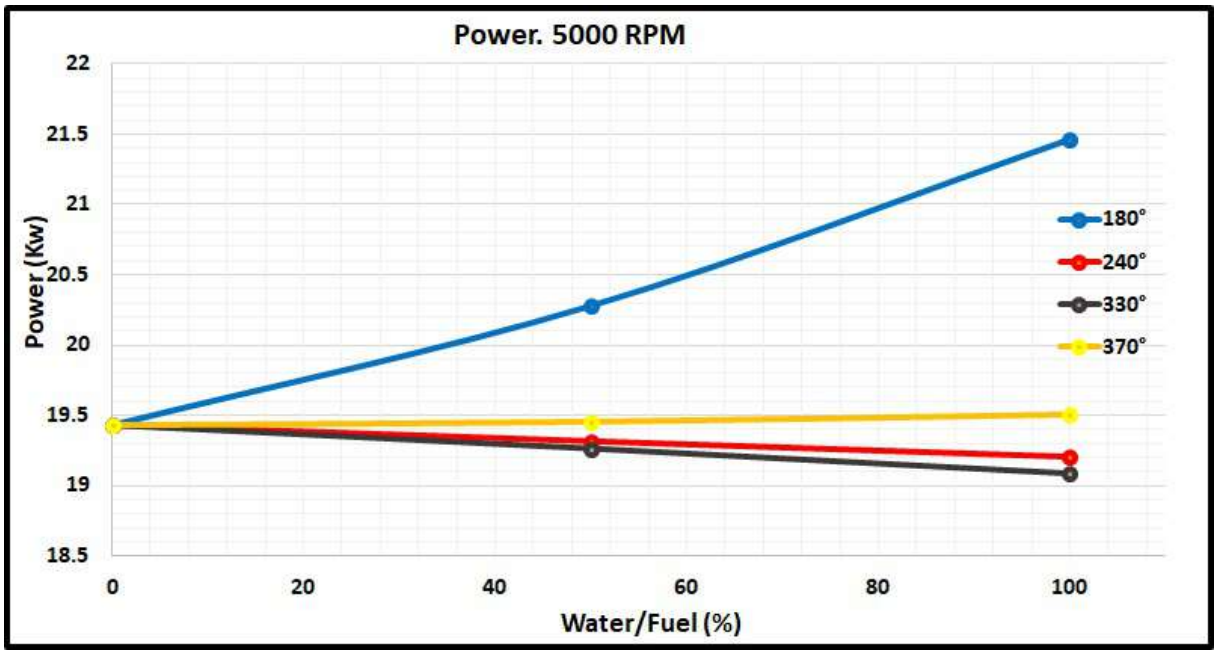

Fig. A.95 – Power 5000 RPM.

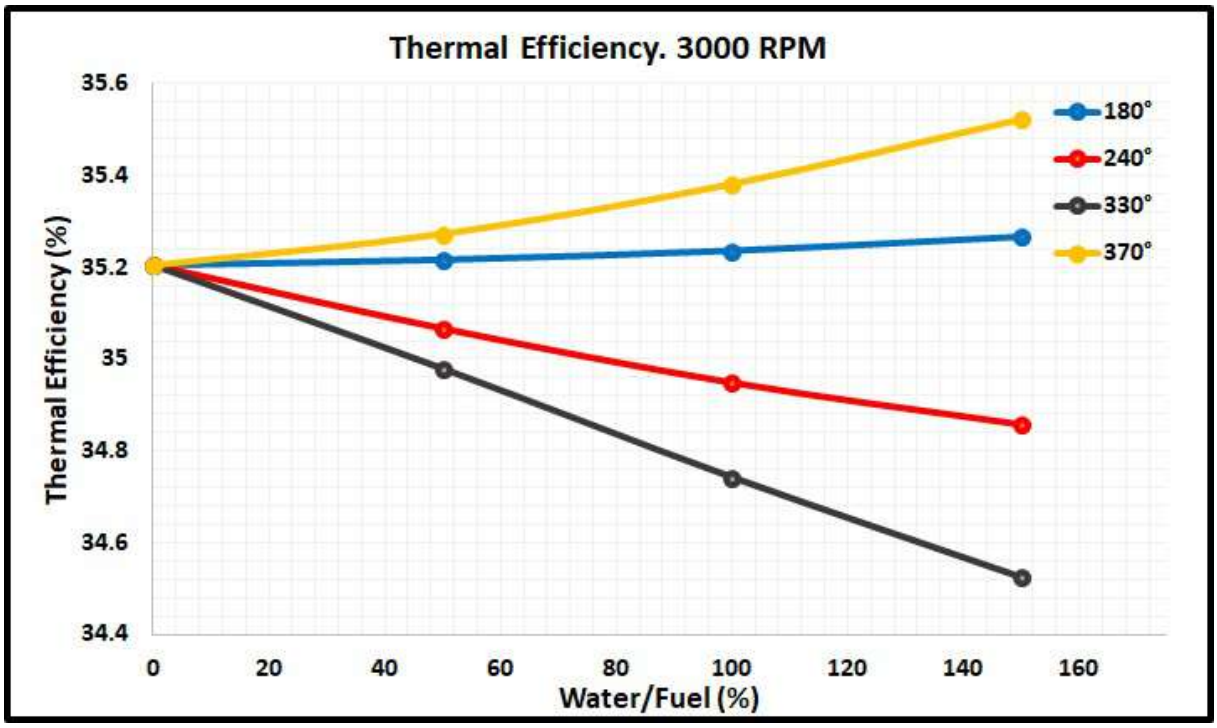

Fig. A.96 – Thermal Efficiency 3000 RPM.

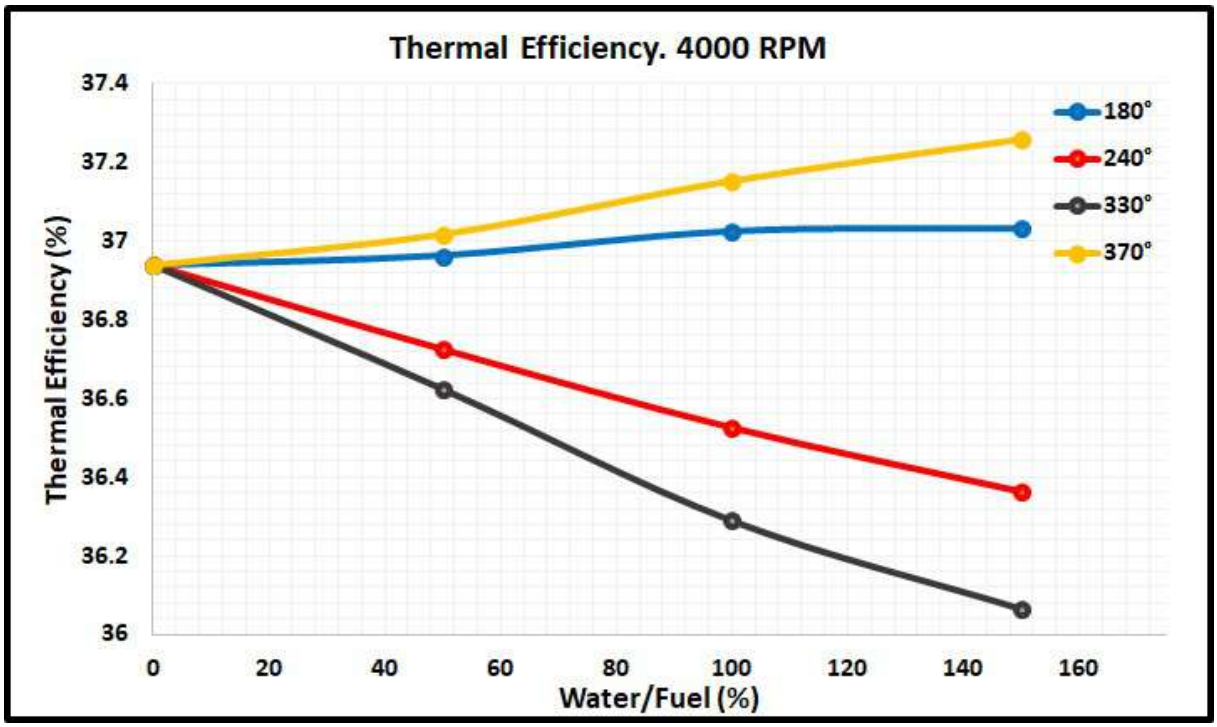

Fig. A.97 – Thermal Efficiency 4000 RPM.

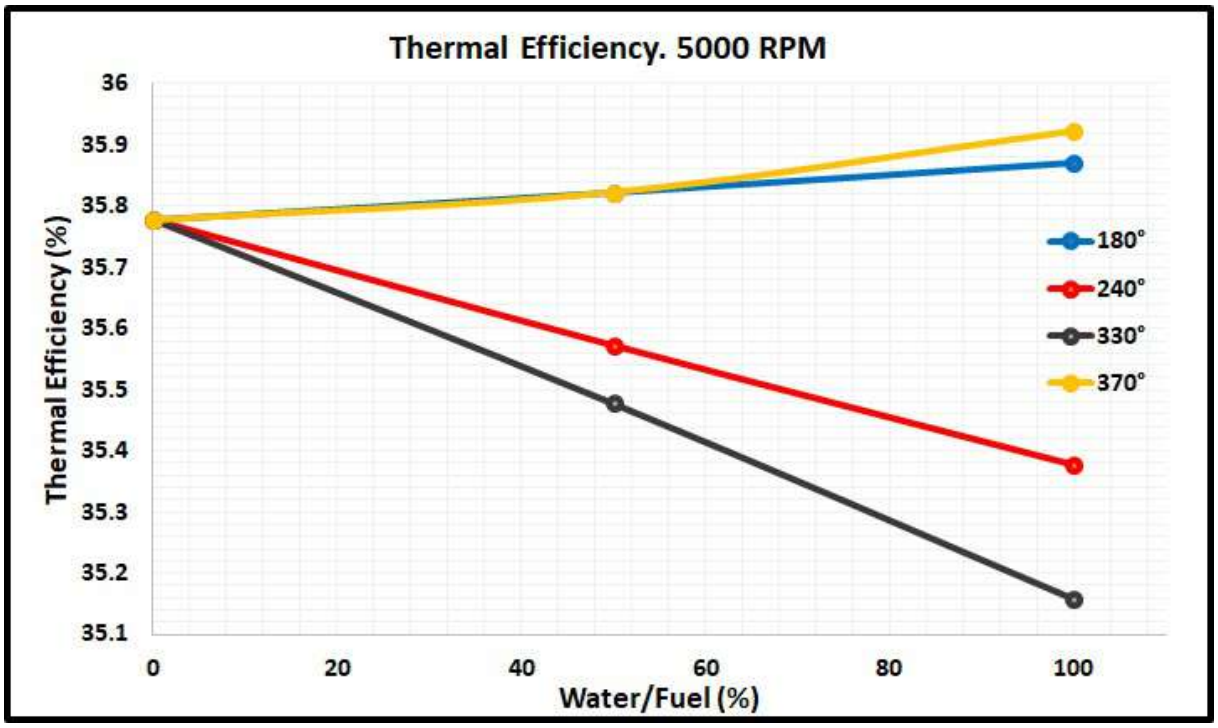

Fig. A.98 – Thermal Efficiency 5000 RPM.

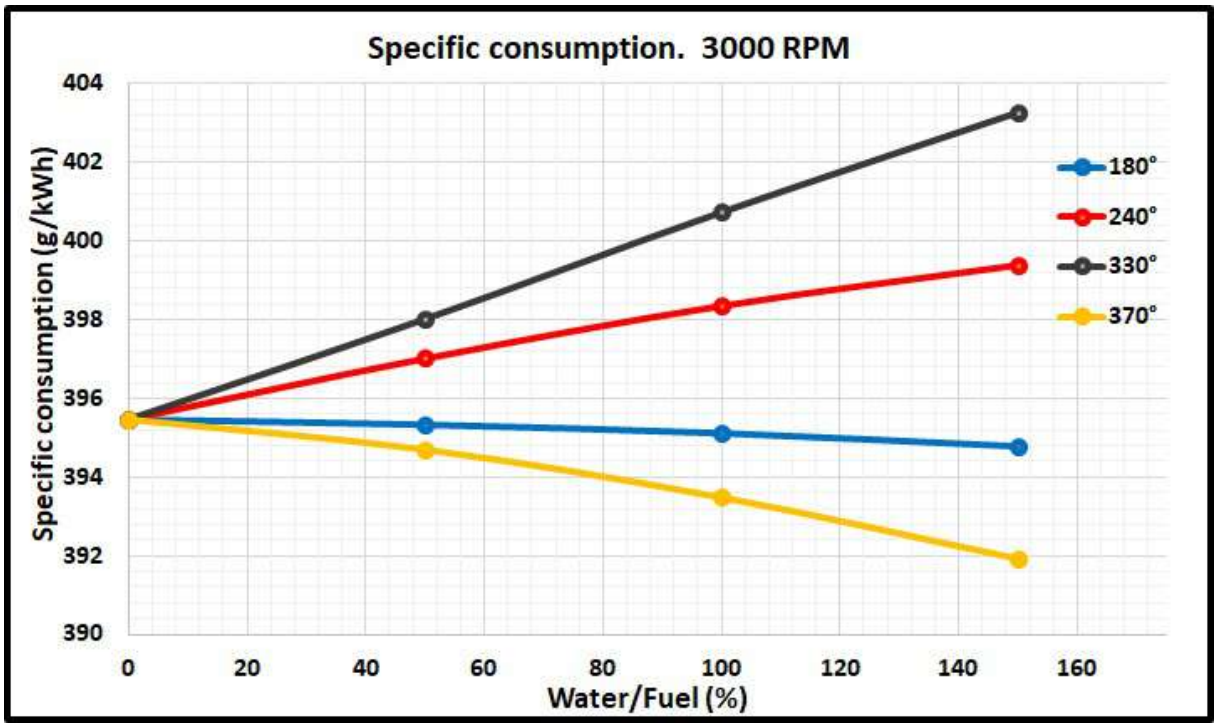

Fig. A.99 – Specific Consumption 3000 RPM.

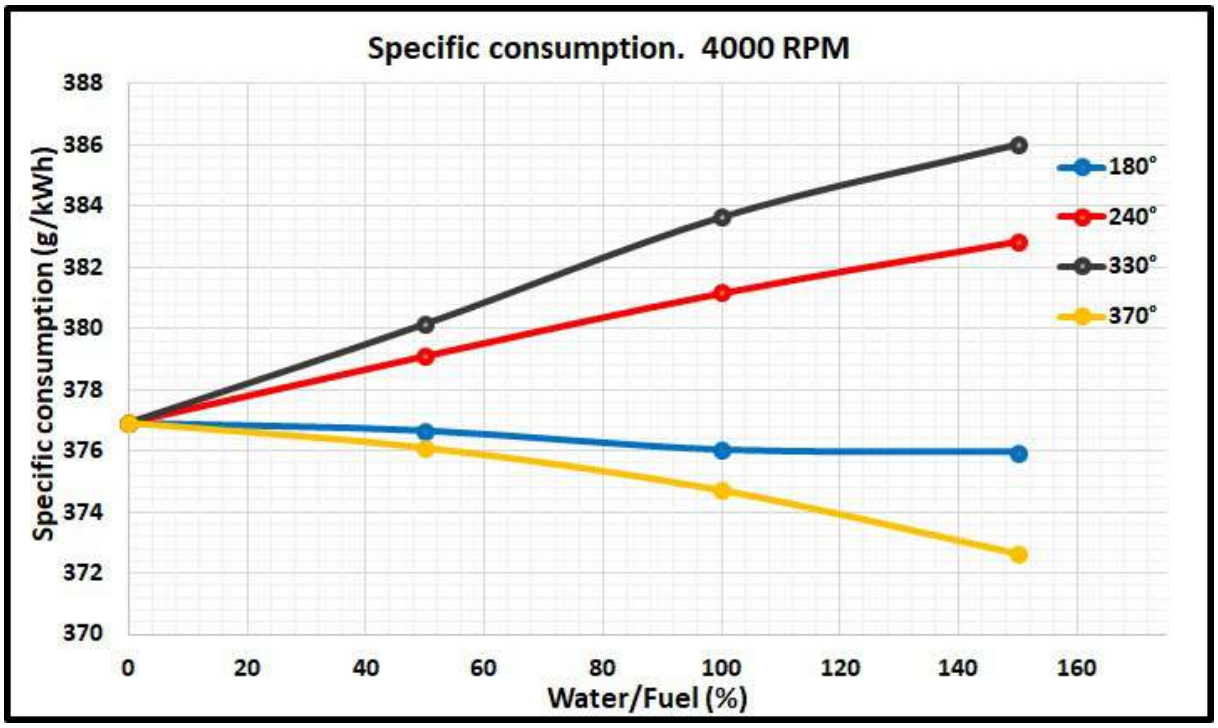

Fig. A.100 – Specific Consumption 4000 RPM.

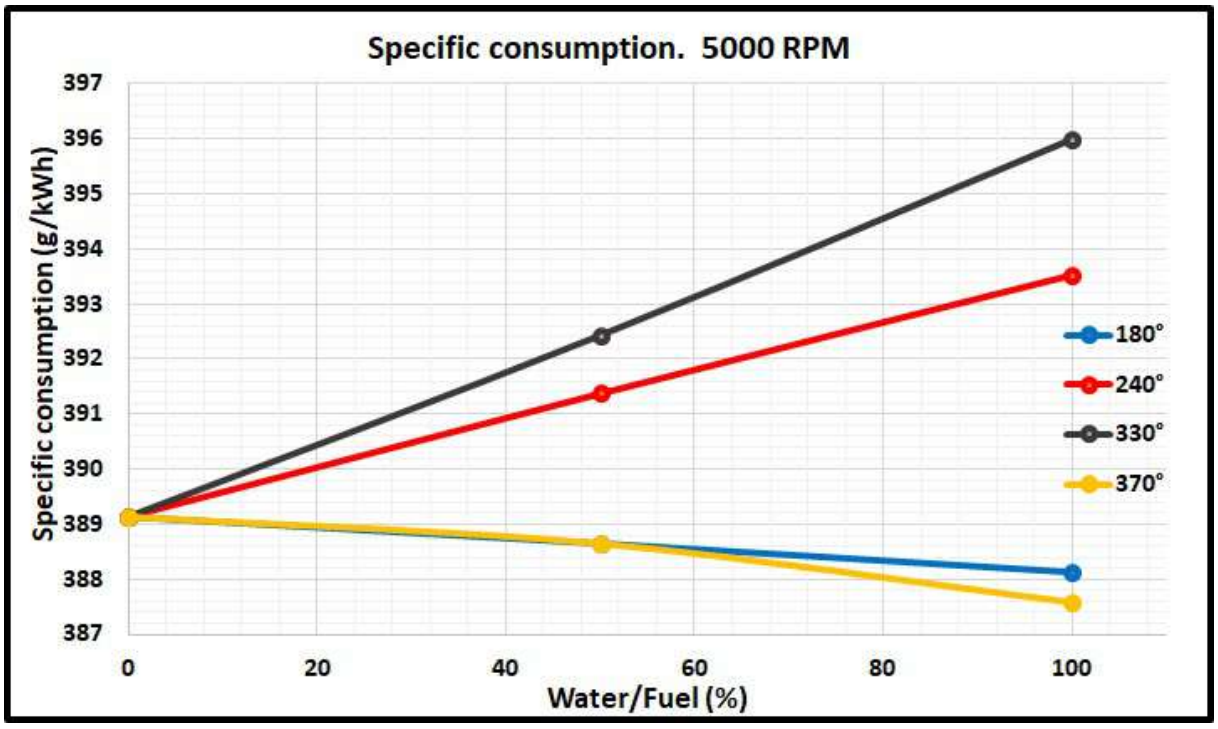

Fig. A.101 – Specific Consumption 5000 RPM.

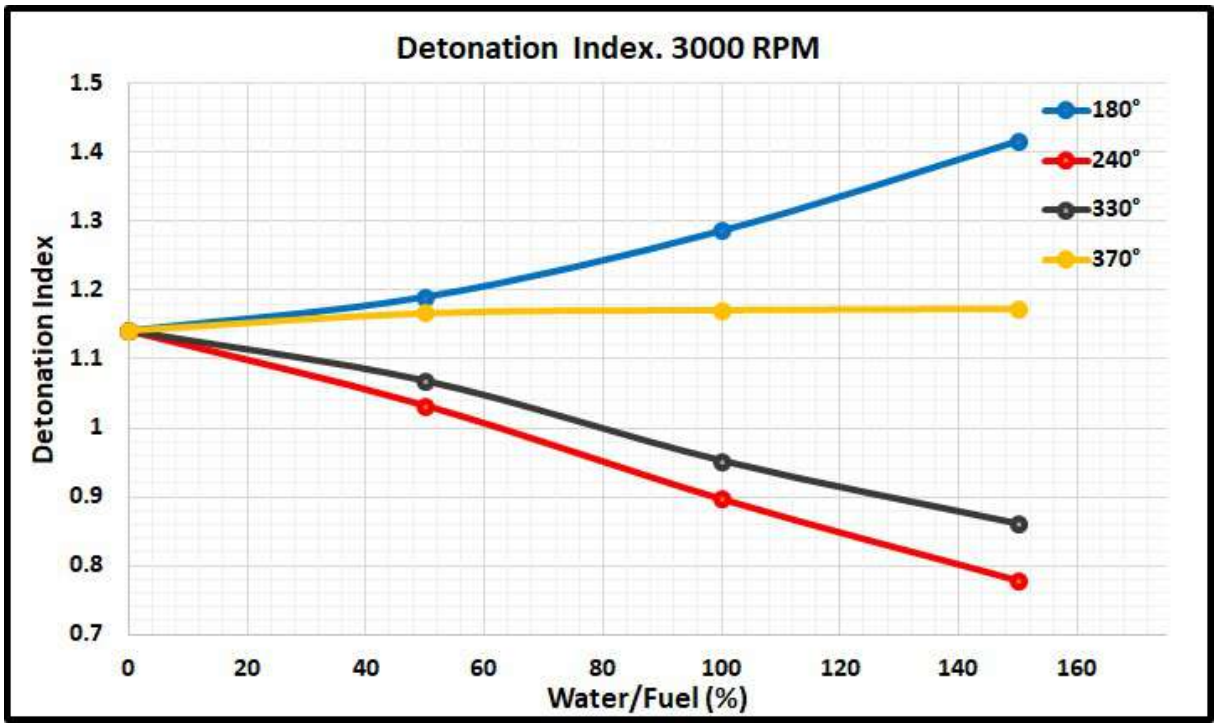

Fig. A.102 – Detonation Index 3000 RPM.

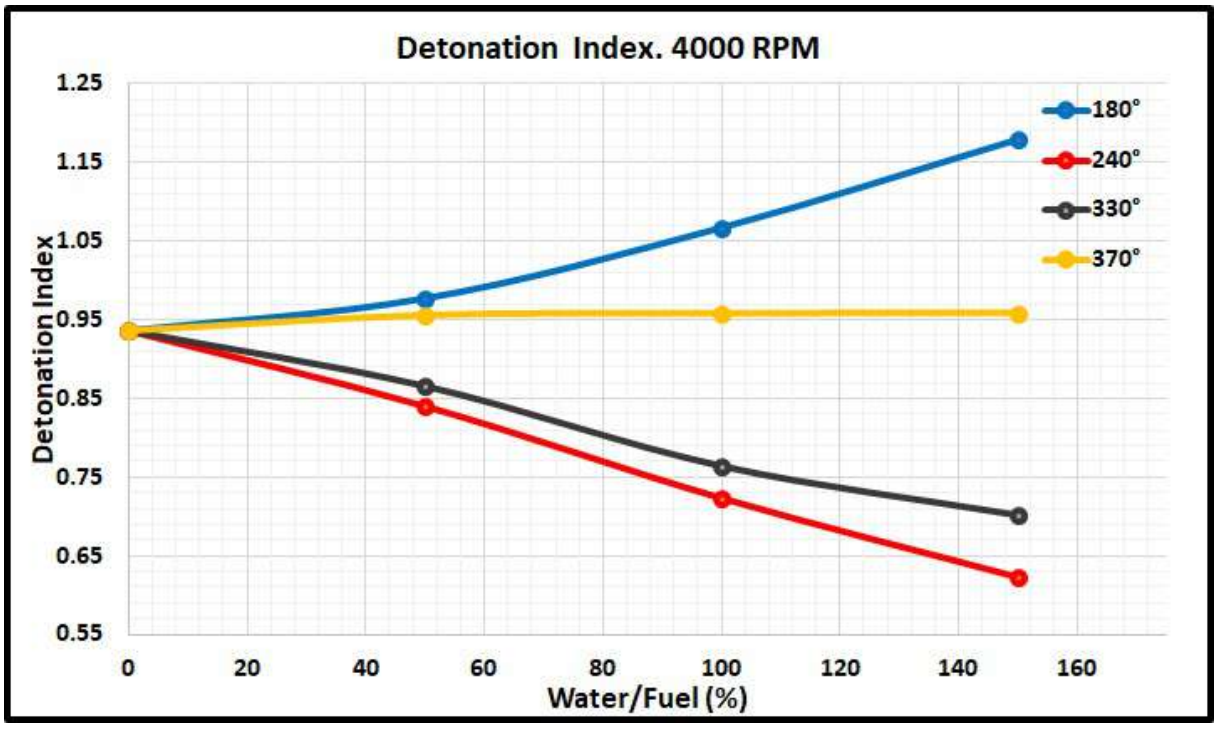

Fig. A.103 – Detonation Index 4000 RPM.

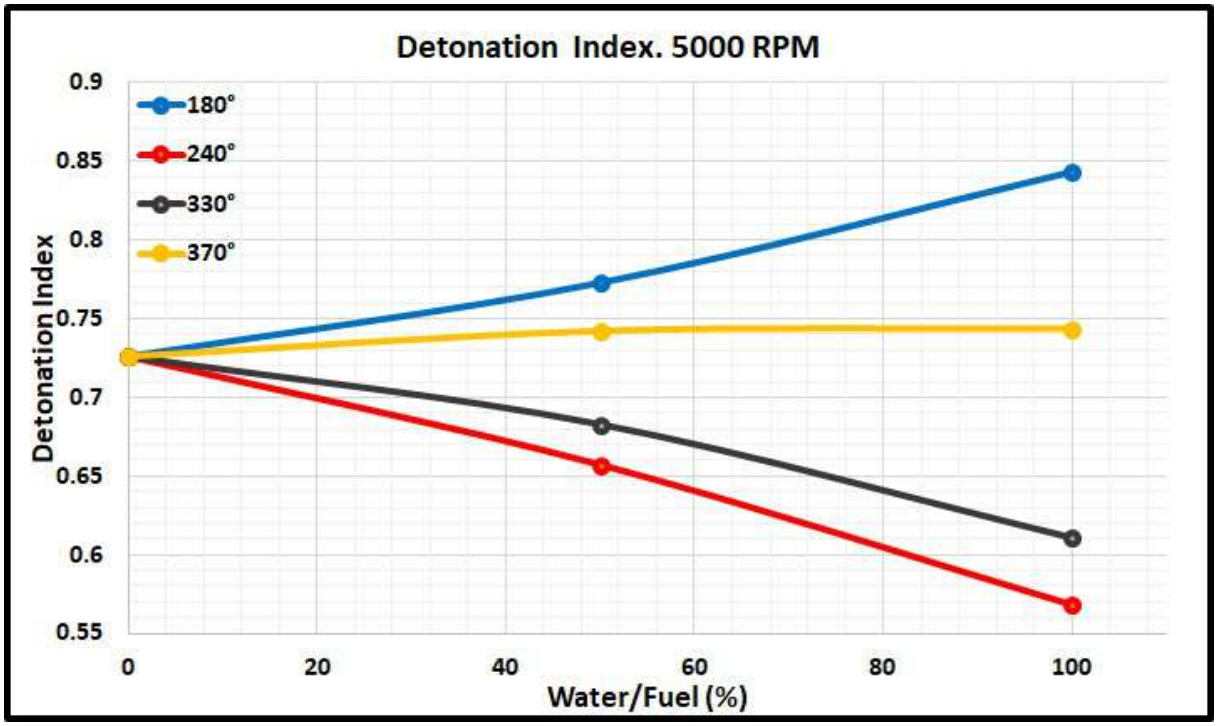

Fig. A.104 – Detonation Index 5000 RPM.

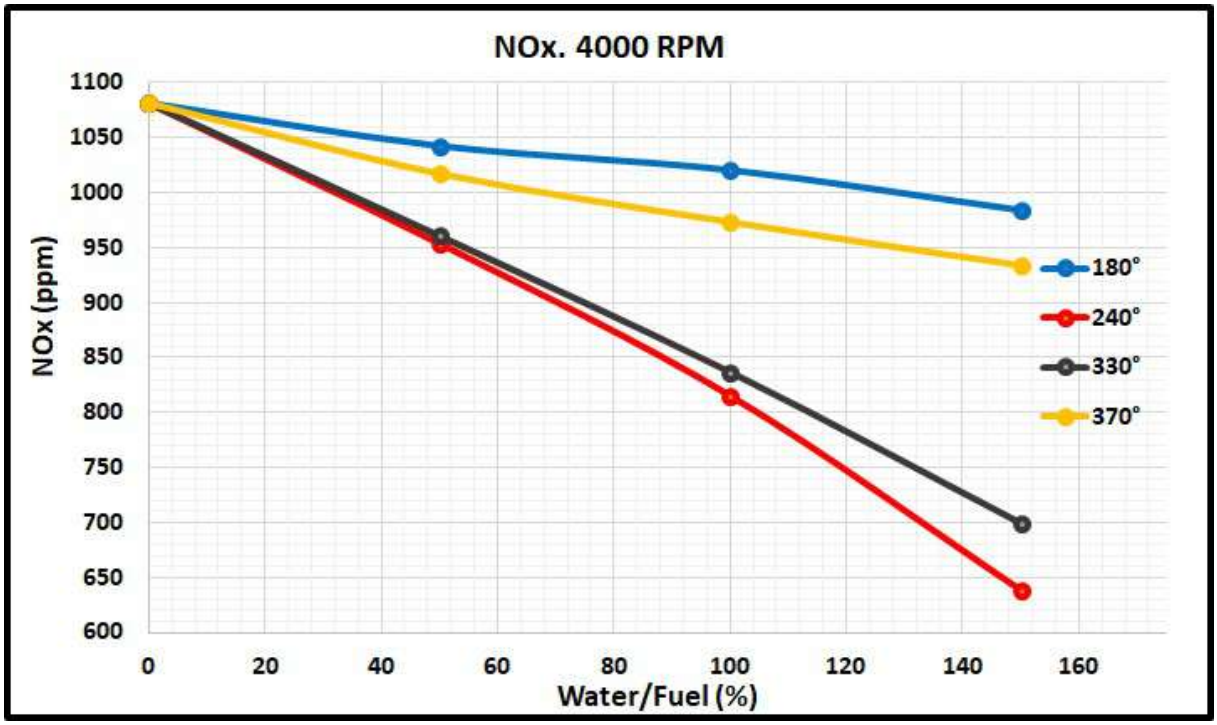

Fig. A.105 – NOx emissions 4000RPM.

B APPENDIX

Table B.1 – Comparison of Performance Variables 1000 RPM (1)

1000 RPM							
	% Water/Fuel	**Power (Kw)**	**Torque (Nm)**	**Thermal Efficiency (%)**	**Volumetric efficiency (%)**	**Instant consumption (kg/h)**	**Specific consumption (g/kWh)**
180° Water injection	***0***	2.750	26.261	30.420	86.489	1.259	457.667
	50	2.793	26.667	30.509	87.575	1.274	456.333
	100	2.847	27.187	30.531	89.224	1.298	456.002
	150	2.928	27.961	30.564	91.672	1.334	455.507
240° Water injection	***0***	2.750	26.261	30.420	86.489	1.259	457.667
	50	2.758	26.332	30.511	86.530	1.258	456.299
	100	2.761	26.363	30.560	86.574	1.258	455.571
	150	2.766	26.413	30.627	86.616	1.257	454.564
	200	2.773	26.476	30.710	86.657	1.257	453.348
	250	2.780	26.543	30.802	86.697	1.256	451.993
330° Water injection	***0***	2.750	26.261	30.420	86.489	1.259	457.667
	50	2.752	26.277	30.447	86.519	1.258	457.263
	100	2.747	26.233	30.403	86.557	1.258	457.921
	150	2.744	26.201	30.374	86.590	1.258	458.351
	200	2.742	26.186	30.365	86.622	1.257	458.488
	250	2.742	26.186	30.373	86.652	1.257	458.376
370° Water injection	***0***	2.750	26.261	30.420	86.489	1.259	457.667
	50	2.762	27.371	30.546	86.481	1.259	455.778
	100	2.768	26.434	30.613	86.469	1.259	454.775
	150	2.776	26.505	30.695	86.452	1.259	453.570

Table B.2 – Comparison of Performance Variables 2000 RPM (1)

2000 RPM							
	% Water/Fuel	**Power (Kw)**	**Torque (Nm)**	**Thermal Efficiency (%)**	**Volumetric efficiency (%)**	**Instant consumption (kg/h)**	**Specific consumption (g/kWh)**
180° Water injection	***0***	6.8843	32.8701	31.5469	100.1934	3.0381	441.3145
	50	7.0691	33.7524	31.5646	102.8313	3.1179	441.0671
	100	7.3813	35.243	31.5947	107.2978	3.2525	440.6473
	150	7.788	37.1851	31.6166	113.1551	3.4294	440.3429
240° Water injection	***0***	6.8843	32.8701	31.5469	100.1934	3.0381	441.3145
	50	6.8832	32.865	31.5467	100.2745	3.0377	441.3178
	100	6.8832	32.8648	31.5522	100.3546	3.0371	441.2415
	150	6.8871	32.8835	31.5753	100.4338	3.0367	440.9188
330° Water injection	***0***	6.8843	32.8701	31.5469	100.1934	3.0381	441.3145
	50	6.8654	32.7798	31.4638	100.2622	3.0378	442.4811
	100	6.8417	32.6665	31.3589	100.3273	3.0374	443.9606
	150	6.8222	32.5738	31.2746	100.3895	3.037	445.157
370° Water injection	***0***	6.8843	32.8701	31.5469	100.1934	3.0381	441.3145
	50	6.9037	32.9625	31.6334	100.1643	3.0384	440.1081
	100	6.9287	33.082	31.7465	100.1255	3.0385	438.5411
	150	6.9562	33.2132	31.8715	100.089	3.0386	436.8202

Table B.3 – Comparison of Performance Variables 3000 RPM (1)

3000 RPM							
	% Water/Fuel	**Power (Kw)**	**Torque (Nm)**	**Thermal Efficiency (%)**	**Volumetric efficiency (%)**	**Instant consumption (kg/h)**	**Specific consumption (g/kWh)**
180° Water injection	***0***	11.9955	38.1828	35.203	105.4644	4.744	395.4807
	50	12.4321	39.5728	35.2154	109.2872	4.915	395.3423
	100	13.0837	41.6468	35.2355	114.9735	5.1696	395.1162
	150	13.8998	44.2445	35.267	122.0606	5.4871	394.7637
240° Water injection	***0***	11.9955	38.1828	35.203	105.4644	4.744	395.4807
	50	11.9478	38.0312	35.0663	105.5566	4.7436	397.023
	100	11.9067	37.9002	34.949	105.6516	4.7431	398.3556
	150	11.8744	37.7972	34.8585	105.7414	4.7425	399.3896
330° Water injection	***0***	11.9955	38.1828	35.203	105.4644	4.744	395.4807
	50	11.9179	37.9357	34.9778	105.5434	4.7436	398.028
	100	11.8362	37.6759	34.7411	105.6216	4.7433	400.7395
	150	11.7609	37.4361	34.5231	105.6955	4.7428	403.2703
370° Water injection	***0***	11.9955	38.1828	35.203	105.4644	4.744	395.4807
	50	12.0195	38.2593	35.2716	105.4322	4.7442	394.7123
	100	12.0572	38.3793	35.3809	105.3895	4.7444	393.4925
	150	12.105	38.5313	35.5226	105.3498	4.7442	391.923

Table B.4 – Comparison of Performance Variables 4000 RPM (1)

4000 RPM							
	% Water/Fuel	**Power (Kw)**	**Torque (Nm)**	**Thermal Efficiency (%)**	**Volumetric efficiency (%)**	**Instant consumption (kg/h)**	**Specific consumption (g/kWh)**
180° Water injection	***0***	16.2939	38.8988	36.9366	102.0611	6.1415	376.9195
	50	16.8733	40.2821	36.9619	105.672	6.3555	376.6613
	100	17.8526	42.6199	37.024	111.6408	6.7131	376.0302
	150	19.0028	45.3658	37.0314	118.8442	7.1442	375.955
240° Water injection	***0***	16.2939	38.8988	36.9366	102.0611	6.1415	376.9195
	50	16.1993	38.673	36.7239	102.1624	6.1412	379.1026
	100	16.1086	38.4565	36.5253	102.2608	6.14	381.164
	150	16.0353	38.2816	36.3636	102.3579	6.1393	382.8587
330° Water injection	***0***	16.2939	38.8988	36.9366	102.0611	6.1415	376.9195
	50	16.1543	38.5655	36.6229	102.1482	6.141	380.1481
	100	16.0052	38.2097	36.2893	102.2305	6.1403	383.6429
	150	15.9052	37.9707	36.0661	102.3058	6.1397	386.0174
370° Water injection	***0***	16.2939	38.8988	36.9366	102.0611	6.1415	376.9195
	50	16.3293	38.9832	37.0158	102.0257	6.1417	376.1131
	100	16.3916	39.132	37.153	101.9845	6.1423	374.724
	150	16.4372	39.241	37.2592	101.949	6.1419	372.6563

Table B.5 – Comparison of Performance Variables 5000 RPM (1)

5000 RPM							
	% Water/Fuel	**Power (Kw)**	**Torque (Nm)**	**Thermal Efficiency (%)**	**Volumetric efficiency (%)**	**Instant consumption (kg/h)**	**Specific consumption (g/kWh)**
180° Water injection	***0***	19.427	37.1028	35.7765	97.3385	7.5598	389.1418
	50	20.279	38.73	35.8213	101.5541	7.8815	388.655
	100	21.4654	40.9959	35.87	107.3874	8.3313	388.127
	150						
240°Water injection	***0***	19.427	37.1028	35.7765	97.3385	7.5598	389.1418
	50	19.3149	36.8887	35.5719	97.4487	7.5595	391.3801
	100	19.2059	36.6806	35.377	97.559	7.5582	393.5363
	150						
330° Water injection	***0***	19.427	37.1028	35.7765	97.3385	7.5598	389.1418
	50	19.2632	36.7901	35.4773	97.433	7.5594	392.424
	100	19.0888	36.4569	35.159	97.5255	7.5587	395.9757
	150						
370° Water injection	***0***	19.427	37.1028	35.7765	97.3385	7.5598	389.1418
	50	19.4523	37.1512	35.8217	97.3027	7.5602	388.6504
	100	19.5074	37.2563	35.9215	97.2612	7.5605	387.5708
	150						

Table B.6 – Comparison of Performance Variables 1000 RPM (2)

1000 RPM				
	% Water/Fuel	**Average pressure indicated (Bar)**	**Detonation Index**	**NOx (PPM)**
180° Water injection	***0***	8.2399	1.5153	622.5
	50	8.3674	1.5026	623.0
	100	8.5305	1.5068	606.3
	150	8.7732	1.542	597.0
240° Water injection	***0***	8.2399	1.5153	622.5
	50	8.2622	1.4035	513.2
	100	8.2717	1.2544	361.1
	150	8.2875	1.1206	187.1
	200	8.3072	1.0041	70.8
	250	8.3283	0.9034	23.1
330° Water injection	***0***	8.2399	1.5153	622.5
	50	8.2448	1.4653	528.3
	100	8.2311	1.3546	394.9
	150	8.2211	1.2602	242.5
	200	8.2164	1.1811	115.7
	250	8.2163	1.117	47.3
370° Water injection	***0***	8.2399	1.5153	622.5
	50	8.2743	1.5635	579.9
	100	8.2941	1.5747	549.4
	150	8.3165	1.5803	523.2

Table B.7 – Comparison of Performance Variables 2000 RPM (2)

2000 RPM				
	% Water/Fuel	**Average pressure indicated (Bar)**	**Detonation Index**	**NOx (PPM)**
180° Water injection	***0***	10.3136	1.2281	605.1
	50	10.5904	1.2507	575.5
	100	11.0581	1.3256	581.2
	150	11.6675	1.4374	559.4
240° Water injection	***0***	10.3136	1.2281	605.1
	50	10.312	1.1175	476.0
	100	10.3119	0.9781	304.4
	150	10.3178	0.8557	135.1
330° Water injection	***0***	10.3136	1.2281	605.1
	50	10.2853	1.1598	488.0
	100	10.2497	1.0458	340.7
	150	10.2206	0.9533	183.2
370° Water injection	***0***	10.3136	1.2281	605.1
	50	10.3426	1.2592	568.8
	100	10.3801	1.2672	543.7
	150	10.4213	1.2688	521.2

Table B.8 – Comparison of Performance Variables 3000 RPM (2)

3000 RPM				
	% Water/Fuel	**Average pressure indicated (Bar)**	**Detonation Index**	**NOx (PPM)**
180° Water injection	***0***	11.9806	1.1411	961.1
	50	12.4167	1.1902	939.8
	100	916		
	150	13.8825	1.4175	886.3
240° Water injection	***0***	11.9806	1.1411	961.1
	50	11.933	1.0325	843
	100	11.8919	0.8965	688.1
	150	11.8596	0.7779	486.2
330° Water injection	***0***	11.9806	1.1411	961.1
	50	11.903	1.0684	848.5
	100	11.8215	0.9523	718.2
	150	11.7463	0.8605	553.5
370° Water injection	***0***	11.9806	1.1411	961.1
	50	12.0046	1.167	919.7
	100	12.0422	1.1716	879.4
	150	12.0899	1.1735	835.9

Table B.9 – Comparison of Performance Variables 4000 RPM (2)

4000 RPM				
	% Water/Fuel	**Average pressure indicated (Bar)**	**Detonation Index**	**NOx (PPM)**
180° Water injection	***0***	12.2052	0.9357	1081
	50	12.6392	0.9769	1042
	100	13.3728	1.0672	1020
	150	14.2344	1.1802	983.5
240° Water injection	***0***	12.2052	0.9357	1081
	50	12.1344	0.8396	953.3
	100	12.0664	0.7226	814.7
	150	12.0115	0.622	637.7
330° Water injection	***0***	12.2052	0.9357	1081
	50	12.1006	0.8652	960.6
	100	11.989	0.7633	836.9
	150	11.914	0.7008	699.7
370° Water injection	***0***	12.2052	0.9357	1081
	50	12.2317	0.955	1017
	100	12.2784	0.9574	973.1
	150	12.3126	0.9582	933.7

Table B.10 – Comparison of Performance Variables 5000 RPM (2)

5000 RPM				
	% Water/Fuel	**Average pressure indicated (Bar)**	**Detonation Index**	**NOx (PPM)**
180° Water injection	***0***	11.6417	0.7256	1019
	50	12.1522	0.7725	985.1
	100	12.8632	0.8431	953.6
	150			
240° Water injection	***0***	11.6417	0.7256	1019
	50	11.5745	0.657	881.5
	100	11.5092	0.5681	733
	150			
330° Water injection	***0***	11.6417	0.7256	1019
	50	11.5436	0.6827	891.6
	100	11.439	0.611	762.3
	150			
370° Water injection	***0***	11.6417	0.7256	1019
	50	11.6569	0.7419	959
	100	11.6899	0.7435	927.6
	150			

Table B.11 – Maximum pressure and temperature values (burned and unburned gas zones) 1000 RPM.

1000 RPM							
	% Water/Fuel	**Maximum pressure reached (MPa)**	**Maximum pressure position (°)**	**Maximum temperature burned gases (K)**	**Position Maximum temperature burned gases Tb (°)**	**Maximum temperature unburned gases (K)**	**Position Maximum temperature unburned gases Tu (°)**
180° Water injection	***0***	5.137	376.3	2257	373.8	879.2	375.8
	50	5.19	376.3	2253	373.8	874.3	375.8
	100	5.275	376.3	2248	373.8	870.0	375.8
	150	5.411	376.3	2245	373.8	866.6	375.8
240° Water injection	***0***	5.137	376.3	2257	373.9	879.2	375.6
	50	5.137	376.3	2167	373.9	853.3	375.6
	100	5.142	376.3	2084	373.9	829.1	375.6
	150	5.151	376.3	2009	373.9	807.1	375.6
	200	5.162	376.3	1941	373.9	786.9	375.6
	250	5.174	376.3	1878	373.9	768.3	375.6
330° Water injection	***0***	5.137	376.3	2257	373.9	879.2	375.8
	50	5.126	376.3	2176	373.9	859.2	375.8
	100	5.118	376.3	2101	373.9	840.8	375.8
	150	5.114	376.3	2034	373.9	824.8	375.8
	200	5.112	376.3	1974	373.9	810.9	375.8
	250	5.114	376.3	1919	373.9	799.1	375.8
370° Water injection	***0***	5.137	376.3	2257	373.9	879.2	375.6
	50	5.135	376.3	2247	371.8	877.9	375.6
	100	5.134	376.3	2247	371.8	877.9	375.6
	150	5.134	376.3	2247	371.8	877.9	375.6

Table B.12 – Maximum pressure and temperature values (burned and unburned gas zones) 2000 RPM

2000 RPM							
	% Water/Fuel	**Maximum pressure reached M(Pa)**	**Maximum pressure position (°)**	**Maximum temperature burned gases (K)**	**Position Maximum temperature burned gases Tb (°)**	**Maximum temperature unburned gases (K)**	**Position Maximum temperature unburned gases Tu (°)**
180° Water injection	***0***	6.447	374.3	2312	371.6	892.2	373.8
	50	6.602	374.3	2306	371.6	888.0	373.8
	100	6.88	374.3	2306	371.6	888.0	373.8
	150	7.248	374.3	2306	371.6	884.4	373.8
240° Water injection	***0***	6.447	374.3	2312	371.7	892.1	373.5
	50	6.443	374.3	2212	371.7	861.2	373.5
	100	6.447	374.3	2122	371.7	832.9	373.5
	150	6.454	374.3	2041	371.7	807.1	373.5
330° Water injection	***0***	6.447	374.3	2312	371.2	892.1	373.6
	50	6.426	374.3	2221	371.2	866.1	373.6
	100	6.411	374.3	2140	371.2	843.0	373.6
	150	6.4	374.3	2068	371.2	823.3	373.6
370° Water injection	***0***	6.447	374.3	2313	371.2	892.2	374.1
	50	6.444	374.3	2313	371.2	892.6	374.1
	100	6.446	374.3	2313	371.2	892.6	374.1
	150	6.446	374.3	2313	371.2	892.6	374.1

Table B.13 – Maximum pressure and temperature values (burned and unburned gas zones) 3000 RPM

3000 RPM							
	% Water/Fuel	**Maximum pressure reached M(Pa)**	**Maximum pressure position (°)**	**Maximum temperature burned gases (K)**	**Position Maximum temperature burned gases Tb (°)**	**Maximum temperature unburned gases (K)**	**Position Maximum temperature unburned gases Tu (°)**
180° Water injection	***0***	7.159	374.2	2476	371.0	909	373.4
	50	7.405	374.2	2471	371.0	904	373.4
	100	7.782	374.2	2471	371.0	904	373.4
	150	8.256	374.2	2471	371.0	904	373.4
240° Water injection	***0***	7.159	374.2	2476	371.0	909	373.6
	50	7.133	374.2	2366	371.0	875.7	373.6
	100	7.118	374.2	2267	371.0	845.5	373.6
	150	7.109	374.2	2179	371.0	818.1	373.6
330° Water injection	***0***	7.159	374.2	2476	371.0	909	373.4
	50	7.116	374.2	2375	371.0	880	373.4
	100	7.081	374.2	2287	370.8	854.7	373.4
	150	7.05	374.2	2207	370.6	833.6	373.4
370° Water injection	***0***	7.159	374.2	2476	370.9	909.6	373.6
	50	7.158	374.2	2478	370.9	909.6	373.6
	100	7.157	374.2	2478	370.9	909.6	373.6
	150	7.157	374.2	2478	370.9	909.6	373.6

Table B.14 – Maximum pressure and temperature values (burned and unburned gas zones) 4000 RPM

4000 RPM							
	% Water/Fuel	**Maximum pressure reached M(Pa)**	**Maximum pressure position (°)**	**Maximum temperature burned gases (K)**	**Position Maximum temperature burned gases Tb (°)**	**Maximum temperature unburned gases (K)**	**Position Maximum temperature unburned gases Tu (°)**
180° Water injection	***0***	7.187	374.3	2577	370.9	920.6	373.6
	50	7.43	374.3	2572	370.9	916.5	373.6
	100	7.847	374.3	2572	370.9	916.5	373.6
	150	8.339	374.3	2572	370.9	916.5	373.6
240° Water injection	***0***	7.187	374.3	2577	371	920.6	373.6
	50	7.152	374.3	2461	371	885.1	373.6
	100	7.125	374.3	2355	371	853.0	373.6
	150	7.107	374.3	2261	371	823.9	373.6
330° Water injection	***0***	7.187	374.3	2577	371	920.6	373.6
	50	7.133	374.3	2469	371	888.7	373.6
	100	7.085	374.3	2374	371	861.2	373.6
	150	7.057	374.3	2293	371	843.2	373.6
370° Water injection	***0***	7.187	374.3	2577	370.8	920.3	373.7
	50	7.189	374.3	2580	370.8	921.3	373.7
	100	7.19	374.3	2580	370.8	921.3	373.7
	150	7.19	374.3	2580	370.8	921.3	373.7

Table B.15 – Maximum pressure and temperature values (burned and unburned gas zones) 5000 RPM

5000 RPM							
	% Water/Fuel	**Maximum pressure reached M(Pa)**	**Maximum pressure position (°)**	**Maximum temperature burned gases (K)**	**Position Maximum temperature burned gases Tb (°)**	**Maximum temperature unburned gases (K)**	**Position Maximum temperature unburned gases Tu (°)**
180° Water injection	***0***	6.77	374.3	2591	370.6	920.3	373.5
	50	7.053	374.3	2587	370.6	917.7	373.5
	100	7.448	374.3	2587	370.6	917.7	373.5
	150						
240° Water injection	***0***	6.77	374.3	2591	370.7	920.3	373.5
	50	6.737	374.3	2470	370.7	884.8	373.5
	100	6.714	374.3	2362	370.7	852.9	373.5
	150						
330° Water injection	***0***	6.77	374.3	2591	370.6	920.3	373.6
	50	6.719	374.3	2480	370.6	889.5	373.6
	100	6.68	374.3	2384	370.6	864.8	373.6
	150						
370° Water injection	***0***	6.77	374.3	2591	370.5	920.3	373.8
	50	6.77	374.3	2593	370.5	920.8	373.8
	100	6.77	374.3	2593	370.5	920.8	373.8
	150						